Mechanistic and quantitative understanding of antibiotic resistance and adaptation of *Escherichia coli* under levofloxacin exposure

Inaugural-Dissertation

to obtain the academic degree

Doctor rerum naturalium (Dr. rer. nat.)

submitted to the Department of Biology, Chemistry, Pharmacy

of Freie Universität Berlin

by

Johanna Seeger

from Berlin

2021

Die vorliegende Dissertation wurde von 2017 bis 2021 unter der Leitung von Prof. Dr. Charlotte Kloft am Institut für Pharmazie der Freien Universität Berlin angefertigt.

Erstgutachterin:	Prof. Dr. Charlotte Kloft
Zweitgutachter:	Prof. Dr. Markus Zeitlinger
Tag der Disputation:	03. August 2021

Selbstständigkeitserklärung

Hiermit versichere ich, dass ich die vorliegende Dissertation selbstständig und nur unter Verwendung der angegebenen Literatur und Hilfsmittel angefertigt habe.

Johanna Seeger

Acknowledgements

It was a great pleasure to perform the present work in the unique and inspiring scientific and social environment at the Department of Clinical Pharmacy and Biochemistry at the Institute of Pharmacy at the Freie Universitaet Berlin, and I would like to express my sincere gratitude to everyone who supported me during this amazing time.

Particularly, I would like to express my deep gratitude to *Prof. Dr. Charlotte Kloft.* Thank you for your trust, your enthusiasm and inspiration; for hearing and considering my (scientific and non-scientific) ideas and concerns. Your encouragement and backing are invaluable.

Further, I would like to express my sincere gratitude to *Dr. Robin Michelet* for the excellent collaboration and valuable discussions, especially for introducing me to the universe of modelling and simulations with endless patience. Thank you for all the scientific and moral support and encouragement, particularly during the last six months of dissertation writing, and for accepting me as office mate during this special time.

Thank you*, Prof. Dr. Sebastian Günther*, from the Department of Pharmaceutical Biology, Institute of Pharmacy, Universitaet Greifswald, for providing PCR protocols, whole genome sequencing of the *E. coli* isolates and introducing me to sequence data analysis.

Thank you, *Prof. Dr. Markus Zeitlinger*, from the Department of Clinical Pharmacology, Medical University of Vienna, for reviewing the present thesis and being a member of the doctoral committee.

Further, I would like to express my deep gratitude to *Dr. Eva Göbgen* for stirring up my passion for science as my supervisor during my elective course and Diploma research. Thank you for introducing me to the *in vitro* infection models with thoroughness and patience, for countless valuable discussions and for your important advice in scientific and non-scientific questions.

Thank you, *Tania Fuhrmann-Selter* and *Corinna Schmidt* for your valuable support in the lab and for being always ready to help with all kinds of experimental challenges. Thank you*, Dr. Ingo Siebenbrodt* for your support and fruitful collaboration in all teaching activities.

I would like to thank *Prof. Dr. Sebastian Wicha* and *Dr. Niklas Hartung* for inspiring discussions, which broadened my perspective, encouraged and guided me especially in the beginning of my doctoral studies.

Thank you, *Josefine Schulz* and *Sebastian Franck*, for being the best office and lab mates I could ever think of. It was a great pleasure to have you right next to me, being always ready to listen, help and share joy and sorrow. Thank you, *Sebastian*, for outstanding discussions, your honest interest and proactive helpfulness. Thanks for encouraging me even from Hamburg, for the Friday afternoon-calls and particularly your moral and scientific support during the last months of writing. Thank you, *Josi,* for inspiring me with your enthusiasm for teaching. I highly enjoyed our mutual understanding and the smooth and efficient collaboration in our joint teaching projects, as we always shared the same ideas without any long discussions. Special thanks for the great experience to establish a novel elective course on communication and medication management and our joint pioneering in the interprofessional teaching project in collaboration with the Charité University Hospital Berlin.

Big thanks for reviewing this dissertation, for valuable comments and helpful discussions to *Sebastian Franck, Luis Ilia, David Busse, Dr. Christine Weiser, Dr. Robin Michelet, Josefine Schulz, Nicole Zimmermann* and *Yomna Nassar*.

Thanks to all present and former members of the “AK Kloft family”, who contributed to a unique working environment and a very special time: *Viktoria Stachanow, Aya Saleh, Dr. Lisa Schmitt, Franziska Kluwe, Dr. Johanna Melin, Dr. Ana-Marija Grišić, Dr. Iris Minichmayr, Ferdinand Weinelt, Alix Demaris, Francis Ojara, Anna Müller-Schöll, Dr. Andrea Henrich, Dr. Lena Klopp-Schulze, Dr. Daniela Burau, Dr. Werner Herrmann, Hacer Bayram* and *Gabriela Karsubke.*

Thanks to *Banafshe Pourshacheraghi* and *Claas Hedtfeld* for trusting me as your mentor in your Diploma and Master research. *Banafshe*, I highly appreciate your enthusiasm, wise ideas and smart questions, which challenged me and let me grow. Thanks for all the stimulating discussions and the great work you did during your Diploma time!

Thanks to all my elective students who generated data in the *in vitro* infection model and provided additional insights: *Charlotte Wieker, Josephin Hinrichs, Julia Paschke, Thuy Trang Vuong, Blerta Nuhu* and *Mergim Domuzeti***.** Very special thanks to the outstanding and incomparable “WPF KOM” group!

Finally, I would like to thank my family and friends: Ich danke meinen *Eltern* für die bedingungslose Unterstützung und ihr unendliches Verständnis, sowie meinen Schwestern *Franziska* und *Christiane* und meinen Neffen *Levi, Justus* und *Luis*, mit denen ich viel zu wenig Zeit verbracht habe. Lieben Dank an meine Freunde für Eure Begleitung und die notwendige Ablenkung, insbesondere an *Katharina, Birgit* und *Marion!*

Abstract

Successful treatment of infectious diseases is increasingly challenging, as emergence and spread of bacterial adaptation and resistance mechanisms threaten the availability of efficacious treatment options. A prerequisite for bacterial eradication and prevention of adaptation and resistance is sufficient antibiotic exposure at target site, which can be obtained by dosing optimisation. For that purpose, a comprehensive understanding of the relationship between pharmacokinetics (PK) and pharmacodynamics (PD), i.e., between antibiotic exposure and effect, is crucial. Currently applied PK/PD parameters and target values are mainly based on the minimal inhibitory concentration (MIC). The informative value of this endpoint measurement is limited, but appropriate alternatives are currently lacking. A comprehensive understanding of exposure-effect relationships requires knowledge about relevant antibiotic resistance and bacterial adaptation mechanisms, which has substantially increased in the last years. However, a link between PK/PD relationships and the underlying mechanisms has not been established yet.

Hence, the present thesis aimed to characterise, quantify, and mechanistically explain bacterial growth-kill behaviour over time. The model compound levofloxacin (LEV) and the bacterial species *Escherichia coli* (*E. coli*) were chosen for the case study, as life-threatening infections with fluoroquinolone resistant *E. coli* strains are of clinically relevant concern.

To characterise growth, kill and regrowth behaviour of three LEV resistant clinical *E. coli* isolates under LEV exposure, time-kill curve investigations in static and dynamic *in vitro* infection models (IVIM) were performed. Mimicking clinically relevant LEV concentration-time (C(t)) profiles, resulting from a 750 mg, 90 min LEV i.v. infusion in plasma, demonstrated the inefficacy of this approved dosing regimen against resistant strains. Bacterial regrowth was observed within 24 h for all strains, but the extent of initial reduction of bacterial concentrations and regrowth differed, even for two strains sharing the same MIC value (8 mg/L).

To understand the genomic background of the observed growth-kill behaviour, a PCR and electrophoresis method was established and mutations in fluoroquinolone resistance determining regions of the isolates were identified by Sanger sequencing. Additionally, whole genome sequencing was performed by collaboration partners, and the sequence types (ST) were determined (ST58, ST88 and ST167). Widespread mutations in *gyrA* and *parC* were identified for all strains. Furthermore, ST88 harboured *qnr* plasmids. The higher LEV susceptibility of ST88 (MIC: 2 mg/L) compared to ST167 (MIC: 8 mg/L) was partly explained by genomic resistance mechanisms, but the reduced susceptibility of ST58 (MIC: 8 mg/L) was not solely explained by the single *gyrA* mutation of the isolate.

To elucidate the contribution of persister formation as a phenotypic adaptation mechanism to the observed growth, kill and regrowth behaviour, an electronic cell counting assay was developed and successfully applied. Filamentation, measured as increased bacterial cell size,

was used as surrogate for persister formation. Assessment of the dynamic changes in bacterial size distributions under static LEV exposure over time implied extensive persister formation of ST88 and ST167, and a comparably small extent of persister formation of ST58.

To quantitatively describe the exposure-effect relationship of LEV against *E. coli* in static and dynamic IVIM experiments, novel PK/PD metrics were introduced, considering the full LEV C(t) profile and bacterial time-kill trajectory: (i) LEV exposure was determined as cumulative area under the LEV C(t) curve, and (ii) the antibiotic effect over time was quantified as cumulative area between the bacterial growth control curve and the time-kill curve, normalised to the area under the growth control curve. Applying these metrics, the exposure-effect relationship was described by a sigmoidal maximum effect (E_{max}) model, combined with an inhibition term. Based on this novel approach, precise parameter estimates for the derived PK/PD parameters, the cumulative area under the LEV C(t) profile causing 50% of the maximum effect ($cumAUC_{50}$) and the cumulative area under the LEV C(t) profile causing regrowth ($cumAUC_{reg}$), were obtained, discriminating the exposure-effect relationship of the strains under static and dynamic LEV exposure.

Finally, gained knowledge about the strain-specific growth-kill behaviour and the underlying adaptation and resistance mechanisms was amalgamated in a three-bacterial-state PK/PD model. Leveraging two bacterial quantification methods, i.e. plate counting and electronic cell counting, allowed discrimination of three bacterial subpopulations: viable, dead and persister cells. Two manifestations of the LEV effect were identified: (i) a LEV concentration-dependent killing effect, decreasing bacterial numbers of viable cells via a sigmoidal E_{max} model, and (ii) an additive increase of the first-order persister formation rate constant, increasing transformation of viable cells into persister cells in presence of LEV. Different LEV potencies of the strains were quantified as strain-specific EC_{50} values, being 5.5-fold higher for ST58 compared to ST88, and 2-fold higher compared to ST167. The largest extent of persister formation for ST88 was confirmed by the highest increase in the persister formation rate constant under LEV exposure for the isolate.

In future, application of electronic cell counting in dynamic IVIM experiments will support refinement of the PK/PD model, as the newly established method was solely applied in static IVIM experiments so far. Further, assessment of PK resistance mechanisms, such as increased expression of efflux pumps or alterations of the outer membrane, decreasing intra-bacterial LEV concentrations, might elucidate the reduced LEV susceptibility of ST58.

Overall, the present thesis highlighted the limitations of the MIC value to guide antibiotic therapy and suggested novel PK/PD parameters. Bacterial adaptation and resistance were quantitatively and mechanistically characterised. The developed PK/PD model elucidated the interplay between different processes determining bacterial growth, kill and regrowth behaviour and facilitates *in silico* simulation of further scenarios, such as alternative LEV dosing

regimens, to ultimately support rational antibiotic dosing and prevent emergence of bacterial adaptation and resistance.

Zusammenfassung

Die erfolgreiche Therapie von Infektionserkrankungen stellt eine zunehmende Herausforderung dar, da die Entstehung und Verbreitung von Antibiotikaresistenz die Verfügbarkeit wirksamer Therapiemöglichkeiten bedroht. Eine Voraussetzung, um Bakterien vollständig abzutöten sowie ihre Anpassung und die Entstehung von Resistenzen zu verhindern, ist eine ausreichende Antibiotikaexposition am Wirkort, die durch optimierte Dosierung erreicht werden kann. Hierzu ist ein umfassendes Verständnis der Beziehung zwischen Pharmakokinetik (PK) und Pharmakodynamik (PD) unerlässlich, also zwischen Antibiotikaexposition und antibiotischem Effekt. Die zurzeit eingesetzten PK/PD-Parameter und ihre Zielwerte basieren überwiegend auf der minimalen Hemmkonzentration (MHK). Die MHK ist als Endpunkt-Messgröße von begrenzter Aussagekraft, jedoch fehlen derzeit angemessene Alternativen. Um Expositions-Effekt-Beziehungen von Antibiotika umfassend zu verstehen, ist die Kenntnis der relevanten Resistenz- und Anpassungsmechanismen der Bakterien essenziell. Obwohl diese in den letzten Jahren bedeutend zugenommen hat, ist der Zusammenhang zwischen PK/PD-Beziehungen und ihren mechanistischen Ursachen bisher wenig erforscht.

Das Ziel der vorliegenden Arbeit war daher, das zeitabhängige bakterielle Wachtsums- und Absterbeverhalten zu charakterisieren, zu quantifizieren und mechanistisch zu erklären. Das Antibiotikum Levofloxacin (LEV) und die bakterielle Spezies *Escherichia coli* (*E. coli*) wurden beispielhaft für diese Fallstudie ausgewählt, da lebensbedrohliche Infektionen mit *E. coli*-Stämmen mit Fluorchinolon-Resistenz von klinisch relevantem Interesse sind.

Um das bakterielle Wachstum, Absterben und Wiederanwachsen drei LEV-resistenter klinischer *E. coli*-Isolate unter LEV-Exposition zu charakterisieren, wurden Untersuchungen in statischen und dynamischen *In-vitro*-Infektionsmodellen (IVIM) durchgeführt. Die Nachahmung klinisch relevanter Konzentrations-Zeitprofile (C(t)-Profile), die nach der Gabe einer 750 mg, 90 min LEV-Infusion im Plasma bestimmt werden, zeigte die Unwirksamkeit dieses zugelassenen Dosierungsschemas bei Infektionen mit resistenten Stämmen. Ein erneutes Anwachsen der Bakterienpopulationen wurde innerhalb von 24 h bei allen Stämmen beobachtet, jedoch mit einem unterschiedlichen Ausmaß des anfänglichen Absterbens und des späteren Wiederanwachsens, selbst für zwei Stämme mit derselben MHK (8 mg/L).

Um die genomischen Ursachen des beobachteten Absterbeverhaltens zu verstehen, wurde eine PCR- und Gelelektrophoresemethode etabliert und wurden Mutationen der Fluorchinolon-Resistenz bestimmenden Regionen der untersuchten Isolate mittels Sequenzierung nach Sanger identifiziert. Zusätzlich wurde das Gesamtgenom der Isolate durch Kooperationspartner sequenziert, und die Sequenztypen (ST) wurden bestimmt (ST58, ST88 und ST167). In allen Isolaten ließen sich weit verbreitete Mutationen der Gene *gyrA* und *parC* festellen. In einem Isolat (ST88) wurden zusätzlich *qnr*-Plasmide identifiziert. Die höhere LEV-

Empfindlichkeit von ST88 (MHK: 2 mg/L) im Vergleich zu ST167 (MHK: 8 mg/L) war teilweise durch genomische Resistenzmechanismen erklärbar, aber die verminderte Empfindlichkeit von ST58 (MHK: 8 mg/L) konnte nicht ausschließlich durch die einzelne *gyrA*-Mutation des Isolates erklärt werden.

Um den Beitrag der Persisterbildung als phänotypischem Adaptationsmechanismus zum beobachteten Wachstums- und Absterbeverhalten aufzuklären, wurde ein Verfahren zur elektronischen Zellzählung entwickelt und erfolgreich eingesetzt. Filamentierung wurde durch Messung der Zellgrößen unter Exposition statischer LEV-Konzentrationen bestimmt und als Surrogat für die Persisterbildung genutzt. Die Untersuchung der dynamischen Änderung der Zellgrößenverteilung von Bakterien, die statischen LEV-Konzentrationen exponiert waren, in Abhängigkeit von der Zeit, deutete auf ausgeprägte Persisterbildung von ST88 und ST167 hin, während ST58 vergleichsweise weniger Persister bildete.

Um die Expositions-Effekt-Beziehung von *E. coli*-Bakterien, die im IVIM statischen und dynamischen LEV-Konzentrationen exponiert waren, quantitativ zu beschreiben, wurden neuartige PK/PD-Messgrößen eingeführt, die das das gesamte LEV C(t)-Profil sowie die gesamte bakterielle Abtötungskurve berücksichtigten: (i) Die LEV-Exposition wurde als kumulierte Fläche unter der LEV C(t)-Kurve berechnet, und (ii) der antibiotische Effekt in Abhängigkeit von der Zeit wurde als kumulierte Fläche zwischen der bakteriellen Wachstumskurve und der Abtötungskurve berechnet und auf die kumulierte Fläche unter der Wachstumskurve normalisiert. Durch die Anwendung dieser Messgrößen konnte die Expositions-Effekt-Beziehung als sigmoidales E_{max}-Modell beschrieben werden, das mit einem Inhibitionsterm kombiniert wurde. Dieser neuartige Ansatz erlaubte die präzise Schätzung der abgeleiteten PK/PD-Parameter, der kumulierten Fläche unter der LEV C(t)-Kurve, die 50% des maximalen Effektes veruracht ($cumAUC_{50}$), und und der kumulierten Fläche unter der LEV C(t)-Kurve, bei der ein Wiederanwachsen der Bakterienpopulation zu beobachten ist ($cumAUC_{reg}$), mit denen die Expositions-Effekt-Beziehung der Stämme unter statischer und dynamischer LEV-Exposition unterschieden werden konnte.

Schließlich ermöglichten die gewonnenen Erkenntnisse über das spezifische Wachstums- und Absterbeverhalten der Stämme und der zu Grunde liegenden Adaptations- und Resistenzmechanismen die Entwicklung eines das bakterielle Wachstums- und Absterbeverhalten charakterisierenden PK/PD-Modells. Durch die zwei eingesetzten Methoden zur Bakterienquantifizierung, zum einen Lebendkeimzahlbestimmung und zum anderen elektronische Zellzählung, konnten drei bakterielle Subpopulationen identifiziert werden: teilungsfähige Zellen, tote Zellen und Persister. Zwei Ausprägungen des LEV-Effektes waren unterscheidbar: (i) ein LEV- konzentrationsabhängiger Abtötungseffekt, der die Anzahl teilungsfähiger Bakterien im Sinne eines sigmoidalen E_{max}-Modells reduzierte, und eine additive Erhöhung der Persisterbildungs-Geschwindigkeitskonstante erster Ordnung unter

LEV-Exposition, die die Transformation teilungsfähiger Zellen in Persisterzellen unter LEV-Einfluss förderte. Unterschiedliche LEV-Wirkstärken wurden durch spezifische EC_{50}-Werte der drei Isolate quantifiziert. Dieser Wert war für ST58 5.5-fach höher als für ST88 und 2-fach höher als für ST167. Das größte Ausmaß der Persisterbildung durch ST88 wurde durch den größten Anstieg der Persisterbildungs-Geschwindigkeitskonstante unter LEV-Einfluss für das Isolat bestätigt.

In Zukunft wird die Anwendung des elektronischen Zellzählungsverfahrens auch in dynamischen IVIM-Experimenten eine Weiterentwicklung des PK/PD-Modelles unterstützen, da die neu entwickelte Methode bisher nur in statischen Experimenten eingesetzt wurde. Weiterhin kann die Untersuchung pharmakokinetischer Resistenzmechanismen wie der gesteigerten Exprimierung von Effluxpumpen und Veränderungen der äußeren Membran, die zu verminderten intrazellulären Antibiotikakonzentrationen führen, zum Verständnis der reduzierten LEV-Empfindlichkeit von ST58 beitragen.

Insgesamt hat die vorliegende Arbeit die Grenzen der MHK als Richtschnur bei der Antibiotikatherapie verdeutlicht und neue PK/PD-Parameter vorgeschlagen. Bakterielle Resistenz- und Anpassungsmechanismen wurden quantitativ und mechanistisch charakterisiert. Das entwickelte PK/PD-Modell klärte das komplexe Zusammenspiel verschiedener Prozesse auf, die das bakterielle Wachstums-, Absterbe- und Wiederanwachsverhalten bestimmten. Es ermöglicht die *in silico* Simulation weiterer Szenarien, wie zum Beispiel alternativer LEV-Dosierungsschemata, um letztendlich die rationale Antibiotikadosierung zu unterstützen und somit zur Verhinderung des Auftretens bakterieller Anpassungs- und Resistenzmechanismen beizutragen.

Table of contents

Abbreviations

AA	Amino acid
ABBC	**A**rea **b**etween the growth control and the **b**acterial killing and regrowth **c**urve
AIC	Akaike Information Criterion
ATCC	American Type Culture Collection
ATU	Area of technical uncertainty
AU	Arbitrary units
AUC	**A**rea **u**nder the (drug) concentration-time **c**urve
AUC_{24h}	**A**rea **u**nder the (drug) concentration-time **c**urve over 24 h
bid	Bis in die (twice daily)
BLAST	Basic Local Alignment Search Tool
C	Concentration
C(t) profile	Concentration-time profile
CAL	Calibrator solution(s)
CAMHB	Cation adjusted Mueller Hinton broth
CASY®	Cell counter and analyser system
CFU	Colony forming units
CI	Confidence interval(s)
CL	Clearence
CLCR	Creatinine clearance
C_{LEV}	Levofloxacin concentration(s)
CLSI	Clinical and Laboratory Standards Institute
C_{max}	Maximum concentration in the dosing interval
C_{nom}	Nominal levofloxacin concentration
C_{tot}	Total levofloxacin concentration
C_u	Unbound levofloxacin concentration
CumABBC	**Cum**ulative **a**rea **b**etween the growth control and the **b**acterial killing and regrowth **c**urve
CumAUC	**Cum**ulative **a**rea **u**nder the (LEV) concentration-time **c**urve
$CumAUC_{50}$	**Cum**ulative exposure causing **50**% of the maximum effect
$CumAUC_{reg}$	**Cum**ulative exposure causing bacterial **reg**rowth
$CumAUC_{reg,dynamic}$	**Cum**ulative exposure causing bacterial **reg**rowth in the **dynamic** *in vitro* infection model
$CumAUC_{reg,static}$	**Cum**ulative exposure causing bacterial **reg**rowth in the **static** *in vitro* infection model
CumAUGC	**Cum**ulative **a**rea **u**nder the **g**rowth **c**ontrol curve
df	Degree(s) of freedom
dIVIM	Dynamic *in vitro* infection model
DNA	Deoxyribonucleic acid
dNTP	Deoxynucleotide triphosphates
dOFV	Difference in objective function value
E. coli	*Escherichia coli*
ECDC	European Centre for Disease Prevention and Control
ECOFF	Epidemiological cut-off
EDTA	Ethylenediaminetetraacetic acid
EHEC	Enterohaemorrhagic *Escherichia coli*
ELS	Extended least squares
EMA	European Medicines Agency
E_{max}	Maximum effect
EPEC	Enteropathogenic *Escherichia coli*
ESBL	Extended spectrum beta-lactamases
EUCAST	European Committee on Antimicrobial Susceptibility Testing
ExPec	Extraintestinal *Escherichia coli*

FACS	Fluorescence-activated cell sorting
f_u	Fraction unbound
GC	Growth Control
GOF	Goodness-of-fit
i.v.	intravenous
IC	Initial condition
ID	Individual identifier
IIV	Interindividual variablility
IVIM	*In vitro* infection model(s)
LEV	Levofloxacin
LLOQ	Lower limit of quatification
MBC	Minimum bactericidal concentration
McF	McFarland turbidity standard
MDR	Multidrug resistance
$MgCl_2$	Magnesium chloride
MIC	Minimal Inhibitory Concentration
MLE	Maximum likelihood estimation
MLST	Multi-locus sequence typing
n	Hill factor (steepness of exposure-effect relationship)
NA	Not applicable
NaCl 0.9%	Sodium chloride solution (0.9%)
NCBI	National Center for Biotechnology
NLME	Nonlinear mixed-effects
NMEC	Neonatal meningitis *Escherichia coli*
ODE	Ordinary differential equations
OFV	Objective function value
P. aeruginosa	*Pseudomonas aeruginosa*
PB	Protein binding
PBP	Penicillin binding protein
PCR	Polymerase chain reaction
PD	Pharmacodynamic(s)
PK	Pharmacokinetic(s)
PMQR	Plasmid-mediated quinolone resistance
Primer F	Forward primer
Primer R	Reverse primer
PsN	Pearl speaks NONMEM®
PTA	Probability of target attainment
Q	Intercompartmental clearance
QC	Quality control sample(s)
qd	Quaque die (once daily)
QRDR	Quinolone resistance determining regions
rcf	Relative centrifugal force
RSE	Relative standard error
RUV	Residual unexplained variablility
S. aureus	*Staphylococcus aureus*
S. pneumoniae	*Streptococcus pneumoniae*
SIR	Sampling importance resampling
sIVIM	Static *in vitro* infection model
ST	Sequence type
TA	Toxin-antitoxin
Taq	*Thermus aquaticus*
TBE buffer	Trishydroxymethylaminomethane-boric acid-ethylenediaminetetraacetic acid buffer
Tris	Trishydroxymethylaminomethane
UPEC	uropathogenic *Escherichia coli*
V_c	Central volume of distribution

V_p	Peripheral volume of distribution
VPC	Visual predictive check
W	Weighting factor
WGS	Whole genome sequencing
WSSR	Weighted sum of squared residuals

Symbols

θ	Typical parameter value for population
Θ	Vector of fixed-effects parameters
η	Random-effects parameter (interindividual variability)
ω^2	Variance of random-effects parameter η
Ω	Variance-covariance matrix of η
ε	Random-effects parameter (residual unexplained variability)
σ	Standard deviation
σ^2	Variance of random-effects parameter ε
∑	Variance-covariance matrix of ε
μ	Arithmetic mean of a population

1 Introduction

1.1 Opportunities and risks of antibiotic therapy

Infectious diseases are a global public health challenge, as effective treatment options are threatened by emergence and spread of antimicrobial resistance. Especially in low- and middle income countries, communicable diseases are among the most frequent causes of death, due to insufficient sanitation and hygiene, as well as limited access to vaccines and effective antimicrobials [1,2]. Globally, 700,000 deaths per year are attributed to antimicrobial resistance, which might increase up to 10 million deaths in 2050, unless effective measures are taken [3]. From a broader perspective, diverse areas of society are involved in development and prevention of antimicrobial resistance and hence, overarching initiatives are needed [4]. For that reason, the World Health Organisation released a “Global action plan on antimicrobial resistance”, addressing different fields of activities, such as educational aspects, surveillance and research, economic aspects and prudent use of antimicrobials [2]. Besides misuse and overuse in human medicines, prophylactic and therapeutic use of antimicrobials in livestock farming is particularly alarming, with 60,000 tonnes of antimicrobials used in animals per year [5]. Antimicrobial resistance can arise from genomic mutations, protecting the microorganisms from an antibiotic compound by preventing the interaction between the drug molecule and its target. Spread of microorganisms harbouring resistance mutations is enhanced by selective pressure resulting from overuse of antibiotics and insufficient antibiotic concentrations at target site, e.g. due to inappropriate antibiotic dosing [6,7]. Further, genetic material, such as plasmids, can be transmitted between microorganisms by horizontal gene transfer, i.e. transformation, transduction and conjugation, enabling exchange and spread of genomic resistance mechanisms [4]. Plasmid-mediated quinolone resistance (PMQR) and beta-lactamases are important examples for transferable genomic resistance mechanisms [8-11]. Additionally, microorganisms can display phenotypic adaptation, such as upregulation of the expression of efflux pumps, resulting in decreased intracellular antibiotic concentrations, or formation of persister cells [8,12]. Persister cells are non-growing bacterial cells, showing a transiently reduced susceptibility to antibiotics, which survive antibiotic exposure and can resume growth of a bacterial population [13]. Formation of persister cells can for example be induced by the so-called “SOS response”, as a consequence of DNA damage caused by fluoroquinolones [14,15].

While currently used antimicrobials are losing their efficacy, efforts in research and development of novel antibiotics are limited. Economic incentives to invest in antimicrobial drug development are missing, because of the high probability of emergence of resistance against novel compounds, before the investment paid off, the typical application of antimicrobials for

the treatment of short-term diseases and the restrained use of innovative treatment options as “last resort” to preserve their efficacy [3,16]. Antibiotic resistance in Gram-negative bacteria, such as *Escherichia coli (E. coli)*, is particularly challenging [17]. Hence, Provenzani et al. recently compiled novel antibiotic agents against Gram-negative organisms, approved by the Food and Drug Administration between 2014 and 2019 [18]: They identified 12 novel compounds, mostly belonging to known antibiotic classes and having specific indications. Further, three antibiotics in the clinical pipeline with “novel” mechanisms of action were described, thereof two inhibitors of bacterial topoisomerases with different binding sites than fluoroquinolones. Hence, further political and financial efforts are required to stimulate antibiotic research and development [19]. Differently, preclinical research on antibiotic compounds is diverse and increasingly focusses on innovative strategies and unconventional concepts, such as antibodies against selected pathogens, antivirulence approaches or phages [16]. Besides development of novel antibiotic agents, repurposing approved drugs for new indications or in new formulations is one important strategy to expand treatment options against microorganisms with reduced susceptibility [4,16]. Furthermore, the concept of antibiotic combination therapy gained increasing attention over the last years [20-23]. Colistin and fosfomycin are examples for repurposed antibiotics with promising *in vitro* activity against *Pseudomonas aeruginosa* (*P. aeruginosa)* combined with other antibiotics [24,25]. Moreover, combining established antibiotics with immunostimulatory agents, such as amoxicillin with monophosphoryl lipid A, can enhance antibiotic efficacy [26].

Another important strategy to maintain efficacy of approved antibiotics is to ensure effective antibiotic concentrations at the site of infection, to eradicate the pathogen and prevent emergence and spread of resistance, by optimised antibiotic dosing. A crucial prerequisite for dosing optimisation is a comprehensive understanding of the relationship between the pharmacokinetics (PK) of an antibiotic compound, determined by both characteristics of the patient and properties of the drug, and the pharmacodynamic (PD) effect against the pathogen. Hence, in 2016, the European Medicines Agency (EMA) released a “Guideline on the use of pharmacokinetics and pharmacodynamics in the development of antimicrobial medicinal products”, which summarises requirements for comprehensive PK/PD analysis, based on preclinical and clinical data, from a regulatory perspective [27]. The basic concepts of PK/PD relationships in the field of antibiotic therapy and their application for PK/PD-guided antibiotic dosing will be outlined in the following chapter.

1.2 Pharmacokinetic/pharmacodynamic relationships in antibiotic therapy

1.2.1 PK/PD parameters and indices

The basic idea of PK/PD-guided antibiotic dosing is to link an exposure metric of a drug to an effect metric in a quantitative way, aiming to predict the expected effect resulting from a certain exposure and vice versa to determine the exposure (PK target) needed to reach a desired effect (PD target). Once a PD target is identified and the required exposure is determined, a dosing regimen can be selected to reach the PK target in an individual patient with an acceptable probability [28]. For that purpose, knowledge about the PK of the drug in a relevant patient population is needed to characterise the relationship between an administered dose and the resulting concentration-time (C(t) profile) of the drug. Based on the widely accepted idea that protein binding of antibiotics reduces their activity, as only the unbound, i.e. "free", fraction is active, PK/PD relationships are typically characterised based on *free* drug concentrations (*f*C) [29-33]. PK metrics, which are most commonly applied to characterise PK/PD relationships, are the maximum free concentration in a dosing interval (fC_{max}), the area under the free concentration-time curve over 24 h ($fAUC_{24h}$) and the cumulative percentage of a 24 h period that the *f*C exceeds the minimal inhibitory concentrations (MIC) of the pathogen in question ($fT_{>MIC}$) [33]. These PK metrics are exemplified for an antibiotic, administered as single intravenous (i.v.) infusion, in Figure 1.1. The MIC value is the most widely used metric quantifying the level of susceptibility or resistance of a certain bacterial strain to a specific antibiotic compound. It enables categorisation of bacterial strains in "susceptible", "susceptible, increased exposure" or "resistant" [34]. The replacement of the previous category "intermediate" in 2017 by the new category "susceptible, increased exposure" addressed a lack of clarity in treating infections caused by pathogens categorised as "intermediate" [35]. However, simplifications are needed when representing a complex phenomenon like antibiotic resistance in a single value. The MIC value is defined as "the lowest concentration of an antimicrobial agent that completely inhibits growth of the organism in the tubes or microdilution wells as detected by the unaided eye" [36]. The definition refers to standardised methods, which are applied to determine a MIC value, described by the Clinical and Laboratory Standards Institute (CLSI): the macrodilution ("tube") method and the microdilution method (chapter 2.2.1.2). According to the CLSI guideline, a defined inoculum of a bacterial suspension is exposed to antibiotic concentrations being multiples or fractions of 1 mg/L, prepared as 2-fold dilution series. After 16 -20 h, the lowest antibiotic concentration preventing visible growth (i.e. visible turbidity) is determined as MIC value [36].

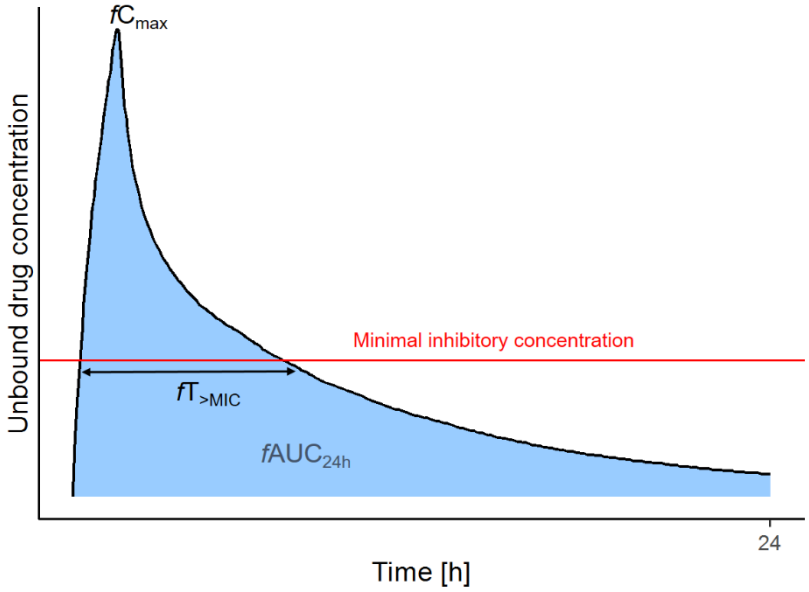

Figure 1.1: Pharmacokinetic metrics, exemplified for a single dose of an antibiotic, administered as 90 min intravenous infusion: maximum free concentration in the dosing interval (fC_{max}), area under the free concentration-time curve over 24 h ($fAUC_{24h}$, blue area) and percentage of a 24 h period that the unbound drug concentration exceeds the minimal inhibitory concentration ($fT_{>MIC}$, arrow and red horizontal line).

PK/PD parameters link a PK metric of an antibiotic compound to the MIC of a pathogen. Most commonly applied PK/PD parameters are the fC_{max}/MIC ratio, the *f*AUC/MIC ratio and the $fT_{>MIC}$ [32,33]. To identify the PK/PD parameter showing the strongest correlation with the antibiotic effect, preclinical *in vitro* or animal studies are performed [28]. An important decision is the measured endpoint, which is finally linked to drug exposure [37]. Commonly, bacterial concentrations in liquid growth medium or bacterial numbers in infected animals are assessed in colony forming units (CFU) and a net static effect, a one- or a two log_{10}–fold decrease in CFU are defined as PD targets [27]. The PK/PD parameter characterising the relationship between exposure and effect best, termed “PK/PD index”, can be identified by relating different PK/PD parameters to the measured PD metric and performing a regression analysis. In this way, the PK/PD relationship can be categorised in either “time-dependent”, with $fT_{>MIC}$ showing the strongest correlation with the effect, or “concentration-dependent”, with fC_{max}/MIC or *f*AUC/MIC predicting the antibiotic effect best [31,32]. Based on the selected PK/PD index, PK/PD target values have been derived, such as 40%-100% $fT_{>MIC}$ for beta-lactam antibiotics [28]. While the PK/PD relationship of beta-lactam antibiotics is typically classified as time-dependent, fluoroquinolones display a concentration-dependent PK/PD relationship [31,38,39]. Mostly, *f*AUC/MIC is identified to be the most appropriate PK/PD index for fluoroquinolones, such as levofloxacin (LEV) [38,40-43]. However, a clear distinction between fC_{max}/MIC and *f*AUC/MIC is not always possible. Preston et al. linked LEV exposure to clinical

outcome parameters of 313 patients receiving LEV therapy for various infections and identified a strong correlation between *f*C_{max}/MIC and *f*AUC/MIC. Here, a *f*C_{max}/MIC of 12.2 was identified as PK/PD target value predicting microbiological eradication and clinical cure best [39]. Once a PK/PD target value is defined, stochastic simulations are leveraged to determine the probability of target attainment (PTA) for a patient population, given the MIC value of the pathogen, a population PK model and a defined dosing regimen [27]. Based on the aggregated knowledge about the PK of a compound, the PK/PD relationship and MIC distributions of relevant pathogens, the European Committee on Antimicrobial Susceptibility Testing (EUCAST) derives clinical breakpoints, discriminating between the three aforesaid categories [27,44]. For LEV against *Enterobacterales,* a MIC ≤ 0.5 mg/L classifies bacterial strains as susceptible and a MIC >1 mg/L as resistant [34], based on a *f*AUC/MIC target of 35.6 "for bacteriostasis", of 67.4 "for 1-$\log_{10}$ reduction", of 140 "for 2-$\log_{10}$ reduction" and a clinical *f*AUC/MIC target of 72, for a standard dosing regimen of 500 mg LEV once daily (quaque die, qd) and a high dosing regimen of 500 mg LEV twice daily (bis in die, bid), administered either i.v. or orally [45]. Differently, the CLSI distinguishes four categories: "susceptible", "susceptible - dose dependent", "intermediate" and "resistant". According to CLSI, an *E. coli* strain displaying a MIC value ≤ 0.5 mg/L is classified as LEV susceptible, a MIC ≥ 2 mg/L classifies an *E. coli* strain as LEV resistant, and a strain with a MIC value of 1 mg/L is categorised as "intermediate". For LEV against *Enterobacteriaceae* "susceptible - dose dependent" is not defined. Different from EUCAST breakpoints, CLSI breakpoints were determined based on a standard LEV dosing regimen of 750 mg qd [46]. However, the present work refers to breakpoints according to EUCAST.

The EMA guideline on the use of PK/PD recommends *in vitro* experiments to describe the PK/PD relationship for various organisms, to assess the effect of multiple C(t) profiles and to study the relationship between drug exposure and emergence of resistance [27]. In so-called "time-kill curve experiments", bacteria are exposed to either static, i.e. constant drug concentrations over time, or to dynamic C(t) profiles. The antibiotic effect is determined by assessing serial bacterial concentrations over time, allowing to characterise the full time-kill trajectory of the bacterial population under antibiotic exposure. At the same time, the bacterial growth curve without antibiotic exposure is assessed, representing disease progression without antibiotic treatment. Bacterial concentrations are displayed on a logarithmic scale over time, characterising the antibiotic effect more comprehensively than the MIC value [47]. Based on time-kill curve experiments, Firsov et al. introduced a PD metric quantitatively exploiting the full bacterial growth-kill trajectory: the **a**rea **b**etween the growth control and the **b**acterial killing and regrowth **c**urve (ABBC), illustrated in Figure 1.2 [48-50].

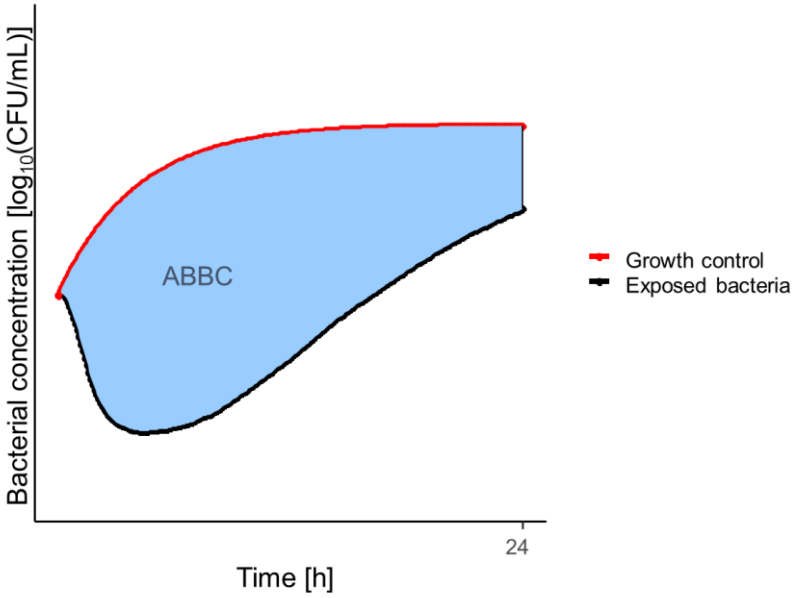

Figure 1.2: Bacterial growth and kill behaviour under antibiotic exposure (black line) and a typical bacterial growth control curve without antibiotic exposure (red line); bacterial concentrations in colony forming units (CFU) per mL on a logarithmic scale against time; blue area: **a**rea **b**etween the growth control and the **b**acterial killing and regrowth **c**urve (ABBC), based on Firsov et al. [48,49,50].

Different *in vitro* infection models (IVIM) to investigate bacterial growth and kill behaviour over time are introduced in the following section.

1.2.2 *In vitro* infection models

Compared to animal models, IVIM provide the advantage that they facilitate systematic and simultaneous assessment of antibiotic exposure, i.e. drug concentrations, and effect, typically bacterial concentrations in CFU/mL, assessed via plate counting assays. Experimental conditions, such as incubation temperature, inoculum concentration or constitution of the growth medium can be controlled to allow for comparison between different bacterial strains, antibiotic C(t) profiles or combinations of different antibiotics [47,51,52]. Furthermore, IVIM are less cost- and resource intensive and provide more flexibility compared to animal models. On the other hand, transferability of results from IVIM experiments to the *in vivo* setting is challenged by the absence of the immune system of the host. However, IVIM can provide valuable insights in exposure-effect relationships, emergence of resistance and allow exploration of different dosing regimens as prerequisite for animal studies and clinical trials [27].

Two main types of IVIM can be distinguished: static IVIM (sIVIM), exposing bacteria to constant drug concentrations, and dynamic IVIM (dIVIM), allowing to mimic antibiotic C(t) profiles.

In **sIVIM** experiments, a defined bacterial inoculum (often 10^6 CFU/mL) is exposed to constant antibiotic concentrations, typically multiples or fractions of the MIC of the exposed bacterial strain. The growth medium is selected according to the requirements of the investigated species. For non-fastidious organisms, Mueller-Hinton broth is usually the medium of choice [36]. Serial samples are drawn over time without replacement of the medium. Hence, the growth medium is not exchanged, limiting bacterial growth without antibiotic exposure by nutrition, space and toxic bacterial metabolites [51]. When stability of the investigated compound under the experimental conditions is not assured, stabilising adjuvants can be used or degradation kinetics of the drug taken into account [21,53,54]. Investigations in sIVIM provide a more comprehensive assessment of the exposure-effect relationship than a single MIC value, because the full bacterial growth-kill trajectory is evaluated. However, static drug concentrations do not reflect *in vivo* conditions, as the PK of the drug is not represented in these *in vitro* models [47].

In **dIVIM experiments**, C(t) profiles resulting from different dosing regimens or routes of administration are mimicked. Given the availability of an appropriate PK model, facilitating *in silico* simulation of C(t) profiles at the site of infection, dIVIM experiments allow to investigate the antibiotic effect resulting from target-site C(t) profiles. Assessment of *in vivo* target-site drug concentrations, e.g. in interstitial space fluid, adipose or muscle tissue, is enabled by the microdialysis technique [47,55-57]. DIVIM can be categorised in diffusion and dilution models. In dilution models, decreasing drug concentrations are obtained by either stepwise or continuous dilution of the growth medium, using peristaltic pumps. In these experimental models, the volume in the culture vessel remains constant and bacterial loss is prevented by membrane filters [47,51,58]. In diffusion models, the driving force of changing drug concentrations is diffusion of drug molecules through a selective permeable membrane, separating two experimental compartments, i.e. culture vessels [59,60]. In the last years, the hollow-fibre technique gained increasing importance [52,61,62]. These advanced diffusion models include cartridges containing numerous hollow fibres, which are inoculated with bacterial suspension. Bacteria are located in the extra-capillary space, outside the hollow fibres, while drug containing medium continuously circulates through the fibres [63]. Various C(t) profiles can be mimicked in the software-controlled system, including multiple dosing over several days [52,61,62].

Data obtained from sIVIM and dIVIM experiments can be utilised to derive PK/PD target values, such as the *f*AUC/MIC ratio for bacteriostasis or a one- or two $\log_{10}$-fold reduction of the bacterial concentrations. Moreover, *in silico* PK/PD modelling can be leveraged to mathematically describe bacterial growth without antibiotic exposure and the antibiotic effect

over time and gain a deeper understanding of the mechanisms driving the observed growth and kill behaviour.

1.2.3 *In silico* PK/PD models

Previously introduced PK/PD parameters relate a single exposure metric, such as fC_{max} or *f*AUC, to the endpoint readout MIC (chapter 1.2.1). Thus, the full antibiotic C(t) profile is reduced to one value either representing a single timepoint of the whole profile (fC_{max}), or the complete profile as a whole (*f*AUC), or a fraction of the profile ($fT_{>MIC}$), while the bacterial time-kill trajectory is not taken into account. PK/PD modelling allows to exploit the full drug C(t) profile and the time course of bacterial concentrations to characterise the exposure-effect relationship over time [64].

PK models are typically developed to characterise the C(t) profile of a drug either in an individual patient or a patient population, based on drug concentrations, determined in plasma or other sampling matrices, the administered dose and route of administration. The complex processes constituting the absorption, distribution, metabolism, and excretion of drug molecules in the body of a patient are represented in a mathematical framework. Here, so-called “compartmental models” are utilised to describe mass transfer of drug molecules in the body, assuming kinetically homogeneous distribution spaces. If first-order kinetics are present or assumed, mass transfer is quantified by first-order rate constants. Based on individual PK parameter estimates, the C(t) profile of a drug in a certain patient can be predicted. Thus, a PK model quantitatively links an administered dose to the resulting C(t) profile [65]. Different approaches have been developed to integrate information on PK in a patient population. The nonlinear mixed-effects (NLME) modelling approach allows to characterise the PK profile of drug for a typical representative of the population and to quantify and explain different levels of variability in the population (chapter 2.4.2) [66]**.** PK models can be applied to *in silico* simulate C(t) profiles resulting from various dosing regimens and routes of administration, e.g. to support antibiotic dosing or to mimic these in C(t) profiles in dIVIM experiments.

In general, **PD models** describe the relationship between drug concentrations and the resulting effects, which can be linear or log-linear, but is mostly characterised by a simple or a sigmodal E_{max} model (Equation 1.1). Here, the concentration-effect relationship is quantified by the maximum effect (E_{max}), the drug concentration required to reach 50% of the maximum effect (EC_{50}), and the Hill factor (γ). E_{max} represents the efficacy of the drug, while the EC_{50} value represents its potency. The Hill factor reflects the steepness of the concentration-effect relationship. In a simple E_{max} model, the Hill factor is fixed to 1 [65,67-69]. The effect can be

represented by measured concentrations of a biomarker, a surrogate marker or a clinical outcome parameter [65,68].

$$E = \frac{E_{max} \cdot C^{\gamma}}{EC_{50}^{\gamma} + C^{\gamma}} \quad (1.1)$$

In the particular case of bacterial growth and killing models, the effect is typically represented by bacterial numbers, assessed in IVIM experiments or animal studies [47]. Different models have been applied to describe the studied biological system “at baseline”, i.e. bacterial growth without antibiotic effect, such as logistic growth models and the Gompertz model [70,71]. Further, the compartmental approach has been introduced to discern bacterial subpopulations, such as susceptible and resistant bacteria, and quantify transformation of bacteria between these “bacterial compartments”. Similar to PK models, first-order rate constants are estimated to quantify processes, such as bacterial growth, death and transition of bacterial cells between subpopulations [64].

Finally, in a **PK/PD model,** a PK model is linked to a PD model, providing a comprehensive description of the dose-exposure-effect relationship. In bacterial growth and kill models, either static or dynamic drug concentrations are related to bacterial numbers over time. The antibiotic effect can be linked to the bacterial death rate constant, accelerating natural death of bacteria, to the bacterial growth rate constant, decelerating bacterial growth, or be implemented as separate killing rate constant [72]. Hence, PK/PD modelling of time-kill curve data quantitatively characterises the exposure-effect relationship over time and can provide mechanistic insights. Once a PK/PD model is developed and its appropriateness and predictive performance is evaluated, the model can be applied to simulate bacterial growth-kill trajectories resulting from various drug concentrations or mimicked dosing regimens.

In the present work, the PD effect of the fluoroquinolone LEV against *E. coli* was assessed in static and dynamic time-kill curve experiments and the exposure-effect relationship was characterised leveraging PK/PD modelling. Hence, the following chapters will introduce the studied antibiotic compound and bacterial organism.

1.3 Characterisation of levofloxacin

1.3.1 Pharmacodynamics of levofloxacin

LEV is the *L*-isomer of the racemic flouoroquinolone ofloxacin and a representative of the third generation of fluoroquinolones (Figure 1.3, [43]). When introduced in the 1980s, the antibiotic class was initially used to treat urinary tract infections, caused by Gram-negative bacteria. Modern fluroquinolones, such as LEV, sparfloxacin and moxifloxacin, display enhanced activity against Gram-positive pathogens [73]. Hence, LEV is indicated for the treatment of a variety of infections, such as pneumonia, acute bacterial exacerbation of chronic bronchitis, complicated urinary tract infections and acute pyelonephritis, as well as skin and soft tissue infections, such as chronic prostatitis [74].

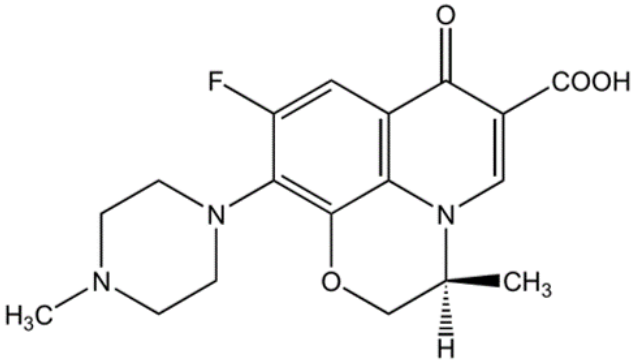

Figure 1.3: Chemical structure of levofloxacin [74].

Fluoroquinolones inhibit bacterial type II topoisomerases, i.e. the gyrase and the topoisomerase IV, which are crucial for bacterial DNA replication [8,9,75]. Bacterial type II topoisomerases are structurally homologous tetramers, consisting of two A subunits (GyrA in gyrase; ParC in Gram-negative topoisomerase IV, GrlA in Gram-positive topoisomerase IV) and two B subunits (GyrB in gyrase; ParE and GrlB in Gram-negative and Gram-positive topoisomerase IV, respectively) [8,76,77]. The A subunits contain the active site tyrosine residue and are encoded on the genes *gyrA*, *parC* and *grlB*, respectively [8], while both A- and B-subunits are involved in fluoroquinolone interaction [75]. In the absence of fluoroquinolones, the bacterial enzymes control DNA topology by inducing and stabilising transient double-strand breaks, enabling unwinding of supercoiled DNA, removing knots and reducing torsional stress [8,9,76]. Fluoroquinolones interact with topoisomerase II-DNA-complexes by constituting Mg^{2+}-mediated ternary complexes, inducing conformational changes in both DNA and enzyme, preventing ligation and thus, inhibiting DNA replication [8,75,76,78]. In Gram-negative organisms, the bacterial gyrase is the primary fluoroquinolone target, while in Gram-positive

bacteria, topoisomerase IV is discussed to be more relevant for the fluoroquinolone effect [8,9,75]. Although distinct physiological roles of gyrase and topoisomerase II have been identified, elevated fluoroquinolone resistance of strains harbouring mutations in both enzymes indicates the ability of type II topoisomerases to mutually compensate for defects [9,78].

Fluoroquinolones have recently gained attention of regulatory authorities due to adverse drug effects, in particular tendinitis and tendon rupture, potentially causing permanent disability [79,80]. Following the recommendations of the Pharmacovigilance Risk Assessment Committee, the EMA released restrictions on fluoroquinolone use in 2018, discouraging fluoroquinolone treatment of mild infections, such as uncomplicated urinary tract or throat infections [80]. In the U.S., the Food and Drug Administration introduced a black box warning for tendinitis and tendon rupture already in 2008. Toxic effects of LEV have been shown *in vitro* and in rats, but the exact mechanism is not elucidated yet. In clinical studies, toxic events were consistently observed in elderly patients, patients with concomitant corticosteroid use, patients with impaired renal function and organ transplant recipients [79]. Thus, for these patient groups, fluoroquinolone use should be generally avoided [80]. Further, fluoroquinolones impaired cartilage and caused arthropathy in juvenile animals. Hence, their use is not recommended in paediatric patients [74]. Prolongation of the electrocardiographic QT_c interval is another severe adverse drug effect of fluoroquinolones, which has been shown to be more pronounced for moxifloxacin compared to LEV [81]. Like for tendon toxicity, a concentration-dependent toxic effect was shown [79,81], highlighting the importance of rational dosing strategies to prevent both, emergence of resistance and toxic effects.

1.3.2 **Pharmacokinetics of levofloxacin**

Currently, the recommended LEV dosing regimen depends on the indication. In Germany, a 500 mg dose is administered either once daily, for the treatment of pyelonephritis or complicated urinary tract infections, or up to twice daily to treat community acquired pneumonia or complicated skin and soft tissue infections. Treatment durations between 7 days and 14 days are recommended for pneumonia, urinary tract infections, pyelonephritis and skin and soft tissue infections, while the recommended treatment duration is 28 days for bacterial prostatitis and up to 8 weeks for inhalational anthrax [82,83]. In the U.S., LEV doses of 750 mg are approved to treat nosocomial and community acquired pneumonia, complicated skin and skin structure infections, complicated urinary tract infections and acute bacterial sinusitis [74].

A linear relationship between the administered LEV dose and the resulting exposure, either in terms of C_{max} or AUC_{24h}, has been shown for a dose range between 50 and 1000 mg [84]. LEV can be administered i.v. and perorally. The oral bioavailability approaches 100% and the

impact of food on absorption is negligible, thus transition between i.v. and oral administration is possible without dosing adjustment [43,84,85]. For i.v. administration, infusion durations of 500 mg in 60 min are recommended [82,83]. After peroral administration, C_{max} in plasma is reached after 1-2 h [74,84,85,86], with C_{max} values ranging between 2.4 mg/L (single dose of 250 mg) and 9.0 mg/L (single dose of 1000 mg) [87]. LEV penetrates well into tissue and body fluids and displays a large volume of distribution of approx. 1.1 L/kg bodyweight [84], i.e. approx. 74 – 112 L [74]. Protein binding (PB) of LEV in plasma is low (approx. 20%-40% [84,85,88]) and independent of plasma concentrations [84]. The primary binding partner is albumin, whereas PB of fluoroquinolones is too low to be affected by hypoalbuminaemia [88]. LEV concentrations in various tissues and body fluids, such as lung tissue and urine, are higher than plasma concentrations [74,84,87,89]. LEV is mainly eliminated via the kidneys, with a fraction excreted unchanged in urine of approx. 87%. Besides glomerular filtration, tubular secretion seems to occur [74]. Moreover, LEV accumulates in urine [87,89,90]. The elimination half-life ranges between 6 and 8 h and hepatic metabolism is negligible. Two metabolites were observed in humans, desmethyl-levofloxacin and levofloxacin-N-oxide, each constituting < 2% of the total administered dose [84]. In agreement with the good tissue distribution and mainly renal elimination, PK of LEV are best described by two-compartemental PK models with first-order elimination [39,42,84,91]. Age, sex and ethnical group or critical illness do not significantly alter LEV PK, but patients with impaired renal function reach significantly higher LEV exposure [42,43,74,84]. Hence, dosing adjustment for patients with impaired renal function according to their creatinine clearance (CLCR) is recommended [74,82].

LEV is indicated for various infections caused by both Gram-positive and Gram-negative bacteria, but also by atypical microorganisms, such as *Chlamydophila pneumoniae* and *Mycoplasma pneumonia* [43,74]. However, this work focussed on LEV effect against *E. coli,* as this pathogen is the most frequent cause of several infections treated with LEV, and fluoroquinolone resistance in *E. coli* is increasingly threatening [17,92].

1.4 *Escherichia coli*

1.4.1 Clinical relevance

E. coli is a representative of the Gram-negative bacterial family of *Enterobacteriaceae* and the most prevalent microorganism of the intestinal flora of humans and warm-blooded animals. The facultative anaerobic rod was first described by the Bavarian paediatrician Theodor Escherich in the 19th century [93]. Besides playing a crucial role for a healthy human microbiome, the facultative pathogenic organism causes severe nosocomial and community acquired infections, such as enteritis, urinary tract infections, septicaemia and neonatal meningitis. Pathogenic *E. coli* strains are classified according to their pathotype, i.e. group of strains belonging to the same species and causing a certain infection [92]. Overall, two main pathogenic *E. coli* types are distinguished: enteric *E. coli* and extraintestinal *E. coli* (ExPec). Important representatives of enteric *E. coli* strains are enteropathogenic *E. coli* (EPEC), primarily causing diarrhoea in children, and enterohaemorrhagic *E. coli* (EHEC), summarising Shiga toxin producing strains, which can cause the haemolytic uremic syndrome, a potentially lethal kidney disease [92,93]. ExPec strains cause infections beyond the intestine, such as uropathogenic *E. coli* (UPEC), being responsible for 80% of urinary tract infections, and neonatal meningitis *E. coli* (NMEC) [92,93]. Antimicrobial resistance of *E. coli* is increasingly alarming, as more than half of the *E. coli* isolates were resistant to at least one of the five antibiotic groups under surveillance of the European Antimicrobial Resistance Surveillance Network (aminopenicillins, carbapenems, third-generation cephalosporins, aminoglycosides and fluoroquinolones) in Europe in 2019, according to the surveillance of antimicrobial resistance report of the European Centre for Disease Prevention and Control (ECDC) [17]. Thus, *E. coli* is the most prevalent pathogen causing antimicrobial-resistant infections, responsible for the largest number of both deaths attributable to infections with resistant pathogens and disability-adjusted life-years [94]. The highest percentage of resistant strains was reported for aminopenicillins (57.1% of all isolates), followed by fluoroquinolones (23.8% of the reported strains) [17].

1.4.2 Growth characteristics and morphology

A prerequisite for *in vitro* investigations of antibiotic effects is a comprehensive understanding of bacterial growth behaviour without antibiotic exposure. The bacterial growth curve, typically assessed by means of plate counting assays, displays bacterial concentrations in CFU/mL on a logarithmic scale over time. Four growth stages can be distinguished: the lag phase, the exponential growth phase, stationary growth and the death phase [95]. Exponential growth of the bacterial population is limited by space, nutrients and potentially toxic bacterial metabolites. In the stationary growth stage, the number of bacterial cells neither decreases nor increases,

which can either be explained by an equilibrium between cell death and division, or by all cells being in a non-dividing state [95]. The stationary stage does not represent a homogenous bacterial population: Bacterial cells may or may not be metabolically active and can resume growth when transferred to fresh growth medium [96]. Moreover, mutants with growth advantages in stationary phase, so-called “GASP mutants”, can occur [95]. The stationary phase is followed by a death phase with declining bacterial concentrations, which can be interrupted by a “post-death” phase, i.e. stagnation of the decline of bacterial concentrations, induced by replicating bacterial subpopulations [95]. The first three stages of the bacterial growth curves can be mathematically described by the Gompertz model, which is applied to characterise various exponential growth processes. In the model, three parameters describe the bacterial growth curve: the tangent in the inflection point, i.e. the maximum growth rate in exponential stage, the x-axis intercept of the tangent, i.e. the lag time, and the asymptote, i.e. the maximum bacterial number in the stationary stage [70,71].

During the different growth stages, alterations in bacterial morphology can be observed. *E. coli* is typically described as cylindrical tube with hemispherical ends [97]. However, in the stationary growth stage, bacterial cells decrease in size and attain an almost spherical shape [96], while fast-growing cells are increased in size [97,98]. *E. coli* cells in the stationary stage have a length of approx. 1.6 µm, which can increase up to 3.9 µm for rapidly growing cells. Investigations of growth and size of *E. coli* in different media showed an association between growth rates and cell volume. The cell width was independent of the growth stage or medium, 1.26 ± 0.16 µm [99]. Bacterial populations with increased cell length at the same time display a large standard deviation around the mean cell length [99,100]. *E. coli* cells harbouring mutations affecting the regulation of cell elongation and division can become very long, up to 750 µm [98].

Cell elongation and division of *E. coli* is controlled by penicillin binding protein 2 (PBP2) and PBP3, respectively. These proteins with transpeptidase activity incorporate disaccharide pentapeptide units into the murein layer, the central layer of the Gram-negative exoskeleton. Along with the cytoplasmic membrane and the outer membrane, the peptidoglycan layer retains shape of the bacterial cell and plays a crucial role for cell elongation [97,98]. The bacterial exoskeleton is a highly dynamic structure, containing a variety of hydrolytic enzymes, binding proteins and chemoreceptors in the periplasmatic space, which constitutes 20%-40% of a Gram-negative bacterium [101]. Surface layers, attached on the outer membrane, contribute to maintain rigidity of the cell envelope and regulate influx and efflux of macromolecules. *E. coli* cells are devoid of a membranous cytoskeleton, i.e. microfilaments or microtubules, but microcompartments in the cytoplasm are built by multienzyme complexes, the nucleoid and other cytoskeletal elements [101].

Reduced susceptibility to antibiotics can be caused by alterations of cells morphology, such as decreased permeability of the outer membrane, reducing net drug uptake and thereby decreasing intracellular antibiotic concentrations (PK resistance). Furthermore, alterations of the antibiotic targets can compromise the antibiotic effect by disrupting the interaction between the antibiotic and its target (PD resistance). Both types of resistance can be enabled by genomic resistance mechanisms, which are introduced with regard to fluoroquinolone resistance in the following chapter.

1.5 Genomic fluoroquinolone resistance mechanisms

Genomic resistance mechanisms can be heritable, such as target-site mutations and chromosomally encoded efflux pumps, or transmitted via horizontal gene transfer of plasmids or transposons [78,102]. Both inherited and acquired resistance mechanisms can confer resistance to multiple antibiotic classes, so-called multidrug resistance (MDR), or to a specific antibiotic or antibiotic class (Figure 1.4).

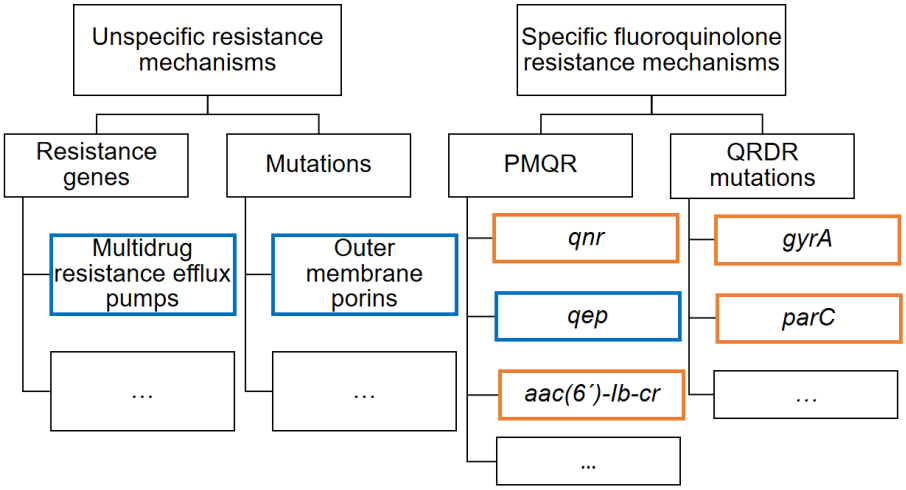

Figure 1.4: Schematic overview of genomic resistance mechanisms with relevance for fluoroquinolone resistance; blue frames indicate pharmacokinetic resistance mechanisms, orange frames indicate pharmacodynamic resistance mechanisms; PMQR: plasmid-mediated quinolone resistance, *qnr:* quinolone resistance gene, *qep:* quinolone efflux pump, *aac(6´)-Ib-cr:* modified aminoglycoside acetyltransferase; QRDR: quinolone resistance determining regions, *gyrA* subunit A of gyrase encoding gene, *parC*: subunit A of topoisomerase IV encoding gene.

Efflux pumps are an important example for **unspecific** antibiotic resistance and can be chromosomally encoded and plasmid-mediated [8]. Incorporated in the bacterial envelope of Gram-positive and Gram-negative bacteria, they enable active efflux of drug molecules and thereby decrease intracellular antibiotic concentrations (PK resistance). MDR efflux pumps propagate resistance against various antibiotics, often in synergy with reduced drug uptake due to outer membrane alterations [9,103]. In Gram-negative bacteria, the lipopolysaccharide layer in the outer membrane of the cell envelope represents a diffusion barrier for hydrophilic antibiotics (Figure 1.5). Drug uptake is realised by chromosomally encoded porin diffusion channels in the outer membrane. Reduced expression or mutations of *omp* genes encoding for these outer membrane porins decrease intracellular drug concentrations and thus, confer PK resistance. Similarly, structural modifications of the outer membrane of Gram-negatives can reduce uptake of antibiotics [103].

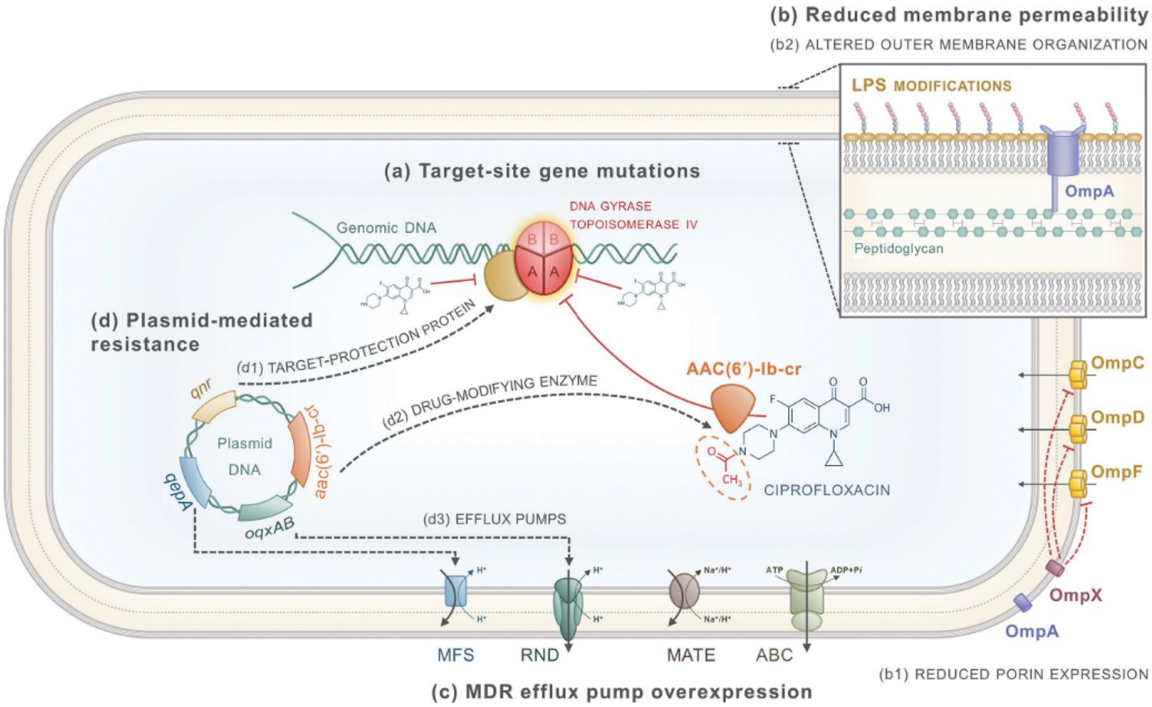

Figure 1.5: Fluoroquinolone resistance mechanisms [103]. Pharmacodynamic (PD) resistance: (a) mutations in quinolone resistance determining regions of the genes encoding for type II topoisomerases. Pharmacokinetic (PK) resistance: (b) Reduced drug uptake due to (b1) reduced expression of porins, (b2) alterations in the lipopolysaccharide (LPS) lager in the outer membrane, (c) increased drug efflux due to increased expression of multidrug resistance (MDR) efflux pumps. (d) Plasmids can confer PK and PD resistance. PD: (d1) *qnr*: target-protecting proteins; (d2) *aac(6´)-Ib-cr:* modification of certain fluoroquinoloes by N-acetylation; PK: (d3) *qepA* and *oqxAB:* plasmid-mediated efflux pumps. Abbreviations: Omp: outer membrane porin, MFS: major facilitator superfamiliy, RND: resistance-nodulation-division, MATE: multiple antibiotic and toxin extrusion, ABC: ATP- binding cassette.

Specific resistance mechanisms, e.g. to beta-lactam antibiotics or fluoroquinolones, can be transmitted via horizontal gene transfer of resistance plasmids. Multiple genes were identified conferring resistance to beta-lactam antibiotics, e.g. encoding for drug degrading enzymes, such as beta-lactamases or carbapenemases. The spread of extended spectrum beta-lactamases (ESBL), encoded on $bla_{CTX\text{-}M}$ genes, is particularly concerning [104]. Three different types of plasmid-mediated fluoroquinolone resistance genes are described: "*qnr"* ("quinolone resistance") genes, quinolone-specific efflux pumps ("*qep"* and *"oqxAB")* and the modified aminoglycoside acetyltransferase *aac(6´)-Ib-cr* [10]. The first *qnr* plasmid was isolated from a clinical *Klebsiella pneumoniae* strain in 1998 [105]. Today, various *qnr* genes have been identified, which encode for structural DNA mimics, competing with fluoroquinolones for binding to bacterial topoisomerases and causing moderately elevated MIC values [8,10,78,106,107]. Similarly, chromosomally or plasmid-mediated efflux pumps cause reduced fluoroquinolone susceptibility, typically below the clinical resistance breakpoint of a

MIC value > 1 mg/L [10,34,103,108]. Furthermore, the acetyltransferase AAC(6´)-Ib-cr inactivates fluoroquinolones with unsubstituted amino nitrogen on the piperazinyl ring, such as ciprofloxacin, but not LEV due to its methyl group in the respective position (Figure 1.3), by N-acetylation [8,78].

Mutations in target enzyme encoding genes, particularly *gyrA* and *parC*, reduce fluoroquinolone susceptibility to a larger extent than PMQR. Mutations result in single amino acid (AA) substitutions, reducing the affinity of fluoroquinolones to the topoisomerase-DNA complex (PD resistance) [78,103]. As the B subunits of the tetrameric enzymes are involved in fluoroquinolone binding, mutations in *gyrB* and *parE*, respectively *grlB,* can also affect susceptibility, but are less frequent than *gyrA* and *parC* mutations [103]. More precisely, alterations near the active site tyrosine residues (position 122 in GyrA and position 120 in ParC) are relevant for fluoroquinolone resistance. Thus, the respective loci were named “quinolone resistance determining regions (QRDR)”. In GyrA, AA residues 67 – 106, and in ParC, AA residues 63 – 102 constitute the QRDR [9,78]. Single mutations in one of the target enzymes reduce susceptibility to a lesser extent than mutations in both target enzymes. This can be explained by fluoroquinolones binding to the secondary target, i.e. to topoisomerase IV, with a higher affinity in case of mutations in the primary target, i.e. in gyrase for Gram-negative bacterial species [78,106]. Multiple QRDR mutations are associated with highly elevated MIC values [9,10,106,109-111]. Most frequent *gyrA* mutations in *E. coli* cause the substitution of a serine residue in position 83 (Ser83), aspartic acid in position 87 (Asp87) and glycine in position 81 (Gly81), while frequent *parC* mutation result in serine substitution in position 80 (Ser80) and glutamic acid in position 84 (Glu84) [8,78,106,109,111]. In general, different fluoroquinolone resistance mechanisms, such as QRDR mutations and *qnr* plasmids, lead to higher MIC values compared to one single mechanism, when coinciding [103].

Knowledge about the genomic background of antibiotic resistance has rapidly increased since whole genome sequencing (WGS) is broadly available. However, reliable prediction of phenotypic resistance from the bacterial genome is not established yet, as a EUCAST report pointed out in 2017 [112]. Bacterial growth under antibiotic exposure is determined by a complex interplay between genomic properties and phenotypic mechanisms, e.g. efflux pump expression in phenotypically adapted persister cells [113]. Thus, clinical implications of sequencing data are still lacking and clinical decision making relies on phenotypic susceptibility testing, comprising diverse genomic and phenotypic mechanisms in the MIC value.

1.6 Bacterial adaptation to antibiotic stress

Antibiotic resistance either pharmacokinetically or pharmacodynamically prevents the drug molecule from binding to its target and hence, resistant bacteria can survive and replicate under antibiotic exposure. Apart from that, bacterial adaptation mechanisms to antibiotic stress, particularly persistence, have gained increasing attention the last years, as they contribute to failure of antibiotic therapy and support emergence of resistance [114,115]. Different from bacteria harbouring genomic resistance mechanisms, persisters are genetically identical to susceptible bacteria. Thus, persistence is a non-heritable, phenotypic, and transient phenomenon [14,116,117]. Persister cells survive antibiotic exposure and can resume growth and give rise to a new bacterial populations in more favourable conditions, e.g. when being transferred to fresh medium [114]. Consequently, persister cells can neither be distinguished from their susceptible kin by genome sequencing, nor does their presence increase the MIC value, as an elevated MIC value indicates the ability of a bacterial population to replicate in presence of an antibiotic [15]. Persister cells have been termed “dormant” cells, as they have been thought to be non-dividing and metabolically inactive, escaping antibiotic action by not expressing antibiotic targets, such as topoisomereases or PBPs [12,14,15,116,118]. However, the term “dormant” is discussed critically, since transformation into the persister state has been elucidated as active stress response mechanism [14,113,114,119]. Further, it has been shown that persister cells do replicate, with a significantly lower growth rate compared to non-persister cells [118,120]. In 2018, persistence was defined and discriminated from phenomena like tolerance and heteroresistance in a consensus statement, developed during a workshop on bacterial resistance and antimicrobial therapy of the European Molecular Biology Organisation [13]. The authors point out that “persistence” refers to a subset of a bacterial population, which is killed by antibiotics with a lower killing rate compared to the susceptible population. Hence, persisters can survive antibiotic exposure, resulting in a biphasic killing curve for the total bacterial population. Bacterial populations arisen from persister subpopulations do not display elevated MIC values. Differently, “heteroresistance” refers to a bacterial subpopulation transiently showing a higher MIC value, whereas “tolerance” indicates that the complete bacterial population survives antibiotic exposure without harbouring resistance mechanisms or displaying an elevated MIC value [13]. According to the origination of persisters, the authors distinguish between “spontaneous persistence” and “triggered persistence”. Balaban et al. first described spontaneous, i.e. stochastic, formation of persister cells prior to antibiotic exposure [120]. In drug-unexposed bacterial populations, persister formation depends on the growth stage, being very low in the lag- and early exponential stage (one in 10^4 to one in 10^6 cells), and increasing considerably in the mid-exponential and stationary phase, up to 1% of the total population [12,14,116,121]. On the other hand, persister formation can be triggered by environmental

conditions, such as starvation, heat, hyperosmotic, acid, oxidative and antibiotic stress [114]. Thus, persister formation is a survival strategy to preserve the bacterial genome under acute stress conditions, comparable to sporulation [122].

The molecular mechanisms controlling persister formation and back-transformation to regular cells have gained increasing interest, as involved regulatory proteins might represent promising novel drug targets to maintain efficacy of antibiotic therapy [123]. The first known regulatory protein involved in persister formation was HipA, encoded by the *hipA* gene, as *E. coli hipA7* mutants ("high persister mutants") showed three orders of magnitude elevated persister fractions compared to an *E. coli* wild type strain [116,120,121]. Keren et al. proposed that besides basic expression of persister proteins, stochastic fluctuation of these proteins in a genetically homogenous bacterial population might control persister formation, depending, among other factors, on the density of the population [12,116,121]. Mechanistically, HipA is a typical representative of a toxin protein, being part of a toxin-antitoxin (TA) module. Toxins in TA modules inhibit a basic bacterial cell function and can be inactivated by complex formation with an antitoxin [114,121]. In case of the *hipBA* module, upregulation of the stable toxin HipA causes arrest of cell division and induces persister formation. The degradable antitoxin HipB is a transcriptional regulator of the *hipBA* operon and represses persister formation [15,114,116,121]. While *hipA* was the first described persister gene, a variety of TA modules involved in regulation of persistence are known today, such as *mazEF* [100] or *recA* and *lexA.* LexA represses the so-called SOS response, while RecA supports cleavage of LexA, inducing persister formation as response to DNA damage. The latter mechanism is especially relevant for persister formation under fluoroquinolone exposure, as these antibiotics induce double strand breaks in the bacterial DNA and thereby trigger SOS response [14,115,123,124]. However, deletion of one of the known persistence regulating proteins does not prevent occurrence of persistence, indicating that different mechanisms regulating persistence can complement each other [114]. Morphological alterations of bacterial cells performing SOS response have been observed and described as "filamentation" [98,100,122-124]. Persister cells continue to grow in length, while cell division is dramatically reduced, resulting in cells with multiple nuclei and considerably increased cell length, up to > 100 µm [98,100,122].

Another phenotypic survival strategy of bacteria, which is often related to persistence, is biofilm formation [12,13,114,125]. Biofilm formation is often associated with indwelling devices, such as catheters or implants [12,114]. Here, bacteria produce a polysaccharide matrix, which protects an antibiotic susceptible bacterial population from the immune system of the host. Susceptible bacteria in a biofilm can be targeted by antibiotic therapy. Different from the planktonic lifestyle, surviving persisters in biofilms are not reached by immune cells and can

therefore resume growth and constitute a new bacterial population, causing recurrent and chronic infections.

Various experimental approaches to investigate persister formation have been developed. On a population level, typically bacterial mutants with increased persister formation are investigated in time-kill curve experiments [14]. Gene expression of regulatory proteins can be assessed by quantitative real time polymerase chain reaction (PCR) [123], and filamentation can be observed applying fluorescence light microscopy or time lapse microscopy [100,113,124]. In addition to cell size, cell viability can be investigated applying fluorescence-activated cell sorting (FACS) [119,124]. On an individual cell level, microfluidic systems have been utilised to observe phenotypic alterations of bacterial cells under antibiotic exposure [120,124].

As interest in persistence has sharply increased in the last years and various *in vitro* approaches have been developed to assess persistence, the authors of the aforementioned consensus statement recommend standardised experimental conditions to assess spontaneous and triggered persistence [13]. In particular, drug-induced persistence should be investigated in bacterial populations in the stationary growth stage, and observation of single cells is recommended. The minimum bactericidal concentration (MBC) can be determined to distinguish between growth inhibition under static exposure to antibiotic concentrations of the MIC and killing at higher concentrations, at the MBC. Antibiotic-induced persistence is associated with higher MBC values, when persister formation is induced under antibiotic concentrations of the MIC. Thus, the MIC does not discriminate persister cells and growing cells, but the MBC is elevated for persisting bacteria [13].

1.7 Objectives

Attainment of adequate antibiotic exposure at target site is crucial to prevent emergence and spread of antibiotic resistance and can be realised by optimised antibiotic dosing. For that purpose, a comprehensive understanding of the exposure-effect relationship is required and pursued in preclinical *in vitro* studies. Here, IVIM are applied to derive PK/PD target values, which are typically based on the MIC value. Although severe limitations of the MIC are well known [47,126,127], appropriate alternatives are currently lacking. To quantify the exposure-effect relationship more adequately, a mechanistic understanding of the underlying processes is required. Knowledge about genomic resistance mechanisms has substantially expanded [112] and bacterial adaptation, such as persister formation, has gained increasing attention in the last years [13]. However, the interplay between genomic resistance, phenotypic adaptation and the PK/PD relationship remains elusive. Hence, the aim of the present thesis was to build a bridge between antibiotic resistance, bacterial adaptation and comprehensive PK/PD analysis to support rational antibiotic dosing. On the grounds of the clinical relevance of *E. coli* infections and fluoroquinolone resistant *E. coli* strains [17], LEV was chosen as a model compound and its effect against three resistant clinical *E. coli* isolates was investigated, pursuing the following concrete objectives:

- Assessment of the growth and kill behaviour of *E. coli* under LEV exposure
  - Assessment of the growth, kill and regrowth behaviour of *E. coli* under exposure to various static LEV concentrations in sIVIM experiments
  - Mimicking of clinically relevant LEV C(t) profiles, resulting from a 750 mg, 90 min i.v. infusion in plasma in dIVIM experiments
  - Assessment of the growth, kill and regrowth behaviour of *E. coli* under exposure to the mimicked LEV C(t) profiles

- Assessment of resistance and adaptation mechanisms
  - Establishment of a PCR-, electrophoresis- and Sanger sequencing-based approach to determine genomic fluoroquinolone resistance mechanisms
  - Determination of genomic resistance mechanisms of three clinical *E. coli* isolates by the established approach
  - Development of an electronic cell counting-based method to quantify persister formation of *E. coli* under LEV exposure
  - Assessment of persister formation of three clinical *E. coli* isolates under LEV exposure over time

- Characterisation of the exposure-effect relationship by informative PK/PD metrics
  - Identification of meaningful exposure and effect metrics based on static and dynamic time-kill curve investigations to characterise the exposure-effect relationship
  - Application of the identified exposure and effect metrics to quantitatively discriminate growth and kill behaviour of three *E. coli* isolates in static and dynamic IVIM experiments
  - Development of informative PK/PD parameters leveraging PK/PD modelling

- Characterisation of the growth, kill and regrowth behaviour of *E. coli* under LEV exposure leveraging NLME modelling

  - Identification of the relevant processes underlying the observed growth, kill and regrowth behaviour
  - Identification and quantification of variability between experimental replicates
  - Quantification of the impact of the *E. coli* strain and exposure pattern (static or dynamic LEV exposure)
  - Exploration of the identified processes for different strains and exposure patterns using stochastic simulations.

2 Materials and methods

2.1 Materials

2.1.1 Chemicals and growth media

Acetic acid-acetate buffer, pH 4.0	
Acetic acid (glacial) LOT: K46507763511	Merck, Darmstadt, Germany
Sodium acetate 0.1 M LOT: 3652564	Merck, Darmstadt, Germany
Agarose NA, specially purified for gel electrophoresis of nucleic acids LOT: 241332	Pharmacia Biotech AB, Uppsala, Sweden
Bacillol® AF, various LOTs	Hartmann, Heidenheim, Germany
Calcium chloride dihydrate LOT: 233199810	Carl Roth GmbH, Karlsruhe, Germany
Casein hydrolysate, bacteriological LOT: 187239333	Carl Roth GmbH, Karlsruhe, Germany
CASY® clean various LOTs	Omni Life Science GmbH, Bremen, Germany
CASY® ton various LOTs	Omni Life Science GmbH, Bremen, Germany
Columbia agar (base), various LOTs	Carl Roth GmbH, Karlsruhe, Germany
DensiCheck™ calibration standards: McF 3.11; LOT: 1001589170 McF 3.02; LOT: 837532901	BioMérieux Inc, Durham, USA
dNTP-Mix (dATP, dCTP, dGTP, dTTP) LOT: 101.546	GeneOn GmbH, Ludwigshafen, Germany
Dream *Taq* DNA Polymerase (5 U/µL) LOT: 00525904	Thermo Fisher Scientific, Schwerte, Germany
Dream *Taq* Green Buffer (20 mM $MgCl_2$) LOT: 00470531	Thermo Fisher Scientific, Schwerte, Germany
Ethanol (> 96%)	Berkel AHK Alkoholhandel, Berlin
Levofloxacin ≥ 97.5% various LOTs	Sigma-Aldrich, St. Louis, Missouri, USA
Lysozyme (50 mg/mL), LOT: 18A2656153	VWR International, Radnor, PA, USA
Magnesium chloride hexahydrate LOT: 293198927	Carl Roth GmbH, Karlsruhe, Germany
Milli-Q® water, purified by Milli-Q Plus®	Millipore Corporation, Eschborn, Germany
Mueller-Hinton broth, unadjusted cation content various LOTs	Oxoid Deutschland GmbH, Wesel, Germany

NoLimits 100 bp DNA fragment LOT: 00547651	Thermo Fisher Scientific, Schwerte, Germany
Nucleic acid extraction kit GF-1	Vivantis technologies, Shah Alam, Malaysia
GF-1 columns and collection tubes, LOT: 12384C-01	
Resuspension Buffer 1 (Buffer R1), LOT: 5233-01	
Resuspension Buffer 2 (Buffer R2), LOT: 5223-02	
Bacterial Genomic Binding Buffer (Buffer BG)	
Wash Buffer (concentrate), LOT: 31970	
Elution Buffer, LOT: 41210	

Primer

gyrA, primer Forward (F) TACACCGGTCAACATTGAG	Thermo Fisher Scientific, Schwerte, Germany
gyrA, primer Revers (R) TTAATGATTGCCGCCGTCGG	
parC, primer F ATGAGCGATATGGCAGAGCGC	
parC, primer R GTGGTGCCGTTAAGCAAA	
qnrA, primer F ATTTCTCACGCCAGGATTTG	
qnrA, primer R GATCGGCAAAGGTTAGGTCA	
qnrB, primer F GATCGTGAAAGCCAGAAAGG	
qnrB, primer R ACGATGCCTGGTAGTTGTCC	
qnrS, primer F ACGACATTCGTCAACTGCAA	
qnrS, primer R AAATTGGCACCCTGTAGGC	
Proteinase K from *Tritirachium album* LOT: SLBQ1035V	Sigma-Aldrich, St. Louis, Missouri, USA
Ringer´s solution LOT: 181767652	B. Braun, Meldungen, Germany

Sodium chloride LOT: 211096	ChemPur, Karlsruhe, Germany
Sodium hypochloride LOT: 454221680	Carl Roth GmbH, Karlsruhe, Germany
TBE Buffer, pH 8.0	
Trishydroxymethylaminomethane (TRIS) hydrochloride, LOT:R8550	ICN Biomedicals, Ohio
Boric acid	Laborchemie Apolda, Apolda, Germany
Ethylenediamine tetraacetic acid (EDTA) disodium salt dihydrate ≥99%, LOT: 470164797	Carl Roth, Karlsruhe, Germany
TE Buffer, pH 8.0	
TRIS hydrochloride, disodium salt dihydrate ≥99%, LOT: 470164797	ICN Biomedicals, Ohio
Ethylenediamine tetraacetic acid (EDTA)	Carl Roth, Karlsruhe, Germany
Sodium hydroxide pellets; LOT: C216998	Merck, Darmstadt, Germany

2.1.2 **Preparation of solutions and growth media**

2.1.2.1 Preparation of sodium chloride solution (0.9%)

Sodium chloride solution, containing 0.9 g NaCl in 100 mL Milli-Q® water was prepared, autoclaved for 15 min at 121°C and 2 bar and used for diluting bacterial samples, taken from the IVIM.

2.1.2.2 Preparation of levofloxacin stock solution

LEV stock solution was prepared according to the CLSI guideline [36]. Potency of the respective batch, determined by the manufacturer according Equation 2.1, was accounted for as given in Equation 2.2. The needed volume of Milli-Q® water to obtain a LEV stock solution of 1000 mg/L or 2000 mg/L, respectively, was calculated accordingly. Aliquots of 1 mL were dispensed in 1.5 mL Safe-Lock tubes and stored at -80°C.

$$Potency = assay\ purity\ \cdot (1 - water\ content) \tag{2.1}$$

$$Volume\ [mL]\ = \frac{weight\ [mg] \cdot potency\ [\frac{\mu g}{mg}]}{concentration\ [\frac{\mu g}{mL}]} \tag{2.2}$$

2.1.2.3 Preparation of acetic acid-acetate buffer (pH 4.0)

LEV quantification was carried out in acetic acid-acetate buffer, which was prepared by dissolving 922.9 mg sodium acetate in 18.0 mL Milli-Q® water and adding 3.0 mL glacial acetic acid. The buffer was adjusted to a pH value between 4.0 and 4.5 using a pH meter.

2.1.2.4 Preparation of TRIS - boric acid - EDTA (TBE) buffer (pH 8.0)

A 10-fold concentrated buffer stock solution was prepared for agarose gel electrophoresis by weighing 107.8 g TRIS-HCl (890 mM) and 55.0 g boric acid (890 mM) and adding 40.0 mL of an EDTA solution (7.45 g in 40 mL, 500 mM). Milli-Q® water was added to reach a total volume of 1.0 L and the pH value was adjusted to 8.0 with 0.1 M NaOH or boric acid using a pH meter. The final 1-fold concentrated electrophoreses buffer was obtained by 1:10 dilution of the buffer stock solution with Milli-Q® water.

2.1.2.5 Preparation of TRIS-EDTA (TE) buffer (pH 8.0)

For reconstitution of lyophilised primers, used for PCR experiments and Sanger sequencing, TE buffer was prepared by weighing 0.038 g EDTA and 0.121 g Tris-HCl in a volumetric flask and adding 100.0 mL Milli-Q® water. The pH value was adjusted to 8.0 using a pH meter.

2.1.2.6 Growth medium preparation and plate casting

For all IVIM model experiments, cation adjusted Mueller-Hinton broth (CAMHB) was used as bacterial growth medium, which was prepared by dissolving 2.1 g dried powder Mueller-Hinton broth in 100.0 mL Milli-Q® water [128]. Cation content was adjusted by adding the needed volume of a 10 mg/mL Ca^{2+} solution and a 10 mg/mL Mg^{2+} solution, to obtain the desired cation content of 25 mg/L Ca^{2+} and 12 g mg/L Mg^{2+}, respectively, as recommended by the CLSI [36]. Next, the solution was autoclaved for 15 min at 121°C and 2 bar, according to the instructions of the manufacturer [129].

Columbia agar plates were used for preparation of bacterial overnight cultures and for bacteria quantification by plate counting during IVIM experiments. For preparation, 42.5 g Columbia agar powder medium was dissolved in 1 L Milli-Q® water by heating until boiling while stirring, until a clear solution was obtained. After autoclaving the liquid medium for 15 min at 121 C and 2 bar, it was poured into sterile petri dishes up to a filling height of of 4 ± 0.5 mm [130] and allowed to solidify under sterile conditions. For sterility control, 2 agar plates per 1 L medium were incubated at 37°C. Only batches without visible bacterial growth after 24 h were accepted.

2.1.3 **Consumables**

Cannulas (various LOTs) BD Microlance™3, 30 mm Sterican 0.80 x 120 mm	Becton Dickinson, Madrid, Spain B. Braun, Melsungen, Germany
CASY® cups	Omni Life Science GmbH, Bremen, Germany
Cellulose acetate syringe filters (0.2 µm, sterile), various LOTs	VWR International, Pennsylvania, USA
Cellulose nitrate filters (0.45 µm, sterile) various LOTs	Sartorius Stedim Biotech GmbH, Göttingen, Germany
Centrifuge tubes with printed graduation and flat caps, 15 mL, LOT: 429CB	VWR International, Pennsylvania, USA
Mµlti® SafeSealTubes, natural (1.5 mL) LOT: 31025020	Carl Roth GmbH, Karlsruhe, Germany
Micro tubes (2 mL), LOT: 72.608	Sarsredt, Nürnbrecht, Germany
Petri dishes polystyrene, Ø 90 mm various LOTs	Waldeck, Münster, Germany
Pipet tips various LOTs epT.I.P.S® Standard/Bulk 0.5 – 20 µL epT.I.P.S® Standard/Bulk 2 – 200 µL epT.I.P.S® Standard/Bulk 100 – 5000 µL	Eppendorf, Hamburg, Germany
PS tubes 14 mL, sterile LOT: E150234K	Greiner Bio-One GmbH, Frickenhausen, Germany
Roti®-Store cryo vials LOT: 185228984	Carl Roth GmbH, Karlsruhe, Germany
Safe-Lock tubes (0.5 mL, 1.5 mL) various LOTs	Eppendorf, Hamburg, Germany
Syringes, various volumes and LOTs	B. Braun, Melsungen, Germany
Tissue culture flasks 25 cm^2 (screw cap with venting position, sterile) various LOTs	TPP Techno Plastic Products, Trasadingen, Switzerland
Tissue culture plates (48 well, sterile) various LOTs	VWR International, Radnor, PA, USA
Ultrafiltration units (cut-off 30 kDa, modified polyethersulfone membrane) various LOTs	VWR International, Radnor, PA, USA
Wellplate (96 wells, transparent, flat bottom)	Marienfeld-Superior, Lauda Königshofen, Germany

2.1.4 **Laboratory devices and equipment**

Analytical balance Mettler AT250	Mettler Instruments, Greifensee, Switzerland
Analytical balance, BP221S	Sartorius AG, Göttingen, Germany
Autoclave, Kronos B23	Newmed, Quattro Castella, Italy
Autoclave, Tuttnauer 2540EL	Tuttnauer, Jerusalem, Israel
Balance MC1	Sartorius AG, Göttingen, Germany
Cell counter and analyser system CASY® TTT; SN: TTT2SA2757	Omni Life Science GmbH, Bremen, Germany
Centrifuge Heraus Pico 17	Thermo Fisher, Osterode, Germany
Digital pH-Meter, pH meter Metrohm (pH range 0 - 13)	Knick Elektronische Messgeräte, Berlin, Germany
Dispenser Ceramus® 2.0 - 10. 0 mL	Hirschmann Laborgeräte GmbH & Co. KG Eberstadt, Germany
Duran® glass bottles (100 mL, 500 mL, 1000 mL)	Schott AG, Mainz, Germany
Dynamic *in vitro* infection model including 3 culture vessels	Constructed by J. Michaels and D. Reese Martin Luther Universitaet Halle-Wittenberg
3-stop tube, Tygon® SI silicone (Ø=1.3 mm, 0.9 mm wall)	Ismatec, Wertheim, Germany
BOLA multiple distributors for bottles, Teflon®	Bohlender GmbH, Gruensfeld, Germany
BOLA screw caps, closed, red, GL 14	Bohlender GmbH, Gruensfeld, Germany
BOLA screw caps, with aperture, red, GL 14	Bohlender GmbH, Gruensfeld, Germany
Connectors, barbed, PP	Ismatec, Wertheim, Germany
GL screw joint system GL 14 for tubes with Ø=0.8 mm	Bohlender GmbH, Gruensfeld, Germany
GL screw joint system GL 14 for tubes with Ø=1.6 mm	Bohlender GmbH, Gruensfeld, Germany
Perforated strainer, Teflon®-coated, GV 050/1/03	Whatman GmbH, Dassel, Germany
Peristaltic pump, MCP process	Ismatec, Wertheim, Germany
Silicon tube, Ø=1.3 mm, 0.90 mm wall	Ismatec, Wertheim, Germany
Teflon® tube, 0.8 x 1.6 mm, Ø=0.40 mm	Schuett24, Goettingen, Germany
Electrophoresis chamber CRVG-SYS	Carl Roth GmbH, Karlsruhe, Germany
Electrophoresis power supply ST 606 T	Gibco-BRL, Carlsbad, USA
Incubator	Heraeus, Hanau, Germany
Inoculation loop sterilizer, Steri Max	WLD-Tec, Göttingen, Germany
Inoculation loops	Carl Roth, Karlsruhe, Germany

Laboratory glass equipment Volumetric flasks (100 mL, 1000 mL) Measuring cylinders (100 mL, 1000 mL) Beaker glasses Funnels	VWR Internatuional GmbH, Darmstadt, Germany
Laminar airflow work bench HB 2448S	Heraeus, Hanau, Germany
Laminar airflow work bench LB-48-C	Heraeus, Hanau, Germany
Laminar airflow work bench safemate 1.8	Euroclone, Pero, Italy
Magnetic stirrer RCT basic	IKA Labortechnik GmbH, Staufen im Breisgau, Germany
Magnetic stirring bars (oval, various sizes)	
McFarland Densiometer DEN-1B	Grant Instruments Ltd, Shepreth, Cambridgeshire, England
Photometer Synergy™ MX	BioTek, Winooski, USA
Pipettes (0.5-10 µL; 10-100 µL; 100-1000 µL; 500–5000 µL) Eppendorf Research Eppendorf Research plus Eppendorf Reference	Eppendorf, Hamburg, Germany
Shaking incubator GFL 3032	GFL Gesellschaft für Labortechnik, Burgwedel, Germany
Thermocycler TC-3000	Biostep® GmbH, Jahnsdorf, Germany
Thermomixer 5436	Eppendorf, Hamburg, Germany
Turbidity meter, DensiCheck®	BioMerieux, Nuertingen, Germany
Ultraviolet lamp No. 880538	Camag AG Co GmbH, Berlin, Germany
Vortexer Reax 2000	Heidolph Instruments GmbH, Schwabach, Germany

2.1.5 **Bacterial strains**

Escherichia coli reference strain ATCC 25922 Levofloxacin MIC=0.032 mg/L	American Type Culture Collection (ATCC), Manassas, Virginia, USA
Escherichia coli patient isolate, Sequence type (ST) 58, Levofloxacin MIC=8 mg/L	Institute for Hygiene and Environmental Medicine, Charité University Hospital Berlin, Germany
Escherichia coli patient isolate, ST88, Levofloxacin MIC=2 mg/L	Institute for Hygiene and Environmental Medicine, Charité University Hospital Berlin, Germany
Escherichia coli patient isolate, ST167, Levofloxacin MIC=8 mg/L	Institute for Hygiene and Environmental Medicine, Charité University Hospital Berlin, Germany

2.1.6 **Software**

CASY® 2.5 version 0.9.11.9	Omni Life Science GmbH, Bremen, Germany
GEN5™ Version 1.10.8	BioTek, Winsooki, USA
Geneious Prime® 11.1	Biomatters, Ltd., Auckland, New Zealand
Microsoft Office Excel 2016	Microsoft Corporation, Redmond, USA
NONMEM 7.4.3	ICON Clinical Research LLC, Gaithersburg, MD, USA
Pirana 2.9.6	Certara Inc., Princeton, NJ, USA
PsN version 4.8.1	Uppsala University, Uppsala, Sweden
R® version 3.6.0, RStudio version 1.2.1335	R foundation for Statistical Computing, Vienna, Austria

2.2 Characterisation of bacterial growth and kill behaviour

Aiming to gain deeper insights in the behaviour of bacterial populations under LEV exposure, various microbiological investigations were performed. The central approach in the presented work were static and dynamic IVIM experiments, which are described in the following chapters (chapters 2.2.2, 2.2.3). Prior to static and a dynamic IVIM experiments, bacteria were cultivated, the MIC values of investigated *E. coli* strains were determined and the impact of LEV binding to components of the growth medium was investigated (chapter 2.2.1). Bacterial and LEV concentrations (C_{LEV}) in samples taken from the IVIM were determined applying previously validated bioanalytical assays.

2.2.1 Microbiological and bioanalytical methods and prior investigations

2.2.1.1 Storage and cultivation of bacteria

Bacterial suspensions were prepared from fresh overnight cultures by suspending bacterial colonies in 3.0 mL autoclaved NaCl 0.9% solution. The bacterial suspension was vortex mixed carefully and adjusted to a turbidity of 3 McF, using a turbidity meter. Aliquots of 0.5 mL were preserved in cryo vials containing beads for long-term storage at - 80°C. 2 days before a microbiological experiment, a cryo vial was opened under sterile conditions, one bead was picked using autoclaved tweezers and bacteria were spread on a Columbia agar plate. After overnight incubation at 37°C, a subculture was derived by picking single colonies from the agar plate, using a sterilised sampling loop and spreading colonies on a fresh agar plate, which was subsequently overnight incubated at 37°C. For each experiment, a fresh overnight culture was prepared from the previous one. Subcultures were kept in the fridge at 4°C for maximum 4 weeks. After 4 weeks, a new subculture was derived from cryo-conserved bacteria as described above.

2.2.1.2 Determination of the minimal inhibitory concentration

The minimal inhibitory C_{LEV} of three clinical *E. coli* isolates were determined by applying the microdilution method according to the CLSI guidelines [36]. A bacterial suspension was prepared by picking 2–4 bacterial colonies from a fresh overnight culture with a sterilised inoculation loop. The colonies were suspended in 3.0 mL autoclaved NaCl 0.9% solution. The bacterial suspension was vortex mixed carefully and adjusted to a turbidity of 0.5 McF, containing approx. $8.8 \cdot 10^7$ CFU/mL [131]. LEV stock solution (1000 mg/L) was sterile filtered (cellulose acetate filter, pore size: 0.2 µm) and diluted in CAMHB to finally obtain C_{LEV} being multiples or fractions of 1 mg/L (Figure 2.1).

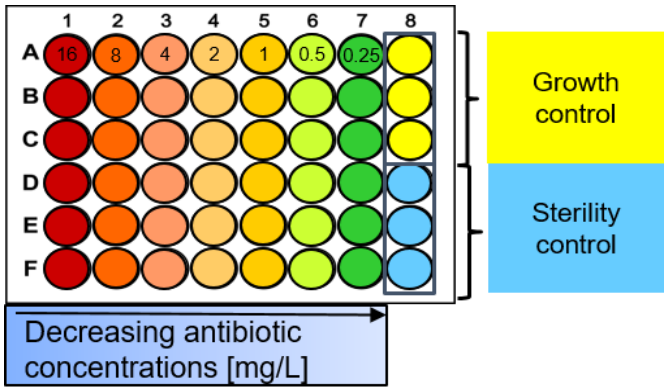

Figure 2.1: Microdilution method to determine the minimal inhibitory concentration. Colours represent antibiotic concentrations being multiples or fractions of 1 mg/L and equal in the wells of each vertical row. Growth control: bacterial suspension without added antibiotic, sterility control: growth medium without antibiotic or bacteria.

900 µL CAMHB were pipetted in each well of 48-well plate. Subsequently, 100 µL of the respective LEV dilution was added to each well (n=6 replicates per LEV dilution and experiment). Finally, 10 µL bacterial suspension were added, resulting in an inoculum concentration of approx. $5 \cdot 10^5$ CFU/mL. In each MIC experiment, sterility controls (1000 µL CAMHB, n=3 per experiment) and growth controls (990 µL CAMHB + 10 µL bacterial suspension, n=3 per experiment) were performed. According to the CLSI, the MIC value was determined as the lowest C_{LEV} inhibiting bacterial growth after 16-20 h of incubation, detected by the unaided eye [36]. For each of the clinical *E. coli* isolates, the assay was performed ≥ 2-fold, while C_{LEV} between 0.25 and 64 mg/L were investigated.

2.2.1.3 Quantification of viable bacteria

For quantification of bacterial CFU in IVIM experiments, a plate counting assay, referred to as “droplet plate assay”, was employed [132]. Different from turbidity-based bacterial quantification methods or electronic cell counting, which assess viable cells, dead cells, debris and non-replicating persister cells, the droplet plate assay quantifies solely viable bacterial cells, i.e bacteria being capable of forming colonies on agar plates. The assay was previously established and validated for *Staphylococcus aureus (S. aureus)*, *Enterococcus faecum* and *E. coli* [21,133,134]. Accordingly, serial 1:10 dilutions were performed with bacterial samples taken from the IVIM, i.e.100 µL bacterial suspension were diluted in 900 µL sterile NaCl 0.9 % solution in a 48-well plate. The number of dilution steps was depending on the expected bacterial concentration in the sample and ranged between 1 and 8, aiming to obtain between 20 and 500 colonies on a quarter agar plate. When very low bacterial concentrations were expected, undiluted samples were plated. 10 drops with a volume of 10 µL, each, were taken

from up to 4 dilutions per sample and each dilution was spread on a quarter Columbia agar plate, resulting in a volume of 100 µL per quarter. Agar plates were kept under sterile conditions on the laminar airflow workbench, until the NaCl 0.9% solution was completely vaporized, and subsequently incubated at 37°C. After 18-24 h, colonies were counted manually and a pictures of agar plates were taken for documentation. Bacterial concentration in the undiluted sample was calculated in CFU/mL, accounting for the different dilution steps. The median of ≤ 4 dilutions per sample was recorded. Of note, this procedure led to different lower limits of quantification (LLOQ) for different samples, depending on the lowest plated dilution. For example, when the first 1:10 dilution was the lowest plated dilution, this resulted in an LLOQ of 10^2 CFU/mL, while the lowest plated dilution of $1:10^3$ resulted in an LLOQ of 10^4 CFU/mL. The LLOQ of each bacterial sample was recorded for later data analysis (chapter 2.4.2.1).

2.2.1.4 Quantification of levofloxacin concentrations and stability

C_{LEV} in IVIM samples were determined applying a previously validated fluorometric assay [135]. LEV stock solution (1000 mg/L) was prepared as described above (chapter 2.1.2.2). Working solutions (C_{LEV}=10 mg/L and C_{LEV}=5 mg/L), calibrator solutions (CAL, n=6) and quality control samples (QC, n=5) in the measurement range between 0.25 and 2.5 mg/L were obtained by diluting the LEV stock solution in CAMHB of the same batch used in the respective experiment. Emissions of CAL, QC and a blank (CAMHB without LEV) were determined using the photometer Synergy™ MX, with an excitation wave length of λ=300 nm and an emission wave length of λ=500 nm. The calibration function was obtained by weighted linear regression (weighting factor $1/y^2$), performed in the photometer software BioTek GEN5™. Only analytical runs meeting the requirements of the EMA guideline for bioanalytical method validation [136] were accepted. CAL, QC, the blank and samples drawn from the IVIM were centrifuged with a relative centrifugal force (rcf) of 1000 *g* for 10 min to remove bacteria. If needed, supernatant of samples was diluted to the measurement range with CAMHB. 200 µL of the (diluted) supernatant were added to 200 µL acetic acid-acetate buffer (pH 4.0-4.5) and vortex mixed carefully. 200 µL of each CAL, QC, the blank and each sample were pipetted in a 96-well plate (transparent, flat bottom) and emissions were determined in triplicate. The arithmetic mean of three measurements was recorded.

C_{LEV} of ≥ 13 samples were determined for each dIVIM experiment. In the sIVIM, constant C_{LEV} were aimed for. LEV stability under the experimental conditions of the sIVIM over 24 h was shown previously for a concentration range between 2 and 16 mg/L [134]. In this work, stability was re-investigated over 3 days for selected C_{LEV} (C_{LEV}=2 mg/L and C_{LEV}=4 mg/L (n=2, each),

C_{LEV}=8 mg/L and C_{LEV}=16 mg/L (n=6, each)). Samples for C_{LEV} determination were taken at t=0 h, t=24 h, t=48 h and at t ≥ 72 h during the sIVIM experiments.

2.2.1.5 Levofloxacin binding to growth medium components

The importance of protein binding (PB) of antimicrobials is well known and accepted, as only the unbound fraction (f_u) of a compound can exhibit antimicrobial activity *in vivo* [29,30]. Antimicrobial activity can also be impaired by binding to components of growth media *in vitro*. Therefore, potential binding of a compound to components of the used growth medium should also be considered in microbiological experiments, especially in case of growth media containing added serum or human albumin [137]. MHB is frequently used as growth medium in microbiological experiments, because it closely resembles human serum regarding osmolality, electrolyte concentrations and pH [128]. The medium contains not further specified beef infusion solids (from 300 g/L), casein hydrolysate (17.5 g/L) and starch (1.5 g/L) [129]. To better mimic human serum conditions in terms of PB, often 4.0 g/dL albumin are added to MHB in microbiological experiments [137], as physiological serum albumin concentrations range between 3.7 and 4.7 g/dL [138]. It has been shown, that addition of 12% albumin reduced the antibiotic effect of moxifloxacin (PB ~38%) and trovafloxacin (PB ~78%) against *Staphylooccus aureus* and *P. aeruginosa,* compared to MHB without additives. These findings indicated that binding to growth medium components might have impaired antimicrobial activity, especially for highly protein bound compounds [139]. Plasma protein binding of LEV is relatively low (~24-38%, [74]). However, binding of LEV to macromolecules in CAMHB was investigated to rule out a relevant impact of PB. Different methods are available to determine the extent of PB of a compound. Most frequently, rapid equilibrium dialysis and ultrafiltration are applied [137]. For convenience of a simple and reliable approach, ultrafiltration was performed in this work. The principle of the ultrafiltration technique separates the f_u from the protein bound fraction by the means of a selectively permeable membrane with a defined cut-off value in an ultrafiltration unit. The drug containing sample is applied to the upper compartment of the ultrafiltration unit, which is subsequently centrifuged. Thereby, the unbound drug molecules are forced to pass through the membrane, while drug molecules bound to macromolecules remain in the upper compartment. The unbound drug concentration (C_u) is determined in the ultrafiltrate [137].

Here, CAL of six C_{LEV} tiers (0.25, 0.5, 1.0, 1.49, 2, 2.49 mg/L) were prepared (n=2 replicates per CAL) and C_{LEV} were determined as described above (chapter 2.2.1.4). Each replicate was measured thrice (Figure 2.2), the arithmetic mean of 3 measurements was determined and the experiment was performed 3-fold.

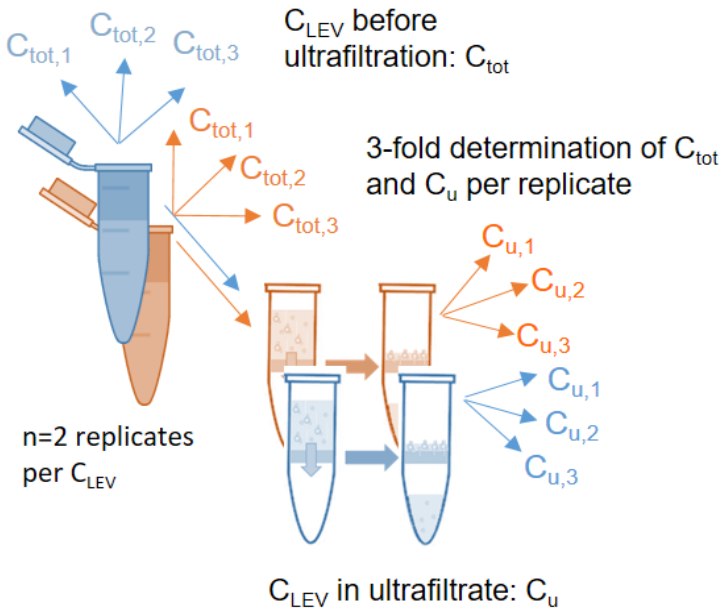

Figure 2.2: Experimental setup to investigate binding of levofloxacin to components of cation adjusted Mueller Hinton broth. C_{LEV}: levofloxacin concentration, C_{tot}: total levofloxacin concentration, C_u: unbound levofloxacin concentration. 6 C_{LEV} (0.25, 0.5, 1.0, 1.49, 2, 2.49 mg/L) were prepared in duplicate (n=2 replicates per C_{LEV}) in each experiment (n=3 experiments) and C_{tot} and C_u of each replicate were determined thrice.

Subsequently, 400 µL of each replicate were pipetted in ultrafiltration units (VWR centrifugal filters, cut-off 30 kD) and centrifuged at 2000 *g* for 30 min. 200 µL of the ultrafiltrate were prepared as described above (chapter 2.2.1.4). Weighted linear regression (emission against nominal C_{LEV} (C_{nom}), weighting factor $1/y^2$) was performed for replicates before ultrafiltration and for ultrafiltrate, respectively. C_{LEV} was determined in triplicate for each replicate, based on the regression functions for CAL before ultrafiltration and in ultrafiltrate, respectively. The arithmetic mean of 3 determinations per replicate was recorded. Aiming to (i) show normal distribution of the differences between C_{LEV} before ultrafiltration and in the respective ultrafiltrate and (ii) answer the question if differences between samples before ultrafiltration and in ultrafiltrate are significant, (i) a Shapiro-Wilk test was carried out and (ii) a paired, 2-sided t-test was performed with a significance level of $\alpha=0.05$. Overall, 108 paired samples were included, the number of degrees of freedom (df) was 107 and variance homogeneity was not assumed.

2.2.2 Static *in vitro* infection model

In all IVIM experiments, the inoculum was prepared as described in 2.2.1.1. LEV stock solution (either 1000 mg/L or 2000 mg/L, depending on the desired C_{LEV}) was sterile filtered and LEV dilutions were prepared in CAMHB. In total, 13 sIVIM experiments were performed, exposing the reference strain *E. coli* ATCC 25922 and three clinical *E. coli* isolates to constant C_{LEV} between 0.25- and 8-fold their MIC (0.5–64 mg/L for the isolates; 0.016-0.064 mg/L for the reference strain) for 1–3 days. In each experiment, one growth control (GC) was performed to monitor bacterial growth under the experimental conditions without antibiotic exposure. 8.9 mL autoclaved CAMHB were pipetted into each cell culture flask (4-5 per experiment) under sterile conditions, and 100 µL of the 1:10 diluted bacterial stock suspension (approx. 10^7 CFU/mL) were added, resulting in an initial bacterial concentration of approx. 10^5 CFU/mL. According to the previously determined lag-time of *E. coli* [134], bacteria were preincubated for 2 h at 35 ± 2°C, aiming to reach the exponential growth stage and a bacterial concentration of 10^6 CFU/mL at t=0 h, when 1.0 mL of the respective LEV dilution was added (GC: 1.0 mL CAMHB). Samples for bacterial quantification were taken at t=0, 0.5, 1, 2, 4, 6, 8, 10 and 24 h in the experiments over 1 day. For the 3-days experiments, additional dense sampling was performed between t=24 and 32 h, one sample was taken at the end of day 2 and one at the end of day 3. Overall, 46 replicates (i.e. time-kill curves of exposed *E. coli* populations) and 13 GC curves were obtained. The specific experimental settings for each of the experiments are presented in Table 7.1.

2.2.3 Dynamic *in vitro* infection model

To investigate the effect of clinically relevant LEV C(t) profiles on three *E. coli* isolates, a dIVIM was leveraged, which was developed based on E. Löwdin et al. and validated for exposing *E. coli* to LEV C(t) profiles previously [58,135,140].

The experimental setup (Figure 2.3) comprised three culture vessels (No.(1)), containing CAMHB, in which the inoculum (prepared as described in chapter 2.2.1.2) was preincubated for 2 h at 35 ± 2°C, in order to reach the exponential growth stage and a bacterial concentration of 10^6 CFU/mL at t=0 h. The three independent culture vessels were connected via a tubing system with three glass bottles (represented in No. (2): “reservoir”). The reservoirs initially contained LEV solution in CAMHB, which was later exchanged with LEV-free CAMHB. In each dIVIM experiment, one GC was performed using drug-free CAMHB for the whole experiment. LEV solution or drug-free CAMHB was pumped into the culture vessels by three peristaltic pumps (No. (3)) with a defined pump rate, aiming to mimic the desired LEV C(t) profile. As afferent and efferent tubes of one culture vessel were inserted in the same peristaltic pump, rates for in- and outflow were equal and volume in the culture vessels was kept constant.

Sterile cellulose nitrate filters (hydrophobic edge, pore size of 0.45 µm) were placed at the outflow tubing to prevent bacterial loss (No. (4)). Efferent tubes were connected with glass bottles, in which the sterile waste was collected (No. (5)). Samples for bacterial and LEV quantification (chapters 2.2.1.3 and 2.2.1.4) were taken from a sampling port with a sterile membrane (No. (6)), using syringes with a 120 mm cannula. The culture vessels were tempered to 35 ± 2°C and the bacterial suspension was stirred with magnetic stirring bars by the magnetic stirring and heating unit (No. (7)).

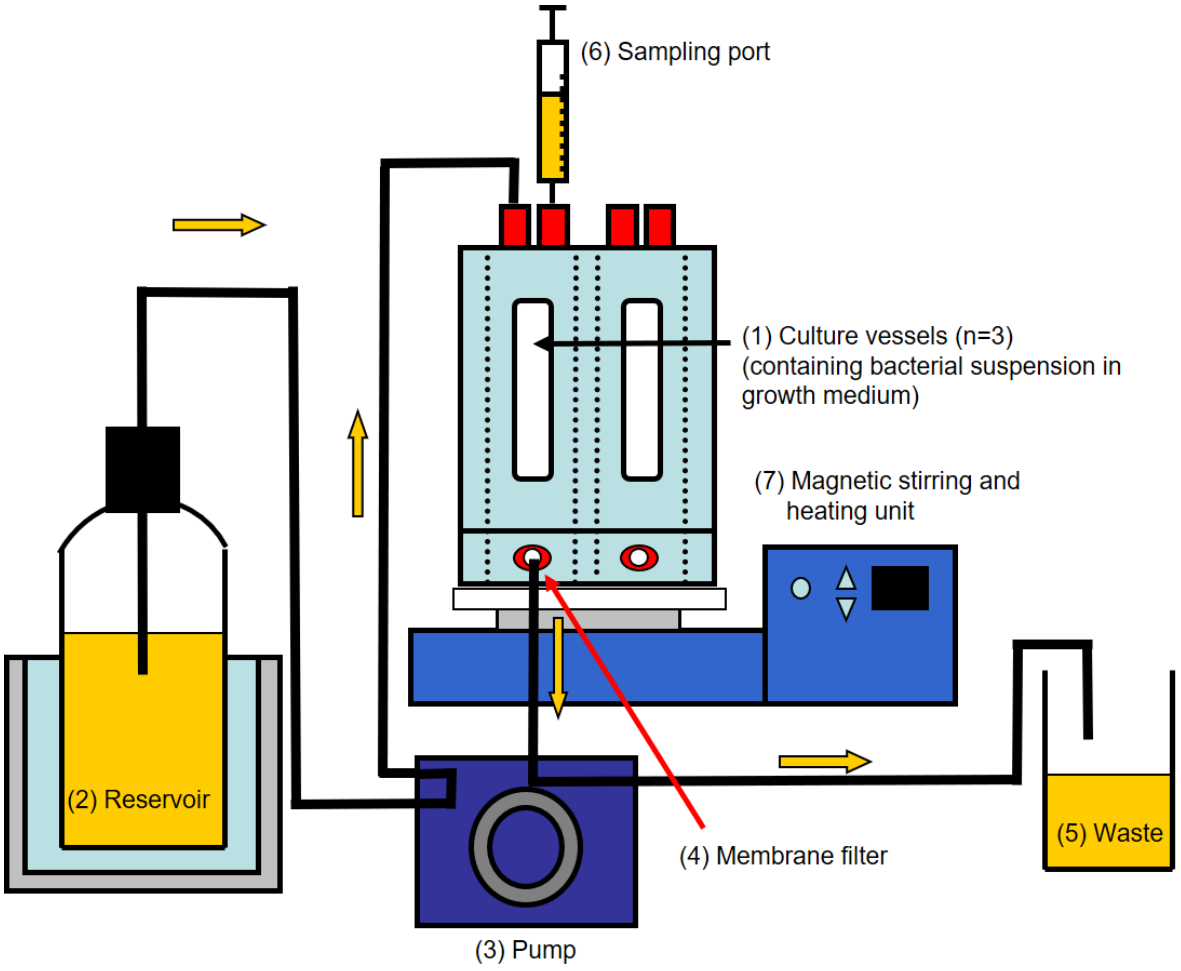

Figure 2.3: Experimental setup of the dynamic *in vitro* infection model, yellow arrows indicate direction of medium flow; explanation: see main text, adapted from [141].

Prior to each dIVIM experiment, all components of the dIVIM (tubing system, glass bottles, culture vessels, screw caps), laboratory equipment (beaker glasses, measuring cylinder, volumetric flask, magnetic stirring bars, tweezers, funnels) and solutions (CAMHB, NaCl 0.9 %, Milli-Q® water) were autoclaved for 15 min at 121°C and 2 bar. Components made from Teflon® (multiple distributors for bottles, strainer for pump tubes, sieves at outflow of culture vessels) were cleaned in sodium hypochlorite solution (12% active chlorine) for 5 min, let dry on the sterile workbench and chlorite crystals were removed with Bacillol® AF. CAMHB was

preincubated at 35 ± 2°C the night before the experiment. The dIVIM was set up under sterile conditions, using tweezers and autoclaved equipment. Membrane filters were moistened with autoclaved Milli-Q® water to ease the placing on top of the sieves at the outflow of each culture vessel. Culture vessels were filled with 90.0 mL CAMHB using a measuring cylinder and funnels. Bacterial suspension was added and after preincubation for 2 h, inflow of LEV solution in CAMHB was initialised by switching on the peristaltic pumps at t=0 h.

Aiming to experimentally mimic clinically relevant LEV C(t) profiles of septic patients in the dIVIM, a previously developed NLME model [55,142] was applied to *in silico* simulate LEV C(t) profiles resulting from a 750 mg, 90 min i.v. infusion in plasma. Parameter estimates and precision of the applied two-compartmental PK model with zero-order infusion and first-order elimination are presented in Table 7.2. In the model, the impact of CLCR on LEV clearance (CL) was incorporated as 1.09% fractional change in CL per mL/min change in CLCR according to Equation 2.3. Interindividual variability (IIV) in CL, central volume of distribution (V_c), peripheral volume of distribution (V_p) and intercompartmental clearance (Q), as well as the covariate effect of CLCR on CL was accounted for in stochastic simulations (n=1000) of LEV C(t) profiles in a septic patient population.

$$CL_{sepsis,i} = \theta\, CL \cdot (1 + 0.0109 \cdot (CLCR_{sepsis,i} - CLCR_{median})) \cdot e^{\eta_{CL,i}} \quad (2.3)$$

$CL_{sepsis,i}$: LEV clearance of septic individual *i*

$\theta\, CL$: typical LEV clearance value for the population

$CLCR_{sepsis,i}$: creatinine clearance of septic individual

$CLCR_{median}$: median creatinine clearance of the population

$\eta_{CL,i}$: individual random effect of clearance for individual *i*

The following experimental parameters were determined aiming to mimic the median LEV C(t) profile of 1000 simulated LEV C(t) profiles: C_{LEV} in the reservoir, infusion duration, pump rate to mimic the increasing part of the C(t) profile ("infusion rate"), elimination pump rate 1, pump rate switch time and elimination pump rate 2. These experimental parameters enabled mimicking zero-order input and biphasic decline of C_{LEV} according to the underlying two-compartmental PK model. Optimal experimental parameters were estimated using the function `optim´ of the R® package `deSolve´ as described previously [134]. The set of parameter values applied to mimic a LEV C(t) profile resulting from a 750 mg, 90 min i.v. infusion in a septic patient is presented in Table 2.1.

Table 2.1: Experimental parameters to mimic a levofloxacin concentration-time profile resulting from a 750 mg, 90 min i.v. infusion in plasma of a septic patient in the dynamic *in vitro* infection model.

Experimental parameter [unit]	Value
LEV concentration in the reservoir [mg/L]	26.2
Infusion duration [min]	90.0
Infusion rate [mL/min]	1.00
Elimination pump rate 1 [mL/min]	1.45
Switch time [min]	126
Elimination pump rate 2 [mL/min]	0.176

In total, n=12 experimental replicates (i.e. dynamic time-kill curves obtained in one culture vessel), exposing three clinical *E. coli* isolates to dynamic LEV C(t) profiles were obtained in seven dIVIM experiments (1-2 replicates per experiment). In six of the experiments, a GC was performed (n_{GC}=6). Different sampling times were chosen, aiming to characterise the full LEV C(t) and bacterial growth and kill trajectory, with dense sampling in the first 10 h (n=4 experiments) or dense sampling between 10 h and 24 h (n=3 experiments, Table 7.3). Additionally, ≥ 13 samples per replicate were taken to quantify C_{LEV} over time (chapter 2.2.1.4).

2.3 Mechanisms of adaptation and resistance

In order to explain and understand the mechanisms driving the observed growth and kill behaviour of *E. coli* under LEV exposure, genomic resistance mechanisms of the clinical isolates, i.e. mutations in QRDR and presence of *qnr* plasmids were investigated. The applied PCR and electrophoresis assays (chapter 2.3.1) were provided by the Institute of Microbiology and Epizootics, Department of Veterinary Medicine, Freie Universitaet Berlin and newly introduced to the Institute of Pharmacy, Department of Clinical Pharmacy and Biochemistry, Freie Universitaet Berlin. To cross-validate PCR and Sanger sequencing, genomic resistance mechanisms were additionally investigated by whole genome sequencing and web-based analysis by the online tool ResFinder 3.2 [143]. For the quantitative assessment of phenotypic adaptation, a novel approach was developed and a proof-of-concept study was carried out (chapter 2.3.2). Prolongation of *E. coli* cells under LEV exposure, referred to as filamentation, was used as surrogate for persister cell formation [122] and assessed with a cell counter and analyser system (CASY®).

2.3.1 Sequencing and genomic resistance mechanisms

2.3.1.1 Bacterial DNA extraction

The nucleic acid extraction kit (GF-1, GeneON) was applied to purify bacterial DNA using a mini-column spin technology and optimised buffers, according to the recommendations of the manufacturer [144]. To comply with the requirements of subsequent PCR amplification, isolation of pure DNA, was enabled by removing impurities, such as cellular debris, proteins or salts during multiple washing steps. The wash buffer was diluted with 40 mL ethanol and the elution buffer was preheated at 65°C according to the manufacturer´s instructions [144]. 5.0 mg lysozyme were dissolved in 100 µL Milli-Q® water, vortex mixed carefully and let rest for 30 min. Single colonies were picked from the freshly prepared overnights cultures of the *E. coli* isolates (chapter 2.2.1.1) with a sterilised inoculation loop and suspended in 100 µL “resuspension buffer 1”. After addition of 10 µL of lysozyme solution and mixing carefully, the suspension was incubated while shaking for 20 min at 37°C. Subsequently, centrifugation was carried out at 10,000 *g* for 3 min, the supernatant was removed carefully and the pellet was suspended in 180 µL “resuspension buffer 2”. Cell lysis was obtained by adding 20 µL proteinase K and incubating while shaking at 65°C, until a clear solution was obtained (at least 20 min). Next, 400 µL bacterial genomic binding buffer (“Buffer BG”) was added and the homogenised solution was incubated at 65°C for 10 min. Subsequently, DNA was precipitated by adding 200 µL ethanol (> 95%) and by careful homogenisation without vortex mixing. For DNA purification, 650 µL sample were applied to a column in a collection tube, which containined a glass filter membrane. The collection tube was centrifuged at 10,000 *g* for 1 min

multiple times, until the total volume was removed from the precipitated DNA. The obtained eluate was discarded. Subsequently, 650 µL diluted wash buffer were applied to the column and centrifugation at 10,000 *g* for 1 min was carried out. The last centrifugation step was repeated once without adding any buffer, to clean the column from ethanol residues. Next, the column was transferred to a clean vial, and 100 µL preheated (65°C) elution buffer were applied to dissolve the DNA. After 2 min resting, centrifugation at 10,000 *g* for 1 min was carried out. To qualitatively control the DNA extraction regarding purity, the $A_{260/280}$ ratio of the obtained DNA solution was determined using the photometer Synergy™ MX. Only samples meeting the target range of $1.7 < A_{260/280} < 1.8$, indicating pure DNA without protein contamination, were accepted and further analysed by PCR and electrophoresis.

2.3.1.2 Amplification of quinolone resistance determining regions and plasmids

In order to investigate genomic fluoroquinolone resistance mechanisms, mutations in the QRDR of *gyrA* and *parC* were assessed by PCR amplification and subsequent DNA sequencing in for three clinical *E. coli* isolates. Furthermore, the presence of the quinolone resistance plasmids *qnrA*, *qnrB* and *qnrS* was investigated, applying a multiplex PCR approach. Preliminary, required solutions and chemicals were prepared: TBE buffer (10-fold and 1-fold concentrated, chapter 2.1.2.4) and TE buffer (chapter 2.1.2.5) were made. The deoxynucleotide (dNTP) mix (20 µL) was diluted in 150 µL 10x Green Buffer (incl. 20 mM $MgCl_2$) and 1150 µL MilliQ® water and stored at -20°C. Primer lyophilisates were reconstituted in 240 µL TE buffer (pH 8.0), obtaining a 100 µM primer stock solution. These stock solutions were mixed and the primer mix was diluted in MilliQ® water (1:10) for subsequent use. For each PCR experiment, a new master mix was prepared, including the diluted dNTP mix (10 mM), forward (F) and reverse (R) primers (primer sequences: chapter 2.1.1) and *Taq* polymerase (volumes of the components: Table 7.4). The DNA ladder used for electrophoresis (NoLimits 100 bp DNA fragment) was reconstituted in 20 µL Tris-HCl buffer (pH 7.6). Amplification of *gyrA* and *parC* and the multiplex PCR of *qnrA*, *qnrB* and *qnrS* were carried out separately with specific thermocycler settings (Table 2.2).

Table 2.2: Thermocycler settings for polymerase chain reaction to amplify *gyrA, parC* and *qnrA/B/S* in *Escherichia coli.*

Step	*gyrA*	*parC*	*qnrA/B/S*
Number of cycles	30	30	25
Predenaturation	94°C/ 3 min	94°C/3 min	94°C/ 3 min
Denaturation	94°C/ 30 s	94°C/ 30 s	94°C/ 30 s
Annealing	58°C/ 30 s	57°C/ 30 s	51°C/ 30 s
Elongation	72°C/ 45 s	72°C/ 45 s	72°C/ 1 min
Endelongation	72°C/ 10 min	72°C/ 10 min	72°C/ 10 min
Pause	10°C / ∞	10°C / ∞	10°C / ∞

Agarose gel electrophoresis (130 volts, 1xTBE buffer) was performed with PCR products in order to prove the presence of *qnrA/B/S* plasmids and monitor the success of *gyrA* and *parC* amplification before performing Sanger sequencing. 6.00 µL of each PCR product and 2.00 µL DNA ladder were applied to a 1.5% agarose gel. After 45 min, PCR products were detected under UV light according to the corresponding size of the DNA ladder fragment (Table 7.5).

2.3.1.3 Sanger sequencing and sequence analysis

In case of detectable bands at fragment sizes of *gyrA* and *parC* on the electrophoresis gel, PCR products were outsourced for Sanger sequencing at LGC Genomics GmbH, Berlin, Germany. Sanger sequencing was performed using an ABI 3730XL DNA sequencer (Thermo Fisher Scientific) with the same set of primers used for PCR. For quality control, PCR products were sequenced in duplicate, using both primer F and primer R. Sanger sequencing was performed for PCR products derived from three clinical *E. coli* isolates before LEV exposure in the IVIM. Additionally, one isolate was cultivated after exposure to a static C_{LEV} of 2 mg/L (1-fold MIC) in the sIVIM for 24 h, DNA was extracted (chapter 2.3.1.1) and Sanger sequencing was performed with both primers.

Sequences were analysed using the software geneious®. Sequence quality was evaluated according to the probability (P) of an incorrect identification of a base for each position of the nucleic acid sequence. The probability of an incorrect base call (P) was quantified by the Phred quality score, representing the probability of an incorrect base call for each position on a logarithmic scale according to Equation 2.4 [145]:

$$Phred\ score = -10\ log_{10} P \tag{2.4}$$

P: Probability of an incorrect base call

According to the fraction of high and low quality base calls, sequences were categorised in quality bins, based on the geneious® default settings (Figure 7.1). Only sequences assigned to the highest quality bin (i.e. Phred score > 40 for min. 90% of the bases and Phred score < 20 for max. 10% of the bases) were further analysed. When no high quality sequence was available, PCR amplification and Sanger sequencing were repeated. As quality control, sequences of one PCR product, obtained with either primer F or primer R, were compared: The complementary sequence of the primer R generated sequence was reversed and pairwise alignment was performed. The percentage of identical bases in the sequences generated by primer F and primer R was calculated. Next, reference sequences for *E. coli gyrA* and *parC* were obtained from the National Center for Biotechnology (NCBI) database [146] and aligned with the sequences of the investigated isolates. For each PCR product, the sequence with the higher quality score (generated by primer F or R) was aligned.

In order to evaluate the relevance of the identified differences between the reference sequence and the PCR products of the isolates with respect to amino acid (AA) alterations, the nucleotide sequences were translated into the corresponding AA sequences. For each PCR product, six possible reading frames were investigated (three forward and three reverse reading frames, each). The correct reading frame was identified by aligning the six AA sequences to a reference protein sequence, obtained from the NCBI database (Table 2.3). The reading frame resulting in the best matching AA sequence best was chosen for further analysis.

Table 2.3: Specification of *gyrA* and *parC* reference sequences, obtained from the National Center for Biotechnology, AA: amino acid.

	gyrA	*parC*
Designation	RYJ34831	AIL 17976.1
Date of modification	08.02.2019	22.10.2014
Sequence length [AA]	875	752
Description	DNA gyrase subunit A [*E. coli* 25922]	DNA topoisomerase IV subunit A [*E. coli* 25922]

Alterations in the AA sequences of the PCR products were identified by visual comparison of the graphical representations of the alignments with the reference proteins. Further, the protein translations of the isolate being investigated before and after LEV exposure in the sIVIM were aligned and visually compared.

2.3.1.4 Whole genome sequencing and sequence typing

In order to validate the newly introduced PCR and sequencing methods, WGS was performed. Contigs, i.e. overlapping DNA sequences, were assembled by the Robert Koch Institute, Berlin, Germany. The Illumina® technology [147] was applied, aiming to confirm identified QRDR mutations and PMQR with an additional method. Additionally, WGS allowed for determination of the sequence types (ST) of the isolates by multi-locus sequence typing (MLST). For that purpose, the MLST-2.0 online tool provided by the Center for Genomic Epidemiology [148] was employed. MLST based on WGS data used a set of housekeeping genes, identified specific nucleotide sequences and assigned a random integer number, the ST, according to the allelic profiles [149,150]. Two sets of housekeeping genes were applied to determine the ST of the isolates: the Warwick medical school scheme and the Pasteur institute scheme. In the following, the isolates are identified by their ST according to the Warwick medical school scheme, as this is most widely spread [151].

For further analysis of the whole genome sequences, the online tool ResFinder 3.2 was employed [143]. The web-based method, provided by the Center for Genomic Epidemiology, used the Basic Local Alignment Search Tool (BLAST®) for identification of resistance mutations and acquired resistance genes in nucleic acid sequences [152].

2.3.2 **Bacterial size distributions and phenotypic adaptation**

Aiming to characterise persister cell formation of *E. coli* under LEV exposure, size distributions of *E. coli* populations have been monitored in the sIVIM. Filamentation of *E. coli* has been described before and was assessed by time-lapse and fluorescence light microscopy, flow cytometry and microfluidic systems [100,119,120,124]. In this work, a novel approach using electronic cell counting based on the CASY® technique was developed. During five sIVIM experiments (chapter 2.2.2), three *E. coli* isolates were exposed to constant C_{LEV} of 1-fold and 2-fold their MIC value for 2 or 3 days, ≥ 10 samples were taken over time and CFU/mL were determined applying the droplet plate assay (chapter 2.2.1.3, Table 7.1). At the same sampling time points, bacterial size distributions were assessed.

2.3.2.1 Setup and principle of electronic cell counter and analyser system

The measurement principle of the CASY® device is based on two electrodes in an electrolyte solution (CASY® ton), generating a steady current flow (Figure 2.4). One of the electrodes is surrounded by a capillary, entailing a hole of a defined diameter, the measuring pore. For measuring bacterial cells, the device was equipped with a 45 µm measuring capillary, i.e. a capillary with a pore size of 45 µm. Bacterial cells were suspended in the electrolyte solution, and a defined volume of cell suspension was drawn into the capillary. When passing the measuring pore, particles and cells caused a voltage drop, which was scanned with a frequency of 1 MHz. Based on the shape and time course of the electrical signal, cell volumes were determined by pulse area analysis. The size distribution of bacteria in a sample was calculated with a resolution of 1024 size channels per measurement, using the linear relationship between measurement signal and cell volume [153]. The size measurement range was set to 0-15 µm, resulting in a channel width of 0.0146 µm.

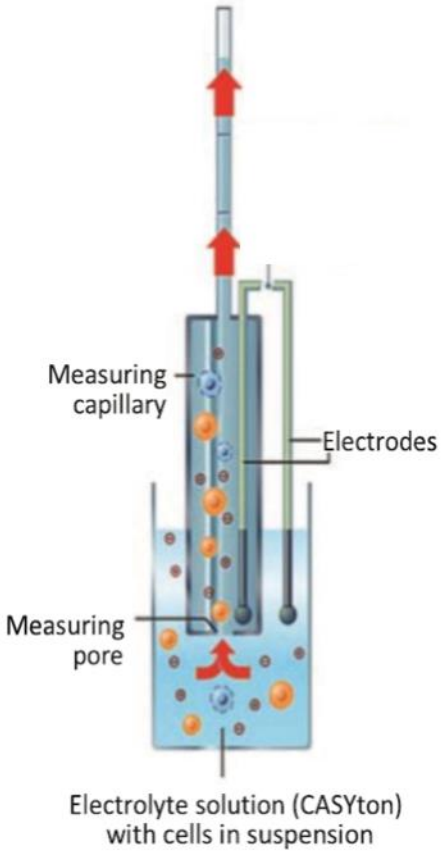

Figure 2.4 Technical setup of the electronic cell counter and analyser system (CASY®); explanation: see main text, adapted from [153].

2.3.2.2 Bacterial quantification and cell size distributions

A sample volume of 200 µL bacterial suspension in CASY® ton was measured (n=1 per sampling time and cell culture flask). Aggregation correction by the device was switched off and the option to set predefined size ranges for “debris”, “dead cells” and “viable cells” was not used, because thresholds were unknown and should be explored.

CASY® ton electrolyte solution was membrane filtered (pore size: 0.2 µm) directly into the measurements vials (CASY® cups) at least 10 min before the measurement, to let air bubble escape before measurement. Background measurements in blank CASY® ton were performed prior to the experiment and intermediately (at each sampling time point > 2 h) and the device was purged until the background signal of blank CASY® ton was < $3 \cdot 10^3$ counts/mL. In each experiment, the signal of a 1:10 dilution series (dilutions: 10^0 – 10^{-5}) of pure CAMHB of the respective batch, kept under the same conditions as bacteria-containing cell culture flasks in the incubator, was assessed at 3 different time points.

For bacterial quantification and determination of cell size distributions with the CASY® device, a bacterial concentration range between $2 \cdot 10^4$ and $2 \cdot 10^5$ counts/mL was aimed for [153]. Therefore, either 100 µL undiluted bacterial suspension, 10^{-1}- or 10^{-2}- diluted samples were processed. 100 µL of the undiluted sample or of the respective dilution were added to 10 mL CASY® ton electrolyte solution (dilution factor: 101), and counts in a sample volume of 200 µL were determined, resulting in a dilution factor of 505 to calculate the counts/mL of the undiluted sample (Figure 7.2).

2.3.2.3 Determination of filamentous bacteria

The CASY® readout, i.e. the raw counts per channel were exported from the software CASY® 2.5 and further processed in the software R®. In a first step, a possible trend in the signal of the blank CAMHB over time in one experiment was evaluated graphically. As no trend in the size distributions was observed over time, the median size distribution of three background measurements per experiment and 10-fold dilution of CAMHB was used for further processing. The CAMHB background signal was accounted for by subtracting the median CAMHB size distribution of the experiment and respective 10-fold dilution from the bacterial size distributions. For example, when the 10^{-1} dilution of a bacterial sample was used for the CASY® measurement, the median of three 10^{-1} dilutions of the background signal, assessed in the same experiment, was subtracted. Here, one measurement comprised the raw counts per channel for 1024 channels, covering a size range between 0 and 15 µm.

Next, the different dilution steps were taken into account by multiplying each background-corrected measurement with $10^{\text{dilution factor}}$ (10-fold dilution series) and 505 (Figure 7.2), to ultimately compare the total counts of one measurement (i.e. the sum of counts over 1024 channels) to the CFU/mL, assessed with the droplet plate assay. For the small size ranges (approx. < 1.2 µm), the counts per channels of the blank CAMHB were higher than the counts of the bacterial samples, resulting in negative background-corrected counts. Based on that observation, the size threshold between assumed debris and bacteria was derived, as larger objects causing a signal higher than the background signal were assumed to be bacterial cells. The size distributions of the three clinical isolates before antibiotic exposure (at t=0 h) were compared graphically and strain-specific debris-bacteria thresholds were determined as the intersection of the size distribution curves and the x-axis (Figure 2.5).

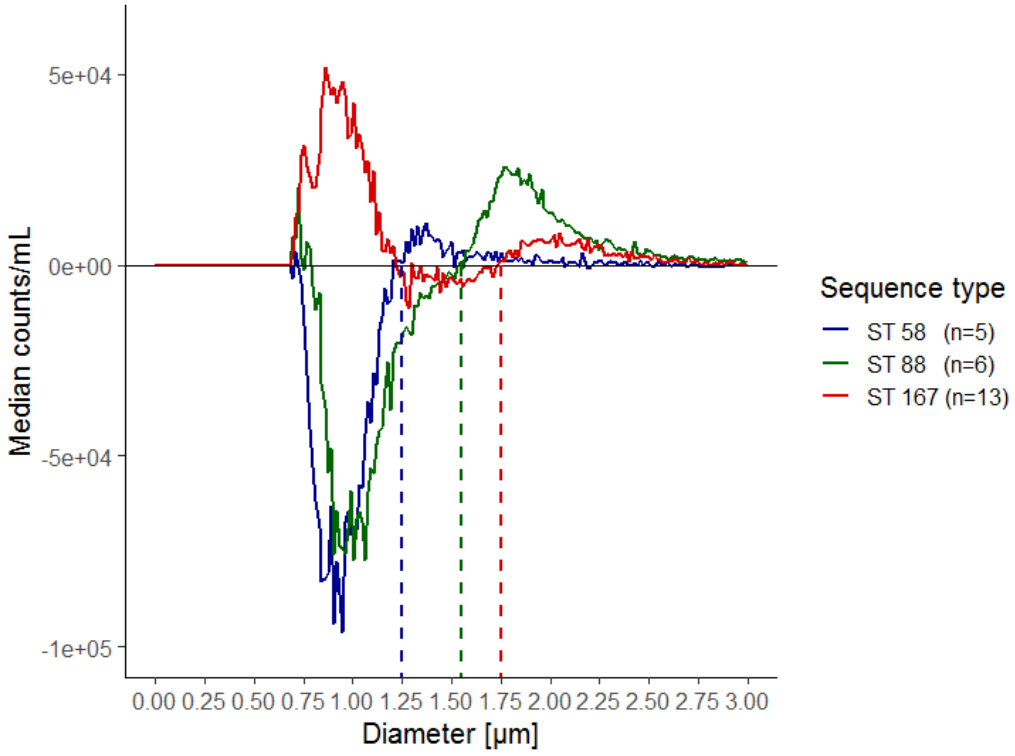

Figure 2.5: Size distribution of 3 *Escherichia coli* isolates before antibiotic exposure in six *in vitro* infection model experiments, median size distribution of n ≥ 5 replicates per isolate, dashed lines illustrate determination of strain-specific thresholds between assumed debris and bacteria as intersection between the size distribution curves and the x-axis; ST: sequence type.

For further analysis, for channels with negative counts, resulting from background correction, zero was imputed (3.34% of all channels). Background- and dilution corrected counts per channel were summarised by grouping the 1024 channels per measurement in size classes and summing up counts within a size class. Different upper size boundaries were explored, aiming to discern “normal size” and “increased size” bacteria. For that purpose, the sum of counts above different thresholds (3, 4, 5 and 6 µm) was depicted over time for the three *E. coli* strains and static LEV exposures (1-fold MIC and 2-fold MIC). Finally, the fraction of total counts belonging to the following four size ranges was determined for each sample and plotted over time of exposure: “Debris” (bacterial diameter < strain-specific threshold); “normal size” (strain-specific threshold < bacterial diameter < 3 µm, [100]) “slightly increased” (3 µm < bacterial diameter < 5 µm) and “extensively increased” (bacterial diameter > 5 µm). Total counts per measurement were calculated as sum of the four size ranges and compared graphically to the CFU/mL, determined with the droplet plate assay (chapter 2.2.1.3). The fractions of the different size ranges were plotted over time; and the fractions of slightly increased and extensively increased cells were compared graphically between the three isolates and LEV exposures.

2.4 Pharmacokinetic/pharmacodynamic modelling and simulations

To comprehensively characterise the exposure-effect relationship of three *E. coli* isolates under static and dynamic LEV exposure, (chapters 2.2.2, 2.2.3), leveraging the insights gained from genomic analysis and phenotypic investigations (chapters 2.3.1, 2.3.2), population-based pharmacometric data analysis was carried out. Different techniques are available to analyse PK and PD data obtained from a population: The naïve pooling approach handles data from a population of multiple individuals (e.g. patients, healthy volunteers or experimental replicates) as being derived from one individual and thereby does not discriminate between IIV, interoccasion variability and residual unexplained variability (RUV), whereas the 2-stage approach assesses the central tendency and the dispersion of the population in two consecutive steps of the analysis [154]. Differently, applying NLME modelling, data derived from a population is evaluated simultaneously [28,66,154].

In a first step, a semi-mechanistic model, linking LEV exposure to the antibiotic effect, was developed to quantitatively characterise the exposure-effect relationship of *E. coli* under LEV exposure. Here, experimental data from multiple replicates in static and dynamic IVIM was pooled and nonlinear regression was performed in the software R®, using the function `optim´ of the package `deSolve´ (chapter 2.4.1). Thereby, informative and easy interpretable PK/PD parameters were derived, but variability between the different experiments and replicates was not taken into account.

To also quantify and explain different levels of variability, as a next step, a NLME PK/PD model was developed using the software NONMEM®, executed by Pearl speaks NONMEM® (PsN) and accessed via Pirana. Beyond discrimination of variability between different experimental replicates and RUV, originating from different bioanalytical methods, this approach enhanced the mechanistic understanding of the underlying processes driving the observed bacterial growth, kill and regrowth behaviour (chapter 2.4.2).

2.4.1 Characterisation of the exposure-effect relationship

Aiming to quantify the exposure-effect relationship of LEV against *E. coli,* identified novel PK/PD metrics, defined as cumulative exposure and effect over time, facilitated exploitation of the full LEV C(t) profile and the complete bacterial growth trajectory. Based on these metrics, novel PK/PD parameters beyond the MIC were derived.

2.4.1.1 PK/PD metrics quantifying the exposure-effect relationship

To account for both time of exposure and the shape of the LEV C(t) profile, the **cum**ulative **a**rea **u**nder the LEV concentration-time **c**urve (cumAUC) was chosen as exposure metric. CumAUC was determined as a function of time (cumAUC(t)), with time starting from 0 (LEV administration) to the end of the static or dynamic IVIM experiment. For the static IVIM, constant C_{LEV} was assumed (chapter 3.1.2). Therefore, cumAUC(t) was calculated based on nominal C_{LEV}. For PD, a novel effect metric, accounting for the complete growth, kill and regrowth trajectory of the isolates, was derived based on the **a**rea **b**etween the GC and the **b**acterial killing and regrowth curve (ABBC), introduced by A. Firsov et al. [48,49,50]. The novel metric was determined by calculating the ABBC **cum**ulatively over time, as cumABBC(t), realised by computing the difference between the area under the bacterial killing and regrowth curve (Figure 2.6, red curve) and the cumulative area under the GC Figure 2.6, black curve) at the respective time (cumAUGC(t)) in the experiment. CumABBC(t) was normalised to cumAUGC(t) by computing the cumABBC(t)/cumAUGC(t) ratio as a function of time (Figure 2.6). Thereby, changing growth dynamics of unexposed bacteria were taken into account and the effect metric was transformed to a scale between 0 (natural growth without antibiotic effect) and 1 (bacterial eradication).

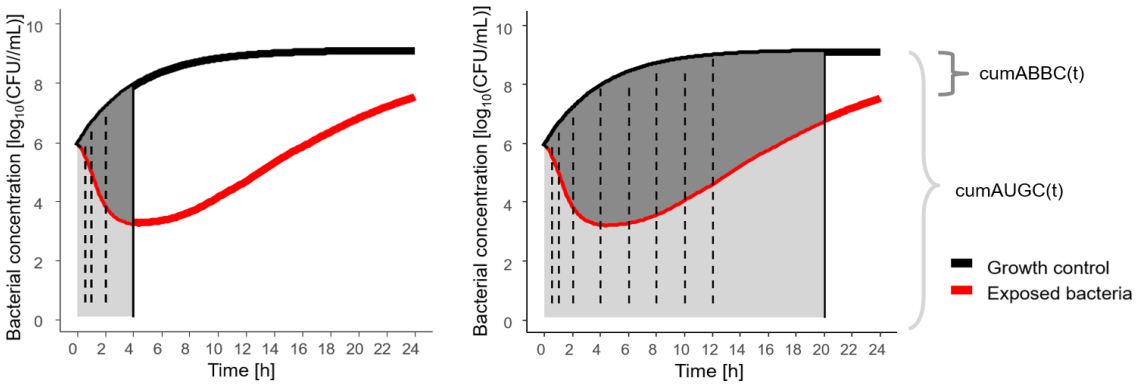

Figure 2.6: Illustration of the novel pharmacodynamic metric, cumABBC(t), to quantify the antibiotic effect based on *in vitro* infection model experiments, exemplified for 2 sampling time points at 4 h (left) with cumABBC(4 h), and at 20 h (right) with cumABBC(20 h); solid vertical lines: sampling time points of assessment, dashed vertical lines: intermediate sampling time points; cumABBC(t): cumulative area between growth control and bacterial killing and regrowth curve as function of time (dark grey area); cumAUGC(t): cumulative area under the growth control curve as function of time (light+dark grey area).

All cumulative areas were determined using the `cumtrapz´ function of the R® package `pracma´, which computed the cumulative integral of y with respect to x by trapezoidal integration with linear interpolation, exemplified for cumAUC(t) in Equation 2.5. CumAUC(t)

was determined over time based on measured (dIVIM) or nominal (sIVIM) C_{LEV} on a linear scale. CumABBC(t) and cumAUGC(t) were computed based on logarithmic bacterial concentrations, determined by the droplet plate assay (chapter 2.2.1.3).

$$cumAUC(t) = \sum_{i=1}^{t} \frac{(C_i + C_{i-1})}{2} \cdot (t_i - t_{i-1}) \quad (2.5)$$

2.4.1.2 PK/PD model development

The novel dynamic PK/PD metrics were applied to graphically explore the antibiotic exposure-effect relationship of LEV against *E. coli* in the sIVIM and dIVIM experiments. Based on these, a simple PK/PD model was developed to derive parameters characterising the exposure-effect relationship quantitatively. During the model development process, ten sIVIM experiments (n = 39 replicates) and seven dIVIM experiments (n = 12 replicates), exposing three clinical isolates, were included. Different mathematical implementations, e.g. ordinary and sigmoidal E_{max} models combined with various inhibition terms, linking cumAUC(t) to cumAUGC(t)-normalised cumABBC(t), were investigated (Table 7.6). Models were compared based on precision of parameter estimates, extent of residual variability and Akaike Information Criterion (AIC). After a sigmoidal E_{max} model with an inhibition term was chosen as final model, two additional sIVIM experiments were conducted (n = 8 replicates), aiming to ultimately obtain a balanced dataset with a comparable number of experiments and replicates for each bacterial strain (Table 7.1). Strain- and exposure pattern- (i.e. static or dynamic exposure) specific PK/PD parameters were estimated.

2.4.1.3 PK/PD parameter estimation

Maximum likelihood estimation (MLE) was applied, seeking to find the set of parameter values describing the exposure and effect data, determined as described above (chapter 2.4.1.1), best. During parameter estimation, the set of parameter values minimising the objective function value (OFV) was pursued, which was computed as the negative sum of the natural logarithm of the individual likelihoods [155]. Given a data vector $y = (y_1, \ldots y_i)$, containing experimental observations (such as experimentally determined values of an antibiotic effect metric), and a defined model, (such as a sigmoidal E_{max} model), MLE identified the parameter vector Θ with greatest likelihood of the observed data by maximising the likelihood function, which can be expressed as the product of probability density functions of the independent variables (such as antibiotic concentrations), $x_1, \ldots x_i$, the parameter Θ and the variance σ^2. A normal distribution of predicted values for an observed value y_i was assumed, with the mean of $\hat{y}$ and a standard deviation of σ. Weighting is a common approach to account for

heteroscedastic errors in (non-)linear regression analysis of bioanalytical data, which are often observed due to inconsistent magnitudes of bioanalytical imprecision. The problem of choosing an appropriate weighting was avoided by utilising the extended least squares (ELS) approach [156]. A proportional residual variability model was specified according to Equation 2.6, and a penalising term was added to avoid negative parameter estimates.

$$ELS = \frac{1}{2} \cdot \sum_{i=1}^{n} \frac{(\hat{y} - y_i)^2}{\sigma^2} + \ln \sigma^2 \quad (2.6)$$

$\hat{y} = predicted\ value\ of\ y$
$y_i = observation\ for\ the\ i^{th}\ individual$
$\sigma^2 = variance$

Two consecutive steps of the minimisation process were performed: In the first step, the Nelder-Mead algorithm was applied, which is a so-called “simplex” method and minimises the objective function by comparing the OFV at (n+1) vertices of a general simplex, followed by replacement of the vertex with the highest OFV [157]. In a second minimisation step, parameter values obtained by the Nelder-Mead method were utilised as initials and the conjugate gradient algorithm was employed to search the flatter surface of the OFV in the neighbourhood of the global minimum [158].

During the model development process, models were compared by the AIC, which is commonly applied to compare non-nested models, as it includes a penalising term increasing the AIC value for a higher number of model parameters (Equation 2.7) [159]. A lower AIC value indicates that a model is superior compared to a model with a higher AIC value.

$$AIC = -2\,LL + 2p \quad (2.7)$$

$LL = natural\ logarithm\ of\ the\ likelihood\ at\ the\ objective\ function\ minimum$
$p = number\ of\ model\ parameters$

2.4.1.4 PK/PD model evaluation and exploration

The final PK/PD model was graphically evaluated by plotting the observed antibiotic exposure-effect curves, stratified per *E. coli* isolate and LEV exposure pattern (i.e. static or dynamic exposure), and overlaying the predictions for the respective isolate and exposure pattern, respectively. To further explore the nature of the exposure-effect relationship, parameter estimation was performed stratified per MIC-normalised LEV exposure (for static, 1-fold MIC and 2-fold MIC, and dynamic exposure pattern). Deterministic simulations were performed for each strain and exposure pattern and the maximum predicted effect (E_{max}) and the corresponding cumulative LEV exposure (cumAUC(t)) value were determined. The property of

an isolate to regrow preferably under exposure to dynamic C_{LEV} was quantified by the ratio between the cumAUC value causing regrowth under static LEV exposure ($cumAUC_{reg,static}$) and the cumAUC value causing regrowth under dynamic LEV exposure ($cumAUC_{reg,dynamic}$) for each strain. The contribution of the two model parameters $cumAUC_{50}$ and $cumAUC_{reg}$ to the antibiotic effect-time trajectories was assessed graphically by plotting the E_{max} model and the inhibition term separately as a function of time for the three isolates and exposure patterns (static, 1-fold MIC and 2-fold MIC, and dynamic exposure). The time and exposure of increasing impact of the inhibition term was determined as ≥ 5% deviation between the trajectory of the E_{max} model term and the full model. The time point of full dominance of the inhibition term was defined as ≤ 5% deviation between the full model and the inhibition term.

2.4.2 **Characterisation of the bacterial growth and kill behaviour**

Building up on the semi-mechanistic model describing the exposure-effect relationship for the different bacterial strains and exposure patterns (chapter 2.4.1), a NLME model was developed to gain a deeper mechanistic understanding and to incorporate quantification of different levels of variability.

2.4.2.1 Dataset generation

Static and dynamic IVIM experiments, exposing three LEV resistant *E. coli* isolates, were included in the NLME model development, while one sIVIM experiment, exposing the LEV susceptible reference strain ATCC 25922 (chapter 2.2.2), was excluded from the analysis. PD observations, i.e. bacterial concentrations, determined by the droplet plate assay (chapter 2.2.1.3), and PK observations, i.e. measured (dIVIM, chapter 2.2.1.4) or nominal (sIVIM) C_{LEV}, were evaluated simultaneously. A NONMEM® specific dataset was generated, in which the individual identifier (ID) represented observations in one experimental replicate, i.e. one cell culture flask in the static or one culture vessel in the dynamic IVIM, respectively, corresponding to a unique bacterial C(t) trajectory and a unique LEV C(t) profile (dIVIM) or constant C_{LEV} (sIVIM). GC curves were included with a corresponding C_{LEV} of 0 mg/L. In addition to standard data items required by NONMEM® [160], the bacterial strain and experiment number were specified and columns to distinguish between static and dynamic LEV exposure and to indicate the nominal C_{LEV} in the sIVIM were implemented (Table 7.7). The “FLAG” column was utilised to distinguish between PK (measured C_{LEV}) and PD (measured bacterial concentrations) observations. All PK and PD observations were transformed into their natural logarithm.

As the **LLOQ** of the droplet plate assay varied between different samples, depending on the lowest plated 10-fold dilution of a sample (chapter 2.2.1.3), it was specified in the dataset

whether an observation was below or above the LLOQ. The corresponding value of the LLOQ for the specific sample was recorded. Observations below the LLOQ were accounted for by applying the so-called “M3 method”. Using this approach, the likelihood of an observation to be above the LLOQ was calculated according to the ELS method, while the likelihood for an observation below the LLOQ was calculated by integrating the density function of the individual prediction, determined by the RUV, from – infinity to the specified LLOQ value [161].

Different meausures to characterise persister cell formation, obtained as described in 2.3.2.3, were specified using the “FLAG” column: the total number of electronic cell counts per mL at a specific time point, the absolute number of electronic cell counts with a diameter > 3 µm per mL, the fraction of counts with a diameter > 3 µm and the absolute number of counts with a diameter > 5 µm per mL.

Beyond the experiments included in the semi-mechanistic PK/PD model (chapter 2.4.1.2), additional dIVIM experiments were included in the analysis: In two replicates, *E. coli* ST58 was exposed to mimicked LEV C(t) profiles resulting from administration of a 500 mg, 60 min LEV i.v. infusion twice daily, [162]. Consequently, two different dosing regimens were specified in the dataset (Table 7.7). Furthermore, LEV C(t) profiles and GC curves obtained in dIVIM feasibility experiments [131] were included in the analysis to inform the model regarding *in vitro* PK in the dIVIM and bacterial growth under the applied experimental conditions. An overview about the different types of experiments, mimicked dosing regimens, exposed bacterial strains and sampling schedules is provided in Table 7.8.

2.4.2.2 Modelling strategy

In a **sequential model development** process, different subsets of the dataset were used (Figure 2.7): In a first step, a “bacterial growth model” was developed based on all GC curves, assessed via the droplet plate assay in the static and in the dynamic IVIM (Figure 2.7, orange frames). Second, static C_{LEV} were linked to viable bacterial CFU/mL, determined by the droplet plate assay, in a “static PK/PD model” (light blue background). For that purpose, all replicates obtained under static LEV exposure were evaluated. Third, a “PK model” was developed to characterise LEV C(t) profiles in the dIVIM, based on measured C_{LEV} in dIVIM experiments (red frame). Fourth, the developed PK model was related to the corresponding bacterial concentrations (viable CFU/mL) and electronic cell counts (chapter 2.3.2.3) in the “final PK/PD model” (Figure 2.7, dark blue background).

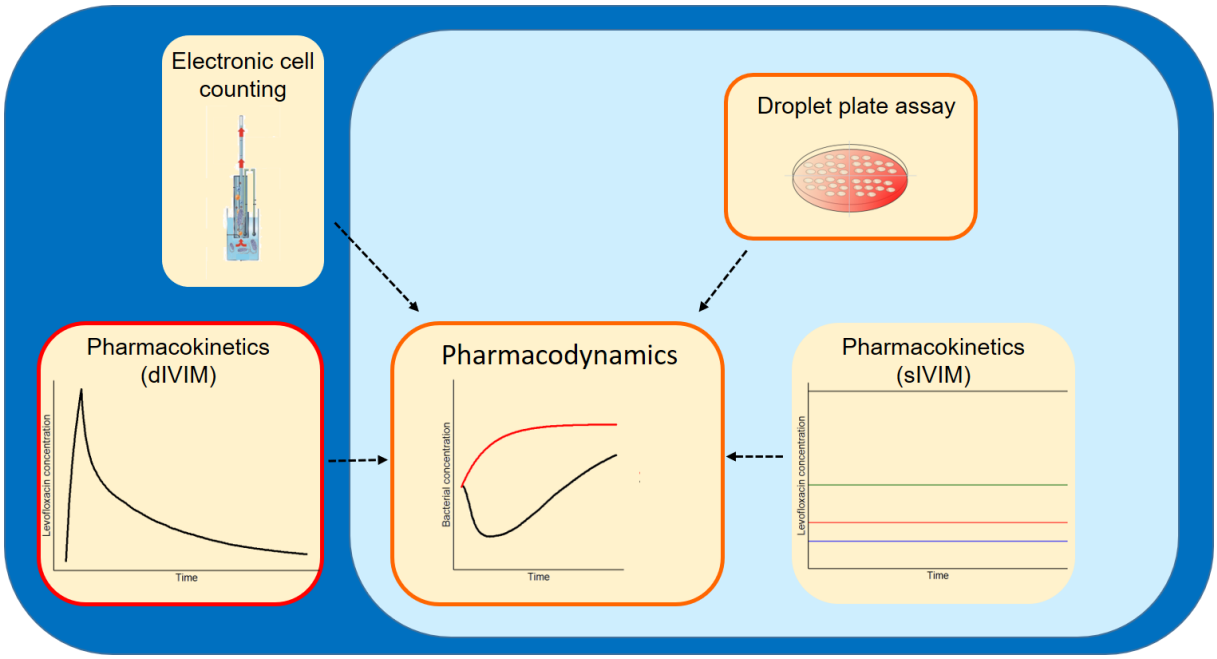

Figure 2.7: Development of a nonlinear mixed-effects pharmacokinetic/pharmacodynamic (PK/PD) model, utilising different subsets of the dataset in a sequential approach: (i) bacterial growth model (orange frames); (ii) static PK/PD model (light blue background); (iii) PK model (red frame); (iv) three-bacterial-state PK/PD model (dark blue background); sIVIM: static *in vitro* infection model, dIVIM: dynamic *in vitro* infection model.

2.4.2.3 Bacterial growth without antibiotic exposure

First, a bacterial growth model was developed to characterise bacterial growth without antibiotic exposure and to identify in the next steps processes being potentially influenced by LEV effects. Here, transformation of bacteria into different phenotypes was modelled as “mass transfer” of bacterial cells between different bacterial subpopulations. Different from PK models, where apparent volumes of distribution are utilised to link a measured drug concentration to the administerd dose of the drug, processes related to bacterial growth and killing were described in the dimension of bacterial numbers in a theoretical volume of 1 mL. This was justified, because all measured bacterial concentrations were determined in the dimension of CFU/mL (droplet plate assay) or electronic counts/mL and hence, differences in volumes between the investigated experimental settings (sIVIM, dIVIM) were not relevant for the analysis.

Bacterial growth control trajectories, assessed in the static and dynamic IVIM, were described by a bacterial life cycle model with a relative growth rate constant ($k_{g,N}$), summarising bacterial growth and natural death in one parameter [54]. The unexposed viable bacterial population (N) reached a maximum number ($popmax$) in the stationary growth stage and bacteria were

allowed to transform into non-cultivable persister cells (P), quantified by the first-order transformation rate constant k_{NP}. Persister cell formation increased with bacterial numbers approximating the maximum population size in the stationary stage according to Equation 2.8. The persister population was assumed to grow with a persister growth rate constant $k_{g,P}$, being an order of magnitude lower compared to viable bacteria [120], according to Equation 2.9. Hence, the persisting bacterial subpopulation contributed to the population maximum to a lesser degree compared to the viable bacterial population (Equations 2.8-2.10, [120]). Back-transformation of persister cells to the cultivable state was quantified by the first-order transformation rate constant k_{PN} , whereby one persister cell was assumed to divide into two viable cells. The initial bacterial number of viable cells (N_0) was estimated, while persister cells were not assumed to be initially present in the inoculum.

$$\frac{dN}{dt} = k_{g,N} \cdot \left(1 - \frac{N + \frac{P}{10}}{popmax}\right) \cdot N - k_{NP} \cdot N + 2 \cdot k_{PN} \cdot P \qquad IC: N_{t=0} = N_0 \qquad (2.8)$$

$$k_{g,P} = \frac{k_{g,N}}{10} \qquad (2.9)$$

$$\frac{dP}{dt} = k_{g,P} \cdot \left(1 - \frac{N + \frac{P}{10}}{popmax}\right) \cdot P + k_{NP} \cdot N - k_{PN} \cdot P \qquad IC: P_{t=0} = 0 \qquad (2.10)$$

2.4.2.4 Bacterial killing and persister formation under static levofloxacin exposure

In the bacterial growth model to describe bacterial growth and kill behaviour under static LEV exposure, two manifestations of the LEV effect were included: A LEV concentration-dependent killing effect (E_{LEV}) was linked to the viable bacterial population N via a sigmoidal E_{max} model according to Equation 2.11. E_{LEV} of a static C_{LEV} was given by the Hill equation (Equation 2.12, [67]) as a function of three effect parameters: the maximum effect (E_{max}), C_{LEV} causing 50% of the maximum effect (EC_{50}) and the Hill factor (γ), determining the steepness of the concentration-effect relationship. For the three *E. coli* isolates, strain-dependent EC_{50} values were estimated.

$$\frac{dN}{dt} = k_{g,N} \cdot \left(1 - \frac{N + \frac{P}{10}}{popmax}\right) \cdot N - k_{NP} \cdot N + 2 \cdot k_{PN} \cdot P - E_{LEV} \cdot N \quad IC: N_{t=0} = N_0 \qquad (2.11)$$

$$E_{LEV} = \frac{E_{max} \cdot C_{LEV}^{\gamma}}{EC_{50}^{\gamma} + C_{LEV}^{\gamma}} \qquad (2.12)$$

A second LEV effect ($k_{P,LEV}$) was additively linked to the transformation rate constant $k_{NP,0}$ according to Equation 2.13, increasing persister cell formation in the presence of LEV in a C_{LEV}-independent manner. The effect on persister cell formation was estimated strain-dependently for $C_{LEV} > 0$ according to Equations 2.13 and 2.14:

$$k_{NP} = k_{NP,0} + k_{P,LEV} \tag{2.13}$$

$$k_{NP,0} = k_{NP} \cdot \frac{N}{popmax} \tag{2.14}$$

The persisting bacterial subpopulation was assumed to be unaffected by the LEV killing effect. Killing of persisters was only enabled after back-transformation into viable bacteria.

2.4.2.5 Pharmacokinetic model for dynamic *in vitro* infection model experiments

Aiming to facilitate a mathematical characterisation of *in vitro* LEV C(t) trajectories, the concept of a two-compartment PK model was utilised, comprising a central and a peripheral compartment with zero-order input and linear elimination. Different from PK models developed based on clinical data, aiming to quantify mass transfer of drug molecules in a biological system, parameter estimates based on *in vitro* LEV C(t) profiles, i.e. clearance (CL), central volume of distribution (V_c), peripheral volume of distribution (V_p) and intercompartmental clearance (Q), did not represent mass transfer of drug molecules in the *in vitro* setting, because the experimental setup comprised only one culture vessel, preventing distribution of LEV molecules into a second compartment (chapter 2.2.3). Hence, PK parameter estimates were not interpretable in terms of distribution or elimination processes in an organism, but rather determined by the applied experimental settings, such as pump rates. The concenpt of a two-compartment PK model was utilised to compare *in vitro* PK parameter estimates to those of the underlying PK model based on *in vivo* data for a septic patient population, which has been used to determine the experimental settings (chapter 2.2.3). Further, it was pursued to link PK model-predicted LEV C(t) profiles to bacterial growth and kill trajectories. Hence, *in vitro* LEV C(t) profiles were charcterised by Equations 2.15 and 2.16, where A_1 and A_2 represented the LEV amount in the central and the peripheral compartment, respectively, in an *in vivo* system. Transition of drug molecules between the two compartments was quantified by the first-order rate constants k_{12} and k_{21}. The elimination rate constant k_{10} represented elimination of LEV molecules from the central compartment.

$$\frac{dA_1}{dt} = -k_{12} \cdot A_1 + k_{21} \cdot A_2 - k_{10} \cdot A_1 \qquad IC: A_{1,t=0} = 0 \qquad (2.15)$$

$$\frac{dA_2}{dt} = k_{12} \cdot A_1 - k_{21} \cdot A_2 \qquad IC: A_{2,t=0} = 0 \qquad (2.16)$$

Different from bacterial growth and killing processes, theoretical mass transfer of drug molecules was described in the dimension of amounts, but transformed into LEV concentrations in the central (C_1) or the peripheral compartment (C_2), respectively, by dividing by the estimated volumes of distribution V_c and V_p (Equations 2.17– 2.21):

$$C_1 = \frac{A_1}{V_c} \qquad (2.17)$$

$$C_2 = \frac{A_2}{V_p} \qquad (2.18)$$

$$k_{12} = \frac{Q}{V_c} \qquad (2.19)$$

$$k_{21} = \frac{Q}{V_p} \qquad (2.20)$$

$$k_{10} = \frac{CL}{V_c} \qquad (2.21)$$

Individual PK parameters were assumed to be log-normally distributed. Hence, an exponential IIV model (chapter 2.4.2.7) was implemented, representing variability between experimental replicates (i.e. culture vessels). Different from patient-derived PK profiles, *in vitro* LEV C(t) trajectories were determined by the chosen “artificial” experimental settings (chapter 2.2.3), affecting different fixed-effects parameters in a similar manner and resulting in strongly correlated PK parameters. Between the strongest correlated parameters V_C and Q, a scaling factor was introduced to quantify the correlation by relating their IIV.

Experimental parameters were determined based on *in silico* simulations of LEV C(t) profiles of a septic patient population, aiming to *in vitro* mimic the median of the simulated LEV C(t) profiles. For these simulations, the covariate effect of the continuous covariate CLCR on CL, identified in the applied PK model based on clinical data [55,142], was taken into account as fractional change according to Equation 2.3 (chapter 2.2.3).

Stochastic simulations (n=1000) were generated based on the developed PK model based on *in vitro* data, applying the fixed-effects parameter estimates and IIV. Median and 95% CI of these simulations were graphically compared to median and 95% CI of simulations (n=1000)

based on the *in vivo* PK model (Table 7.2, [55,142]), which was used to derive the experimental settings (chapter 2.2.3).

2.4.2.6 PK/PD model of bacterial growth and kill behaviour under static and dynamic levofloxacin exposure

The PK model describing LEV C(t) trajectories in the dynamic IVIM experiments (chapter 2.4.2.5) was linked to the PK/PD model developed based on static IVIM experiments (chapter 2.4.2.4) and evaluated with the full dataset, including both PK and PD data (GC, static and dynamic exposure). Parameters of the PK model as well as parameters characterising bacterial growth and persister formation were fixed, while parameters characterising the LEV effect were re-estimated based on the full dataset. For static exposure, nominal C_{LEV} was linked to bacterial numbers and for the dynamic exposure pattern, individual LEV C(t) profiles, predicted by the PK model, were imputed. As the PK/PD model was developed based on viable bacterial CFU, determined by the droplet plate assay (chapter 2.2.1.3), no direct measure for persister cell formation had been implemented so far. Hence, in the last step, different measures were explored to further inform persister cell formation, leveraging investigations of size distributions by electronic cell counting described in chapter 2.3.2.3. The PK/PD model was extended by a bacterial compartment representing dead cells, either originating from natural death ($k_d \cdot N$), or from LEV induced death of viable bacteria ($E_{LEV} \cdot N$) according to Equation 2.22. By implementing a death rate constant k_d, the natural growth and killing processes were discerned, allowing to alternatively explore implementation of E_{LEV} as effect on k_d. In the final PK/PD model, natural death and LEV-dependent killing were implemented as separate processes, with natural death being only enabled for the viable bacterial population, not for persisters. Consequently, $k_{g,N}$ represented solely natural growth, independent from bacterial death or killing.

The total electronic cell counts were leveraged as a measure for the aggregated bacterial numbers in the three compartments according to Equations 2.22 – 2.24, where P represented the persisting bacterial cells, N represented the viable bacterial cells and D the dead bacterial cells. Incorporating the total electronic cell counts to inform these bacterial compartments enabled estimating numbers of dead cells and persister cells being present in the inoculum before LEV exposure. Furthermore, the full dataset including the total electronic cell counts was exploited to investigate alternative options to implement the LEV effect on k_{NP}, such as a simple and a sigmoidal E_{max} model.

$$\frac{dD}{dt} = k_d \cdot N + E_{LEV} \cdot N \qquad IC: D_{t=0} = D_0 \qquad (2.22)$$

$$CASY\ total\ =\ P + N + D \tag{2.23}$$

$$\frac{dN}{dt} = k_{g,N} \cdot \left(1 - \frac{N + \frac{P}{10}}{popmax}\right) \cdot N - k_{NP}\ \cdot N + 2 \cdot k_{PN}\ \cdot P -\ E_{LEV}\ \cdot N -\ k_d\ \cdot N \tag{2.24}$$

$$IC\colon N_{t=0}\ =\ N_0$$

Log-normal distribution of individual PD parameters was assumed and hence, an exponential IIV model was implemented in a stepwise approach. The forward inclusion and backward deletion technique was utilised [163], based on the difference in OFV (dOFV) as decision criterion to include or delete IIV on a fixed-effect parameter (dOFV of ≥ 3.84 indicating statistical significance, $p < 0.05$, df=1). RUV was implemented as a proportional RUV model, corresponding to additive RUV in the log domain, as individual $\varepsilon_{i,j}$ values were assumed to be normally distributed for both PK and PD observations. RUV was assumed to be mainly attributed to bioanalytical imprecision. Hence, three separate RUV values were estimated, corresponding to the employed bioanalytical methods: a fluorometric assay to determine C_{LEV} (chapter 2.2.1.4), the droplet plate assay to determine viable bacteria (chapter 2.2.1.3) and the electronic cell counting assay to determine total numbers of bacterial cells in the three bacterial compartments (chapter 2.3.2). RUV of PD observations was estimated jointly for growth controls and exposed bacteria.

2.4.2.7 Pharmacokinetic/pharmacodynamic nonlinear mixed-effects modelling

The term “nonlinear mixed-effects” indicates that a nonlinear relationship between the estimated parameters and the dependent variable, e.g. drug or bacterial concentrations, is characterised, distinguishing between fixed-effect parameters, characterising a process for a typical representative of the population, and random-effects parameters, characterising the variability between individuals of the population [66]. In the area of PK/PD NLME modelling, the term “population” often refers to a group of patients or, like in the present work, comprises a group of individual experimental replicates (chapter 2.4.2.1). Thereby, all observations, e.g. drug concentrations determined in plasma of a patient or bacterial concentrations assessed in an IVIM experiment, can be fully exploited, because also individuals or replicates being less informative than others, e.g. because of contributing less observations, can be included in the analysis. Hence, NLME modelling is especially beneficial when data is sparse or imbalanced. A NLME model comprises three components: (i) the structural submodel, describing the concentration-time trajectory of a typical representative of a population, (ii) the stochastic submodel, representing the different levels of intra- and interindividual variability and, potentially, (iii) the covariate submodel, defining the relationship between individual characteristics and model parameters [164].

The structural submodel is a mathematical representation of a complex system, describing the dependent variable of interest as function of input and model parameters. In the context of PK/PD modelling, it represents physiological processes determining a C(t) profile, e.g. of a drug in human plasma, or bacterial numbers in *in vitro* models. Hereby, complex systems are simplified by assuming kinetically homogenous distribution spaces, so-called “compartments”, to which observed amounts of the quantity of interest can evenly distribute. Parameters quantifying the mass transfer of drug molecules, or - in the context of bacterial growth models - bacterial cells, and the volumes of compartments constitute the fixed-effects parameter vector Θ, describing the typical C(t) trajectory of the population.

The stochastic submodel comprises different levels of variability, such as IIV, variability within one individual (interoccasion variability) and RUV, quantified by the random-effects parameters. As PK parameters are positive and typically right-skewed distributed, PK data is often logarithmically transformed and a log-normal distribution of PK parameters is assumed [154,165]. Here, the individual parameter estimate $\theta_{i,k}$ is related to the typical population parameter value θ by an exponential IIV model (Equation 2.25), describing the deviation between the individual parameter $\theta_{i,k}$ of the i^{th} individual for the k^{th} parameter and the typical parameter value θ_k for the population [154]:

$$\theta_{i,k} = \theta_k \cdot e^{\eta_{i,k}} \tag{2.25}$$

The individual random-effects parameters η_k of all individuals *i* are assumed to be normally distributed, with a mean of zero and a variance ω^2. Variances of random-effect parameters quantifying the IIV (e.g. with two parameters: ω_1^2, ω_2^2) are denoted in the Ω matrix. When random effects are not correlated, the Ω matrix can be reduced to the diagonal vector. For correlated random effects, covariance terms are added and represented as off-diagonal elements in the Ω matrix (Equation 2.26).

$$\Omega = \begin{pmatrix} \omega_{1,1}^2 & \omega_{2,1}^2 \\ \omega_{1,2}^2 & \omega,_{2,2}^2 \end{pmatrix} \tag{2.26}$$

For easier interpretation, it is common to report the variance by transforming the parameter estimate of ω^2 to the corresponding coefficient of variation (CV, %) according to Equation 2.27:

$$CV, \% = \sqrt{e^{\omega_k^2 - 1}} \cdot 100 \tag{2.27}$$

RUV comprises variability from various sources, such as bioanalytical imprecision or model misspecification. The random-effect parameters $\varepsilon_{i,j}$ characterises the deviation between observations and individual predictions, based on the individual model parameters, for the i^{th} individual and the j^{th} observation. The individual predictions can be linked to the observations applying different residual variability models, such as additive, proportional, combined or

exponential residual variability models. Similarly to $\eta_{i,k}$ values, $\boldsymbol{\varepsilon}_{i,j}$ values are assumed to be normally distributed with a mean of zero and a variance σ^2, which constitute the ∑ matrix [164].

The covariate model facilitates quantification of the impact of a certain characteristic, such as age, sex or renal function of a patient on the individual estimate for a specific fixed-effects parameter. Covariates can be continuous, if their values are not interrupted, or categorical, if values constitute distinct classes [69]. In this work, the bacterial strain (ST58, ST88 or ST167) and the experimental setting (static or dynamic IVIM) were investigated as categorical covariates. Three alternatives for covariate implementation were explored: (i) estimation of distinct fixed-effect parameters for each bacterial strain or experimental setting, (ii) estimation of the absolute change from the population estimate (Equation 2.28), and (iii) estimation of the fractional change from the population estimate (Equation 2.29). Implementation as absolute or fractional change, respectively, are exemplified for the investigated covariate effect of the static experimental setting compared to the dynamic setting as reference on the maximum bacterial number ($popmax$) in Equation 2.28 and 2.29:

$$\theta\ popmax_{static} = \theta\ popmax_{dynamic} + \theta_{absoulte\ change} \tag{2.28}$$

$$\theta\ popmax_{static} = \theta\ popmax_{dynamic} \cdot (1 + \theta_{fractional\ change}) \tag{2.29}$$

For **parameter estimation**, MLE is applied, as described above (chapter 2.4.1.3). In addition to the fixed-effects parameters vector $\boldsymbol{\Theta}$, the random-effects parameter matrices $\boldsymbol{\Omega}$ (IIV) and ∑ (RUV) are estimated. Hence, the likelihood function can be expressed as the product of the individual probability density functions according to Equation 2.30:

$$L_i(\theta, \omega^2, \sigma^2|Y_i) = p(Y_i|\theta, \omega^2, \sigma^2) = \prod_{j=1}^{n} L\left(\theta, \omega^2, \sigma^2|Y_{ij}\right) \tag{2.30}$$

The set of parameter values minimising the OFV, calculated as minus twice the natural logarithm of the likelihood, is sought during the estimation process. Different estimation algorithms are available, such as first-order estimation, first-order conditional estimation, first-order conditional estimation with interaction and Laplacian conditional estimation [154]. In this work, the Laplacian method was applied, enabling application of the so-called “M3 method” to account for observations below the LLOQ (chapter 2.4.2.1) [161,166].

2.4.2.8 Nonlinear mixed-effects model evaluation

The model development process was guided by numerical and basic graphical model evaluation techniques and plausibility of parameter estimates. Nested models were compared using the likelihood ratio test, calculating the dOFV of two competing models, which was determined as minus twice the natural logarithm of the likelihood. A model was considered to be superior, when for one parameter difference a decrease in OFV was ≥ 3.84, which indicates statistical significance at the 0.05 significance level, assuming a χ^2 distribution with one degree of freedom [69]. AIC was used to compare between non-nested models (chapter 2.4.1.3). For graphical model evaluation, key diagnostic plots were generated: To assess the so-called goodness-of-fit (GOF), observed concentrations were plotted against population predictions and individual predictions. Here, narrow and even distribution of data points around the line of identity was aimed for, indicating no bias in the structural model [167]. Conditional weighted residuals were determined according to Hooker et al. [168] and depicted against time, individual and population predictions and observed concentrations to investigate the appropriateness of the stochastic submodel, indicated by data points scattering narrowly and randomly around y=0.

Parameter precision and accuracy of key models was assessed by the sampling importance resampling (SIR) technique, providing more reliable metrics of parameter uncertainty than the relative standard error of parameter estimates, calculated based on the variance-covariance matrix [169,170]. SIR does not take any distributional assumptions and is therefore superior in cases of complex models, when the assumption of normally distributed model parameter estimates may not be justified. The SIR algorithm comprises three iteratively performed steps: In the first step (sampling), M parameter vectors are randomly sampled from a proposal distribution. Second, importance weighting is performed by computing an importance ratio for each sampled parameter vector. The weighting factor represents the probability of the sampled parameter vector to belong to the “true”, i.e. unknown, parameter distribution. Hence, parameter vectors with a high importance ratio are sampled with a higher probability in the third step, when m new parameter vectors are sampled from the pool of M simulated vectors. A new proposal distribution is then obtained by fitting a multivariate Box-Cox distribution to the resamples [170]. In this work, the first proposed distribution was based on the covariance matrix and three iterations were performed, with a samples/resamples ratio of 5 (first iteration: 500 samples, 100 resamples; second iteration: 1000 samples, 200 resamples, third iteration: 2000 samples, 400 resamples). SIR was considered successful, when the proposed dOFV distribution in the last iteration was below the reference χ^2 distribution with degrees of freedom equal to the number of estimated parameters. When the obtained dOFV distribution was not

entirely below the reference distributions, three additional SIR iterations were performed, based on the last new proposal distribution.

Simulation-based model evaluation techniques were applied for key models. The **predictive performance** of the PK model was evaluated by stratified visual predictive checks (VPC) for the two *in vitro* mimicked dosing regimens, before linking predicted *in vitro* C_{LEV} to bacterial numbers in the final PK/PD model. 1000 stochastic simulations based on the PK model, assuming log-normally distributed fixed-effects parameters and including IIV, were performed based on the developed PK model for each dosing regimen. The median, 5^{th} and 95^{th} percentile of observations were graphically compared to the respective percentiles of the simulations, including the 90% confidence interval (CI) around each percentile. Predictive performance of the final PK/PD model was evaluated by stratified VPCs for bacterial numbers in static and dynamic IVIM experiments. Additionally, the median and 90% CI around the median of the simulated fraction of bacterial numbers being below the LLOQ was graphically compared to the observed fraction of bacterial concentrations below the LLOQ.

Robustness of the PK model was evaluated utilising case deletion diagnostics, aiming to identify influential experimental replicates by excluding those replicates showing multiple observed C_{LEV} outside of the 90% prediction interval of the VPC. PK parameters were re-estimated for the datasets excluding those replicates and estimates were compared to those obtained based on the full dataset. Robustness of the final PK/PD model, based on both static and dynamic IVIM experiments and two different bacterial quantification assays was evaluated by re-estimating all parameters simultaneously. Parameter estimates were compared to those obtained previously in the sequential model development process, based on the final PK/PD model.

2.4.2.9 Nonlinear mixed-effects model exploration

Stochastic simulations (n=1000) based on the final PK/PD model were performed to investigate the trajectories of bacterial numbers of the three bacterial subpopulations for the respective three *E. coli* isolates. The LEV killing effect and the effect on persister formation were analysed graphically and compared between the isolates. The impact of the two discerned LEV effects was investigated by simulating two scenarios: (i) The killing effect was omitted by fixing E_{max} to 0, and solely persister cell formation was assumed, and (ii) the effect on persister cell formation was omitted by fixing $k_{P,LEV}$ to 0 (n=1000 simulations, each). Trajectories of bacterial populations were compared between the simulated scenarios.

2.5 Statistics

In addition to specific numerical evaluation techniques, introduced in 2.4, some general statistical metrics and methods were applied. Statistical analyses were performed in R®/RStudio [171,172].

2.5.1 Descriptive statistics

To characterise the central tendency and dispersion of a vector of measured or simulated data, the following metrics were applied [173]:

- Arithmetic mean $$\bar{x} = \frac{1}{n} \cdot \sum_{i=1}^{n} x_i \quad (2.31)$$
- Median $$\tilde{x} = \begin{cases} x_{\frac{n+1}{2}} & for\ uneven\ n \\ \frac{1}{2}\left(x_{\frac{n}{2}} + x_{\frac{n}{2}+1}\right) & for\ even\ n \end{cases} \quad (2.32)$$
- Variance $$\sigma^2 = \frac{\sum_{i=1}^{n}(x_i - \bar{x})^2}{n-1} \quad (2.33)$$
- Standard deviation $$\sigma = \sqrt{\sigma^2} \quad (2.34)$$
- Coefficient of variation (CV,%) $$CV, \% = \frac{\sigma}{\bar{x}} \cdot 100 \quad (2.35)$$

- Percentiles: The n^{th} percentile indicates the value in a vector of observations below which n% of the observations fall.
- Confidence interval: The confidence interval representing a confidence level of e.g. 95% (95% CI) indicates the lower and upper limit of the range of possible values in which a point estimate falls with a probability of 95%.

2.5.2 **Linear regression**

Linear regression analysis was performed to characterise the relationship between an emission value, determined by a fluorometric assay (chapter 2.2.1.4) and the corresponding C_{LEV} of the sample. For that purpose, slope and intercept of a linear regression model were estimated using the weighted least squares method, assuming a heteroscedastic error. Measured emission values (y) were linked to C_{nom} of CAL (x) according to equation 2.36:

$$y = slope \cdot x + intercept \tag{2.36}$$

Slope and intercept were estimated using the weighted least squares methods, aiming to minimise the weighted sum of squared residuals (WSSR) by applying a weighting factor $W_i = \frac{1}{y^2}$.

$$WSSR = \sum_{i=1}^{i=n} (\hat{y} - y_i)^2 \cdot \frac{1}{y^2} \tag{2.37}$$

$\hat{y} = predicted\ value\ of\ y$
$y_i = \ observed\ value\ of\ y$

The coefficient of determination R^2 was computed to evaluate the goodness of fit of the calibration function. Linear regression was performed using the `lm´ function in R®.

2.5.3 **Hypothesis testing**

The Shapiro-Wilk normality test was applied to show normal distribution of differences between C_{LEV} of samples before ultrafiltration and in ultrafiltrate of the respective samples (chapter 2.2.1.5). For parametric comparison between paired samples, a two-sided t-test was carried out. The test value t was calculated according to equation 2.38:

$$t = \frac{\frac{\sum d_i}{n}}{\sqrt{\frac{\sum d_i^2 - \frac{(\sum d_i)^2}{n}}{n \cdot (n-1)}}} \tag{2.38}$$

$d: difference\ of\ paired\ samples\ x_i - y_i$
$n: number\ of\ pairs$
$df = n - 1$

3 Results

3.1 Characterisation of bacterial growth and kill behaviour

In the following chapter, insights in bacterial growth and kill behaviour under static and dynamic LEV exposure in IVIM experiments are presented. Prior to IVIM experiments, the MIC values of three clinical *E. coli* isolates were determined (chapter 3.1.1). To ensure controlled and reproducible experimental conditions, (i) LEV stability in the sIVIM over three days was shown (chapter 3.1.2) and (ii) the impact of potential LEV binding to components of the growth medium was investigated (chapter 3.1.3). Time-kill experiments were performed under static LEV exposure (chapter 3.1.4) and finally mimicking clinically relevant LEV C(t) profiles in the dynamic IVIM (chapter 3.1.5).

3.1.1 Minimal inhibitory concentration

The MIC values of the three *E. coli* isolates were determined as the lowest C_{LEV} inhibiting bacterial growth after 16-20 h of incubation [36], as 2 mg/L for the *E. coli* isolate ST88 (Figure 7.3), while the MIC value of ST58 (Figure 3.1) and ST167 (Figure 7.4) was 8 mg/L. No visible growth was detected in the sterility controls, while growth controls displayed visible turbidity.

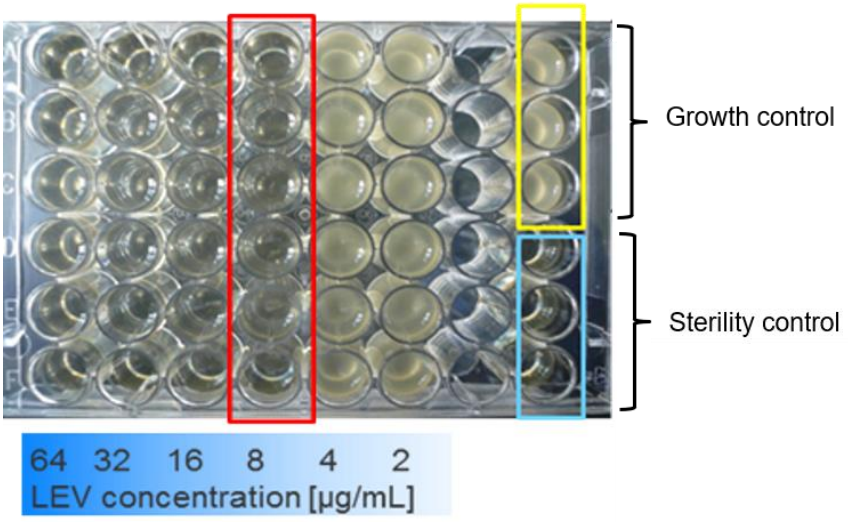

Figure 3.1: Minimal inhibitory concentration (MIC), determined by the microdilution method, exemplified for *Escherichia coli* sequence type 58. Levofloxacin (LEV) concentrations in each well in a row are displayed below the corresponding vertical row; growth control (yellow frame): bacterial suspension without LEV addition; sterility control (blue frame): growth medium without bacteria or drug; red frame indicates LEV MIC of the isolate (8 mg/L).

3.1.2 Levofloxacin stability in the static *in vitro* infection model

Stability of C_{LEV} in the static IVIM was investigated for a concentration range between 2 mg/L and 16 mg/L over three days. All measured C_{LEV} were within ±15% of the nominal concentration (Figure 3.2), corresponding to the accepted bioanalytical imprecision of the applied fluorometric assay [135]. No trend of decreasing C_{LEV}, indicating degradation of the compound, was observed within ≥ 72 h.

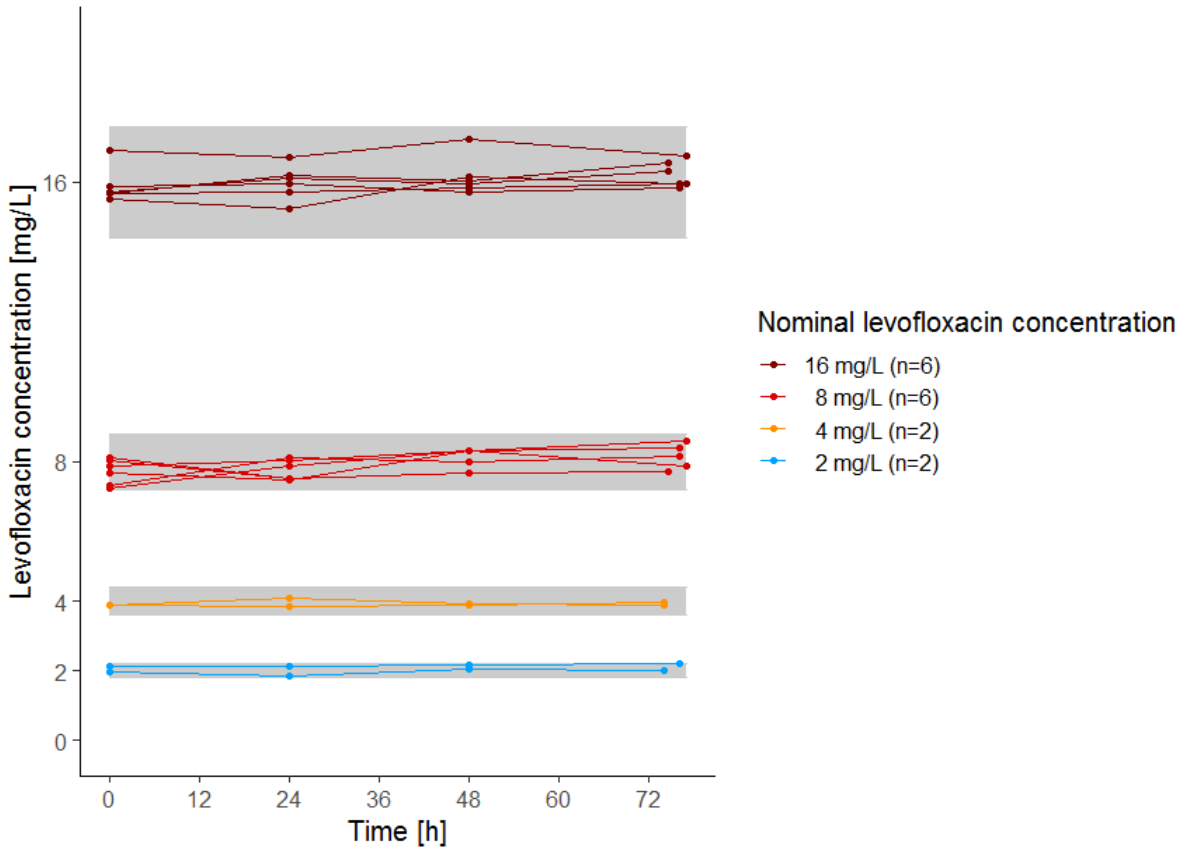

Figure 3.2 Levofloxacin stability in the static *in vitro* infection model over 3 days, colours: respective levofloxacin concentrations, shaded areas: ±15% deviation of nominal concentration, points: measured levofloxacin concentrations, lines connect measurements in one replicate.

3.1.3 Levofloxacin binding to growth medium components

The impact of LEV binding to macromolecules in the bacterial growth medium was investigated by performing calibration according to the fluorimetric LEV quantification assay (chapter 2.2.1.4). Ultrafiltration of CAL was carried out to separate protein bound molecules from the f_u of LEV in the sample. Calibration functions obtained before ultrafiltration and in ultrafiltrate were compared. Overall, slope and intercept values were lower for the regression function of CAL before ultrafiltration, compared to the regression functions of the ultrafiltrate (Table 3.1, Figure 3.3). Linearity was acceptable ($R^2 \geq 0.98$) for each of the three experiments and for linear regression based on merged measurements of experiment 1, 2 and 3.

Table 3.1: Intercept, slope and coefficient of determination (R^2) of calibration functions for levofloxacin quantification before ultrafiltration and in ultrafiltrate, obtained from three experiments (n=2 replicates per experiment and 3-fold measurement of each replicate), and from merged data of three experiments; AU: arbitrary units.

Experiment	Sample	Intercept [AU]	Slope [(AU·mL)/µg]	R^2
1	Before ultrafiltration	-18.4	13461	0.9989
	Ultrafiltrate	241	13755	0.9991
2	Before ultrafiltration	137	15174	0.9985
	Ultrafiltrate	553	15165	0.9991
3	Before ultrafiltration	-138	15405	0.9948
	Ultrafiltrate	41.3	15516	0.9939
1 - 3 (merged)	Before ultrafiltration	1.24	14583	0.9881
	Ultrafiltrate	284	14742	0.9902

The prerequisite for a two-sided, paired t-test was met, as differences between C_{LEV} before ultrafiltration and in the respective ultrafiltrate were normally distributed (Shapiro-Wilk test, $p = 0.116$; Figure 7.5). H_0 ($\mu(C_{LEV,cal,before\ ultrafiltration}) = \mu(C_{LEV,cal,ultrafiltrate})$) was not rejected with a confidence level of $p > 0.95$, indicating no difference between C_{LEV} in CAL before ultrafiltraton and in C_{LEV} in ultrafiltrate.

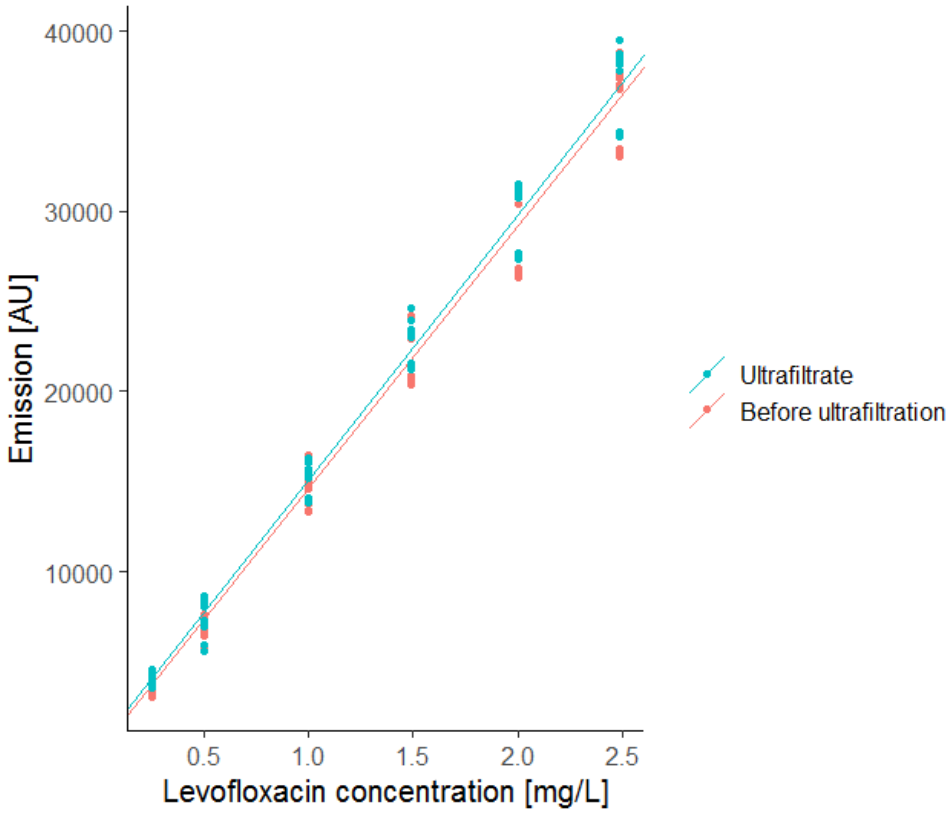

Figure 3.3: Calibration functions for levofloxacin quantification in cation adjusted Mueller Hinton broth in ultrafiltrate (blue line) and before ultrafiltration (red line), obtained from three single experiments (n=2 replicates per levofloxacin concentration and experiment, 3-fold determination of each replicate); points represent arithmetic mean of 3 single determinations per replicate in arbitrary units (AU) against nominal levofloxacin concentration, solid lines: weighted linear regression ($1/y^2$).

Comparison between calculated C_{LEV} according to the respective calibration function obtained before ultrafiltration and in ultrafiltrate, respectively, and C_{nom} showed strong agreement (R^2=0.9924, Figure 3.4).

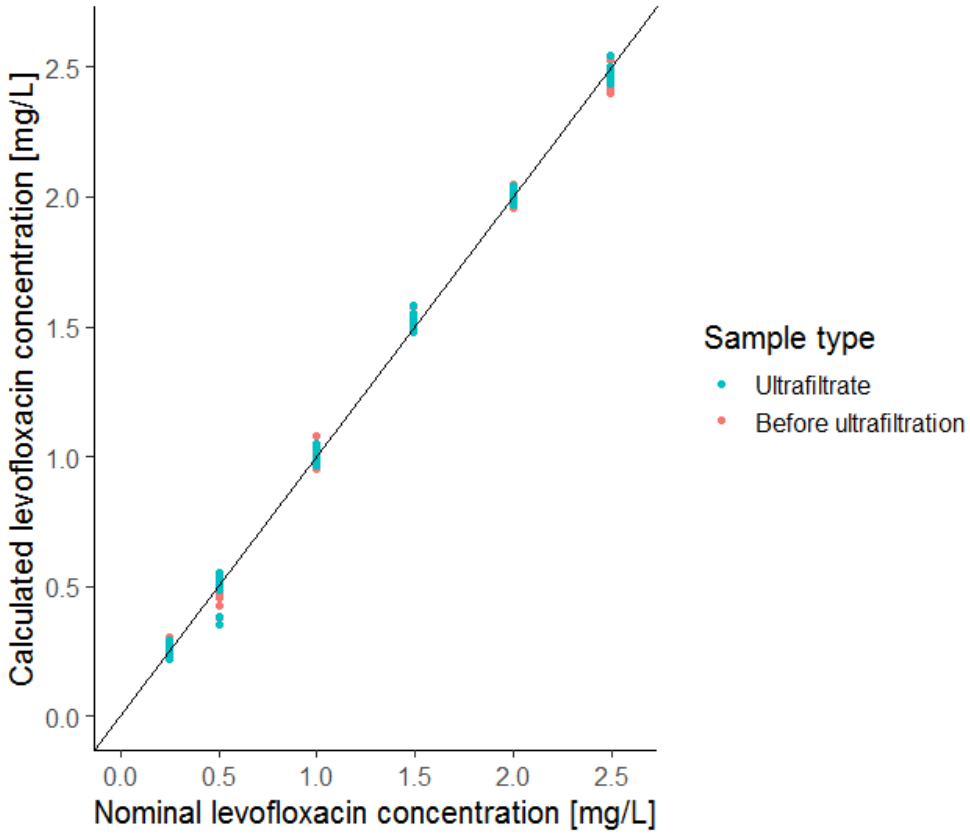

Figure 3.4: Levofloxacin concentration [mg/L], calculated based on linear regression functions for calibrator solutions in ultrafiltrate (blue points) and before ultrafiltration (red points) against nominal levofloxacin concentrations; solid line: weighted ($1/y^2$) linear regression function (slope: 0.993, intercept: 0.00220, R^2=0.9924), n=108.

3.1.4 Static *in vitro* infection model experiments

Before exposing three LEV resistant clinical *E. coli* isolates to constant C_{LEV} in the sIVIM, the reference strain *E. coli* ATCC 25922 was investigated under exposure to static C_{LEV} between 0.016 mg/L (0.5-fold MIC) and 0.064 mg/L (2-fold MIC), aiming to characterise the growth kill behaviour of a LEV susceptible strain (Figure 3.5). Additionally, a GC was performed to assess bacterial growth without antibiotic exposure. Starting from an inoculum concentration between $3.4 \cdot 10^6$ CFU/mL (GC) and $8 \cdot 10^6$ CFU/mL (2-fold MIC exposure), C_{LEV}-dependent growth-kill trajectories were observed: The GC displayed exponential growth between t=0 h and t=6 h and subsequently, constant bacterial concentrations were maintained in the stationary growth stage until the end of the experiment at t=25 h, with a final bacterial concentration of $1.3 \cdot 10^{10}$ CFU/mL. Under exposure to 0.5-fold the MIC of the susceptible strain (0.032 mg/L), bacteria were reduced to a minimum concentration of 10^4 CFU/mL at t=6 h, representing a 2.4 $\log_{10}$-

fold reduction compared to the initial bacterial concentration at t=0 h ($5.4 \cdot 10^6$ CFU/mL). Afterwards, regrowth was observed, nearly reaching the initial concentration of $2.5 \cdot 10^6$ CFU/mL at t=25 h. A similar shape of the growth-kill trajectory was observed for bacteria under 1-fold MIC exposure: After a 4.4 $\log_{10}$-fold initial decline of bacterial concentration below the LLOQ of the droplet plate assay for the respective sample (100 CFU/mL) within 2 h, regrowth was observed within 24 h, reaching $7.4 \cdot 10^4$ CFU/mL after 25 h. Similarly, bacteria exposed to the 2-fold MIC were reduced to a concentration below 100 CFU/mL within 1.5 h and displayed regrowth up to $5.5 \cdot 10^2$ CFU/mL within 25 h.

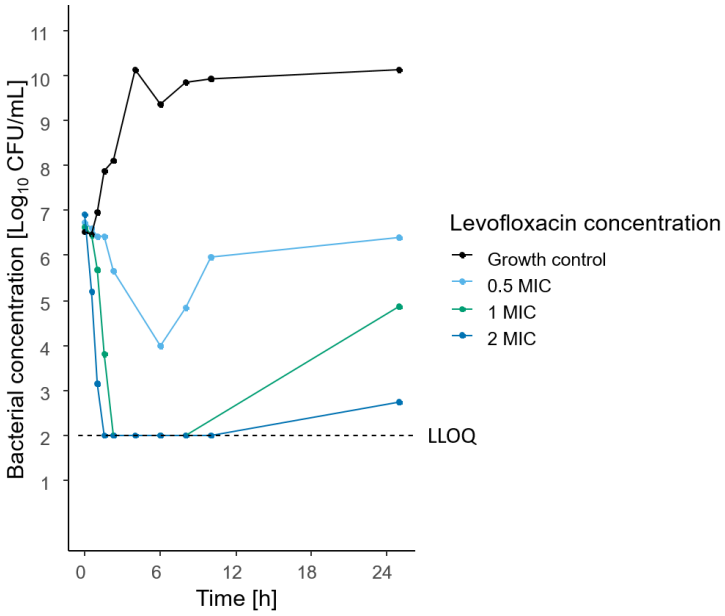

Figure 3.5: Growth-kill behaviour of *Escherichia coli* ATCC 25922 under exposure to constant levofloxacin concentrations in a static *in vitro* infection model experiment (n=1 per levofloxacin concentration), colours: levofloxacin concentrations, normalised to the minimal inhibitory concentration of the strain (MIC=0.032 mg/L), black line: growth control (GC), points: bacterial concentrations, quantified as colony forming units (CFU) per mL, dashed line: lower limit of quantification (LLOQ), experimental settings: see Table 7.1.; ATCC: American Type Culture Collection.

Bacterial growth without antibiotic exposure was comparable between the reference strain ATCC 25922 and the three clinical isolates (Figure 3.5 and Figure 3.6, black symbols and lines). Furthermore, the shape of time-kill trajectories of the resistant isolates under LEV exposure were similar to the LEV susceptible strain for the respective MIC-normalised C_{LEV}. Like the reference strain, the *E. coli* isolates displayed an initial reduction of bacterial concentrations, mostly followed by regrowth, when exposed to static C_{LEV} of 1-fold their MIC (Figure 3.6). However, the extent of the initial decline, time of the minimum bacterial concentration and magnitude of regrowth were strain-specific:

ST58: When exposed to C_{LEV} of 0.5-fold the MIC (light blue points and line, n=1 replicate), ST58 showed delayed growth reaching a bacterial concentration one order of magnitude below the GC ($5 \cdot 10^8$ CFU/mL) after 24 h. When exposed to static C_{LEV} of 1-fold the MIC (green points and lines, n=4 replicates), bacterial concentration of the isolate was reduced between 0.5- and 2 $\log_{10}$-fold, representing the smallest extent of initial bacterial killing compared to the other isolates. The minimal bacterial concentration was observed between t=4 h and t=10 h, followed by regrowth within 24 h up to > 10^8 CFU/mL for all replicates exposed to 1-fold MIC. Being exposed to C_{LEV} of 2-fold MIC (dark blue points and lines, n=5 replicates), the isolate displayed regrowth after initial bacterial reduction within 24 h in 3 replicates to > 10^3 CFU/mL. For 2 replicates being exposed for 3 days, regrowth was observed up to the magnitude of the GC (10^{10} CFU/mL) at t=76 h. Eradication (i.e. bacterial concentrations below the LLOQ at t=24 h) was observed under exposure to C_{LEV} of 4-fold MIC (red points and lines, n=2 replicates) and under exposure to 8-fold the MIC (pink points and line, n=1). Of note, the LLOQ of the droplet plate assay differed between samples belonging to one replicate (chapter 2.2.1.3).

ST88: When exposed to C_{LEV} of 0.25-fold its MIC (yellow points and line, n=1), ST88 displayed delayed growth and reached final bacterial concentrations of the magnitude of the GC at t=27 h ($1.2 \cdot 10^{10}$ CFU/mL). Final concentrations were one order of magnitude lower compared to the GC when exposed to C_{LEV} of 0.5-fold MIC (n=3). Under 1-fold MIC exposure (n=5), the bacterial population was reduced to minimal concentrations between 10^3 CFU/mL and $3 \cdot 10^5$ CFU/mL between t=4 h and t=6 h. Following, the bacterial population of ST88 displayed regrowth up to > 10^8 CFU/mL within 24 h in all replicates. Under exposure to C_{LEV} of 2-fold the MIC (n=5), bacterial concentrations declined to a minimum 3 $\log_{10}$-fold lower compared to the initial bacterial concentration, followed by slight bacterial regrowth up to ≥ 10^2 CFU/mL within 24 h in 2 replicates and up to > 10^8 CFU/mL at t= 73.5 h in 2 further replicates. Exposed to C_{LEV} of 4-fold the MIC, bacterial eradication within 24 h was observed (n=1).

ST167: When ST167 was exposed to C_{LEV} of 0.5-fold MIC in on replicate, bacterial concentrations decreased below the LLOQ, followed by regrowth reaching bacterial concentrations comparable to the GC ($8 \cdot 10^8$ CFU/mL). Under exposure to C_{LEV} of 1-fold the MIC (n=7), the bacterial population reached its minimum concentration of approx. 10^3 CFU/mL between 2 h and 6 h, followed by regrowth up to $4.3 \cdot 10^5$ within 24 h in one replicate and > 10^8 CFU/mL within 48 h in three more replicates. In three replicates, bacterial eradication was observed under exposure to 1-fold MIC within 48 h. Being exposed to C_{LEV} of 2-fold its MIC (n=7), ST167 displayed regrowth up to > 10^3 CFU/mL in two replicates within 24 h and 28 h, respectively, and eradication within ≥ 48 h in 4 replicates.

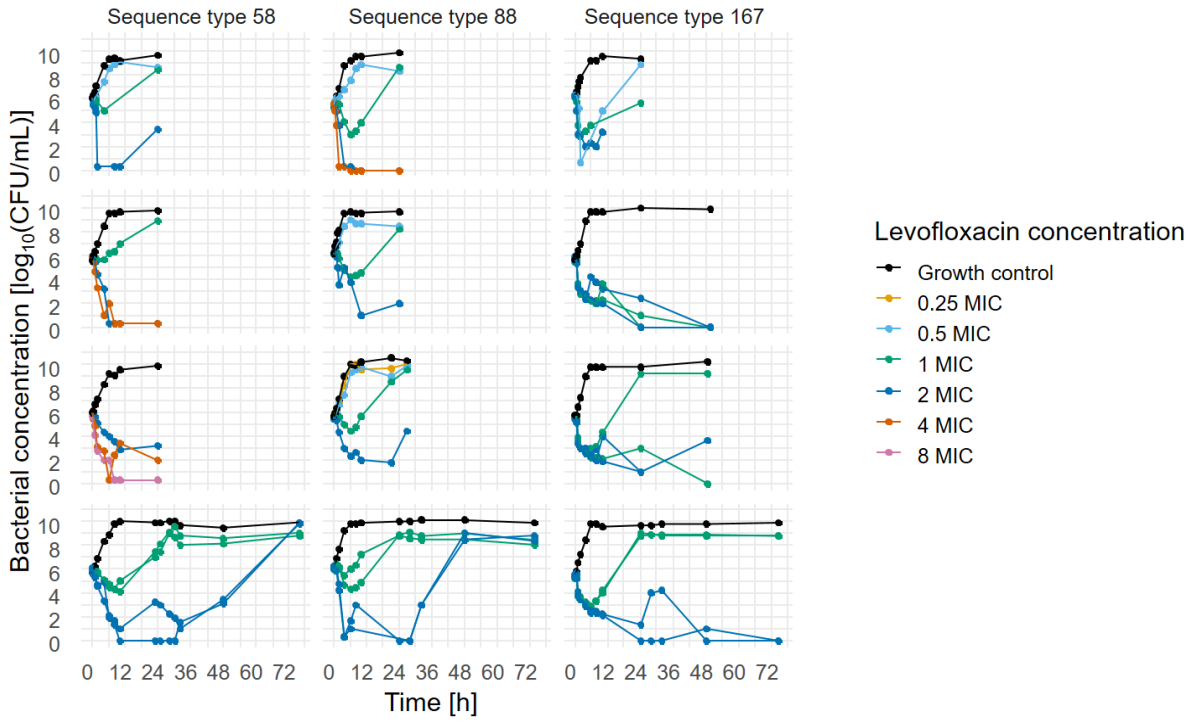

Figure 3.6: Growth-kill behaviour of 3 *Escherichia coli* isolates (left: sequence type 58, middle: sequence type 88, right: sequence type 167) under exposure to constant levofloxacin concentrations in 12 static *in vitro* infection model experiments, colours: levofloxacin concentrations, normalised to the minimal inhibitory concentration (MIC) of the isolate, black lines: growth behaviour of unexposed bacteria, points: bacterial concentrations, quantified as colony forming units (CFU) per mL, experimental settings: see Table 7.1.

3.1.5 Dynamic *in vitro* infection model experiments

In the dynamic *in vitro* infection model, clinically relevant LEV C(t) profiles resulting from a 750 mg, 90 min i.v. infusion in plasma were successfully mimicked (Figure 3.7). According to the underlying two-compartmental PK model with zero-order infusion and first-order elimination, C_{max} was followed by a biphasic decline of C_{LEV}. 89.4% of measured C_{LEV} were within the 95% CI of 1000 simulated C(t) profiles in plasma of septic patients, based on the PK model used to derive the experimental settings (chapter 2.2.3).

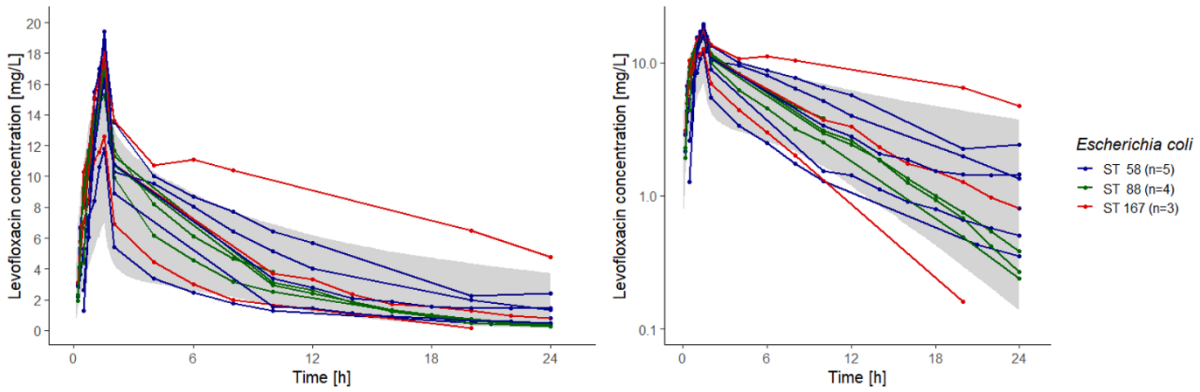

Figure 3.7: Levofloxacin concentration-time profiles resulting from a 750 mg, 90 min intravenous infusion in plasma; mimicked in a dynamic *in vitro* infection model (n=12 replicates), experimental settings based on a two-compartmental pharmacokinetic model with zero-order infusion, shaded area: 95% confidence interval of 1000 levofloxacin concentration-time profiles in plasma of septic patients simulated *in silico*; left: linear scaling; right: semilogarithmic scaling; points: measured concentrations, colours: 3 exposed *Escherichia coli* isolates; ST: sequence type.

C_{max} was reached at t_{max}=1.5 h in all replicates (n=12) and ranged from 11.8 to 19.4 mg/L, while the AUC_{24h} ranged between 47.0 mg·h·L^{-1} and 216 mg·h·L^{-1} (Table 3.2). However, no trend was observed towards lower or larger exposure, in terms of C_{max} and AUC_{24h} values, for one of the isolates. Experimentally observed C_{max}/MIC ratios ranged between 1.48 and 8.95 and AUC_{24}/MIC ratios between 5.87 and 49.0. For one replicate, the AUC_{24h} could not be determined, as the C_{LEV} at t=24 h was missing.

Table 3.2: Pharmacokinetic (PK) and pharmacodynamic (PD) parameters and PK/PD indices in dynamic *in vitro infection* model experiments (n=12 replicates), exposing three clinical *Escherichia coli* isolates to levofloxacin concentration-time profiles resulting from a mimicked single administration of a 750 mg, 90 min intravenous infusion in plasma for 24 h; ST: Sequence type, MIC: Minimal inhibitory concentration, AUC_{24h}: area under the levofloxacin concentration-time profile over 24 h, C_{max}: maximum concentration in the dosing interval.

ST	MIC [mg·L^{-1}]	Levofloxacin C_{max} [mg·L^{-1}]	Levofloxacin AUC_{24h} [mg·h·L^{-1}]	C_{max}/MIC [unitless]	AUC_{24}/MIC [unitless]
58	8	18.9	151	2.36	18.9
58	8	18.5	127	2.31	15.9
58	8	11.8	47.0	1.48	5.87
58	8	16.4	102	2.05	12.75
58	8	19.4	74.2	2.43	9.28
88	2	16.8	78.6	8.40	39.3
88	2	17.9	-*	8.95	-*
88	2	15.3	95.3	7.65	47.6
88	2	17.0	98.0	8.50	49.0
167	8	12.6	54.3	1.58	6.78
167	8	17.3	216	2.16	27.0
167	8	18.1	107	2.26	13.4

* AUC_{24h} not available due to missing C_{LEV} at t=24 h.

Overall, bacterial growth without antibiotic exposure was comparable between the three exposed isolates (Figure 3.8, dashed lines) and similar to bacterial growth in the sIVIM. The exponential growth stage was observed between t=0 h and t=6 h and bacterial concentrations remained constant in the stationary growth stage until the end of the experiment at t=24 h. Different from the sIVIM, bacterial concentrations reached approx. 10^9 CFU/mL in the stationary stage for all isolates, compared to approx. 10^{10} CFU/mL in the sIVIM (Figure 3.6 and Figure 3.8, black lines). Under exposure to the mimicked LEV C(t) profiles, which were comparable between the three strains, the shapes of bacterial concentrations-time trajectories were similar to time-kill curves in the static IVIM, with a strain-dependent initial decline and regrowth within 24 h in all replicates (n=12, Figure 3.8, solid lines). Initial bacterial reduction was maximum 4 log_{10}-fold (below the lower limit of quantification of the droplet plate assay) for ST88 (green points and lines) after 2-4 h, while ST58 (blue points and lines) was only reduced ≤ 2 log_{10}-fold, reaching minimum bacterial concentrations between 2-8 h. Despite sharing the same MIC value of LEV, ST167 (red points and lines) was reduced to a larger extent than ST58, reaching 4 log_{10}-fold reduction between 6 and 10 h. While ST58 and ST167 displayed regrowth reaching final bacterial concentrations mostly of the magnitude of the GC (10^9 CFU/mL) after 24 h, ST88 reached final concentrations at t=24 h below the initial concentration ($7 \cdot 10^3$ to $3.3 \cdot 10^5$ CFU/mL).

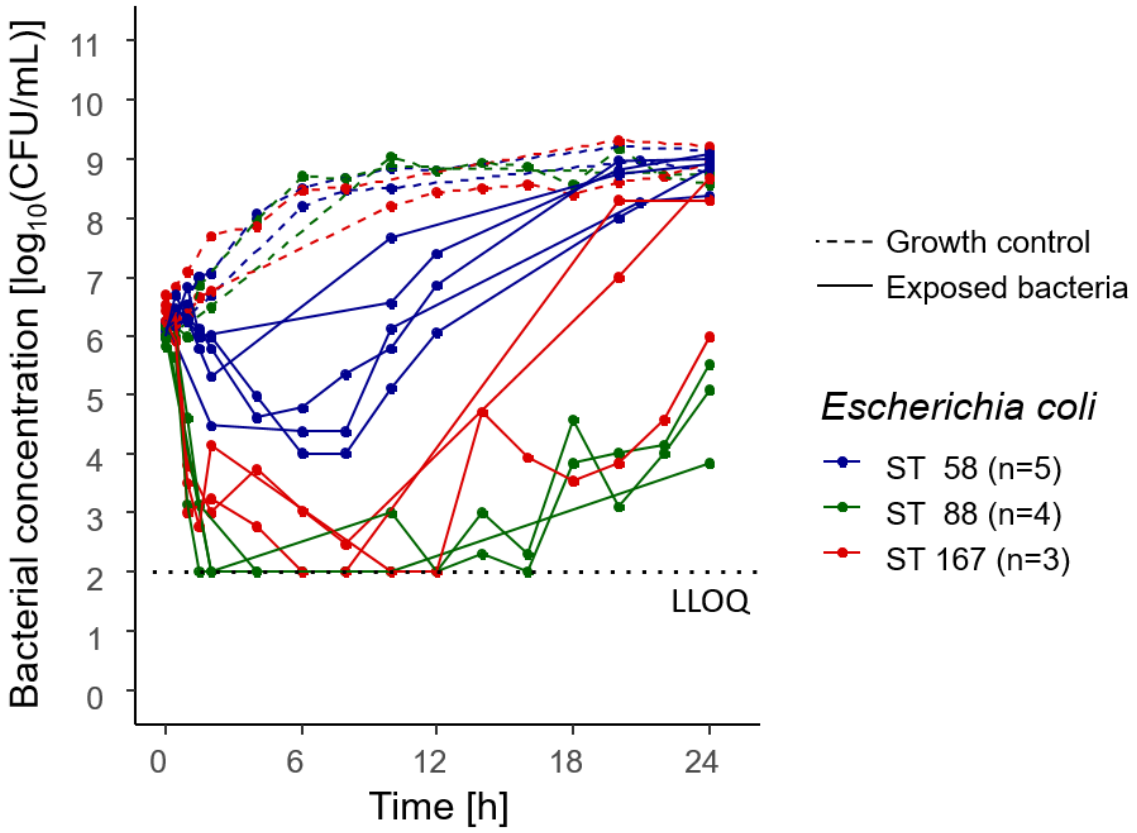

Figure 3.8: Growth-kill behaviour of 3 *Escherichia coli* isolates under exposure to levofloxacin concentration-time profiles resulting from a 750 mg, 90 min intravenous infusion in plasma, mimicked in a dynamic *in vitro* infection model (n=12 replicates, solid lines), and growth control curves of unexposed bacteria (n=6 replicates; dashed lines), points: bacterial concentrations, quantified as colony forming units (CFU) per mL, dotted horizontal line: lower limit of quantification (LLOQ); colours: 3 exposed *Escherichia coli* isolates; ST: sequence type.

3.2 Mechanisms of adaptation and resistance

In the following chapters, insights into the contribution of genomic resistance mechanisms and phenotypic adaptation to the observed strain-specific growth, kill and regrowth behaviour of three *E. coli* isolates are presented. First, genomic resistance mechanisms, i.e. mutations in QRDR of *gyrA* and *parC* of the isolates and presence of *qnrA, qnrB* and *qnrS* plasmids were investigated (chapter 3.2.1). For that purpose, PCR amplification and Sanger sequencing were performed (chapter 2.3.1), sequences were analysed in the software geneious® and results were compared to the web-based analysis of whole genomes sequences of the isolates, utilising the online tool ResFinder 3.2 [143]. Second, a novel method to quantify persister cell formation as postulated mechanism of phenotypic adaptation was developed and applied (chapter 2.3.2). Using electronic cell counting to determine cell size distributions of bacterial populations under LEV exposure in the static IVIM allowed for quantification of filamentous cells and unveiled strain-specific persister cell formation (chapter 2.3.2).

3.2.1 Sequencing and genomic resistance mechanisms

3.2.1.1 Sanger sequencing and sequence analysis

Bacterial DNA fulfilling the desired $A_{260/280}$ ratio was obtained for each *E. coli* isolate from a bacterial subculture which was not exposed to LEV in the IVIM previously and for one isolate (ST88), which was cultivated after being exposed to a C_{LEV} of 2 mg/L (corresponding to the MIC value of the isolate) in the static IVIM for 24 h. The electrophoresis gels showed clear bands for the PCR products of *gyrA* and *parC* obtained from all DNA samples, indicating successful DNA extraction and amplification of QRDR, which was confirmed by successful Sanger sequencing of these PCR products. For the multiplex PCR products of *qnrA/B/S* of *E. coli* ST58 and ST167, no bands were detectable, indicating that the isolates did not harbour *qnrA/B/S* plasmids. Clear bands were visible at 500 bp for PCR products of *qnrA/B/S* amplification of *E. coli* ST88 before and after LEV exposure in the IVIM (Figure 3.9).

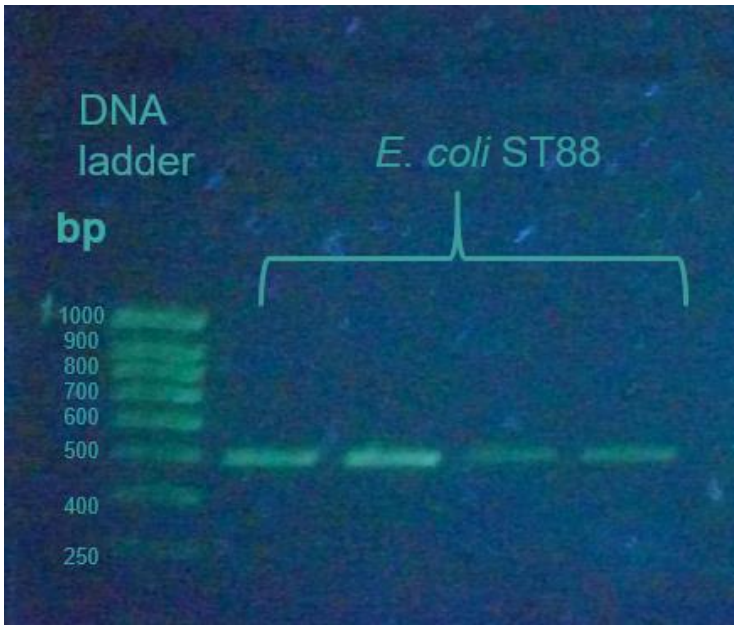

Figure 3.9: Electrophoresis gel with multiplex polymerase chain reaction (PCR) products (n=4) of the fluoroquinolone resistance plasmids *qnrA/B/S,* in *Escherichia coli (E. coli)* ST88, DNA extracted before *in vitro* levofloxacin exposure, and DNA ladder, bands of joint PCR products of *qnrA/B/S* plasmids at 500 base pairs (bp), ST: sequence type.

For all PCR products, high quality sequences (i.e. Phred score > 40 for ≥ 90% of the bases and Phred score < 20 for ≤ 10% of the bases) of both *gyrA* and *parC,* using either primer F or primer R for Sanger sequencing, were obtained and leveraged for further analysis (Table 7.9). Alignment of sequences belonging to one PCR product obtained with the two primers showed > 90% identical bases for all PCR products. Aligning the PCR products with NCBI reference sequences showed ≥ 96.7% identity, indicating sufficient quality of the sequences used for further analysis of mutations in QRDR.

In a next step, DNA sequences were translated into proteins applying six possible reading frames for each sequence and the correct reading frame was identified by alignment with a reference AA sequence. Alterations in the AA sequence of the isolates were determined by comparing the resulting protein sequences to a reference sequence (Figure 3.10).

The *gyrA* mutation Ser83Leu was detected in each of the three isolates. In addition, ST167 harboured the *gyrA* mutation Asp87Asn and the *parC* mutation Ser81Ile.

Further, the nucleic acid sequences of ST88 before and after LEV exposure in the static IVIM were aligned (Figure 3.11). Comparison of the DNA sequences before and after exposure showed 100% identical bases in the protein-coding regions.

Figure 3.10: Alignments of quinolone resistance determining regions (QRDR) for 3 *Escherichia coli* isolates (ST58, ST88 and ST167) with reference sequences; panels A, B, C: parts of protein sequences displaying the *gyrA* alterations Ser83Leu (red circles) and Asp87Asn in ST167 (blue circle); panel D: *parC* alteration Ser81Ile in ST167 (violet circle). Dark green bar represents identical residues between two sequences; annotations [146] describing the functionality of the protein in grey, yellow (CDS: coding sequence) and light green bar, letters represent amino acids: Ala/A: alanine; Arg/R: arginine; Asn/N: asparagine; Asp/D: aspartic acid; Cys/C: cysteine; Gln/Q: glutamine; Gly/G: glycine; His/H: histidine; Ile/I: isoleucine; Leu/L: leucine; Lys/K: lysine; Met/M: methinonine; Phe/F: phenylalanine; Pro/P: proline; Ser/S: serine; Thr/T: threonine; Trp/W: tryptophan; Tyr/Y: tyrosine; Val/V: valine.

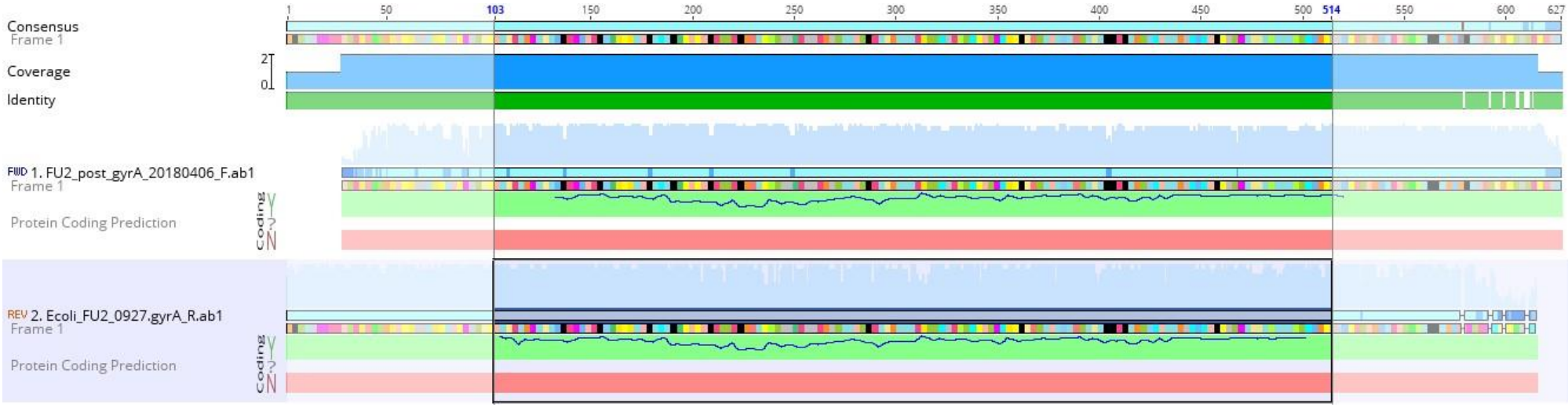

Figure 3.11: Alignment of *gyrA* sequences of *Escherichia coli* sequence type 88, obtained before and after exposing the isolate to a levofloxacin concentration of 2 mg/L for 24 h in the static *in vitro* infection model, including protein coding prediction based on EMBOSS protein analysis [174]. Blue bar represents identical bases with consensus sequence, dark green bar represents identical bases between two sequences; light blue histogram indicates base call quality; blue protein coding prediction graph in light green area indicates protein coding regions in the nucleic acid sequence (non-coding regions: blue graph in red area).

3.2.1.2 Whole genome sequencing and sequence typing

Aiming to validate results obtained with the newly introduced methods, WGS of *E. coli* isolates was performed and relevant mutations for antibiotic resistance and acquired resistance genes were identified using ResFinder 3.2 [143]. Further, MLST was successfully carried out for all investigated sequences, applying both MLST schemes available in MLST-2.0. Identity with the reference alleles was 100% for each gene and each isolate, and the length of alignments of the reference sequences and the respective investigated alleles was equal for all genes (n=7 for scheme 1 and n=8 for scheme 2), indicating a "perfect match" for each of the investigated sequences [149]. According to the Warwick medical school scheme, the isolates were identified as ST58, ST88, and ST167 (Table 3.3, Figure 7.6).

Previously found mutations in QRDR of *gyrA* and *parC* were confirmed by applying ResFinder 3.2 for identification of genomic resistance mechanisms. However, the replacement of serine by isoleucine in ST167 was allocated to position 80, instead of position 81 (Figure 3.10). Further, no mutations were detected in the genes encoding for the subunit B of the type II topoisomerases (*gyrB* and *parE*). Confirming the electrophoresis results (Figure 3.9), *qnr* plasmids were detected in ST88 and could be specified as *qnrS1.* In addition, acquired antibiotic resistance mechanisms to other antibiotic classes were identified and are presented in Table 7.10.

Table 3.3: Sequence types according to 2 multilocus sequence typing (MLST) schemes, levofloxacin minimal inhibitory concentrations (MIC), mutations in quinolone resistance determining regions (QRDR) and acquired fluoroquinolone resistance mechanisms of 3 investigated *Escherichia coli* isolates.

Sequence type (Warwick medical school)	Sequence type (Pasteur institute)	MIC [mg/L]	Mutations in QRDR		Acquired fluoroquinolone resistance
			gyrA	*parC*	
58	24	8	Ser83Leu	WT	-
88	66	2	Ser83Leu	WT	*qnrS1*
167	877	8	Ser83Leu Asp87Asn	Ser80Ile	-

Ser: serine, Leu: leucine, Asp: aspartic acid, Asn: asparagine, Ile: isoleucine, WT: wild type, *qnrS1:* quinolone resistance gene S1.

3.2.2 Bacterial size distributions and phenotypic adaptation

Size distributions of the three *E. coli* isolates ST58, ST88 and ST167 were assessed under LEV exposure in sIVIM experiments using electronic cell counting. Based on increasing cell sizes, indicating filamentation of LEV exposed bacteria, the contribution of persister cell formation to the observed bacterial regrowth was investigated (chapter 2.3.2) In a first step, strain-specific diameter thresholds to discriminate between debris and bacterial cells were identified (chapter 2.3.2.3): 1.25 µm for ST58, 1.55 µm for ST88, and 1.75 µm for ST167 (Figure 7.7). Secondly, different size thresholds to distinguish between regular and increased bacteria were explored graphically (Figure 3.12). The shapes of the time courses of the investigated size classes were similar for the GC curves of the isolates (Figure 3.12, top). As all counts above the respective threshold (3, 4, 5 and 6 µm) were added up to the upper limit of the full measurements size range (15 µm), counts in the respective size class were lower for higher boundaries. Similarly to the GC curves, the shapes of the curves representing counts of LEV exposed bacteria were comparable between the investigated size range boundaries (3, 4, 5 and 6 µm). Under exposure to C_{LEV} of 1-fold MIC or 2-fold MIC, a steep increase in bacterial counts in the size class > 3 µm was observed in the first 6 h of the experiments, followed by constant or slightly decreasing counts > 3 µm between t=6 h and t=12 h. Under exposure to C_{LEV} of 1-fold MIC (Figure 3.12, middle), a steep increase between t=12 h and the end of the experiment followed for all size ranges and for all strains. For ST58 and ST88, similar trajectories were observed under exposure to C_{LEV} of 2-fold the MIC value, while for ST167, bacterial counts remained constant between t=12 h and the end of the experiments (Figure 3.12, bottom).

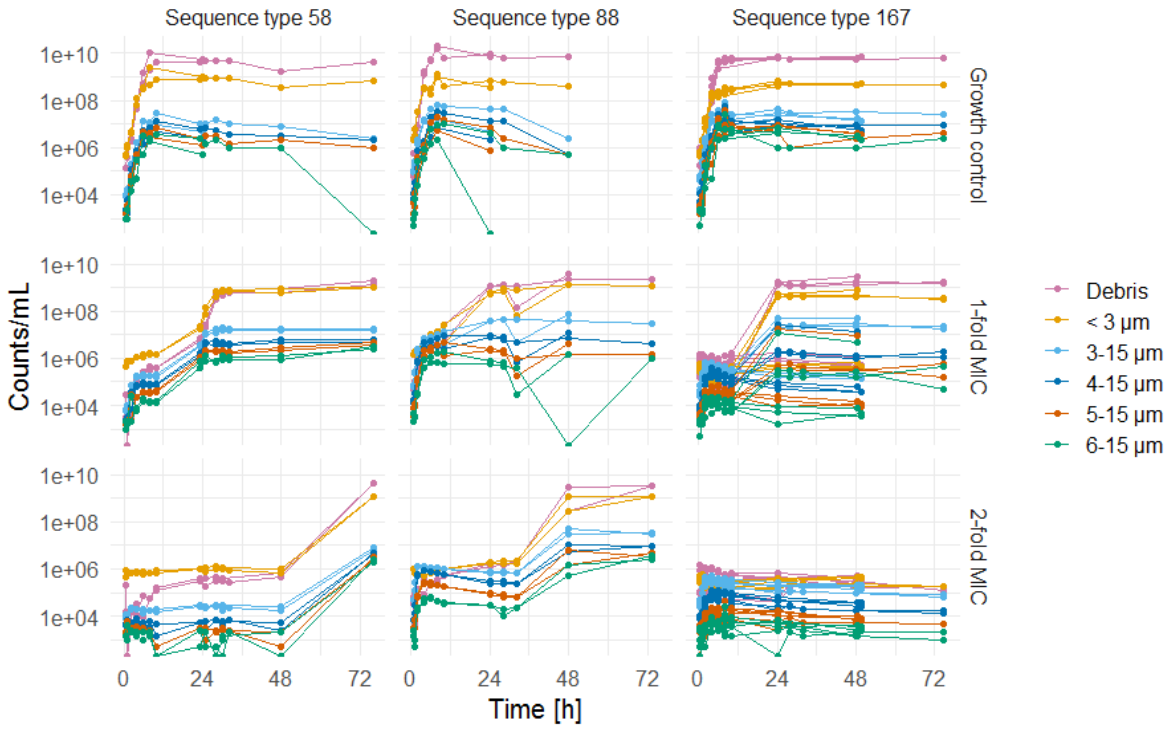

Figure 3.12: Bacterial counts, determined by electronic cell counting, for three *Escherichia coli* isolates (ST58: n=1 experiment, ST88: n=1 experiment, and ST167: n=3 experiments), without antibiotic exposure (growth control, top), and under exposure to levofloxacin concentrations (C_{LEV}) of 1- and 2-fold the minimal inhibitory concentration (MIC) of the isolates in static *in vitro* infection model experiments (n=2 replicates per C_{LEV} and experiment, n=1 growth control per experiment). Pink points and lines: counts in size range between 0 µm and strain-specific threshold: 1.25 µm (ST58), 1.55 µm (ST88) or 1.75 µm (ST167); yellow points and lines: bacterial counts < 3 µm; light blue points and lines: counts > 3 µm; dark blue, red and green points and lines: counts of prolonged bacterial cells, colours represent different lower boundaries for the "increased" size range.

Graphical comparison of the total counts, i.e. the sum of counts of all size ranges, with viable CFU/mL, determined by the droplet plate assay, showed comparable growth control curves (Figure 3.13, top). When decreasing viable bacterial concentrations were determined by the droplet plate assay, electronic counts/mL constantly remained at the inoculum concentration. Regrowth of viable bacteria was represented in increasing electronic cell counts, resulting in similar electronic cell counts compared to viable bacterial concentrations at the end of the experiment for regrown bacterial populations.

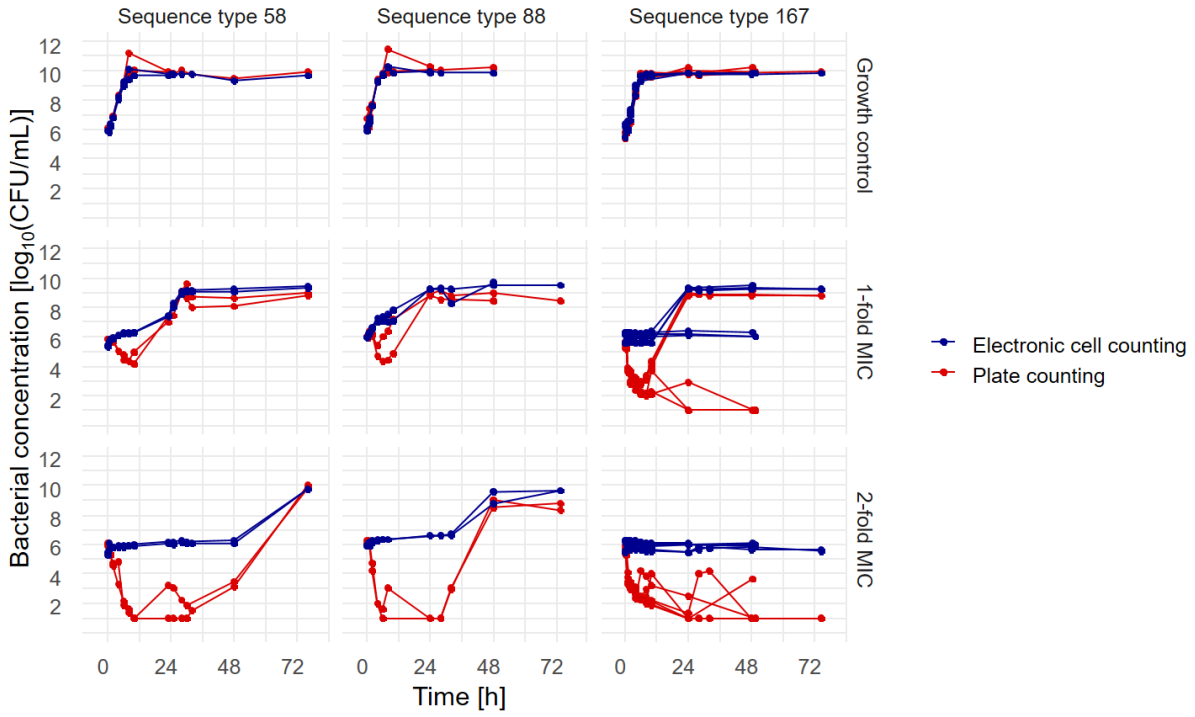

Figure 3.13: Bacterial concentrations in static *in vitro* infection model experiments, without antibiotic exposure (top), and exposing three *Escherichia coli* isolates (ST58, left column; ST88, middle column; and ST167, right column) to levofloxacin concentrations of 1- (middle) and 2-fold (bottom) the minimal inhibitory concentration (MIC), quantified by electronic cell counting (blue symbols and lines) and plate counting (red symbols and lines), n ≥ 2 replicates per bacterial strain and LEV concentration.

The fractions of different bacterial cell size ranges of the total electronic counts were comparable between the growth controls of the three isolates (Figure 7.8, Figure 7.9, Figure 7.10, left panels). In growing bacterial populations without antibiotic exposure, cell diameters were mainly below 3 µm, with a small fraction of cells displaying slightly increased diameters in the beginning of the exponential growth stage. In the stationary growth stage, the majority of cells displayed a diameter < 3 µm for all isolates.

Under exposure to C_{LEV} of 1-fold the MIC of the respective isolate, bacterial cells with slightly increased diameter (> 3 µm) were observed (Figure 7.8, Figure 7.9, Figure 7.10, middle panels). While the fraction of cells with slightly or extensivly increased cell size (> 5 µm) differed beween the isolates, a time-dependent pattern was comparable between the strains: In the beginning of the experiments, bacteria with slightly increased cell size occurred, when bacterial killing was observed in the droplet plate assay. A small fraction of extensively increased cells with a diameter > 5 µm was detected in that stage for all of the strains, being

most pronounced for ST88, and similarly small for ST58 and ST167. The fraction of extensively increased cells expanded, when viable bacterial counts, quantified by the droplet plate assay, decreased. For all isolates, increased bacterial cells were detectable as long as regrowth of viable bacteria was obsereved. The fraction of prolonged cells decreased, when concentrations of regrown bacterial populations had reached the extent of the GC in the stationary growth stage after approx. 24 h.

Exposed to C_{LEV} of 2-fold their MIC, ST88 and ST167 showed high fractions of slightly increased cells and extensively increased cells in a time-dependent manner (Figure 7.8, Figure 7.9, Figure 7.10, right panels). For ST58, the fractions of slightly and extensively increased cells were small and comparable to the GC of the isolate (Figure 7.8). For ST88 under exposure to C_{LEV} of 2-fold MIC, the fraction of slightly increased cells increased rapidly, when viable counts were reduced in the first 6 h of the experiment (Figure 7.9). At the same time, the fraction of extensively increased cells increased until t=10 h. In the stationary stage, the fraction of increased cells remained at a low level. For ST167, the initial fraction of increased cells before LEV exposure was different between the experiments, but comparable for two replicates obtained in one experiment (Table 7.8, Figure 7.10: ID 84 and ID 85: experiment 26, ID 88 and ID 89: experiment 27, ID 93 and ID 94: experiment 28). A lower fraction of increased cells after termination of the regrowth phase compared to the killing- and regrowth phase was observed for all isolates.

For all isolates, a higher fraction of increased cells (> 3 µm) was observed under LEV exposure compared to unexposed bacterial populations (Figure 3.14). The fraction > 3 µm increased in the first 2-4 h of the experiment, reaching its maximum between t=2 h and t=4 h (Table 3.4). The extent of filamentation was largest for ST88 under exposure to C_{LEV} of 2-fold the MIC, with a maximum of 85.5% cells showing increased diameters at t=2 h (Figure 3.14, middle, orange lines). For ST167, filamentation was more pronounced under exposure to C_{LEV} of 1-fold the MIC, reaching its maximum of 64.9% increased cells at t=2 h (Figure 3.14, bottom, green lines). Comparatively low fractions of increased cells were observed for ST58, with a maximum of 11.7% under exposure to C_{LEV} of 1-fold the MIC at t=4 h. Subsequently, fractions of increased cells declined. For ST58, all bacterial cells displayed a “normal” size after 24-36 h, while increased diameters were observed for approx. 20% of the bacterial cells of ST167 under 2-fold MIC exposure until the end of the experiment. Filamentation was observed for ST88 until t=48 h under exposure to 2-fold the MIC.

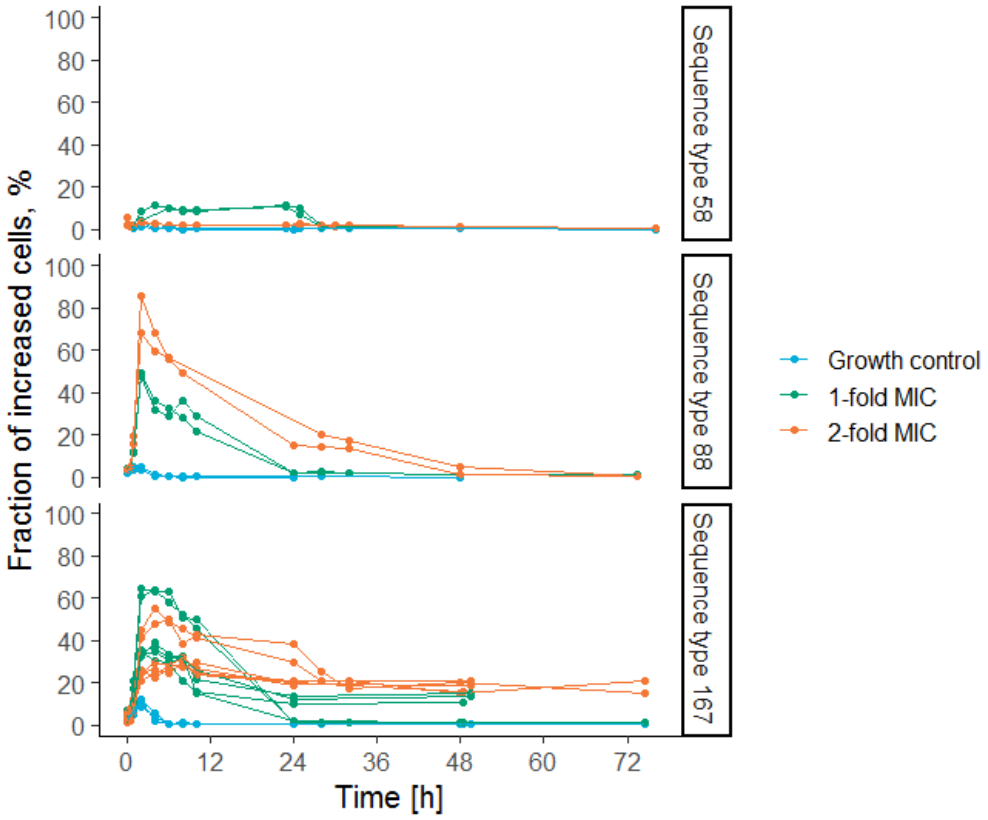

Figure 3.14: Fraction of bacterial cells with increased diameter (> 3 µm) of three *Escherichia coli* isolates (ST58: n=1 experiment, ST88: n=1 experiment, and ST167: n=3 experiments) without levofloxacin (LEV) exposure (growth control) and under exposure to LEV concentrations (C_{LEV}) of 1- and 2-fold the minimal inhibitory concentration (MIC) in static *in vitro* infection model experiments (n=2 replicates per C_{LEV} and experiment, n=1 growth control per experiment); blue points and lines: growth control without LEV exposure; green points and lines: exposure to 1-fold MIC of the isolate, orange points and lines: exposure to 2-fold the MIC.

Table 3.4: Maximum fraction of cells with increased diameter (> 3 µm) and time of maximum for 3 *Escherichia coli* isolates (Sequence type 58, 88 and 167) under levofloxacin exposure in 5 static *in vitro* infection model experiments.

Sequence type	Maximum fraction of increased cells, %	Time at maximum of increased cells [h]
58	11.7	4
88	85.5	2
167	64.9	2

3.3 Pharmacokinetic/pharmacodynamic modelling and simulations

PK/PD modelling was performed, aiming to amalgamate insights from different experimental approaches to quantify and mechanistically characterise the strain-specific growth, kill and regrowth behaviour under static and dynamic LEV exposure. First, a semi-mechanistic model was developed, based on cumulative areas as novel PK and PD metrics (chapter 3.3.1) and PK/PD parameters were derived to quantitatively discriminate between the investigated strains and exposure patterns. Second, mechanistic understanding of the underlying processes was enhanced by developing a PK/PD NLME model (chapter 3.3.2).

3.3.1 Characterisation of the exposure-effect relationship

3.3.1.1 PK/PD metrics quantifying the exposure-effect relationship

As exposure metric, the cumAUC(t) was introduced (chapter 2.4.1.1). For sIVIM experiments, LEV cumAUC(t) increased linearly over time, while for the dynamic exposure pattern, a steep increase in C_{LEV} in the beginning of a C(t) profile and decreasing C_{LEV} in the terminal part were represented in a sigmoidal LEV cumAUC(t) trajectory (Figure 3.15). Maximum LEV cumAUC(t) values, observed at the end of each experiment, were approx. 7-fold higher for static exposure (1536 mg·h·L^{-1}, resulting from 24 h exposure to C_{LEV}=64 mg/L) compared to the dynamic exposure pattern (216 mg·h·L^{-1}). Of note, for the dynamic exposure pattern, no trend towards higher or lower drug exposure for one of the isolates was observed (Figure 3.15, left, Figure 3.7).

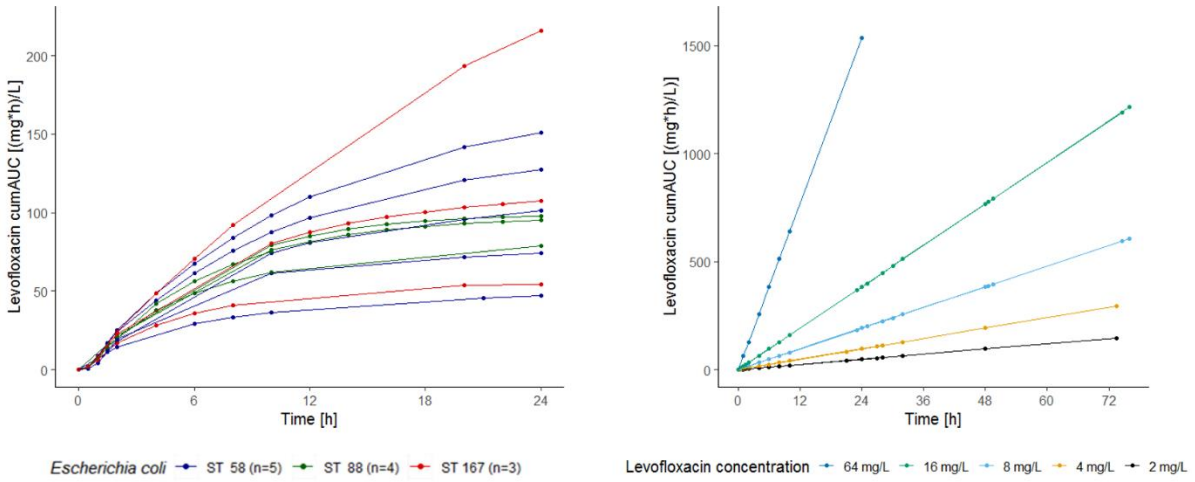

Figure 3.15: Levofloxacin exposure metric, determined as cumulative area under the concentration-time curve (cumAUC) over time in *in vitro* infection model experiments, left: exposure metric over time, resulting from mimicking a 750 mg, 90 min intravenous infusion in plasma in **dynamic** *in vitro* infection model experiments (n=12 replicates), colours: 3 exposed *Escherichia coli* isolates, right: exposure metric over time in **static** *in vitro* infection model experiments, colours: nominal levofloxacin concentrations, points: sampling times, ST: sequence type.

As effect metric, the cumAUGC(t)-normalised cumABBC(t) was employed. The maximum effect was observed at the sampling time point of the minimum bacterial concentrations, before regrowth occurred. In the sIVIM, the maximum normalised effect was similar for the investigated isolates (ST58: 0.818, ST88: 0.852, ST167: 0.858, Figure 3.16, right) and rather determined by the MIC-normalised static C_{LEV} (Figure 7.11). However, distinct effect-time trajectories were observed for static exposure to 0.5- and 1-fold the MIC, but the maximum effect was similar for 2-fold MIC exposure and higher concentrations. Contrary, under dynamic LEV exposure, the maximum normalised effect quantitatively demonstrated differences in bacterial growth and kill behaviour of the strains (0.377 (ST58) – 0.706 (ST88), Figure 3.16, left). Bacterial regrowth was represented by decreasing effect-time trajectories.

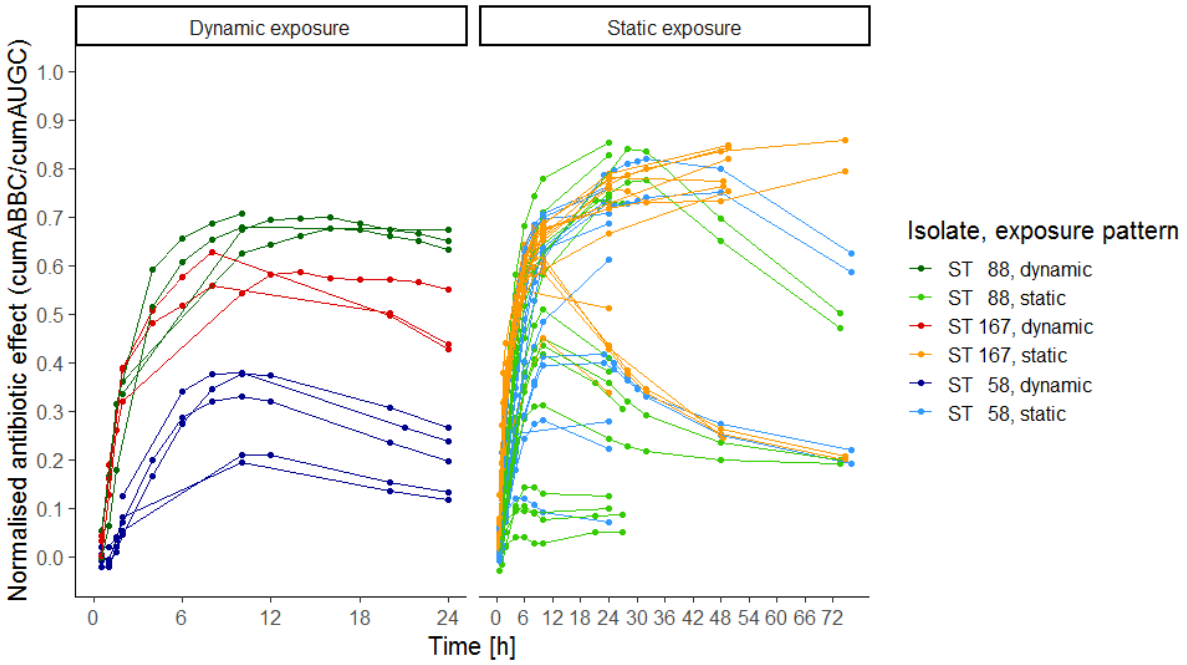

Figure 3.16: Antibiotic effect of levofloxacin against *Escherichia coli*, determined as the cumulative area between the growth control and the bacterial killing and regrowth curve (cumABBC(t)), normalised to the area under the growth control curve (AUGC(t)) of unexposed bacteria over time in *in vitro* infection model experiments; left: effect of levofloxacin concentration-time profiles resulting from mimicking a 750 mg, 90 min intravenous infusion in plasma in **dynamic** *in vitro* infection model experiments (n=12 replicates), right: effect of constant levofloxacin concentrations in **static** *in vitro* infection model experiments (n=43 replicates), colours: 3 *Escherichia coli* isolates under dynamic (dark green, red and blue) and static (light green, orange and light blue) exposure, points: sampling times, ST: sequence type.

Relating the exposure and effect metrics, cumAUC(t) and cumAUGC(t)-normalised cumABBC(t), respectively, initially sigmoidally increasing exposure-effect curves were observed for static and dynamic LEV exposure, and regrowth was represented by a decline in the normalised cumABBC(t) at higher exposure (Figure 3.17). For static exposure, the decline was less pronounced (smaller slope) compared to the dynamic exposure pattern, probably as a consequence of the linearly increasing incremental LEV cumAUC(t) for static LEV exposure, compared to decreasing increments of LEV AUC in the terminal part of dynamic C(t) profiles (Figure 3.15). Exposure-effect curves, obtained from both static and dynamic IVIM experiments, unveiled different LEV potencies for the investigated isolates: For ST58 (blue curves), a higher exposure was required to observe an increasing effect compared to the other isolates (Figure 3.17). Under dynamic exposure, the extent of the maximum normalised effect was different for the three strains. The exposure-effect curves obtained from sIVIM experiments demonstrated the strain-specific exposure needed to reach similar effects for the three isolates.

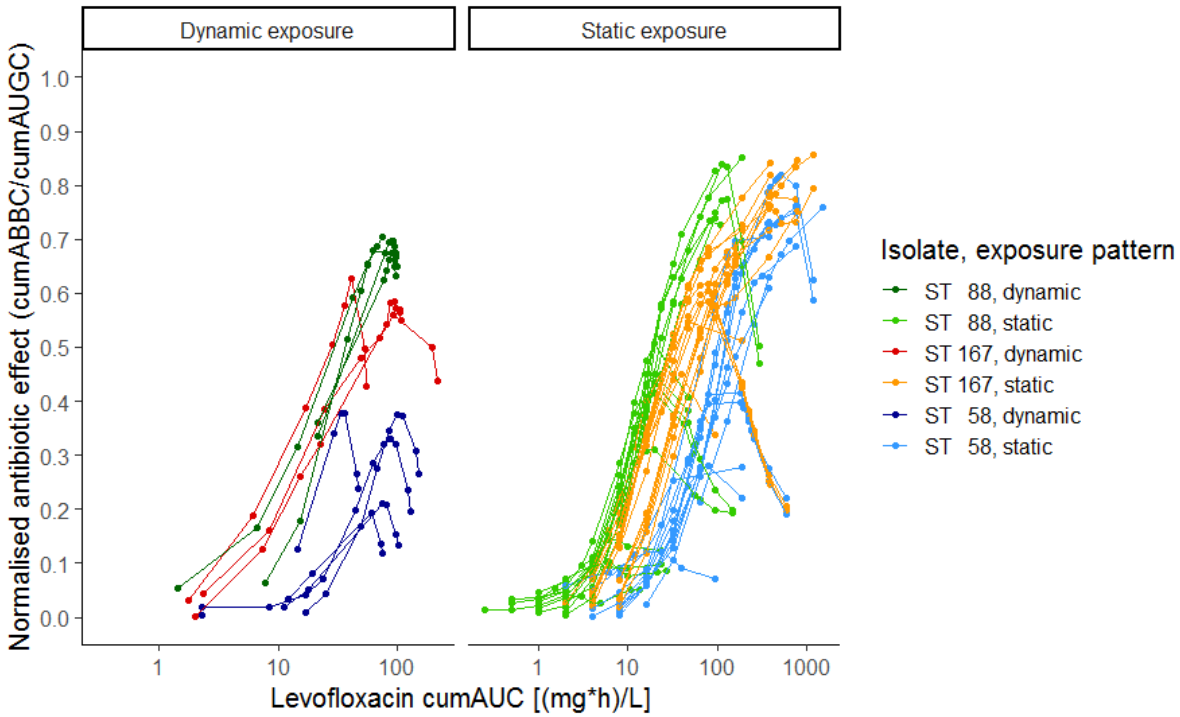

Figure 3.17: Exposure-effect relationship of levofloxacin against *Escherichia coli* in static and dynamic *in vitro* infection model experiments, exposure determined as cumulative area under the levofloxacin concentration-time curve (cumAUC(t)), effect determined as cumulative area between the growth control and the bacterial killing and regrowth curve (cumABBC(t)), normalised to the area under the growth control curve (cumAUGC(t)), left: exposure-effect relationship resulting from mimicking a 750 mg, 90 min intravenous infusion in plasma in **dynamic** *in vitro* infection model experiments (n=12 replicates), right: exposure-effect relationship of constant levofloxacin concentrations in **static** *in vitro* infection model experiments (n=43 replicates), colours: 3 *Escherichia coli* isolates under dynamic (dark green, red and blue) and static (light green, orange and light blue) exposure, points: sampling times, ST: sequence type.

3.3.1.2 Parameter estimates and stratification per exposure pattern

Different mathematical implementations were investigated to characterise the exposure-effect relationship (Table 7.6, Table 7.11). In comparison to a sigmoidal E_{max} model without inhibition term, the exposure-effect curves were better described by sigmoidal E_{max} models including an inhibition term. Thereby, the observed decreasing effect, representing regrowth, was accounted for. As the effect was normalised to the cumAUGC(t), an effect > 1 was not plausible and consequently, E_{max} was fixed to 1 in the final model (Equation 3.1):

$$Effect = \frac{cumABBC(t)}{cumAUGC(t)} = \frac{cumAUC(t)^n}{cumAUC_{50}^n + cumAUC(t)^n} \cdot \frac{1}{1 + \frac{cumAUC(t)}{cumAUC_{reg}}} \quad (3.1)$$

In the PK/PD model, the sigmoidally increasing effect in the first part of the exposure-effect course (Figure 3.17) was primarily determined by the $cumAUC_{50}$ value, with a steeper increase in effect for a lower $cumAUC_{50}$ estimate of a strain. Bacterial regrowth, represented by a decrease in antibiotic effect at higher exposure at later time points, was determined by the LEV $cumAUC_{reg}$ value: Small $cumAUC_{reg}$ estimates represented regrowth at lower cumulative LEV exposure, while high $cumAUC_{reg}$ estimates resulted in a negligible impact of the inhibition term and therefore reduced the PK/PD model to a sigmoidal E_{max} model (i.e. only left part in Equation 3.1). For each isolate, $cumAUC_{50}$ and the Hill factor (n) were jointly estimated for static and dynamic exposure, while $cumAUC_{reg}$ was estimated separately ($cumAUC_{reg,static}$ and $cumAUC_{reg,dynamic}$).

The observed differences between the strains in initial bacterial reduction were quantified by their $cumAUC_{50}$ estimates, being smallest for ST88, followed by ST167 (almost 2-fold higher), and being largest for ST58 (more than 5-fold higher compared to ST88, Table 3.5), indicating the highest LEV susceptibility for ST88, in line with the lower MIC value of this isolate (2 mg/L). However, differences in the exposure-effect relationship between ST58 and ST167, sharing the same MIC value (8 mg/L), were observed: The initial bacterial reduction was less pronounced for ST58, which was quantified by a more than 3-fold higher $cumAUC_{50}$ estimate compared to ST167 (158 vs. 49.4 $mg \cdot h \cdot L^{-1}$).

$CumAUC_{reg}$ estimates revealed strain-dependent differences between the exposure patterns: The $cumAUC_{reg,static}$ estimate was smallest for ST88, followed by ST167 (5-fold higher) and ST58 (9.5-fold higher compared to ST88), being in line with the order of the $cumAUC_{50}$ estimates. However, the $cumAUC_{reg,dynamic}$ estimate was smallest for ST58, followed by ST88 and ST167. The $cumAUC_{reg,static}$/$cumAUC_{reg,dynamic}$ ratio indicated the tendency of an isolate to regrow preferably under exposure to clinical relevant LEV C(t) profiles mimicked in the dynamic setting, being more pronounced for higher values. Comparing the static setting with constant LEV exposure to the dynamic setting with clinically relevant LEV C(t) profiles, the $cumAUC_{reg,static}$/$cumAUC_{reg,dynamic}$ ratio was < 1 for ST88 (0.885), different from ST58 (12.6) and ST167 (3.55), indicating a higher tendency to regrow under static exposure for the isolate.

Table 3.5: Parameter estimates and parameter imprecision of a sigmoidal E_{max} model combined with an inhibition term, describing the exposure-effect relationship of levofloxacin against 3 clinical *Escherichia coli* isolates in static and dynamic *in vitro* infection model experiments.

Parameter [unit]	Estimate (RSE, %)
Sequence type 58	
$cumAUC_{50}$ [mg·h·L^{-1}]	158 (9.45)
Hill	1.02 (5.49)
$cumAUC_{reg,dynamic}$ [mg·h·L^{-1}]	248 (34.6)
$cumAUC_{reg,static}$ [mg·h·L^{-1}]	3132 (36.5)
$cumAUC_{reg,static}$/$cumAUC_{reg,dynamic}$ ratio	12.6
Proportional residual variability, %CV	4.00 (11.8)
Sequence type 88	
$cumAUC_{50}$ [mg·h·L^{-1}]	28.6 (7.85)
Hill	1.25 (5.37)
$cumAUC_{reg,dynamic}$ [mg·h·L^{-1}]	373 (34.9)
$cumAUC_{reg,static}$ [mg·h·L^{-1}]	330 (22.9)
$cumAUC_{reg,static}$/$cumAUC_{reg,dynamic}$ ratio	0.885
Proportional residual variability, %CV	4.33 (11.7)
Sequence type 167	
$cumAUC_{50}$ [mg·h·L^{-1}]	49.4 (7.54)
Hill	0.961 (6.62)
$cumAUC_{reg,dynamic}$ [mg·h·L^{-1}]	473 (39.2)
$cumAUC_{reg,static}$ [mg·h·L^{-1}]	1679 (20.3)
$cumAUC_{reg,static}$/$cumAUC_{reg,dynamic}$ ratio	3.55
Proportional residual variability, %CV	3.33 (11.3)

Abbreviations: RSE: Relative standard error (imprecision of parameter estimates); $cumAUC_{50}$: exposure, determined as cumulative area under the levofloxacin concentration-time curve, causing 50% of the maximum effect, $cumAUC_{reg,static}$: exposure causing regrowth in a static *in vitro* infection model, $cumAUC_{reg,dynamic}$: exposure causing regrowth in a dynamic *in vitro* infection model, Hill: Hill factor (steepness of exposure-effect relationship), CV: coefficient of variation.

3.3.1.3 Model evaluation and exploration

The final PK/PD model overall well captured the central tendency of observed data for the three investigated isolates (Figure 3.18, top) and two exposure patterns (Figure 3.18, bottom). Stratification per strain and exposure pattern demonstrated strain-specific characteristics of the exposure-effect relationship: While predicted exposure-effect curves were largely overlapping for ST88 (Figure 3.18, upper panel, middle), a higher maximum effect was reached for ST58 and ST167 under static exposure (Figure 3.18, light blue and orange points and lines) compared to the dynamic exposure pattern (dark blue and red points and lines). Predictions for the dynamic exposure pattern illustrated the strain-specific exposure-effect relationship (Figure 3.18, lower panel, left), while for static exposure, also the MIC-normalised C_{LEV} determined the effect (Figure 7.11).

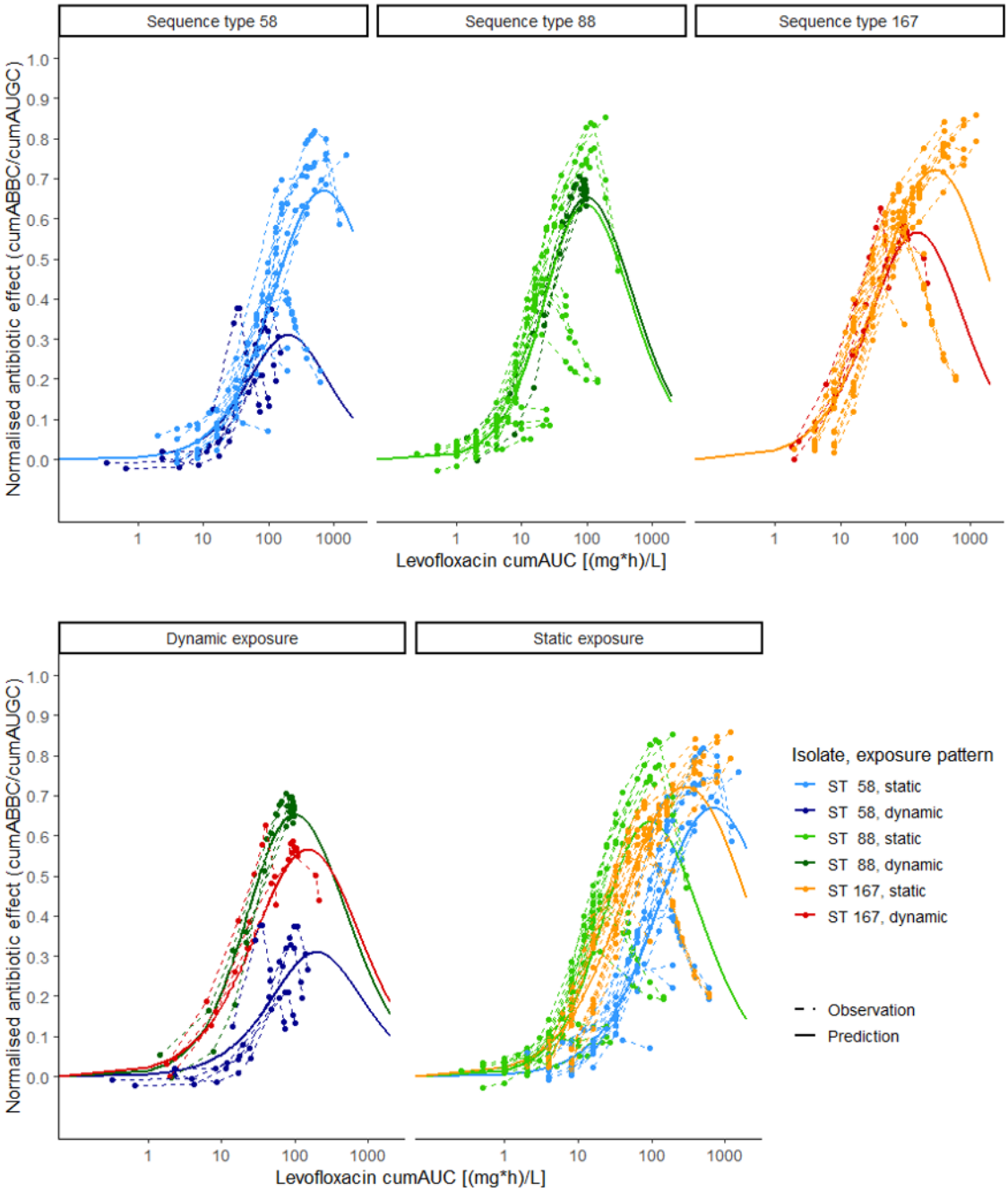

Figure 3.18: Exposure-effect relationship of levofloxacin against *Escherichia coli* in static and dynamic *in vitro* infection model experiments, exposure determined as cumulative area under the levofloxacin concentration-time curve (cumAUC(t)), effect determined as cumulative area between the growth control and the bacterial killing and regrowth curve (cumABBC(t)), normalised to the area under the growth control curve (cumAUGC(t)), observations (points and dashed lines) and predictions (solid lines) based on E_{max} model with inhibition term, colours: 3 *Escherichia coli* isolates under dynamic (dark green, red and blue) and static (light green, orange and light blue) exposure, upper panel: exposure-effect relationship per isolate, lower panel: exposure-effect relationship per exposure pattern, ST: sequence type.

To further elucidate the impact of the static C_{LEV} on the exposure-effect relationship, parameters were estimated stratified per exposure pattern and MIC-normalised C_{LEV} for static exposure (Table 3.6). For ST58 and ST167, $cumAUC_{50}$ estimates were comparable between dynamic exposure and static exposure to 1-fold MIC, while the $cumAUC_{50}$ estimates for 2-fold MIC exposure were much higher for these isolates. Differently, for ST88, the $cumAUC_{50}$ value was 1.6-fold higher for the dynamic exposure pattern compared to 2-fold MIC exposure (32.2 $mg \cdot h \cdot L^{-1}$ vs 19.7 $mg \cdot h \cdot L^{-1}$). $CumAUC_{reg}$ estimates were beyond the maximum observed exposure for ST58 and ST167 under static exposure to C_{LEV} of 2-fold MIC (Figure 3.15, right). Differently, for ST88, $cumAUC_{reg}$ was 1.5-fold higher under dynamic exposure compared to static exposure to 2-fold MIC and more than 20-fold higher compared to static exposure to 1-fold MIC, respectively, indicating a tendency of the isolate to display regrowth under static rather than under dynamic exposure.

Table 3.6: Parameter estimates and parameter imprecision of a sigmoidal E_{max} model combined with an inhibition term, describing the exposure-effect relationship of levofloxacin against 3 clinical *Escherichia coli* isolates in static and in the dynamic *in vitro* infection model experiments, stratified per exposure pattern (static exposure to 1-fold MIC, 2-fold MIC and dynamic exposure).

Parameter [unit]	**Estimate (RSE, %)**		
	C_{LEV}=1 MIC	**C_{LEV}=2 MIC**	**C_{LEV}=dynamic**
Sequence type 58			
$cumAUC_{50}$ [$mg \cdot h \cdot L^{-1}$]	75.6 (10.2)	106 (4.87)	83.0 (30.5)
Hill	1.31 (7.02)	1.34 (4.35)	1.28 (12.5)
$cumAUC_{reg}$ [$mg \cdot h \cdot L^{-1}$]	167 (10.8)	2643 (17.1)	87.5 (44.0)
Proportional residual variability, %CV	0.925 (22.4)	0.802 (19.8)	4.85 (24.0)
Sequence type 88			
$cumAUC_{50}$ [$mg \cdot h \cdot L^{-1}$]	12.6 (5.67)	19.7 (3.64)	32.2 (10.1)
Hill	1.57 (4.77)	1.65 (3.95)	1.20 (8.04)
$cumAUC_{reg,}$ [$mg \cdot h \cdot L^{-1}$]	29.7 (7.40)	397 (10.2)	615 (44.7)
Proportional residual variability, %CV	0.737 (19.8)	0.580 (20.4)	0.695 (24.0)
Sequence type 167			
$cumAUC_{50}$ [$mg \cdot h \cdot L^{-1}$]	28.9 (8.71)	64.6 (4.66)	27.2 (8.45)
Hill	1.36 (8.92)	1.05 (4.62)	1.28 (7.64)
$cumAUC_{reg,}$ [$mg \cdot h \cdot L^{-1}$]	333 (13.5)	3956 (20.3)	195 (14.2)
Proportional residual variability, %CV	3.09 (17.9)	0.781 (17.1)	0.703 (26.2)

RSE: Relative standard error (imprecision of parameter estimates); $cumAUC_{50}$: exposure, determined as cumulative area under the levofloxacin concentration-time curve, causing 50% of the maximum effect, $cumAUC_{reg}$: exposure causing regrowth, MIC: minimal inhibitory concentration, Hill: Hill factor (steepness of exposure-effect relationship), CV: coefficient of variation.

Deterministic simulations for the three isolates and two exposure patterns illustrated the strain-specific characteristics of the exposure effect relationship (Figure 3.19): While for ST58 and ST167 the simulated exposure-effect curves for dynamic exposure (red lines) and static exposure to 1-fold MIC (blue lines) were comparable, for ST88, the predicted E_{max} was similar between dynamic exposure and static exposure to 2-fold MIC (0.696 vs 0.757) but requiring almost 2-fold higher LEV exposure in the dynamic setting (136 $mg \cdot L \cdot h^{-1}$ vs 76.0 $mg \cdot L \cdot h^{-1}$, Table 3.7).

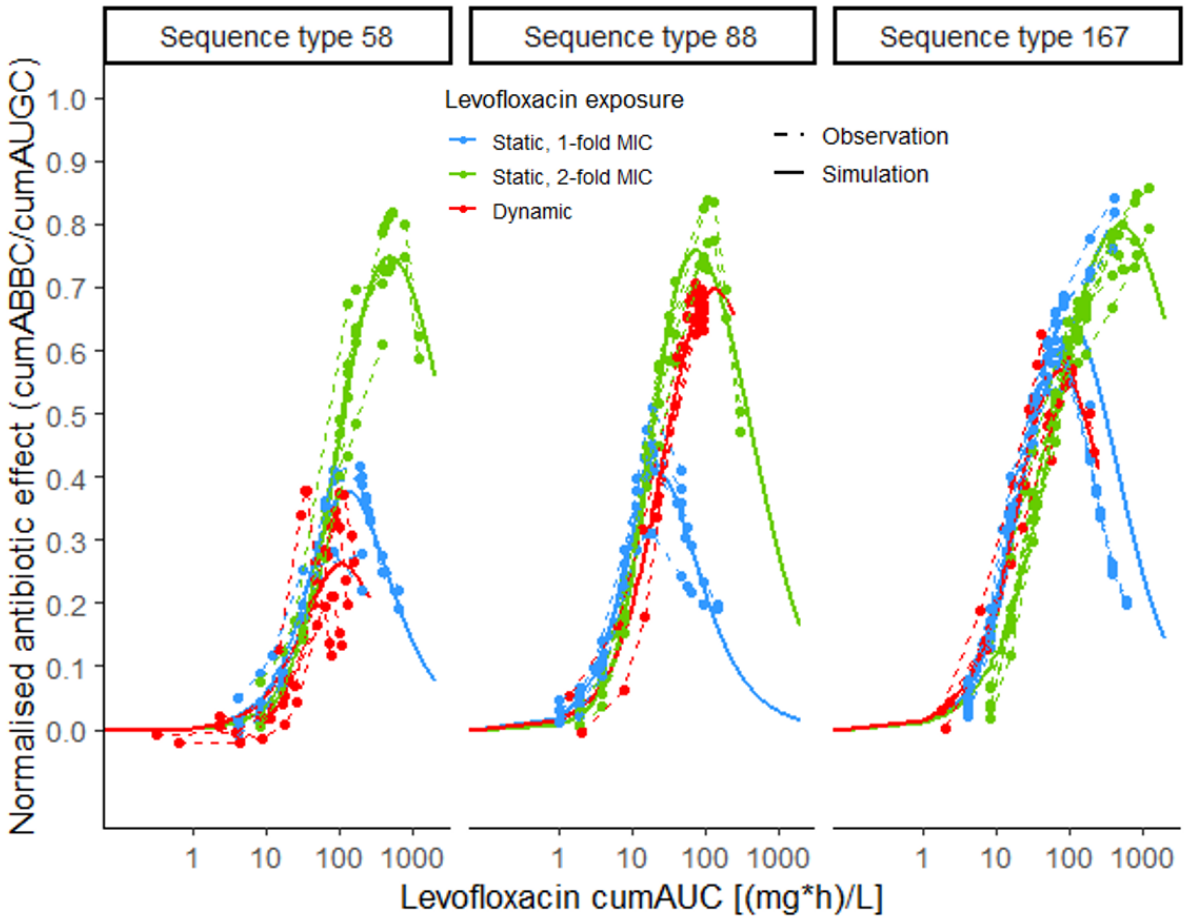

Figure 3.19: Exposure-effect relationship of levofloxacin against *Escherichia coli* in static and dynamic *in vitro* infection model experiments, stratified per exposure pattern (blue: static, 1-fold MIC; green: static, 2-fold MIC; red: dynamic); exposure metric: cumulative area under the levofloxacin concentration-time profile (cumAUC(t)); effect metric: cumulative area between the growth control and the bacterial killing and regrowth curve (cumABBC(t)), normalised to the area under the growth control curve (cumAUGC(t)), observations (points and dashed lines) and deterministic simulations (solid lines) based on E_{max} model with inhibition term, MIC: minimal inhibitory concentration.

For ST58, predicted E_{max} under dynamic exposure was much smaller than that from static exposure to 1-fold MIC (0.261 vs 0.337), with only 18.6% lower cumulative LEV exposure (105 mg·h·L^{-1} vs 129 mg·h·L^{-1}, Table 3.7). At the same time, LEV exposure at the maximum effect was 4.6-fold higher comparing exposure to 2-fold MIC in the static to the dynamic setting (486 vs 105 mg·h·L^{-1}). For ST167, E_{max} was smaller in the dynamic setting compared to static exposure to 1-fold MIC (0.567 vs 0.650), with a 22.9% smaller exposure at the maximum effect. Consequently, for ST58 and ST167, insufficient exposure in the dynamic setting might have contributed more to regrowth compared to ST88.

Table 3.7: Levofloxacin exposure at predicted maximum effect (E_{max}), determined as cumulative area under the levofloxacin concentration-time curve ($cumAUC_{max}$), and E_{max}, determined as cumulative area between the growth control and the bacterial killing and regrowth curve (cumABBC(t)), normalised to the area under the growth control curve (cumAUGC(t)), and cumulative exposure in 24 h (cumAUC(24 h)) for 3 *Escherichia coli* isolates, predictions based on the developed E_{max} model with inhibition term, stratified per exposure pattern: static exposure to 1-fold minimal inhibitory concentration (MIC), static exposure to 2-fold MIC and dynamic exposure to a levofloxacin concentration-time profile resulting from mimicking a 750 mg, 90 min intravenous infusion in plasma in dynamic *in vitro* infection model experiments.

	C_{LEV}=1 MIC	C_{LEV}=2 MIC	C_{LEV}=dynamic
Sequence type 58			
$cumAUC_{max}$ [mg·h·L^{-1}]	129	486	105
E_{max}	0.377	0.747	0.261
cumAUC(24 h) [mg·h·L^{-1}]	192	384	77.6
Sequence type 88			
$cumAUC_{max}$ [mg·h·L^{-1}]	23.0	76.0	136
E_{max}	0.406	0.757	0.696
cumAUC(24 h) [mg·h·L^{-1}]	48	96	77.6
Sequence type 167			
$cumAUC_{max}$ [mg·h·L^{-1}]	96.0	493	74.0
E_{max}	0.650	0.796	0.567
cumAUC(24 h) [mg·h·L^{-1}]	192	384	77.6

The separate trajectories of the killing process, described by the E_{max} model term, and the regrowth process, characterised by the inhibition term, demonstrated the changing impact of the two processes determining the exposure-effect relationship and unveiled the relation between the two parameters, $cumAUC_{50}$ and $cumAUC_{reg}$ and the full normalised effect (Figure 3.20, Table 3.8).

Three phases of the effect-time trajectories were identified: In the first phase, the killing process predominantly (up to 95%) determined the effect, illustrated by the overlapping trajectories of the E_{max} model term and the full model (Figure 3.20, coloured dashed and solid lines). The second phase (transition phase) was determined by the two opposing processes and comprised the intersection of the killing and the regrowth trajectories (Table 3.8, Figure 3.20: exemplified for ST58 under static exposure to 2-fold MIC, black horizontal and vertical dashed lines). In the third phase, regrowth predominantly (up to 95%) determined the effect (Figure 3.20: overlapping dotted and solid lines). With increasing impact of the inhibition term, the effect was reduced to a strain-specific extent. Differences between the strains were more pronounced in the dynamic setting than under static exposure. The predicted E_{max} was both influenced by the steepness of the effect-time trajectory and the slope of the inhibition term. E_{max} was similar for the isolates under static exposure to LEV concentrations of 2-fold MIC, but different in the dynamic setting. The predicted effect increased later under exposure to 1-fold MIC (blue solid lines) compared to 2-fold MIC (green solid lines). Additionally, effect-time curves were steeper for exposure to static LEV concentrations of 2-fold MIC compared to 1-fold MIC. The impact of the inhibition term, reversing the effect at later time points, was more pronounced for static exposure to 1-fold MIC compared to 2-fold MIC. Under exposure to dynamic LEV concentrations, the impact of the inhibition term was most pronounced for ST58 and smallest for ST88.

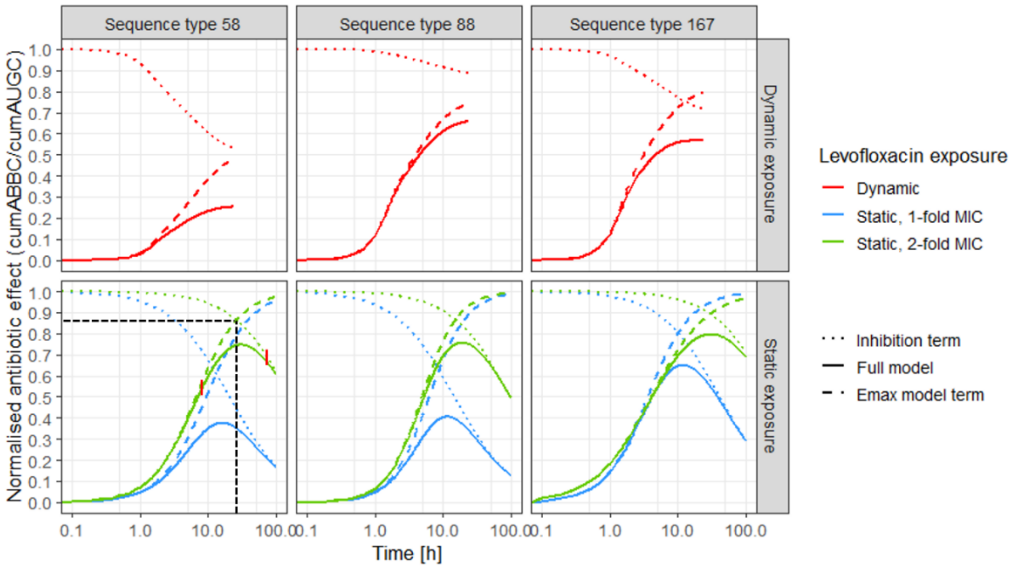

Figure 3.20: Predicted effect (solid lines) of levofloxacin over time against 3 *Escherichia coli* isolates (left: sequence type 58, middle: sequence type 88, right: sequence type 167) in *in vitro* infection model experiments, based on the E_{max} model with inhibition term; and predictions based only on the separate inhibition term (regrowth process, dashed lines) and only on the E_{max} model term (killing process, dotted lines); upper panel: predictions for dynamic exposure (red), lower panel: predictions for static exposure to 1-fold MIC (blue) and 2-fold MIC (green), black horizontal and vertical dashed lines indicate the intersection between killing and regrowth trajectories, exemplified for sequence type 58, static 2-fold exposure; vertical red lines indicate three phases of exposure-effect relationship: “killing phase”, “transition phase”, “regrowth phase”; MIC: minimal inhibitory concentration.

Table 3.8: Dominance* of killing and regrowth processes in the three different phases of the effect-time trajectories (Figure 3.20, red vertical lines in lower left panel) of three *Escherichia coli* isolates under exposure to static levofloxacin (LEV) concentrations (1- and 2-fold the minimal inhibitory concentration (MIC) of the isolate), based on parameter estimates stratified per exposure pattern.

	Sequence type 58		**Sequence type 88**		**Sequence type 167**	
C_{LEV} = 1-fold MIC	Time [h]	Effect	Time [h]	Effect	Time [h]	Effect
Dominance of killing process (Higher impact of E_{max} term)	≤ 1.10	≤ 0.0539	≤ 0.80	≤ 0.358	≤ 2.20	≤ 0.320
Intersection of killing and regrowth trajectories	13.3	0.610	8.7	0.630	10.1	0.803
Dominance of regrowth process (Higher impact of inhibition term)	≥ 90.0	≥ 0.179	≥ 41.0	≥ 0.252	≥ 31.4	≥ 0.541
C_{LEV} = 2-fold MIC						
Dominance of killing process (Higher impact of E_{max} term)	≤ 8.70	≤ 0.560	≤ 5.30	≤ 0.503	≤ 13.1	≤ 0.737
Intersection of killing and regrowth trajectories	26.2	0.863	15.3	0.866	29.9	0.892
Dominance of regrowth process (Higher impact of inhibition term)	≥ 60.0	≥ 0.697	≥ 29.5	≥ 0.732	≥ 66.0	≥ 0.750

*Dominance defined as ≤ 5% deviation from prediction based on full model (Figure 3.20, red vertical lines in lower left panel)

3.3.2 Characterisation of the bacterial growth and kill behaviour

The developed semi-mechanistic PK/PD model characterised the exposure-effect relationship of LEV against three *E. coli* isolates and quantitatively discriminated between strains and exposure patterns. In a next step, a NLME model was developed to enhance the mechanistic understanding of the underlying processes and quantify different levels of variability in the experimentally derived data. In this chapter, results of the main steps in the sequential model development process (chapter 2.4.2.2) are presented.

3.3.2.1 Bacterial growth without antibiotic exposure

The bacterial growth model without LEV exposure comprised two bacterial compartments: viable bacterial cells, which were assumed to be cultivable by means of the droplet plate assay, and non-cultivable persister cells (chapter 2.4.2.3, Figure 3.21).

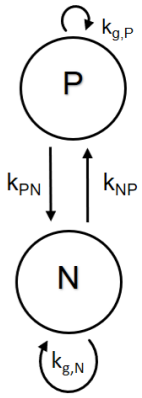

Figure 3.21: Schematic representation of the bacterial growth model. P: persisting bacteria; N: viable bacteria; $k_{g,N}$: first-order growth rate constant of viable bacteria; $k_{g,P}$: first-order growth rate constant of persisting bacteria; k_{NP}: first-order transformation rate constant N to P; k_{PN}: first-order transformation rate constant P to N.

Bacterial growth parameters were plausible, precisely estimated (RSE < 25%, Table 3.9), and in agreement with regard to the experimental settings: The estimated number of bacteria in the inoculum (N_0) was $10^{5.9}$ CFU, while the experimentally adjusted inoculum concentration was 10^6 CFU/mL. IIV of N_0 was small (4.9%, CV) and precisely estimated (RSE 12.6%). Growth behaviour of unexposed bacteria was similar between the three investigated isolates, but different between the two investigated experimental settings: A relevant impact of the experimental setting (i.e. static or dynamic IVIM) on the relative growth rate constant and the maximum bacterial number was identified. Without accounting for the experimental setting, predicted bacterial numbers were systematically higher (up to +1 $\log_{10}$CFU) than observed bacterial concentrations for the static and lower (up to -1 $\log_{10}$CFU) for the dynamic IVIM

experiments (Figure 7.12). Both the relative growth rate constant $k_{g.N}$ and the maximum bacterial number $popmax$ were affected by the experimental setting (Figure 7.13). Hence, the experimental setting was implemented as categorical covariate: Two different relative growth rate constants were estimated for the static and the dynamic IVIM (k_{g,N_DYN} and k_{g,N_STAT}). The maximum bacterial number in the static IVIM was best linked to the maximum bacterial number in the dynamic setting as fractional change of $popmax$ (Equation 2.29). Implementation of the covariate effect of the experimental setting on $k_{g,N}$ and on $popmax$ decreased IIV of $popmax$ (5.5%, CV vs 1.7%, CV) and the AIC (dAIC: - 65.3). Bacterial growth was faster (relative growth rate constant 1.81 h^{-1} vs. 1.15 h^{-1}) and resulted in a higher $popmax$ value in the static compared to the dynamic IVIM, with a 11.2 % higher maximum bacterial number on a logarithmic scale in the sIVIM.

Table 3.9: Parameter estimates and imprecision of the final bacterial growth model for three *Escherichia coli* isolates.

Parameter [unit]	Estimate (RSE, %)	Estimate (RSE, %) (based on SIR)	95% CI (based on SIR)
Bacterial growth parameters			
θ k_{g,N_DYN} [h^{-1}]	1.15 (6.2)	**1.15 (5.01)**	1.03 – 1.27
θ k_{g,N_STAT} [h^{-1}]	1.81 (4.1)	**1.81 (2.63)**	1.72 – 1.91
θ N_0 [log_{10}(CFU)]	5.90 (0.9)	**5.90 (1.03)**	5.77 – 6.02
θ $popmax$ [log_{10}(CFU)]	8.75 (0.6)	**8.75 (0.60)**	8.65 – 8.86
θ Fractional change $popmax$ [log_{10}(CFU)]	0.112 (7.7)	**0.112 (7.20)**	0.0947 – 0.127
Transformation rate constants			
θ k_{NP} [h^{-1}]	0.0 (6.6)	**$9.96 \cdot 10^{-7}$ (14.9)**	$7.25 \cdot 10^{-7}$ – $1.28\ 10^{-6}$
θ k_{PN} [h^{-1}]	$9.87 \cdot 10^{-2}$	**$9.87 \cdot 10^{-2}$ (12.9)**	$7.25 \cdot 10^{-2}$ – $1.23 \cdot 10^{-1}$
Interindividual variability, %CV			
ω N_0	4.90 (12.6)	**4.86 (29.4)**	3.66 – 6.36
ω $popmax$	1.73 (22.3)	**1.67 (30.7)**	1.30 – 2.19
Additive residual unexplained variability			
σ	55.9 (6.10)	**55.9 (4.71)**	50.9 – 61.3

RSE: Relative standard error (obtained from the variance-covariance matrix); %CV: coefficient of variation (calculated according to Equation 2.27); CI: confidence interval, determined by the sampling importance resampling (SIR) method; k_{g,N_DYN}: relative growth rate constant in the dynamic *in vitro* infection model, k_{g,N_STAT}: relative growth rate constant in the static *in vitro* infection model; N_0: bacterial inoculum number in colony forming units (CFU) on a log_{10} scale; $popmax$: maximum bacterial number in the stationary growth stage in the dynamic *in vitro* infection model in CFU on a log_{10} scale, fractional change of $popmax$: according to Equation 2.29, k_{NP}: persister formation rate constant, k_{PN}: back-transformation rate constant, θ: fixed-effects parameter, ω: random-effects parameter (interindividual variability), σ: random-effects parameter (residual unexplained variability).

3.3.2.2 Bacterial killing and persister formation under static levofloxacin exposure

In a second step, the effect of static LEV exposure was linked to bacterial C(t) trajectories in the static PK/PD model (chapter 2.4.2.4, Figure 3.22).

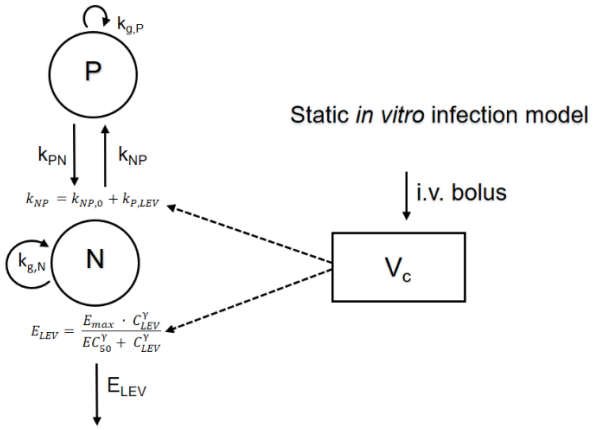

Figure 3.22: Schematic representation of the static PK/PD model. P: persisting bacteria; N: viable bacteria; $k_{g,N}$: first-order growth rate constant of viable bacteria; $k_{g,P}$: first-order growth rate constant of persisting bacteria; k_{NP}: first-order transformation rate constant N to P, $k_{NP,0}$: first-order transformation rate constant N to P without levofloxacin effect; $k_{P,LEV}$: strain-specific additive increase of persister cell formation under levofloxacin exposure; k_{PN}: first-order transformation rate constant P to N; E_{LEV}: levofloxacin induced killing process, quantified by a sigmoidal E_{max} model; E_{max}: maximum bacterial killing effect; C_{LEV}: static levofloxacin concentration; EC_{50}: strain-specific levofloxacin concentration required to reach 50% of the maximum effect; γ: Hill factor (steepness of concentration-effect relationship).

Bacterial growth without antibiotic exposure was taken into account by fixing the bacterial growth parameters k_{g,N_STAT} and N_0 as well as related IIV to parameter values estimated for unexposed bacteria in the sIVIM (Table 3.9). In the static PK/PD model, the fractional change of $popmax$ compared to the dynamic setting could not be estimated, as replicates obtained in the dIVIM were not included yet. Hence, the maximum bacterial number in the sIVIM was estimated solely based on static GC data, accounting for the relative growth rate in the static experimental setting, and $popmax$ was fixed to the respective value ($10^{9.73}$ CFU). Antibiotic effect parameters, describing bacterial killing by a sigmoidal E_{max} model and increased persister cell formation under LEV exposure by an additive increase of the first-order persister formation rate constant k_{NP} were successfully estimated (Table 3.10).

Table 3.10: Parameter estimates and imprecision of the pharmacokinetic/pharmacodynamic model for three *Escherichia coli* isolates under static levofloxacin exposure.

Parameter [unit]	Estimate (RSE, %)	Estimate (RSE, %) (based on SIR)	95% CI (based on SIR)
Bacterial growth parameters			
θ k_{g,N_STAT} [h^{-1}]	1.81 FIX	**1.81 FIX**	**-**
θ N_0 [log_{10}(CFU)]	5.90 FIX	**5.90 FIX**	**-**
θ $popmax$ [log_{10}(CFU)]	9.73 FIX	**9.73 FIX**	**-**
Transformation rate constants			
θ k_{NP} [h^{-1}]	$1.0 \cdot 10^{-6}$ FIX	**$1.0 \cdot 10^{-6}$ FIX**	**-**
θ k_{PN} [h^{-1}]	0.10 FIX	**0.10 FIX**	**-**
Killing effect parameters			
θ E_{max} [h^{-1}]	6.88 (5.50)	**6.88 (7.86)**	5.98 – 81.5
θ $EC_{50,1}$ [mg/L]	14.1 (6.90)	**14.1 (9.02)**	11.9 – 17.1
θ $EC_{50,2}$ [mg/L]	3.10 (8.10)	**3.10 (9.42)**	2.63 - 3.78
θ $EC_{50,3}$ [mg/L]	2.33 (28.4)	**2.33 (48.8)**	0.307 - 4.58
θ $Hill$ [-]	2.45 (9.60)	**2.45 (12.8)**	1.85 - 3.04
Persister formation effect parameters			
θ $k_{P,LEV1}$ [h^{-1}]	$1.4 \cdot 10^{-4}$ (98.6)	**$1.41 \cdot 10^{-4}$ (74.9)**	$4.41 \cdot 10^{-5}$ – $4.47 \cdot 10^{-4}$
θ $k_{P,LEV2}$ [h^{-1}]	$8.0 \cdot 10^{-5}$ (165)	**$8.37 \cdot 10^{-5}$ (140)**	$1.75 \cdot 10^{-5}$ – $4.63 \cdot 10^{-4}$
θ $k_{P,LEV3}$[h^{-1}]	$3.33 \cdot 10^{-2}$ (9.40)	**$3.33 \cdot 10^{-2}$ (22.9)**	$1.97 \cdot 10^{-2}$ – $4.80 \cdot 10^{-2}$
Interindividual variability, %CV			
ω $k_{g,N}$	27.5 FIX	**27.1 FIX**	-
ω N_0	4.90 FIX	**4.10 FIX**	-
ω $popmax$	1.70 FIX	**5.50 FIX**	-
Additive residual unexplained variability			
σ	2.42 (8.0)	**2.42 (4.01)**	2.27– 2.65

RSE: Relative standard error (obtained from the variance-covariance matrix); %CV: coefficient of variation (calculated according to Equation 2.27); CI: confidence interval, determined by the sampling importance resampling (SIR) method; E_{max}: maximum levofloxacin effect on bacterial killing according to Equation 2.11 and 2.12, $EC_{50,1}$: levofloxacin concentration (C_{LEV}) causing 50% of the maximum killing effect for sequence type (ST) 58, $EC_{50,2}$, C_{LEV} causing 50% of the maximum killing effect for ST88, $EC_{50,3}$: C_{LEV} causing 50% of the maximum killing effect for ST167, $Hill$: Hill factor (steepness of concentration-effect relationship), $k_{P,LEV1}$: levofloxacin-dependent additive increase in persister cell formation (according to Equation 2.13 and 2.14) for ST58, $k_{P,LEV2}$: levofloxacin-dependent additive increase in persister cell formation for ST88, $k_{P,LEV3}$: levofloxacin-dependent additive increase in persister cell formation for ST167, θ: fixed-effects parameter, σ: random-effects parameter (residual unexplained variability).

A relevant impact of the bacterial strain on the killing effect parameter EC_{50} and on the additive increase of persister formation under LEV exposure ($k_{P,LEV}$) were identified. Hence, the bacterial strain was implemented as categorical covariate by estimating strain-dependent EC_{50} and $k_{P,LEV}$ values. EC_{50} estimates were in the range of experimentally investigated C_{LEV} and corresponded to C_{LEV} of approx. 1.8-fold the MIC for ST58 (MIC: 8 mg/L), 1.6-fold the MIC for ST88 (MIC: 2 mg/L) and was below the MIC for ST167 (approx. 0.3-fold the MIC of 8 mg/L),

indicating different LEV potencies for the isolates. Although ST58 and ST167 shared the same MIC value, a more than 6-fold higher C_{LEV} was required to reach 50% of the maximum killing effect for ST58, indicating a higher initial susceptibility for ST167. Despite of the 4-fold higher MIC value of ST167 compared to ST88, EC_{50} values were similar and 95% CI of EC_{50} estimates were overlapping between the two isolates. Differently, the LEV effect on persister cell formation was similar for ST58 and ST88, with approximately 100 additional CFU per one million CFU transforming into the persister phenotype per hour under LEV exposure (additive increase of $k_{P,LEV}$: $1.41 \cdot 10^{-4} \cdot h^{-1}$ and $8.37 \cdot 10^{-5} \cdot h^{-1}$, respectively). For ST167, the increase in the first-order rate constant under LEV exposure was much higher, with approx. $3.33 \cdot 10^{4}$ additional CFU per one million CFU and hour turning into persister cells (additive increase of $k_{P,LEV}$: $3.33 \cdot 10^{-2} \cdot h^{-1}$).

The assumption of χ^2-distributed dOFV did not hold true for persister formation effect parameters and hence, parameter uncertainty could not be reliably computed from the standard errors of parameter estimates. Therefore, SIR was applied to derive 95% CI representing the true parameter uncertainty distribution more appropriately and indicating precisely estimated killing effect parameters (chapter 2.4.2.8).

3.3.2.3 Pharmacokinetic model for dynamic *in vitro* infection model experiments

As a next step, a PK model was developed to characterise *in vitro* mimicked LEV C(t) profiles. PK parameters of a two-compartment model with zero-order infusion and first-order elimination were precisely estimated (Table 3.11). Overall, parameter estimates were in good agreement with parameter estimates of the underlying PK model based on *in vivo* data for a septic patient population, which has been used to determine the experimental settings (chapter 2.2.3), accounting for the covariate effect of CRCL on CL (Equation 2.3, [55,142]). While CL and V_c were estimated significantly higher based on IVIM data ("*in vitro* model"), V_p and Q were estimated significantly higher in the model based on LEV C(t) profiles in patients ("*in vivo* model").

Table 3.11: Parameter estimates and imprecision of pharmacokinetic (PK) parameters of the final PK model for levofloxacin concentrations in dynamic *in vitro* infection model experiments (n=21 experimental replicates), mimicking a 750 mg, 90 min i.v. infusion (n=14 replicates) or a 500 mg, 60 min i.v. infusions twice daily (n=7 replicates); determined by sampling importance resampling (SIR), parameter estimates of the underlying PK model [55,142] based on *in vivo* levofloxacin concentrations (n=39 patients); θ $\boldsymbol{CL}$ calculated based on the median creatinine clearance for the septic subpopulation (n=7, median creatinine clearance: 73.2 mL/min), and 1.09% change in CL per mL/min change in creatinine clearance, according to Equation 2.3.

Parameter [unit]	Estimates *in vitro* (RSE, %)	95% CI, *in vitro*	Estimate *in vivo,* sepsis (RSE, %)*
Pharmacokinetic parameters			
θ CL [L·h^{-1}]	8.90 (10.7)	7.21 – 10.9	6.24 (7.1)
θ V_c [L]	28.3 (8.80)	23.8 – 33.3	21.7 (9.5)
θ V_p [L]	42.1 (7.71)	35.6 – 48.9	64.4 (7.3)
θ Q [L·h^{-1}]	26.6 (14.7)	19.5 – 34.6	60.3 (9.3)
θ SF [unitless]	1.39 (14.6)	0.994 – 1.78	-
Interindividual variability, %CV			
ω CL	57.3 (27.1)	44.7 – 77.3	40.2 (34)
ω V_c	42.0 (36.5)	29.9 – 60.1	51.8 (23)
ω V_p	28.3 (66.1)	15.8 – 49.5	42.4 (36)
ω Q	ω V_c · SF		46.6 (62)
Proportional residual unexplained variability, %			
σ	26.9 (4.34)	24.9 – 29.2	8.75 (22)

RSE: Relative standard error, determined by SIR, *RSE based on bootstrap results (n=200); %CV: coefficient of variation (calculated according to Equation 2.27); CI: confidence interval, determined by SIR; CL: clearance, V_c: central volume of distribution, V_p:peripheral volume of distribution, Q: intercompartmental clearance, SF: scaling factor, relating ω V_c to ω Q. θ: fixed-effects parameter, ω: random-effect parameter (interindividual variability), σ: random-effect parameter (residual unexplained variability).

Overall, these deviations in parameter estimates, particularly the lower total volume of distribution ($V_c + V_p$) *in vitro* (70.4 L) compared to *in vivo* (86.1 L) resulted in higher simulated median C_{max} values *in vitro* compared to *in vivo* for both mimicked dosing regimens (Table 3.12, Figure 3.23). As a consequence of the higher *in vitro* LEV clearance, C_{min} values in the terminal phase of the C(t) profiles were lower for simulated LEV C(t) profiles based on the *in vitro* model compared to simulated C_{min} values based on the *in vivo* model. Yet, *in vitro* mimicked C(t) profiles were overall comparable to simulations based on the *in vivo* data and hence, LEV PK was appropriately mimicked in the dIVIM.

Table 3.12: Secondary pharmacokinetic (PK) parameters of simulated levofloxacin concentration-time profiles (n=1000 simulations) based on the developed PK model for dynamic *in vitro* infection model experiments and on a PK model based on levofloxacin concentration-time profiles in patients [55,142].

	In vitro model		*In vivo* model	
	500 mg bid	750 mg qd	500 mg bid	750 mg qd
$C_{max,1}$ [mg/L]	10.7	13.7	9.22	11.7
$C_{max,2}$ [mg/L]	12.1	NA	11.3	NA
$C_{min,1}$ [mg/L]	1.49	0.606	2.17	1.50
$C_{min,2}$ [mg/L]	1.89	NA	3.18	NA
AUC_{24h} [mg·h·L^{-1}]	94.3	77.5	104	91.2

C_{max}: maximum levofloxacin concentration in the dosing interval, C_{min}: minimum levofloxacin concentration in the dosing interval, AUC_{24h}: area under the levofloxacin concentration-time curve over 24 h, bid: bis in die (twice daily), qd: quaque die (once daily), NA. not applicable.

V_c and Q were highly correlated in the *in vitro* setting, as experimental determinants influenced the parameters in a similar fashion and, hence, a scaling factor formally correlating V_C and Q by relating their IIV was estimated to be 1.39 (0.994 – 1.78 , Table 3.11). However, IIV of CL in the experimental setting was higher compared to IIV of CL *in vivo,* while IIV of central and peripheral volume of distribution was higher *in vivo.* As a consequence, 95% CI of simulations based on the *in vitro* model, accounting for IIV and assuming log-normal distribution of PK parameters, were smaller in the increasing and larger in the decreasing part of the C(t) profiles compared to simulations based on the *in vivo* model (Figure 3.23, blue and yellow shaded areas). However, 95% CI of simulations based on the *in vitro* and the *in vivo* model were largely overlapping, demonstrating the clinical relevance of the *in vitro* mimicked LEV C(t) profiles.

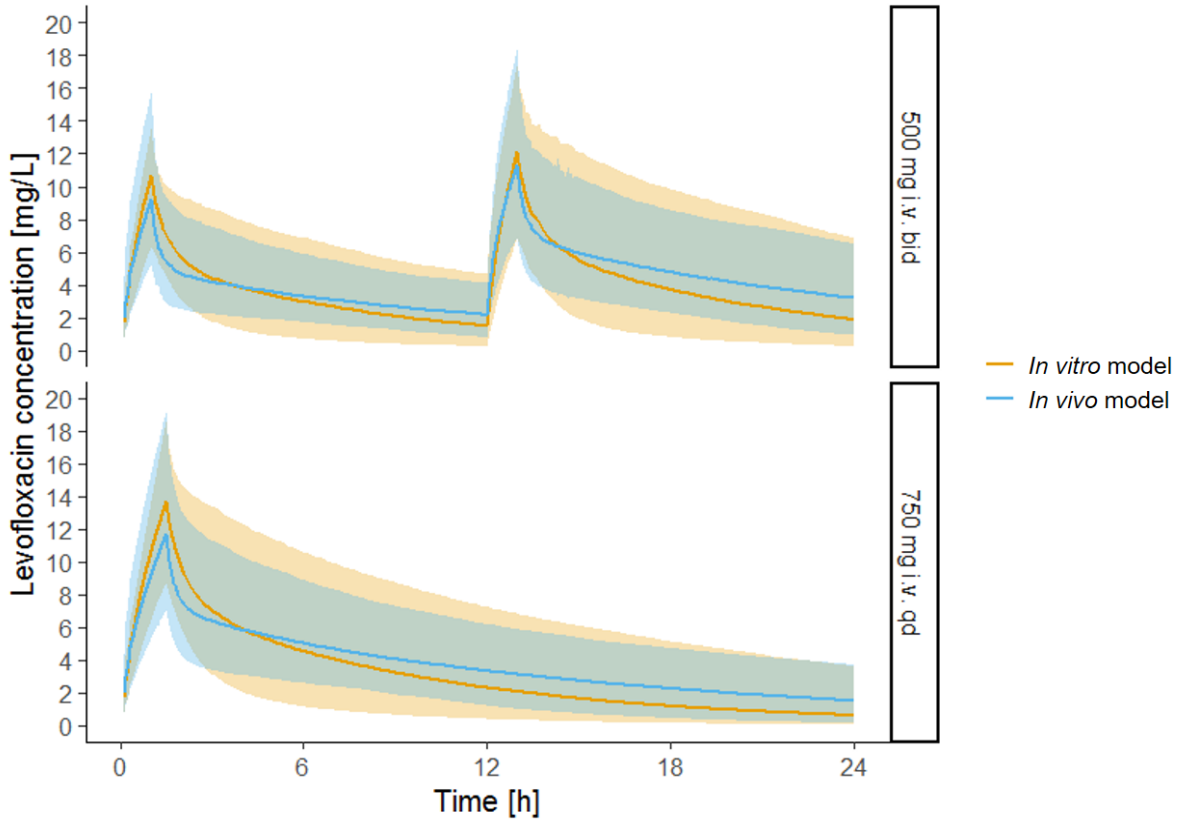

Figure 3.23: Median and 95% confidence intervals of simulated levofloxacin concentration-time profiles resulting from a 500 mg, 60 min i.v. infusion bid (top) and 750 mg, 90 min i.v. infusion qd (bottom); simulations based on pharmacokinetic (PK) model for levofloxacin in *in vitro* infection model experiments (yellow lines and areas, n=1000 simulations per dosing regimen), and on a PK model based on levofloxacin concentration-time profiles in patients (blue lines and areas) [55,142]. **Abbreviations:** i.v.: intravenous, bid: bis in die (twice daily), qd: quaque die (once daily).

3.3.2.4 Three-bacterial-state PK/PD model

Finally, the developed PK model was linked to the bacterial growth and kill model in a "three-bacterial-state PK/PD model", including bacterial concentration-time trajectories under static and dynamic LEV exposure and two different methods to quantify bacterial concentrations: the droplet plate assay and electronic cell counting (Figure 3.24; NONMEM® script: chapter 7.3). To characterise LEV C(t) trajectories in the dIVIM, PK parameters were fixed to the parameter estimates of the final PK model (Table 3.11), while for the sIVIM experiments, nominal C_{LEV} was imputed. Leveraging the total electronic cell counts as a measure for the aggregated bacterial number in three bacterial compartments described the observed bacterial trajectories best and allowed to estimate initial bacterial numbers in the persister cell compartment (N_P) and in the dead cell compartment (N_D). The bacterial number in the dead cell compartment originated both from natural death, quantified by the death rate constant k_D , and LEV induced killing. Bacterial growth parameters and rate constants quantifying transformation into the persisting phenotype and back-transformation (k_{NP} and k_{PN}) and k_d were re-estimated including all unexposed bacterial growth trajectories, obtained in the static and in the dynamic IVIM, and were fixed when estimating the LEV effect parameters.

The killing effect was best characterised by a sigmoidal E_{max} model and quantified by the effect parameters E_{max}, γ and $EC_{50.}$. While E_{max} and γ were jointly estimated for the three *E. coli* isolates, strain-specific EC_{50} values were estimated. Differently, LEV effect on persister cell formation was best described as an additive increase of the persister formation rate constant k_{NP} , quantified as $k_{P,LEV}$. Implementation of a simple or sigmoidal E_{max} model to characterise LEV effect on persister cell formation resulted in implausible effect parameter estimates, increased AIC and was therefore not pursued further. Linking the killing effect to k_D instead of describing a separate killing process did not significantly decrease AIC or change parameter estimates. Therefore, a change of the structural model was not deemed justified. Parameter estimates and imprecision of the final three-bacterial-state PK/PD model are presented in Table 3.13.

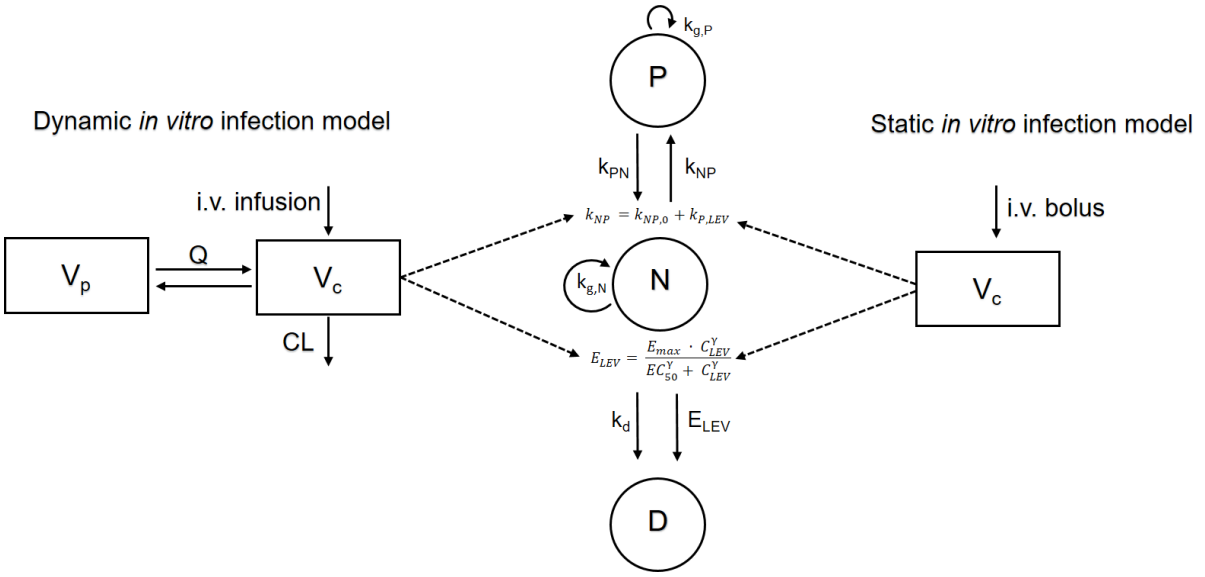

Figure 3.24: Schematic representation of the three-bacterial-state PK/PD model, describing the effect of levofloxacin against *Escherichia coli* in static and dynamic *in vitro* infection model experiments. **Abbreviations:** i.v.: intravenous; CL: clearance, V_c: central volume of distribution, $V_{p:}$ peripheral volume of distribution, Q: intercompartmental clearance, P: persisting bacteria, N: viable bacteria, D: dead cells, $k_{g,N}$: first-order growth rate constant of viable bacteria, $k_{g,P:}$ first-order growth rate constant of persisting bacteria, k_{NP}: first-order transformation rate constant N to P, $k_{NP,0}$: first-order transformation rate constant N to P without levofloxacin effect, $k_{P,LEV}$: strain-specific additive increase of persister cell formation under levofloxacin exposure, k_{PN}: first-order transformation rate constant P to N, $k_{d:}$ first-order death rate constant, E_{LEV}: levofloxacin induced killing process, quantified by a sigmoidal E_{max} model, $E_{max:}$ maximum bacterial killing effect, C_{LEV}: levofloxacin concentration (either static, i.e. nominal levofloxacin concentration, or dynamic, i.e. PK model predicted levofloxacin concentration), EC_{50}: strain-specific levofloxacin concentration required to reach 50% of the maximum effect, γ: Hill factor (steepness of concentration-effect relationship).

Table 3.13: Parameter estimates and imprecision of the three-bacterial-state pharmacokinetic/pharmacodynamic model for three *Escherichia coli* isolates under levofloxacin exposure in static and dynamic *in vitro* infection model experiments, parameters fixed to values obtained in the sequential model development process due to plausibility of parameter estimates.

Parameter [unit]	Estimate (RSE, %)	Estimate (RSE, %) based on SIR	95% CI based on SIR
Pharmacokinetic parameters			
θ CL [L·h^{-1}]	8.90 FIX	**8.90 FIX**	-
θ V_c [L]	28.3 FIX	**28.3 FIX**	-
θ V_p [L]	42.1 FIX	**42.1 FIX**	-
θ Q [L·h^{-1}]	26.6 FIX	**26.6 FIX**	-
θ SF [-]	1.39 FIX	**1.39 FIX**	-
Bacterial growth parameters			
θ k_{g,N_DYN} [h^{-1}]	1.15 FIX	**1.15 FIX**	-
θ k_{g,N_STAT}[h^{-1}]	1.81 FIX	**1.81 FIX**	
θ k_d [h^{-1}]	0.0123 FIX	**0.0123 FIX**	-
θ N_0 [log$_{10}$(CFU)]	5.90 FIX	**5.90 FIX**	-
θ N_P [log$_{10}$(CFU)]	2.47 (0.9)	**2.20 (7.08)**	1.81 – 2.41
θ N_D [log$_{10}$(CFU)]	0.74 (73.8)	**0.910 (11.0)**	0.623 – 0.993
θ $popmax$ [log$_{10}$(CFU)]	8.75 FIX	**8.75 FIX**	-
θ Fractional change $popmax$ [log$_{10}$(CFU)]	0.112 FIX	**0.112 FIX**	-
Transformation rate constants			
θ k_{NP} [h^{-1}]	1.0·10^{-6} FIX	**1.0·10^{-6} FIX**	-
θ k_{PN} [h^{-1}]	0.10 FIX	**0.10 FIX**	-
Killing effect parameters			
θ E_{max} [h^{-1}]	7.37 (1.40)	**7.32 (11.0)**	5.54 – 8.61
θ $EC_{50,1}$ [mg/L]	19.9 (20.3)	**17.2 (15.5)**	12.6 – 23.8
θ $EC_{50,2}$ [mg/L]	4.15 (0.40)	**3.10 (16.2)**	2.48 – 4.42
θ $EC_{50,3}$ [mg/L]	7.53 (0.10)	**8.46 (10.5)**	6.86 – 10.3
θ $Hill$ [-]	1.60 (0.10)	**1.90 (7.80)**	1.55 – 2.13
Persister formation effect parameters			
θ $k_{P,LEV1}$ [h^{-1}]	8.94·10^{-2} (9.10)	**1.11·10^{-1} (10.7)**	8.69·10^{-2} – 1.32·10^{-1}
θ $k_{P,LEV2}$ [h^{-1}]	1.52 ·10^{-1}(9.70)	**1.79·10^{-1} (8.45)**	1.48·10^{-1}- 2.05·10^{-1}
θ $k_{P,LEV3}$ [h^{-1}]	3.03·10^{-3} (0.40)	**4.34·10^{-3} (24.7)**	2.23·10^{-3} – 6.41·10^{-3}
Interindividual variability (PK), %CV			
ω CL	56.7 (7.0)	**71.3 (28.1)**	49.8 – 96.1
ω V_c	39.1 FIX	**39.1 FIX**	-
Interindividual variability (PD), %CV			
ω E_{max}	39.2 (0.0)	**33.4 (26.9)**	23.6 – 42.0
Proportional residual unexplained variability, %			
σ_{PK}	35.6 (14.7)	**35.5 (4.49)**	33.0 – 39.0
Additive residual unexplained variability			
$\sigma_{droplet\ plate}$	2.25 (0.0)	**2.20 (3.22)**	2.09 – 2.37
σ_{CASY}	1.24 (14.7)	**1.22 (4.64)**	1.14 – 1.35

RSE: Relative standard error (obtained from the variance-covariance matrix); CI: confidence interval, determined by the sampling importance resampling (SIR) method; %CV: coefficient of variation (calculated according to Equation 2.27).
Pharmacokinetic (PK) parameters: CL: clearance, V_c: central volume of distribution, V_p :peripheral volume of distribution, Q: intercompartmental clearance, SF: scaling factor, relating ω V_c to ω Q.
Pharmacodynamic (PD) parameters, related to bacterial growth: k_{g,N_DYN}: growth rate constant in the dynamic *in vitro* infection model, k_{g,N_STAT}: growth rate constant in the static *in vitro* infection model, k_d: death rate constant, N_0: inoculum number in colony forming units (CFU) on a $\log_{10}$ scale, N_P: initial bacterial number in persisting subpopulation on a $\log_{10}$ scale; N_D: initial number of dead bacterial cells on a $\log_{10}$ scale, $popmax$: maximum bacterial number in the stationary growth stage in the dynamic *in vitro* infection model in CFU on a $\log_{10}$ scale, fractional change of $popmax$: according to equation 2.29, k_{NP} : persister formation rate constant, k_{PN} : back-transformation rate constant.
PD parameters, related to LEV effect: E_{max}: maximum levofloxacin effect on bacterial killing according to Equation 2.11 and 2.12, $EC_{50,1}$: levofloxacin concentration (C_{LEV}) causing 50% of the maximum killing effect for sequence type (ST) 58, $EC_{50,2}$ C_{LEV} causing 50% of the maximum killing effect for ST88, $EC_{50,3}$: C_{LEV} causing 50% of the maximum killing effect for ST167, $Hill$: Hill factor (steepness of concentration-effect relationship), $k_{P,LEV1}$ levofloxacin-dependent additive increase in persister cell formation (according to Equation 2.13 and 2.14) for ST58, $k_{P,LEV2}$: levofloxacin-dependent additive increase in persister cell formation for ST88, $k_{P,LEV3}$: levofloxacin-dependent additive increase in persister cell formation for ST167.
θ: fixed-effects parameter, ω: random-effects parameter (interindividual variability), σ: random-effects parameter (residual unexplained variability).

Overall, LEV effect parameters estimated based on the full dataset were comparable to parameter estimates solely based on static IVIM experiments and bacterial quantification by means of the droplet plate assay. SIR increased precision of parameter estimates for most parameters and provided more reliable assessment of parameter uncertainty compared to the covariance matrix, but did not result in significant changes of parameter estimates. The maximum initial killing effect E_{max} was 1.1-fold higher for the full dataset compared to estimation solely based on sIVIM experiments (7.32 h^{-1} vs. 6.88 h^{-1}). Accordingly, EC_{50} values were approx. 1.2- fold higher compared to static exposure for ST58 (17.2 vs 14.1 mg/L) and 3.6-fold higher for ST167 (8.46 vs 2.33 mg/L), indicating that higher C_{LEV} were required to achieve 50% of the maximum effect in the dIVIM for these isolates. However, EC_{50} for ST88 was the same estimated based on the full dataset compared to static experiments (3.10 mg/L). Differences between the isolates in LEV potency were even more pronounced accounting for both static and dynamic IVIM experiments, with a 5.5-fold higher EC_{50} value for ST58 (17.2 mg/L) compared to ST88 (3.10 mg/L) and a 2-fold higher EC_{50} value compared to ST167 (8.46 mg/L). Furthermore, the additive increase in persister cell formation under LEV exposure, quantified by strain-specific $k_{P,LEV}$ values, was estimated three orders of magnitude higher based on the full dataset, including the total electronic cell counts as a measure for the aggregated bacterial number of three bacterial compartments for ST58 and ST88 compared to estimates based on static experiments: For ST58, approx. 10^5 additional CFU per one million CFU and hour transformed into the persisting phenotype under LEV exposure (compared to 141 additional CFU per one million CFU and hour based on static experiments), and for ST88, $1.79 \cdot 10^5$ CFU per one million CFU and hour turned into persister cells (compared to 84 CFU

estimated based on static experiments). These findings might be explained by additional information on the persister cell compartment provided by the total electronic cell counts, which were solely obtained in static, not in dynamic IVIM experiments. For ST167, persister cell formation increased $4.34 \cdot 10^3$ CFU per one million CFU and hour under LEV exposure, estimated based on the full dataset (vs. $3.33 \cdot 10^4$ in the static PK/PD model), indicating a lower increase in persister cell formation under dynamic exposure for the isolate. Overall, the extent of persister cell formation under LEV exposure was highest for ST88, with strain-dependent differences in the impact of the exposure pattern. High IIV in LEV clearance was estimated based on the full dataset (71.3%), while IIV in E_{max} values was moderate. Proportional RUV was split up in three RUV values, associated with three employed bioanalytical assays, and was largest for the droplet plate assay and smallest for C_{LEV}.

3.3.2.5 Nonlinear mixed-effects model evaluation

Appropriateness of the structural **bacterial growth model** was evaluated stratifying per bacterial strain and experimental setting (static or dynamic IVIM), utilising basic GOF plots (chapter 2.4.2.8). Bacterial growth without antibiotic exposure was adequately characterised for the three investigated *E. coli* isolates. Accounting for the two different experimental settings as categorical covariate, GOF plots showed population and individual predictions of bacterial numbers narrowly and randomly scattering around the line of identity (Figure 3.25). Observed and predicted maximum bacterial numbers were one order of magnitude higher for the static compared to the dynamic experimental setting.

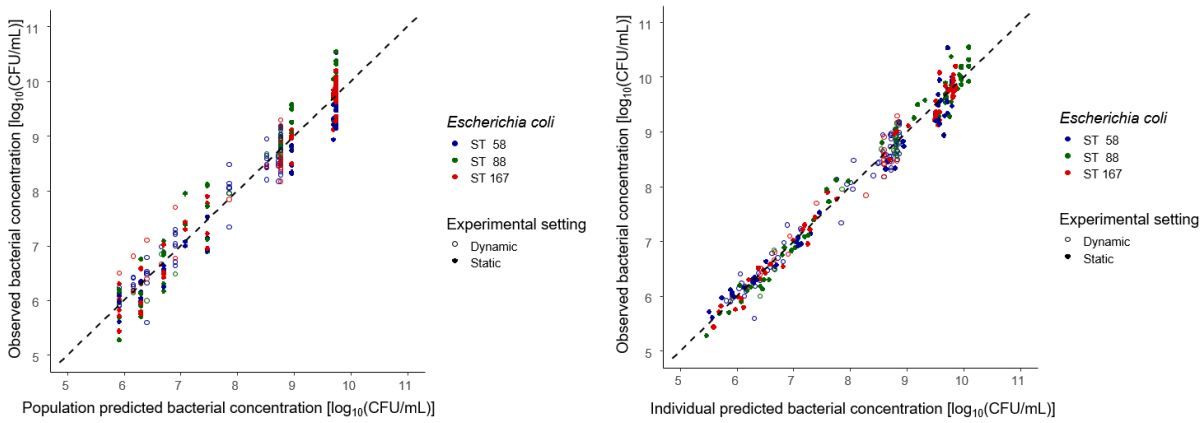

Figure 3.25: Observed bacterial concentrations of three *Escherichia coli* strains (ST58, ST88 and ST167) in growth control replicates in dynamic (open circles) and static (filled circles) *in vitro* infection model experiments, versus population predictions (left) and individual predictions (right) based on the final bacterial growth model, dashed lines: lines of identity, symbols: bacterial concentrations, colours: bacterial strains; CFU: colony forming units, ST: sequence type.

Conditional weighted residuals were in an acceptable range (between -2.95 and +3.37) and did not show any trends for one isolate or exposure pattern over time or bacterial concentration (Figure 3.26).

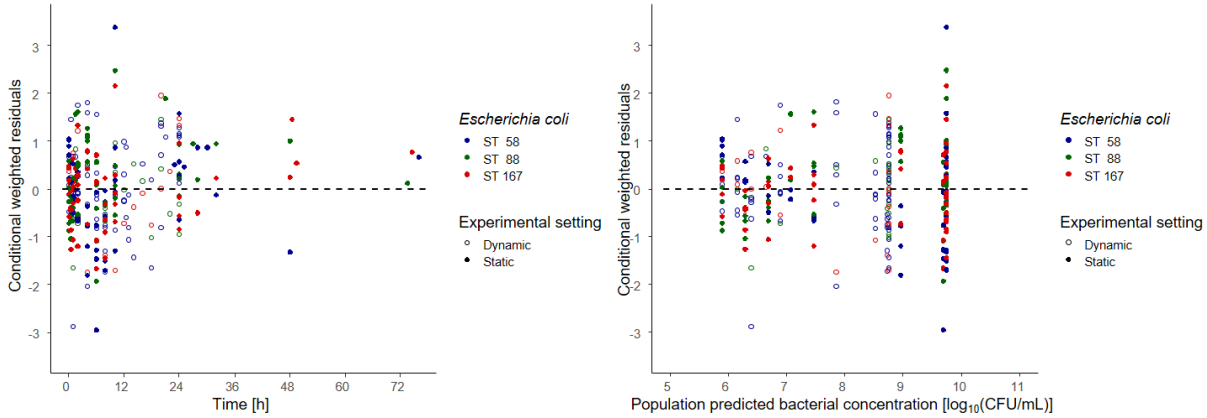

Figure 3.26: Conditional weighted residuals (CWRES) versus time (left) and population predictions (right) of bacterial concentrations in growth control replicates of three *Escherichia coli* strains (ST58, ST88 and ST167) in dynamic (open circles) and static (filled circles) *in vitro* infection model experiments, dashed lines: CWRES=0; symbols: CWRES, colours: bacterial strains; CFU: colony forming units, ST: sequence type.

The **static PK/PD model** was evaluated stratifying per bacterial strain and MIC-normalised C_{LEV}. Overall, the central tendency of bacterial concentrations in the sIVIM was adequately characterised by the PK/PD model for three *E. coli* isolates under LEV exposure (Figure 3.27). For ST58 and ST88 under 2-fold MIC exposure and for ST167 under 1-fold MIC exposure, observed bacterial concentrations were for some observations much higher than population predictions and individual predictions, which could most likely be explained by a large experimental variability for exposure to C_{LEV} around the MIC. However, no systematic trend was observed for one bacterial isolate or MIC-normalised C_{LEV}, indicating that the structural model adequately characterised growth and kill behaviour of the three isolates in the sIVIM. Conditional weighted residuals were between -2.54 and +3.28, indicating no major bias in the structural model (Figure 3.28).

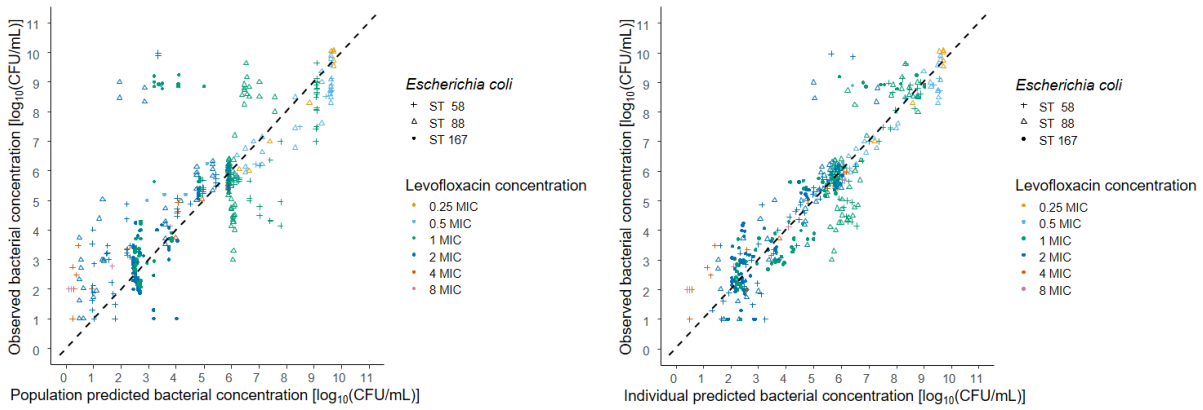

Figure 3.27: Observed bacterial concentrations of three *Escherichia coli* strains (ST58, ST88 and ST167) under levofloxacin exposure in static *in vitro* infection model experiments, versus population predictions (left) and individual predictions (right) based on the final static PK/PD model, dashed lines: lines of identity, symbols: bacterial strains; colours: levofloxacin concentration, normalised to the minimal inhibitory concentration (MIC) of the isolate, CFU: colony forming units, ST: sequence type.

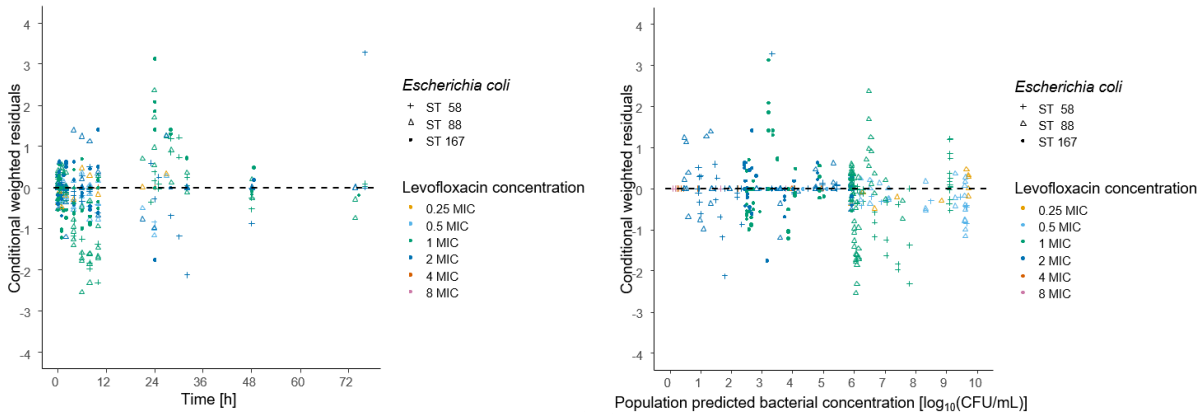

Figure 3.28: Conditional weighted residuals (CWRES) versus time (left) and population predictions (right) of bacterial concentrations of three *Escherichia coli* strains (ST58, ST88 and ST167) under levofloxacin exposure in static *in vitro* infection model experiments, dashed lines: CWRES=0; symbols: bacterial strains; colours: levofloxacin concentration, normalised to the minimal inhibitory concentration (MIC) of the isolate, CFU: colony forming units, ST: sequence type.

The structural **PK model** was evaluated stratified per mimicked dosing regimen (Figure 3.29). Observed C_{LEV} versus population predictions scattered randomly around the line of identity, showing no trend towards over- or underprediction for one of the dosing regimens (Figure 3.29, upper panel). However, individual predictions, being determined by the structural and the stochastic submodel were slightly larger compared to observations (Figure 3.29, lower panel). Overprediction of individual C_{LEV} was more pronounced for the 500 mg bid dosing regimen (Figure 3.29, green symbols) compared to the 750 mg qd dosing regimen (orange symbols).

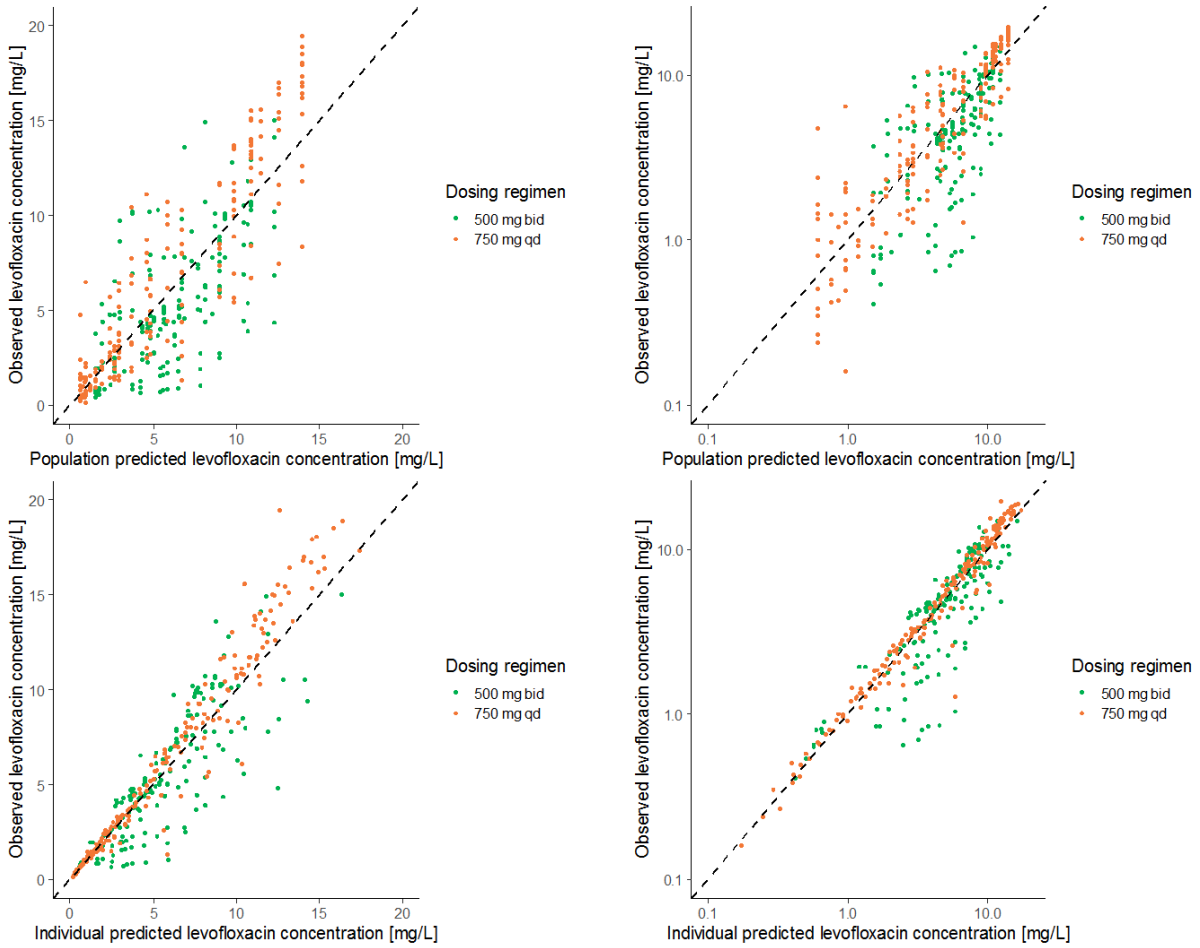

Figure 3.29: Observed levofloxacin (LEV) concentrations in dynamic *in vitro* infection model experiments, mimicking LEV concentration-time profiles resulting from administration of 500 mg, 60 min LEV i.v. infusions twice daily (bid, green symbols, n=7 replicates) or a 750 mg, 90 min i.v. LEV infusion once daily (qd, orange symbols, n=14 replicates) versus population predictions (upper panel) and individual predictions (lower panel) based on the final pharmacokinetic model, left: linear scaling: right: logarithmic scaling; dashed lines: lines of identity, symbols: LEV concentrations.

Conditional weighted residuals were overall in an acceptable range (between -3.0 and +2.6, Figure 3.30). A trend towards overprediction was indicated by a larger fraction of negative compared to positive residuals. For the 500 mg bid dosing, more negative residuals were observed compared to the 750 mg qd dosing regimen, especially after the second LEV administration at t=12 h (Figure 3.30, left). No trend in conditional weighted residuals was observed for population predictions of C_{LEV} (Figure 3.30, right).

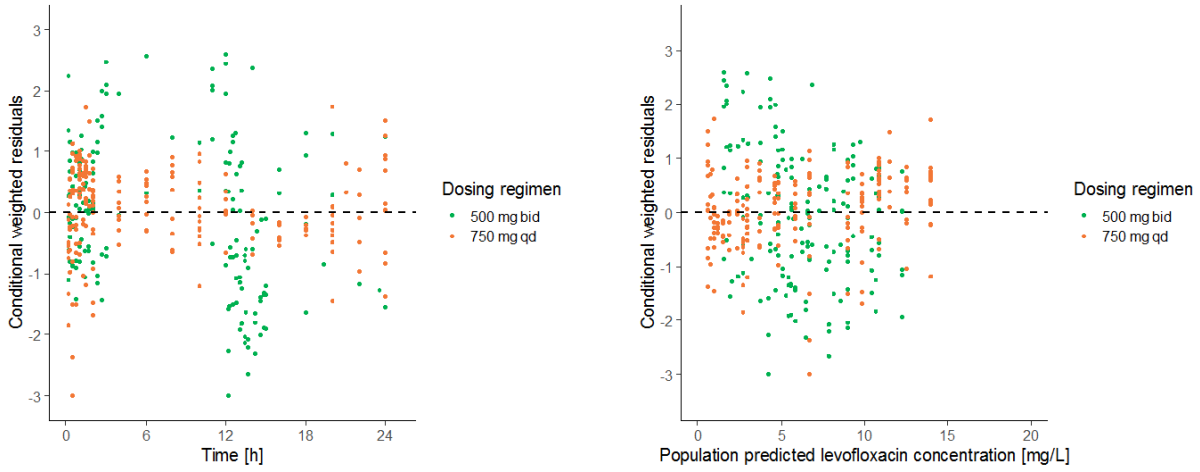

Figure 3.30: Conditional weighted residuals (CWRES) versus time (left) and population predictions (right) of levofloxacin (LEV) concentrations in dynamic *in vitro* infection model experiments, mimicking LEV concentration-time profiles resulting from administration of 500 mg, 60 min LEV i.v. infusions twice daily (bid, green symbols, n=7 replicates) or a 750 mg, 90 min i.v. LEV infusion once daily (qd, orange symbols, n=14 replicates), dashed lines: CWRES=0; symbols: CWRES.

The predictive performance of the PK model was evaluated by VPCs, stratified for the two mimicked dosing regimens (Figure 3.31, Figure 3.32).

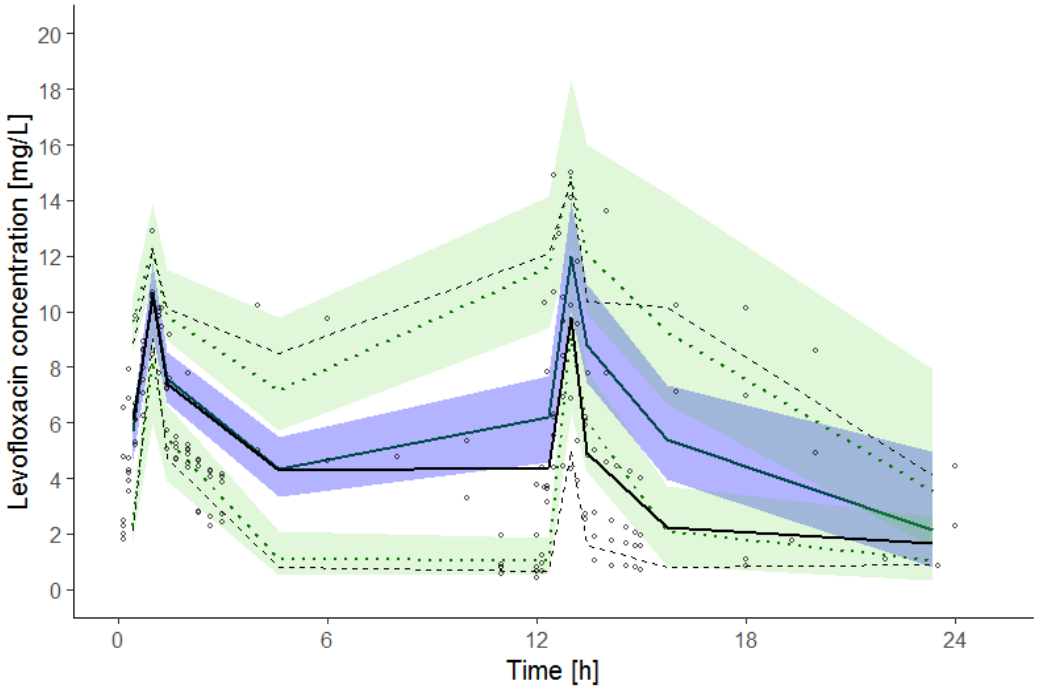

Figure 3.31: Visual predictive check (n=1000 simulations) for the *in vitro* pharmacokinetic model, based on experimental levofloxacin (LEV) concentration-time profiles resulting from a 500 mg, 60 min intravenous LEV infusion twice daily, mimicked in dynamic *in vitro* infection model experiments (black symbols, n=7 replicates), black solid line: median of observed LEV concentrations, black dashed lines: 5^{th} and 95^{th} percentile of observations, green solid line and blue shaded area: median and 90% confidence interval of simulations, green dashed lines and green shaded areas: 5^{th} and 95^{th} percentile and 90% confidence interval of simulations.

For the 500 mg bid dosing regimen, percentiles of observations were mostly within the 90% CI of respective percentiles of 1000 simulated LEV C(t) profiles (Figure 3.31). Yet, observed C_{LEV} after the second administration at t=12 h showed high experimental variability, represented in larger observation intervals compared to the first administration at t=0 h. However, some observations were above the 90% prediction interval of simulated C_{LEV}, which were mainly contributed by ID 10, while C_{LEV} below the 90% prediction interval were mainly contributed by ID 3 and ID 4 (Figure 7.14).

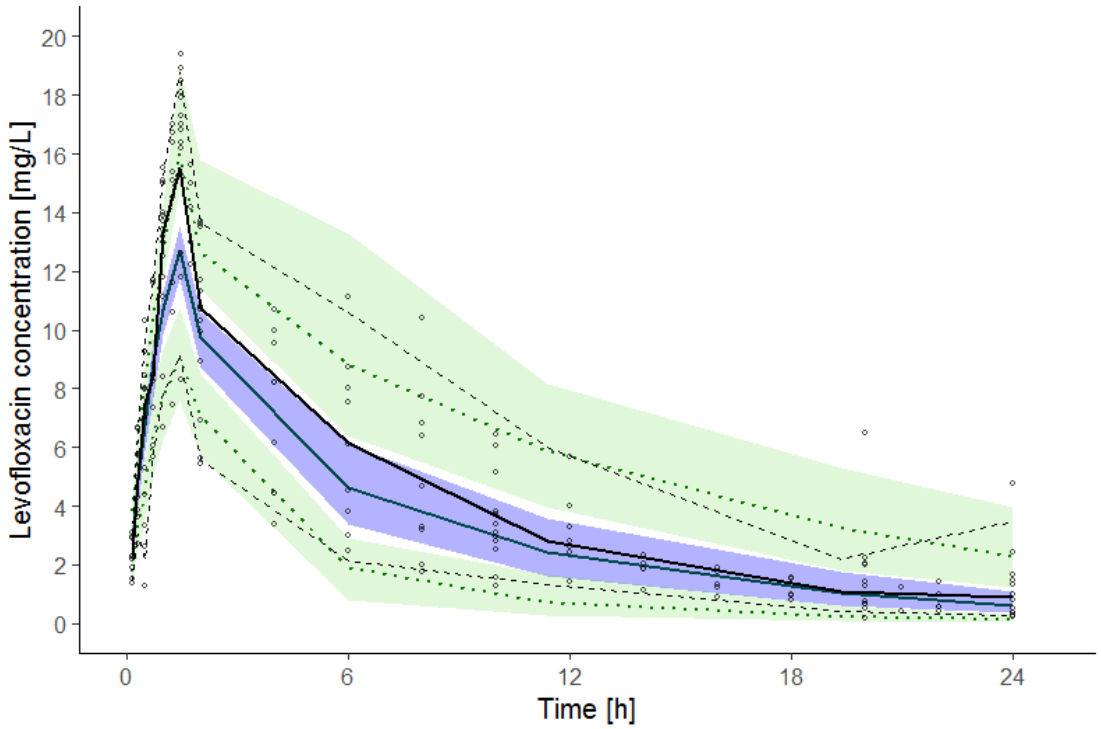

Figure 3.32: Visual predictive check (n=1000 simulations) for the *in vitro* pharmacokinetic model, based on experimental levofloxacin (LEV) concentration-time profiles resulting from a 750 mg, 90 min intravenous LEV infusion, mimicked in dynamic *in vitro* infection model experiments (black symbols, n=14 replicates), black solid line: median of observed LEV concentrations, black dashed lines: 5th and 95th percentile of observations, green solid line and blue shaded area: median and 90% confidence interval of simulations, green dashed lines and green areas: 5th and 95th percentile and 90% confidence interval of simulations.

Overall, the PK model showed adequate predictive performance for C_{LEV} observed in experimental replicates mimicking the 750 mg qd dosing regimen (Figure 3.32). Observed C_{LEV} above the 90% prediction interval were mainly contributed by ID 20 (Figure 7.15). Hence, case deletion diagnostics were performed (chapter 2.4.2.8) to investigate the influence of single IDs on parameter estimates. However, only ID 4 was identified as influential individual, with a dOFV of 4.46 and a covariance ratio > 1, indicating that exclusion of ID 4 increased parameter imprecision. As conspicuously high or low C_{LEV} were observed for ID 3, ID 4, ID 10 and ID 20, PK parameters were re-estimated excluding these IDs one after the other. Apart from a lower RUV when excluding ID 4 (24.5% vs 26.9%), parameter estimates were within the 95% CI of parameter estimates based of the full dataset, derived by the SIR technique (Table 7.12). Hence, no ID was excluded from further analysis.

Robustness of the **three-bacterial-state PK/PD model** was evaluated by re-estimating all parameters simultaneously. Overall, re-estimated PK and bacterial growth parameters were comparable to those obtained based on the developed bacterial growth and PK model (Table 3.13, Table 3.14). However, the initial number of viable cells N_0 was underestimated (5.28 compared to 5.90), and the killing effect parameters E_{max} and EC_{50} and the strain-dependent persister formation effect parameter $k_{P,LEV}$ were estimated higher for the three bacterial strains compared to previous results. Killing effect parameters were precisely estimated (RSE ≤ 15.2%, based on SIR) and discriminated between LEV potency of ST58 (EC_{50}: 38.2 mg/L), ST88 (EC_{50}: 7.31 mg/L) and ST167 ($EC_{50:}$ 18.6 mg/L). Although the magnitude of the killing effect parameter estimates was higher compared to sequentially estimated parameters, the order of EC_{50} values of the three strains did not change (ST58 > ST167 > ST88), when all parameters were estimated simultaneously. In contrast, the order of the strains regarding their $k_{P,LEV}$ values was different to sequentially estimated parameters, being highest for ST167 ($1.39 \cdot 10^5$ additional CFU per one million CFU and hour) and lowest for ST58 (191 additional CFU per one million CFU and hour). Of note, parameter precision was higher for $k_{P,LEV}$ of ST167 compared to previous results (9.74% vs 24.7% RSE, based on SIR), while P_{LEV} of ST58 and ST88 were less precisely estimated (25.9% and 22.4% RSE, respectively, based on SIR).

Table 3.14: Simultaneously re-estimated parameter values and imprecision of the three-bacterial-state pharmacokinetic/pharmacodynamic model; describing growth and kill behaviour of three *Escherichia coli* isolates under levofloxacin exposure in static and dynamic *in vitro* infection model experiments.

Parameter [unit]	Estimate	Estimate (RSE, %) based on SIR	95% CI based on SIR
Pharmacokinetic parameters			
θ CL [L·h^{-1}]	9.17	**9.17 (12.0)**	7.45 – 12.0
θ V_c [L]	27.6	**27.6 (11.7)**	21.1 - 34.1
θ V_p [L]	44.2	**44.2 (8.77)**	35.7 – 50.9
θ Q [L·h^{-1}]	27.9	**27.9 (14.1)**	20.0 – 35.1
θ SF [-]	0.996	**0.966 (25.5)**	0.395 – 1.40
Bacterial growth parameters			
θ k_{g,N_DYN} [h^{-1}]	1.72	**1.72 (10.3)**	1.37 – 2.04
θ k_{g,N_STAT} [h^{-1}]	2.51	**2.51 (6.08)**	2.15 - 2.75
θ k_d [h^{-1}]	0.0369	**0.0269 (19.7)**	0.0165 – 0.0370
θ N_0 [log$_{10}$(CFU)]	5.28	**5.28 (1.27)**	5.16 – 5.42
θ N_P [log$_{10}$(CFU)]	2.72	**2.72 (8.46)**	2.21 – 3.10
θ N_D [log$_{10}$(CFU)]	0.45	**0.450 (22.9)**	0.287 – 0.711
θ $popmax$ [log$_{10}$(CFU)]	8.74	**8.74 (1.46)**	8.46 – 8.98
θ Fractional change $popmax$ [log$_{10}$(CFU)]	0.0924	**0.0924 (16.2)**	0.065 – 0.127
Transformation rate constants			
θ k_{NP} [h^{-1}]	0.0	**$1.06 \cdot 10^{-6}$ (25.1)**	$6.47 \cdot 10^{-7}$ – $1.65 \cdot 10^{-6}$
θ k_{PN} [h^{-1}]	0.467	**0.467 (9.87)**	0.343 – 0.518
Killing effect parameters			
θ E_{max} [h^{-1}]	9.60	**9.60 (9.72)**	7.76 – 11.3
θ $EC_{50,1}$ [mg/L]	38.2	**38.2 (15.2)**	27.6 – 50.2
θ $EC_{50,2}$ [mg/L]	7.31	**7.31 (13.4)**	5.66 – 9.40
θ $EC_{50,3}$ [mg/L]	18.6	**18.6 (14.0)**	14.6 – 24.5
θ $Hill$ [-]	1.01	**1.01 (9.93)**	0.836 – 1.22
Persister formation effect parameters			
θ $k_{P,LEV1}$ [h^{-1}]	$1.9 \cdot 10^{-4}$	**$1.91 \cdot 10^{-4}$ (25.9)**	$7.56 \cdot 10^{-5}$ – $2.65 \cdot 10^{-4}$
θ $k_{P,LEV2}$ [h^{-1}]	$7.78 \cdot 10^{-2}$	**$7.78 \cdot 10^{-2}$ (22.4)**	$4.93 \cdot 10^{-2}$ – $1.14 \cdot 10^{-1}$
θ $k_{P,LEV3}$ [h^{-1}]	$1.33 \cdot 10^{-1}$	**$1.39 \cdot 10^{-1}$ (9.74)**	$1.09 \cdot 10^{-1}$ – $1.59 \cdot 10^{-1}$
Interindividual variability (PK), %CV			
ω CL	58.0	**58.0 (19.3)**	45.2 – 70.4
ω V_c	44.4	**44.3 (34.7)**	29.7 – 61.6
Interindividual variability (PD), %CV			
ω E_{max}	24.3	**24.3 (25.4)**	18.4 – 31.2
Proportional residual unexplained variability (PK), %			
σ_{PK}	35.6	**35.6 (4.58)**	32.4 – 39.0
Additive residual unexplained variability (PD)			
$\sigma_{droplet\ plate}$	2.58	**2.58 (3.26)**	2.44 – 2.77
σ_{CASY}	1.37	**1.37 (5.64)**	1.23 – 1.54

RSE: Relative standard error (obtained from the variance-covariance matrix); CI: confidence interval, determined by the sampling importance resampling (SIR) method; %CV: coefficient of variation (calculated according to Equation 2.27).
Pharmacokinetic (PK) parameters: CL: clearance, V_c: central volume of distribution, V_p :peripheral volume of distribution, Q: intercompartmental clearance, SF: scaling factor, relating ω V_c to ω Q.
Pharmacodynamic (PD) parameters, related to bacterial growth: k_{g,N_DYN}: growth rate constant in the dynamic *in vitro* infection model, k_{g,N_STAT}: growth rate constant in the static *in vitro* infection model, k_d: death rate constant, N_0: inoculum number in colony forming units (CFU) on a $\log_{10}$ scale, N_P: initial bacterial number in persisting subpopulation on a $\log_{10}$ scale; N_D: initial number of dead bacterial cells on a $\log_{10}$ scale, $popmax$: maximum bacterial number in the stationary growth stage in the dynamic *in vitro* infection model in CFU on a $\log_{10}$ scale, fractional change of $popmax$: according to equation 2.29, k_{NP} : persister formation rate constant, k_{PN} : back-transformation rate constant.
PD parameters, related to LEV effect: E_{max}: maximum levofloxacin effect on bacterial killing according to Equation 2.11 and 2.12, $EC_{50,1}$: levofloxacin concentration (C_{LEV}) causing 50% of the maximum killing effect for sequence type (ST) 58, $EC_{50,2}$ C_{LEV} causing 50% of the maximum killing effect for ST88, $EC_{50,3}$: C_{LEV} causing 50% of the maximum killing effect for ST167, $Hill$: Hill factor (steepness of concentration-effect relationship), $k_{P,LEV1}$ levofloxacin-dependent additive increase in persister cell formation (according to Equation 2.13 and 2.14) for ST58, $k_{P,LEV2}$: levofloxacin-dependent additive increase in persister cell formation for ST88, $k_{P,LEV3}$: levofloxacin-dependent additive increase in persister cell formation for ST167.
θ: fixed-effects parameter, ω: random-effects parameter (interindividual variability), σ: random-effects parameter (residual unexplained variability).

Appropriateness of the three-bacterial-state PK/PD model model was shown for C_{LEV} (Figure 7.16, Figure 7.17), bacterial concentrations assessed via droplet plate assay (Figure 7.18, Figure 7.19) and electronic cell counting (Figure 7.20). Adequate agreement between observed bacterial concentrations and individual and population predictions is exemplified by GOF plots for bacterial concentrations under LEV exposure in the dIVIM (Figure 3.33). No trend was observed for any of the strains, but lower bacterial concentrations compared to population predictions were observed for bacteria under exposure to LEV C(t) profiles mimicking a 500 mg bid administration, indicating a potential bias for this dosing regimen in the structural submodel (Figure 3.33, left, green symbols). However, the tendency was not visible comparing observations to individual predictions (Figure 3.33, right), indicating appropriateness of the stochastic submodel. Overall, the appropriateness of the model for the 500 mg bid dosing regimen could not be comprehensively evaluated, as it was only investigated exposing one isolate (ST58).

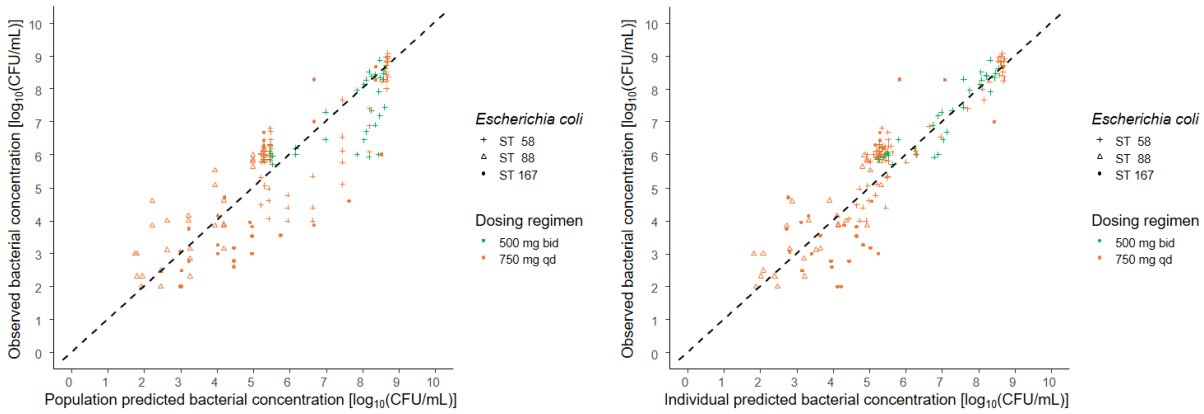

Figure 3.33: Observed bacterial concentrations of three *Escherichia coli* isolates under levofloxacin (LEV) exposure in dynamic *in vitro* infection model experiments, mimicking LEV concentration-time profiles resulting from administration of 500 mg, 60 min LEV i.v. infusions twice daily (bid, green symbols, n=7 replicates) or a 750 mg, 90 min i.v. LEV infusion once daily (qd, orange symbols, n=14 replicates) versus population predictions (left) and individual predictions (right) based on the final three-bacterial-state pharmacokinetic/pharmacodynamic model, dashed lines: lines of identity, symbols: bacterial strains; CFU: colony forming units, ST: sequence type.

Conditional weighted residuals were in an acceptable range (between -2.01 and +2.23) and did not show a bias for any of the isolates or dosing regimens (Figure 3.34).

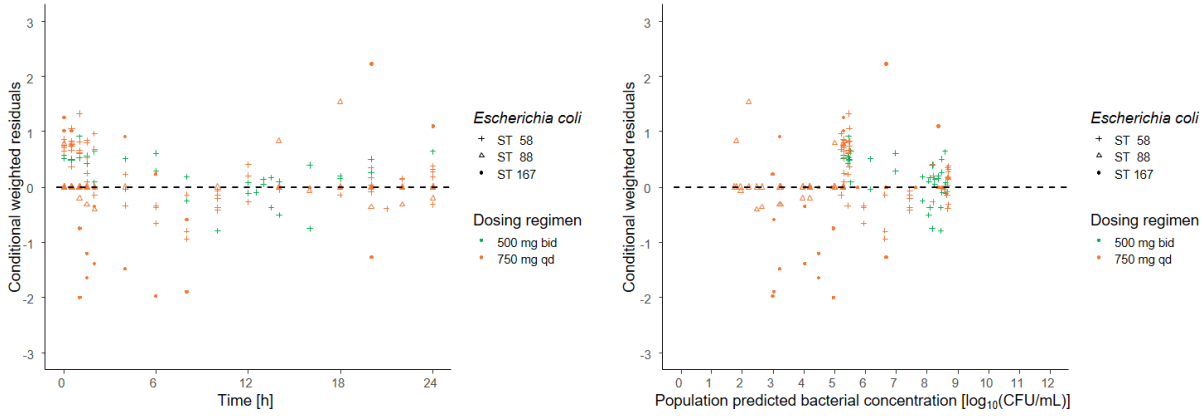

Figure 3.34: Conditional weighted residuals (CWRES) versus time (left) and population predictions (right) of bacterial concentrations of three *Escherichia coli* strains (ST58, ST88 and ST167) under levofloxacin (LEV) exposure in dynamic *in vitro* infection model experiments, mimicking LEV concentration-time profiles resulting from administration of 500 mg, 60 min LEV i.v. infusions twice daily (bid, green symbols, n=7 replicates) or a 750 mg, 90 min i.v. LEV infusion once daily (qd, orange symbols, n=14 replicates), dashed lines: CWRES=0; symbols: bacterial strains; CFU: colony forming units, ST: sequence type.

The VPC showed adequate predictive performance of the three-bacterial-state PK/PD model for the growth and kill behaviour of three *E. coli* isolates under exposure to dynamic LEV C(t) profiles resulting from a 750 mg, 90 min i.v. infusion and for ST58 under exposure to mimicked LEV C(t) profiles resulting from administration of a 500 mg, 60 min i.v. infusion twice daily (Figure 3.35, upper panel). The median of observed bacterial concentrations (black solid line) was mainly within the 90% CI around the median of simulated bacterial numbers (green solid line and blue shaded area) for the three isolates and two dosing regimens. The fraction of bacterial numbers below the LLOQ of the droplet plate assay (100 CFU/mL, horizontal black dashed line) was adequately captured (Figure 3.35, lower panel). For exposure of ST58 to the 500 mg, 60 min i.v. infusions twice daily, no bacterial concentrations below the LLOQ of the droplet plate assay were observed [131,162], in line with the median prediction of the fraction of bacterial numbers below the LLOQ for this dosing regimen (Figure 3.35, lower panel, green solid line covered by black solid line).

The VPC for bacterial time-kill trajectories in the sIVIM showed overall good agreement between observed bacterial concentrations and simulated bacterial numbers for the three isolates under static exposure to C_{LEV} between 0.25-fold and 8-fold the MIC, with small deviations for ST88 under exposure to 2- and 4-fold the MIC value of the isolate (Figure 7.21).

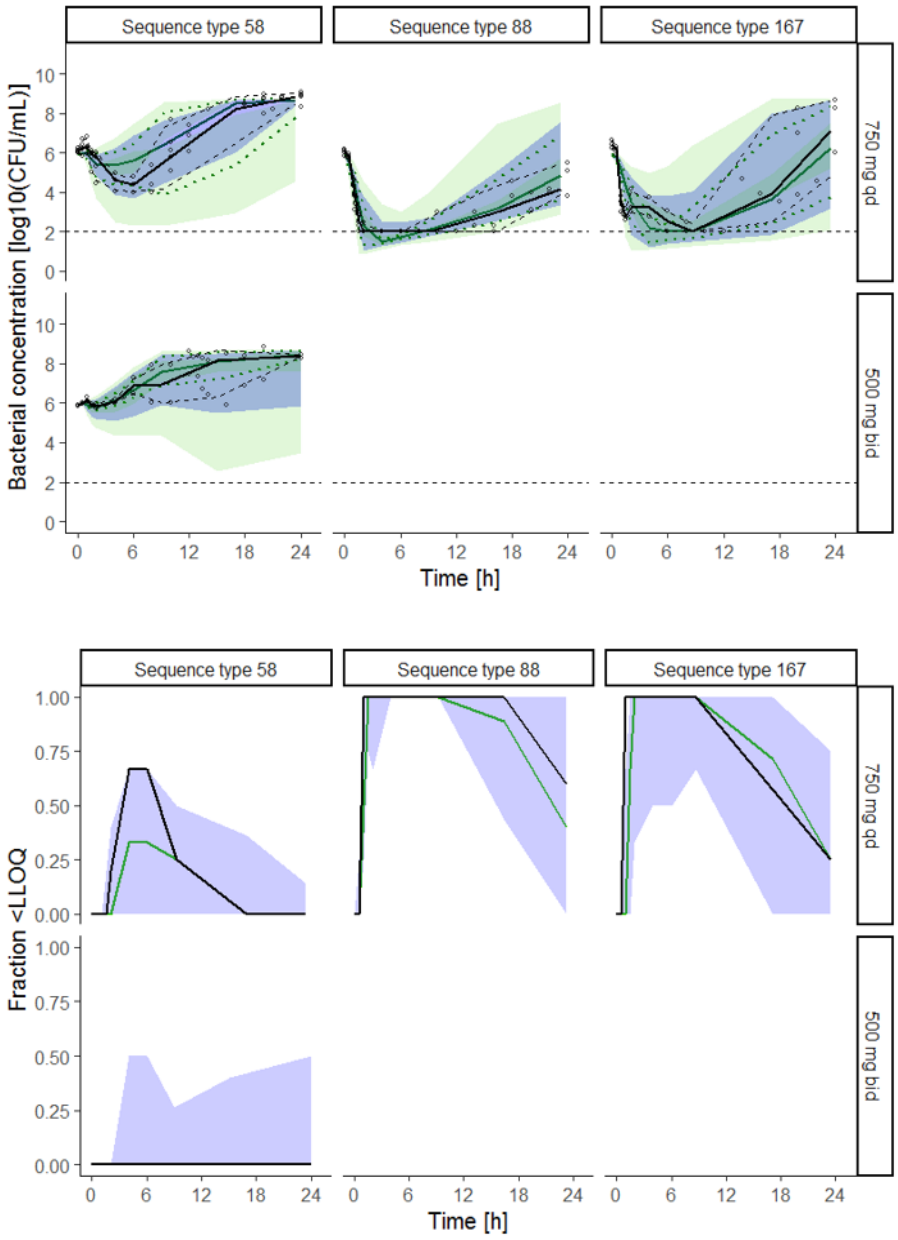

Figure 3.35: Visual predictive check (n=1000 simulations) of the three-bacterial-state pharmacokinetic/pharmacodynamic model for growth and kill behaviour of three *Escherichia coli* isolates (Sequence type 58, 88 and 167) under levofloxacin (LEV) exposure in dynamic *in vitro* infection model experiments, mimicking LEV concentration-time profiles resulting from administration of a 750 mg, 90 min i.v. LEV infusion once daily (qd, upper panels) or 500 mg, 60 min LEV i.v. infusions twice daily (bid, lower panels) and fraction of bacterial concentrations being below the lower limit of quantification (LLOQ); black solid line: median of observations, black dashed lines: 5th and 95th percentile of observations, green solid line and blue shaded area: median and 90% confidence interval of simulations, green dashed lines and green areas: 5th and 95th percentile and 90% confidence interval of simulations; black dashed line at y=2: LLOQ=10^2 CFU/mL.

3.3.2.6 Nonlinear mixed-effects model exploration

Stochastic simulations were leveraged to graphically explore the trajectories of the three discerned bacterial subpopulations under static LEV exposure and under exposure to dynamic LEV C(t) profiles (Figure 3.36). Under simulated exposure to static C_{LEV} (Figure 3.36, A), at C_{LEV} ≥ 2-fold MIC for ST58 and ST88, initial killing and regrowth was observed within 24 h and the median of simulated bacterial numbers of the persister subpopulation (red solid lines) exceeded median of the growing bacterial subpopulations (green solid lines). For ST167, simulated trajectories of growing bacteria did not show regrowth within 24 h and the persister subpopulation exceeded the growing bacterial population under exposure to C_{LEV} ≥ 1-fold MIC. For all isolates under simulated dynamic exposure to the 750 mg, 90 min i.v. infusion (Figure 3.36, B, left), the simulated number of growing bacteria was initially reduced, which was followed by regrowth. Under simulated exposure to two 500 mg, 60 min i.v. infusions (Figure 3.36, right), the growing subpopulation of ST58 showed no initial reduction, but delayed growth, while ST88 and ST167 showed initial killing and regrowth, with a second killing and regrowth phase after the second administration at t=12 h. The persisting subpopulation increased with a strain-specific extent, being largest for ST88, followed by ST58 and being smallest for ST167, in agreement with the estimated $k_{P,LEV}$ values of the isolates. For ST88 and ST167, the median number of persister cells exceeded the median number of growing bacteria in the dynamic experimental setting under exposure to both dosing regimens. For ST58, the median of the growing bacterial subpopulation remained above the persisting subpopulation for 24 h under dynamic exposure to both simulated dosing regimens.

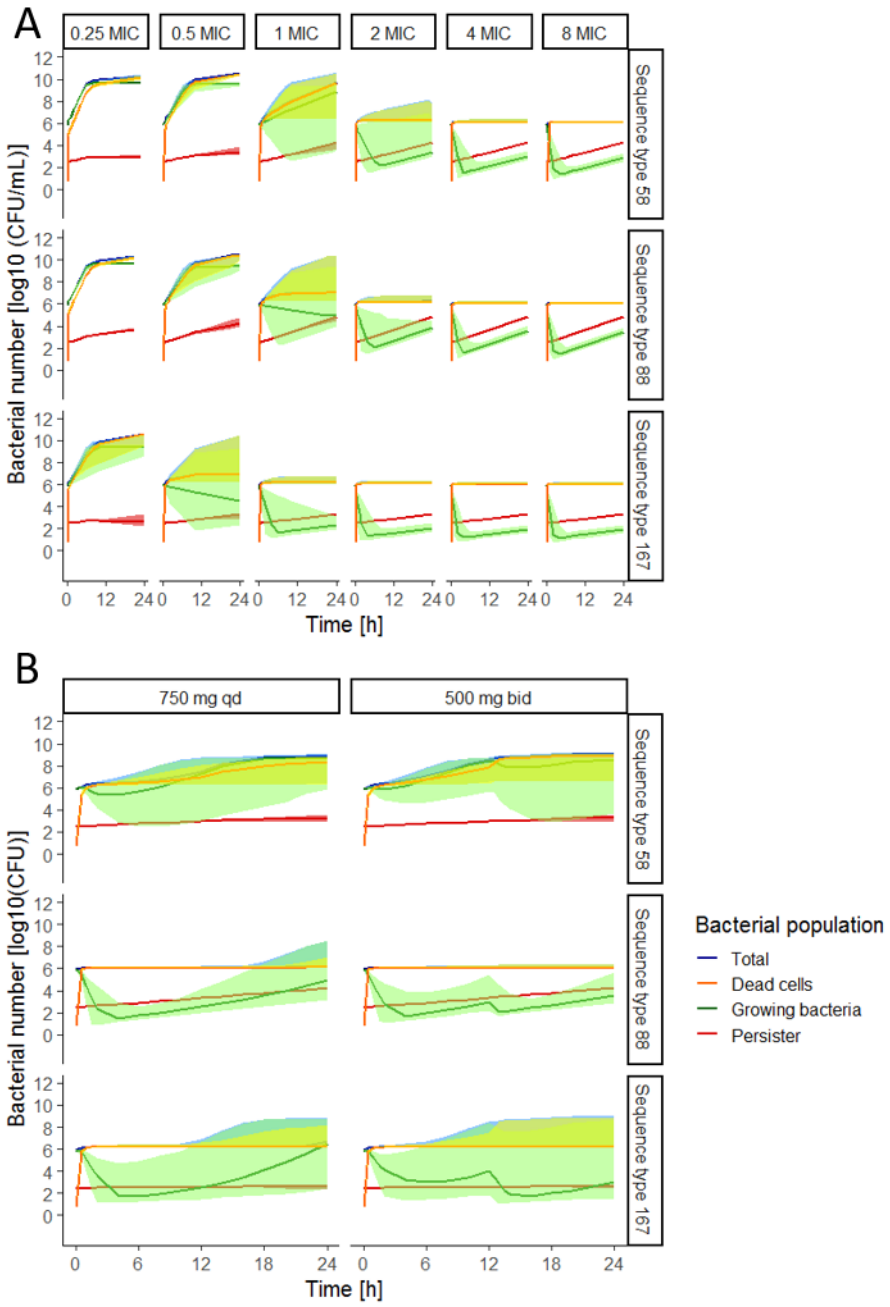

Figure 3.36: Medians (solid lines) and 90% confidence intervals (shaded areas) of simulated bacterial numbers in different bacterial populations over time under levofloxacin (LEV) exposure in static (A) and dynamic (B) *in vitro* infection model experiments, exposing the three *Escherichia coli* isolates (sequence type 58, 88 and 167) to constant LEV concentrations between 0.25- and 8-fold the minimal inhibitory concentration (MIC) of the isolate, and LEV concentration-time profiles resulting from a 750 mg, 90 min i.v. infusion once daily (qd, B, left), and from 500 mg, 60 min LEV i.v. infusions twice daily (bid, B, right); colours: bacterial populations; n=1000 simulations; CFU: colony forming units.

Fractional bacterial numbers over time in the dIVIM (Figure 7.22, top) demonstrated that the simulated persister fraction was negligible for ST58 under dynamic LEV exposure to 500 mg

bid and 750 mg qd i.v. infusions. High simulated persister fractions emerged for ST88 and ST167 under dynamic LEV exposure to both simulated dosing regimens. Strain-dependent persister formation was simulated under static LEV exposure ≥ 2-fold the MIC for ST58, ≥ 1-fold the MIC for ST88 and ≥ 0.5-fold the MIC for ST167 (Figure 7.22, middle). The fraction of persister cells was negligible for unexposed bacteria (Figure 7.22, bottom).

The median C_{LEV} - dependent killing effect, simulated omitting the effect on persister formation by fixing $k_{P,LEV}$ to 0 (chapter 2.4.2.9) followed the C(t) profile in the dIVIM and was much higher than the constant additive effect on persister formation, simulated omitting the killing effect by fixing E_{max} to 0 (Figure 7.23, left). The killing effect was largest for ST88, followed by ST167 and ST58, in agreement with the EC_{50} estimates of the isolates ($EC_{50,2} < EC_{50,3} < EC_{50,1}$). For ST58, the effect on persister formation declined below the killing effect at t=18 h (Figure 7.23, right).

Simulations omitting the LEV effect on persister cell formation showed similar shaped trajectories of the growing bacterial subpopulation compared to simulations accounting for both LEV effects (Figure 3.37 vs Figure 3.36). Increasing persister numbers were simulated under static exposure, being most pronounced for ST88. Under simulated dynamic exposure, the initial number of persisting bacteria remained constant.

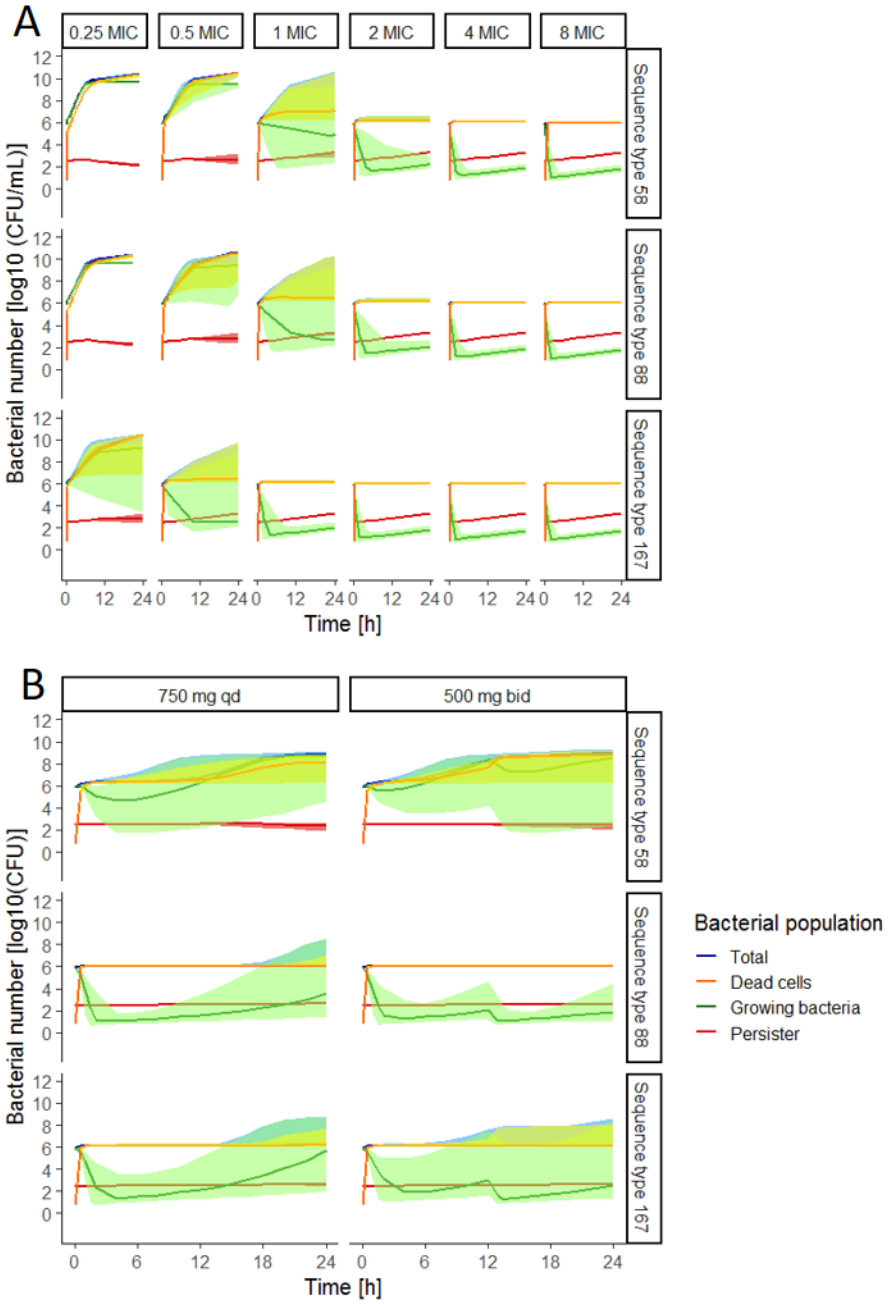

Figure 3.37: Medians (solid lines) and 90% confidence intervals (shaded areas) of simulated bacterial numbers in different bacterial populations over time, omitting the effect on persister formation when exposing three *Escherichia coli* isolates (sequence type 58, 88 and 167) to static levofloxacin (LEV) concentrations between 0.25- and 8-fold the minimal inhibitory concentration (MIC) of the isolate (A), and in dynamic *in vitro* infection model experiments (B), mimicking LEV concentration-time profiles resulting from a 750 mg, 90 min i.v. infusion once daily (qd, B, left) and from 500 mg, 60 min LEV i.v. infusions twice daily (bid, B, right), n=1000 simulations; CFU: colony forming units.

Bacterial numbers, simulated without LEV killing effect were comparable to bacterial growth curves (Figure 7.24). Simulated bacterial numbers in the persisting subpopulation remained on the initial concentration for ST58, increased over time for ST88 and decreased for ST167 under both static and dynamic LEV exposure.

4 Discussion

In the present chapter, results of *in vitro* investigations of growth and kill behaviour of three *E. coli* isolates under LEV exposure in static and dynamic IVIM experiments are discussed (chapter 4.1) and linked to the investigated bacterial adaptation and resistance mechanisms (chapter 4.2). Two PK/PD models, which were developed to (i) quantify the observed exposure-effect relationship using novel PK/PD parameters and to (ii) comprehensively understand the underlying mechanisms of the observed growth, kill and regrowth behaviour are critically discussed with regard to relevant literature (chapter 4.3).

4.1 Investigations of bacterial growth and kill behaviour

Preliminary to sIVIM experiments, LEV stability under the experimental conditions of the sIVIM was shown for C_{LEV} between 2 and 16 mg/L, being within ±15% of nominal C_{LEV} over three days. These findings confirmed previous results, obtained under equal conditions in the same laboratory, showing LEV stability over 24 h (C_{LEV}: 2–16 mg/L, maximum -10% compared to nominal C_{LEV}) [134]. As C_{LEV} did not show a decreasing trend over time, the observed variability was attributed to imprecision or inaccuracy of the applied fluorometric assay, which was quantified as ≤ 7.69% CV and ≤ ±15.2% RE, respectively [135]. Beyond the investigated concentration range, Matos et al. showed LEV stability in Mueller Hinton broth over 48 h at 37°C for C_{LEV}=0.4 mg/L (97.4 ± 4.58% recovery) and 12 mg/L (97.3 ± 3.95% recovery) [175]. In the present investigations, C_{LEV} between 0.5 mg/L and 64 mg/L were applied in sIVIM experiments. Thus, LEV was assumed to be also stable in sIVIM experiments in concentrations of 32 mg/L (n=2 replicates) and 64 mg/L (n=1 replicate).

Investigations of LEV binding to components of the growth medium were performed to justify comparison between C_{LEV} determined *in vitro* in CAMHB and unbound plasma concentrations. Although binding of LEV to plasma proteins *in vivo* is relatively low (between 20% and 40%), with albumin being the predominant binding partner, and concentration independent [84,85,88], an impact of binding to growth medium components should be ruled out. The presented findings suggested a difference in fluorescence signals of CAL before ultrafiltration and in ultrafiltrate, indicating that calibration should always be performed in medium from the same batch as the medium used in the experiment, in which samples were obtained. In case of relevant LEV binding to proteins in CAMHB, $C_{LEV,cal}$ of ultrafiltrate would have been lower compared to $C_{LEV,cal}$ before ultrafiltration, as protein bound drug molecules do not pass the filter membrane and therefore are not detectable in ultrafiltrate [137]. As no statistical significant difference in $C_{LEV,cal}$ before and after ultrafiltration was detected, C_{LEV} determined in CAMHB

samples taken from the IVIM were unbound concentrations and therefore comparable with unbound concentrations *in vivo*. Thus, a relevant impact of LEV binding to components of growth medium was ruled out. However, to mimic *in vivo* protein binding, Zeitlinger et al. suggested addition of 12% albumin to Mueller-Hinton broth [139]. Their investigations showed a relevant impact of albumin addition on the killing effect of moxifloxacin (PB ~38%) and trovafloxacin (PB ~78%) against *S. aureus* and *P. aeruginosa* in sIVIM experiments. Moreover, diverse supplements to bacterial growth medium, such as erythrocytes, thrombocytes or human serum have been used to mimic target-site conditions in different *in vitro* investigations. Time-kill curve experiments have been carried out in human body fluids, such as urine, bile or cerebrospinal fluid [176]. Comparing growth-kill behaviour of *E. coli* ATCC 25922 under ciprofloxacin exposure in CAMHB without supplement to CAMHB containing 50% erythrocytes showed decreased antibiotic activity of ciprofloxacin in CAMHB containing erythrocytes [177]. However, the static and dynamic IVIM utilised in the present work were previously validated for LEV against *E. coli* [135] and applied using CAMHB without any supplements [134]. Hence, addition of albumin or other supplements to growth medium was not implemented in these investigations for the sake of consistency and comparability to previous investigations. Feasibility of using supplemented media in the applied dIVIM and potential impact on the killing effect remains to be investigated.

MIC values of the investigated *E. coli* isolates have been determined under standardised conditions according to CLSI guidelines [36]. According to EUCAST susceptibility breakpoints, the investigated isolates were LEV resistant, as their MIC values exceeded the clinical breakpoint for LEV against *Enterobacterales* of 1 mg/L [34]. However, MIC determinations need to be interpreted cautiously, as their capability to predict *in vivo* susceptibility is limited [126,127]. The MIC serves as classification criterion to categorise bacterial isolates in “resistant”, “susceptible”, or “susceptible, increased exposure” [34]. Clinical decisions on antibiotic therapy are still widely based on the categorisation of the isolated pathogen, although assay variability of MIC determinations is high and can be discerned in inter-strain differences, intra-laboratory variability and inter-laboratory variability [126]. Both biological variability, i.e. differences in susceptibility of different bacterial strains belonging to one species, and variability resulting from assay variation (e.g. incubation time, temperature or inoculum preparation) challenge the rationale for the MIC as guiding principle in antibiotic therapy [127,178]. Further, visual detection of turbidity is highly subjective and does not account for bacterial growth below the visually detectable limit of 10^7 - 10^8 CFU/mL [127]. These limitations can result in inadequate classification of a bacterial isolate and consequently in inappropriate choice of the antibiotic agent, when isolates exhibit MIC values close to the clinical breakpoint [179]. Clinical susceptibility breakpoints represent the MIC value discerning between

pathogens with high probability of a successful treatment and a high probability of therapeutic failure when a standard dosing regimen of the respective antibiotic agent is administered, based on PTA analysis [27,44]. The category “susceptible, increased exposure” has been introduced to account for pathogens with a high probability of therapeutic success, when increased target-site exposure is achieved, e.g. by adjusting the dosing regimen [35]. The desired PK/PD target is typically a value of a certain PK/PD parameter, such as *f*AUC/MIC, fC_{max}/MIC or $fT_{>MIC}$, which has been shown to be correlated with a PD target, such as 1- or 2-log_{10}-fold reduction of bacterial concentration or bacteriostasis *in vitro* [27]. However, these parameters are based on the MIC as endpoint measurement and do not account for the full bacterial growth and kill trajectories over time. Furthermore, apart from the technical and biological variability associated with MIC determinations, only a 2-fold dilution series of an antibiotic agent is investigated according to CLSI guidelines [36]. Consequently, an MIC value of 1.0 mg/L can be interpreted as a value > 0.5 mg/L and < 2.0 mg/L, even when experimental conditions are well controlled [34]. To account for the resulting uncertainty, EUCAST implemented the “Area of Technical Uncertainty” in breakpoint tables [180]. When a determined MIC value falls within this range, it is recommended to repeat the MIC determination, use an alternative approach, downgrade the susceptibility category or include uncertainty in the report [34]. A clinical breakpoint does not account for genomic resistance mechanisms of bacterial strains. Differently, epidemiological cut-off (ECOFF) values represent the highest MIC value of an organism devoid of phenotypically detectable acquired resistance mechanisms, i.e. distinguishes between wild type and non-wild type bacteria [181]. Consequently, an ECOFF value accounts for genomic resistance mechanisms, but does not necessarily predict the probability of successful treatment, as both wild-type and non-wild type organisms may or may not be clinically susceptible [182]. According to the ECOFF value of 0.25 mg/L, based on the international MIC distribution of LEV against *E. coli,* the investigated isolates belonged to the non-wild type population (Figure 7.25). The discrepancies between clinical breakpoints and ECOFF values point out that organisms harbouring genomic resistance mechanisms are not necessarily classified as resistant in terms of clinical breakpoints, which applies for example to an *E. coli* isolate with an MIC value of 0.5 mg/L. A reliable relationship between genomic resistance mechanisms and clinically relevant resistance is not established yet [112]. Hence, IVIM investigations are recommended to characterise the PK/PD relationship of an antibiotic compound and different bacterial species comprehensively in preclinical studies [27]. In the following chapters, IVIM investigations are discussed in the light of the MIC values of the isolates and their genomic fluoroquinolone resistance mechanisms.

4.1.1 Static *in vitro* infection model

In the first place, IVIM investigations are generally applied to identify the most predictive PK/PD parameter to describe the exposure-effect relationship of a certain compound and organism. Second, when the best suited parameter is identified, IVIM experiments are employed to derive target values for a desired effect, such as 2 log_{10}-fold reduction of bacterial load [38,47,52]. Furthermore, leveraging additional techniques, such as fluorescence microscopy, FACS analysis or determination of endotoxin release can elucidate adaptation and resistance mechanisms occurring in the investigated experimental setting [100,183,184]. Even though LEV was introduced into the Asian market in 1993 and is approved in the U.S. since 1996 [79], few *in vitro* investigations of its effect against *E. coli* have been published. Drago et al. performed static IVIM experiments, exposing two susceptible *E. coli* strains to C_{LEV} between 0.5- and 4-fold their MIC [185]. Similar to the present investigations of the susceptible strain ATTC 25922, under exposure to 1-fold the MIC, initial reduction of the bacterial load was followed by regrowth within 24 h. Differently, under exposure to 0.5-fold the MIC, Drago et al. did not observe initially decreasing bacterial concentrations, but delayed growth. Exposing the LEV susceptible strains to static concentrations of 2- and 4-fold the MIC resulted in eradication within 24 h. Lee et al. obtained comparable results investigating LEV susceptible *E.coli* strains, isolated from chicken, in poultry serum [186]. Here, bacterial concentrations remained at the inoculum concentration under exposure to 0.5-fold MIC, while initial killing and regrowth was observed under exposure to 1-fold MIC. Exposed to higher C_{LEV}, bacterial load was reduced to the LLOQ of the applied plate counting assay. Differently, in the present investigations, the LEV susceptible strain *E. coli* ATCC 25922 showed regrowth under 2-fold MIC exposure. Here, only one replicate of the time-kill curve experiment exposing the LEV susceptible strain was performed. However, these results indicate that even for a susceptible strain, devoid of genomic resistance mechanisms, static exposure to C_{LEV} of the MIC of the strain might not be sufficient to attain eradication.

The LEV resistant *E. coli* strain ST167 was previously exposed to C_{LEV} between 2 and 16 µg/mL in the sIVIM for 24 h [134]. In agreement with the present results, the bacterial isolate displayed initial bacterial reduction, followed by regrowth within 24 h under exposure to C_{LEV}=8 mg/L. Similarly, eradication was observed under exposure to C_{LEV}=16 mg/L within 24 h. However, the MIC of the isolate was determined to be 4 mg/L, instead of 8 mg/L. This discrepancy might be explained by slightly different inoculum preparation or incubations times within the defined timeframe of 16-20 h and can be seen as an example for the intra-laboratory variability described by Mouton et al. [126]. However, time-kill curves were comparable, when nominal C_{LEV} are considered instead of MIC-normalised concentrations. Compared to the other investigated isolates, the shape of time-kill curves of ST167 was similar for each respective

MIC-normalised C_{LEV} (Figure 3.6), but extent of initial decrease of bacterial concentrations differed and was highest for ST167 and lowest for ST58 under 1-fold MIC exposure, although the same MIC value was determined for the two strains. Typically, time-kill curve experiments are carried out for 24 h, due to potential scarcity of nutrients and space in the static setting [51]. Here, sIVIM experiments were performed for up to three days without observing a decline in GC curves, showing feasibility of sIVIM experiments for > 24 h. Moreover, regrowth was observed under exposure to 2-fold MIC in at least one replicate for all three strains at t > 24 h, indicating that longer experiments can provide additional insights and bacterial adaptation might be missed in shorter experiments. Compared to simple MIC determinations, static time-kill curves provide the advantage of quantifying the bacterial growth and kill behavior over time, but they do not account for the pharmacokinetic profile of the antibiotic compound at target-site [47,51,52]. Hence, different types of dIVIM were developed to investigate the antibiotic effect mimicking target-site exposure [51].

4.1.2 Dynamic *in vitro* infection model

The effect of LEV against *Streptococcus pneumonia* (*S. pneumonia*) was investigated in a dIVIM by Tasso et al., who mimicked pulmonary LEV C(t) profiles by stepwise withdrawal and replacement of LEV containing growth medium in a cell culture flask, resulting in stepwise dilution of the medium [187]. Using this approach, they mimicked LEV C(t) profiles in pulmonary tissue resulting from eight different dosing regimens. The investigated *S. pneumonia* strain (LEV MIC: 1 mg/L) displayed regrowth under mimicked administration of 250 mg or 500 mg LEV in 24 h and was successfully eradicated under exposure to the mimicked dosing regimens with either higher dose or shorter dosing interval. This approach might represent target-site conditions more appropriately than constant drug exposure, but a stepwise dilution approach is still inferior to mimicking human C(t) profiles based on PK models in a dIVIM. Apart from limitations related to the used growth medium and the absence of the immune system of the host, dIVIM are capable of mimicking clinically relevant C(t) profiles and allow for comprehensive PK/PD analysis, when both bacterial and antibiotic concentrations are determined over time.

In the present dIVIM investigations, clinically relevant LEV C(t) profiles were successfully mimicked (Figure 3.7). Determination of C_{LEV} using a validated fluorometric assay allowed for thorough analysis of the exposure-effect relationship *in vitro.* The observed experimental variability was quantified and partly explained applying a NLME modelling approach (chapters 3.3.2 and 4.3.2). Of note, no trend towards lower or larger exposure, in terms of C_{max} and AUC_{24h} values, was observed for one of the investigated *E. coli* isolates (Table 3.2), allowing to attribute differences in the observed growth-kill behaviour between the isolates to strain-

specific characteristics. The PK/PD target values for 1 log_{10} reduction (*f*AUC/MIC: 67.4) and 2-log_{10} reduction (*f*AUC/MIC: 140), respectively, reported by EUCAST based on Drusano et al [38,45], were not reached for any of the isolates (Table 3.2), even when mimicking C(t) profiles resulting from the highest approved dose of 750 mg [74]. Hence, the observed regrowth of the resistant strains was expected. However, the PK/PD target for "bacteriostasis" (*f*AUC/MIC: 35.6) was attained for ST88 in three replicates, resulting in regrowth with final concentrations below the initial concentration after 24 h (Figure 3.8).

Regrowth under exposure to LEV C(t) profiles after single administration of 500 mg and 750 mg, respectively, was also observed by Odenholt and Cars, who administered a single LEV dose to reach initial C_{LEV} of 4 and 6 mg/L, respectively, and subsequently mimicked a half-life of 7 h in a dIVIM [41]. While *E. coli* ATCC 25922 (MIC according to [41]: 0.016 mg/L) was eradicated, *E. coli* M12 (MIC: 0.5 mg/L) displayed regrowth within 24 h under exposure to both mimicked dosing regimens. Similarly, *E. coli* ST167 was initially reduced 3-4 log_{10}-fold when exposed to mimicked C(t) profiles resulting from a 500 mg, 30 min i.v. infusion using the same dIVIM as in the present investigations [134]. The extent of initial reduction was larger mimicking a C(t) profile resulting from a 750 mg, 90 min i.v. infusion (below the LLOQ of the assay) and regrowth was observed later compared to the 500 mg dose (t=6-10 h compared to t=4 h). Of note, a higher inoculum concentration was applied in previous investigations, mimicking a 500 mg, 30 min i.v. infusion (10^7 CFU/mL instead of 10^6 CFU/mL). Hence, the so-called "inoculum effect", i.e. attenuated killing for higher inoculum concentrations, might also have contributed to the smaller effect, next to lower exposure [188,189]. In a clinical study, Pea et al. found that a dosing regimen of 500 mg LEV bid was beneficial for pathogens causing complicated and catheter-associated urinary tract infections and presenting MIC values > 8 mg/L [89]. Similarly, higher doses of LEV (1000 mg) have been shown to be capable of eradicating *E. coli* strains with MIC values ≤ 32 mg/L causing urinary tract infections [87]. However, a single dose of 750 mg was equally effective as 1000 mg, as LEV exposure in urine was much higher compared to C_{LEV} in plasma. Accordingly, Stein et al. suggest the implementation of urine-specific breakpoints to account for accumulation of LEV and consequently higher exposure in urine, allowing for successful treatment of urinary tract infections caused by "resistant" strains according to clinical breakpoints [87]. DIVIM can be applied to mimic C(t) profiles of antibiotic compounds resulting from different dosing regimens at target-site, e.g. in urine, and to derive appropriate PK/PD indices and PK/PD target values. Based on a PK model, LEV C(t) profiles in plasma and urine were simulated to streamline *in vitro* investigations [190]. However, the experimental design of elaborate dIVIM investigations can be further optimised, e.g. to identify most informative sampling timepoints [191]. In a next step, alternative LEV dosing regimens, such as 1000 mg qd, and the effect of resulting target-

site C(t) profiles, can be investigated in further dIVIM experiments. Alternatively, the developed NLME PK/PD model can be applied to *in silico* simulate bacterial time-kill curves under various LEV dosing regimens. Thereby, the PD effect of multiple LEV C(t) profiles on the investigated *E. coli* isolates can be further explored without a need to perform *in vitro* investigations.

Observed differences between the strains in extent of initial bacterial reduction, time and extent of regrowth, even for the two isolates with equal MIC values (ST58 and ST167) were not expected and have not been described in similar investigations before. Ambrose et al. showed the impact of the bacterial growth rate on LEV effect against *S. aureus* in a hollow-fibre infection model [192]. Lower bacterial growth rates were obtained by supplementing the growth medium with up to 10% NaCl solution, resulting in a reduced killing effect for lower growth rates. In the present investigations, NLME modelling was applied to estimate individual relative growth rate constants of replicates in sIVIM and dIVIM experiments (chapter 3.3.2, Figure 7.13). Relative growth rate constants were different under static and dynamic exposure, which might have contributed to differences in the exposure-effect relationship between the static and the dynamic experimental setting (chapter 3.3.1). Singh et al. exposed three *E. coli* strains to ascending C_{LEV} in a hollow-fibre infection model and investigated the impact of target-site mutations in *gyrA* and *parC* and efflux pump expression on the growth behaviour of the strains [193]. They point out that efflux pump upregulation might play an underestimated role in fluoroquinolone resistance. To further elucidate bacterial adaptation and resistance mechanisms driving the observed growth-kill behaviour of the three isolates, further genomic and phenotypic investigations were performed.

4.2 Bacterial resistance and adaptation mechanisms

4.2.1 Genomic resistance

Bacterial DNA extraction, followed by PCR amplification of QRDR and *qnr* plasmids and agarose gel electrophoresis of PCR products were newly introduced to the Department and successfully carried out for three *E. coli* isolates. *GyrA* and *parC* sequences were obtained by Sanger sequencing of PCR products and analysed in the software geneious®. High sequence quality was assured by evaluating the fraction of positions with a Phred quality score > 90, indicating a low probability of an incorrect base call ($P < 10^{-4}$, chapter 2.3.1.3). Further, high agreement (> 90%) between sequences obtained by Sanger sequencing applying primer F and primer R indicated reproducible sequencing results (Table 7.9). QRDR mutations of the isolates were determined by translating DNA sequences into proteins, which were then compared to reference AA sequences of *gyrA* and *parC*. Additionally, the determined QRDR mutations (Table 3.3) were confirmed by WGS. However, the identified replacement of serine by isoleucine was incorrectly allocated to position 81 in the Sanger sequencing based approach (Figure 3.10) instead of position 80 (Table 3.3). This was most likely caused by an incorrect identification of the reading frame during sequence analysis, which could potentially have been avoided by trimming the low quality ends of DNA sequences before translating into AA sequences [194]. The protein alterations identified by WGS are widely spread and known to be associated with fluoroquinolone resistance (chapter 1.5). Wohlkonig et al. provided a structural explanation for the importance of the *gyrA* residues Ser83 and Asp87 by presenting a crystal structure of moxifloxacin in complex with *Acinetobacter baumannii* in 2010 [76], while the relevance of these *gyrA* residues has already been described before for multiple Gram-negative bacterial species. In *E. coli*, Ser83 is most commonly replaced by leucine, tryptophane or alanine, while Asp87 can be replaced by asparagine, valine, glycine, tyrosine or histidine [9]. Similarly, the relevance of the identified *parC* mutation Ser80 and potential replacement by leucine, isoleucine and arginine have been described [9]. Since the first *qnr* plasmid was identified in *Klebsiella pneumonia* in 1998 [105], several studies investigated the impact of *gyrA* and *parC* mutations and *qnr* plasmids on phenotypic fluoroquinolone resistance, mainly linking MIC values to genomic properties of bacterial isolates [10,77,78,106,109]. In general, MIC values were higher for a higher number of QRDR mutations and mutations in both *gyrA* and *parC* [8,106,109]. Additional presence of *qnr* plasmids typically increased MIC values, but *qnr* plasmids alone did not cause clinically relevant fluoroquinolone resistance, i.e. MIC values higher than the clinical breakpoint of 1 mg/L [10,34,78]. Vinué et al. suggested that presence of *qnr* plasmids might facilitate selection of mutants with *gyrA* or *parC* mutations under ciprofloxacin exposure and therefore might increase selective pressure [77]. *Qnr* plasmids compete with fluoroquinolones for gyrase binding by mimicking the DNA in structure,

size and electronic properties [10]. The present investigations did not identify any novel *gyrA* or *parC* mutations in the *qnr* harbouring isolate ST88 after exposure to static C_{LEV} of the MIC for 24 h (Figure 3.11). However, exposure for 24 h might have been too short to select novel mutants, as Vinué et al. exposed the *E. coli* strains for 72 h.

The detected genomic resistance mechanisms only partly explained the differences in LEV susceptibility between the *E. coli* isolates, quantified by the novel PK/PD parameter $cumAUC_{50}$ in the semi-mechanistic PK/PD model (chapter 3.3.1) and the strain-specific EC_{50} estimates in the NLME model (chapter 3.3.2), both indicating the highest susceptibility for ST88, followed by ST167 and the lowest susceptibility for ST58. Given the number of *gyrA* and *parC* mutations and *qnr* plasmids, a higher LEV susceptibility of ST88 compared to ST167 was plausible, but the elevated resistance level of ST58 was unexpected with regard to the single *gyrA* mutation of the isolate. The potential contribution of fitness costs due to the higher number of mutations harboured by ST167 might play a role in the lower resistance level of the isolate compared to ST58, as resistance mutations might be associated with fitness costs [108,195,196]. However, the role of fitness costs in fluoroquinolone resistance is discussed controversially: Marcusson et al. investigated the impact of fluoroquinolone resistance mutations (*gyrA, parC* and the efflux regulating gene *marR*) on relative fitness in growth competition assays, comparing growth of mutants harbouring specific mutations to the wild type. They identified that an *E. coli* strain harbouring the same *gyrA* and *parC* mutations as ST167 did not show significantly lower fitness compared to the wild type, but additional *marR* mutations decreased fitness of the investigated strains [195]. Differently, Machuca et al. showed that *E. coli* strains harbouring the efflux pump gene *qepA2,* associated with *gyrA/parC* mutations displayed lower fitness in growth competitions assays than the wild type, but additional *marR* mutations compensated for these fitness costs [108]. In the present investigations, individual growth rate constants of the *E. coli* strains, estimated based on the growth control replicates in dynamic and static IVIM experiments, have been compared during the NLME model development (Figure 7.13, top). In the dynamic setting, ST167 displayed lower individual growth rates compared to the other isolates, which might be explained by the additional *parC* mutation of the isolate and might have contributed to the lower susceptibility compared to ST58. However, in the sIVIM, individual growth rates of ST58 were lower compared to the other isolates. On the other hand, lower replications rates have been shown to be associated with a lower LEV effect, suggesting higher susceptibility for higher replication rates [192]. Of note, the estimated relative growth rate constants cannot be directly compared to replication rates, as they summarise bacterial growth and natural death in one parameter, representing the “net bacterial growth”. Hence, the complex interplay between fluoroquinolone resistance mutations, growth rates and growth and kill behaviour needs to be further elucidated. Moreover, alterations of membrane permeability

due to downregulation of the outer membrane proteins *OmpF* and *OmpC* or overexpression of efflux pumps, such as *marR*, *qepR* or the AcrAB complex might have played a role [77,193], but were not further investigated. As the investigated genomic resistance mechanisms did not fully explain the differences in the exposure-effect relationship of the three isolates, investigations of size distributions were performed to quantify the contribution of persister cell formation, indicated by filamentation.

4.2.2 **Phenotypic adaptation**

Fluoroquinolones are known to induce adaptation to antibiotic stress in *E. coli* by developing persistent subpopulations [14,100,115,116,122,123]. In 2019, a consensus statement by Balaban et al. clarified the mechanistic differences between “persistence”, “tolerance” and “resistance”: While resistance enables bacteria to replicate in the presence of an antibiotic, the term “persistence” refers to a bacterial subpopulation being able to survive antibiotic exposure by adapting its metabolism and potentially resume growing in presence of the antibiotic. Differently, the term “tolerance” refers to a total bacterial population surviving antibiotic treatment [13]. Persistence can be detected by imaging techniques, because cell division of persister cells is halted, which causes alteration of cell morphology, including visible and quantifiable elongation. The emergence of elongated *E. coli* cells under antibiotic exposure, also refered to as “filamentation”, is mostly investiagted by time-lapse microscopy, FACS or microfluidic systems [100,120,123,124]. In the present work, electronic cell counting based on the coulter counter principle was established as complementary approach to quantify all bacterial cells in a sample and characterise the size distribution of a bacterial population [197-200]. An electronic cell counting method using a CASY® device was applied, which enabled rapid and simple quantification of viable bacteria, dead cells and persister cells during time-kill curve experiments, while the applied plate counting assay solely quantified viable cells. Fractions of cell counts in defined size ranges were determined to explore the extent of filamentation for the three investigated isolates, being largest for ST88 under exposure to 2-fold MIC (Figure 3.14, Figure 7.9). This observation was confirmed by the $cumAUC_{reg,static}$ estimate in the semi-mechanistic PK/PD model (Table 3.5), being lowest for ST88. The $cumAUC_{reg,static}/cumAUC_{reg,dynamic}$ ratios indicated the property of an isolate to regrow preferably in dIVIM experiments, under exposure to decreasing antibiotic concentrations, and was < 1 for ST88, indicating that the isolate displayed regrowth preferably under static LEV exposure. Dynamics of cell size distributions, investigated in sIVIM experiments, agreed with this trend, showing pronounced filamentation for ST88 and ST167 and less pronounced increase in cell diameter for ST58. The NLME modelling approach enabled quantification of LEV effect on persister cell formation by estimating the strain-specific additive increase of the first-order rate constant k_{NP}, being highest for ST88 (Table 3.13). In the present investigations, the electronic

cell counting approach to quantify persister cells was not applied in dynamic experiments, potentially explaining different $k_{P,LEV}$ estimates based on the static and the full dataset (Table 3.10, Table 3.13, chapter 4.3.2). As a next step, size distribution assessment in dIVIM experiments could provide additional insights in filamentation under exposure to decreasing C_{LEV} and hence elucidate the interplay between decreasing C_{LEV} and persister cell formation for the *E. coli* strains. Similar to the present investigations, Khan et al. observed filamentation of *E. coli* under static ciprofloxacin exposure, being most pronounced under exposure to 0.5-fold and 1-fold MIC between t=1 h and t=4 h [183]. Furthermore, time-dependent changes of size distributions were observed for the three investigated isolates under LEV exposure and in the growth controls (Figure 7.8, Figure 7.9, Figure 7.10). Similarly, growth-stage dependent persister cell formation of *E.coli* under antibiotic exposure has been shown before, being low in the early exponential growth stage and increasing in the late exponential stage [14,116]. Dynamically changing cell size distributions of growing *E.coli* populations without antibiotic exposure have already been described by Toennies et al., who observed decreasing cell sizes in the exponential stage, utilising the coulter counter technique [200]. In the present investigations of unexposed bacteria, cells with increased diameter were detected in the beginning of the experiments, indicating rapidly replicating bacteria being in the in the early exponential growth stage. However, the initial fraction of increased bacteria varied between the strains and between experiments (Figure 7.8, Figure 7.9, Figure 7.10). Different lag times of the isolates, resulting in different growth stages after equal preincubation time of 2 h for all strains, could provide an explanation for the observed strain-specific differences in initial size distributions (Figure 2.5). In previous investigations, lag time of ST167 has been determined to be approx. 2 h [134]. The same lag time was assumed for ST58 and ST88 in these investigations, but different growth rates of the strains (Figure 7.13), potentially associated with fitness costs due to resistance mutations, might require adjustment of preincubation times to ensure comparable growth stages of isolates, when the antibiotic is added. The observation of different initial fractions of increased cells between experiments investigating the same strain (Figure 7.10) might be explained by persister cell formation during the preincubation time and variability in experimental conditions, such as inoculum concentration and incubation temperature. Balaban et al. point out that persistence might already be induced in the overnight culture, triggered by stress signals, such as starvation [13]. Hence, different conditions while preparing the overnight cultures might also have contributed to variability of initial size distributions.

Determination of a distinct threshold to discern viable *E. coli* and persister cells is challenging, as in addition to the growth-stage dependency, cell sizes vary between different strains and growth conditions [98,99]. Hence, it was deemed most reasonable to leverage the total number

of bacterial counts in a sample as a metric for the aggregated bacterial numbers of three bacterial compartments (dead, growing and persister cells) in the NLME model. This approach was free of assumptions regarding size thresholds and enabled implementation of a “dead cells” compartment in the PK/PD model and estimation of initial bacterial numbers in the persister and in the dead cell compartment (chapter 3.3.2, Table 3.13, Figure 3.24). Based on the PK/PD model, simulated trajectories of bacterial numbers belonging to the subpopulations confirmed the highest extent of persister cell formation for ST88 under LEV exposure, being quantified by the highest $k_{P,LEV}$ estimate of the isolate (Table 3.13, Figure 3.36).

Electronic cell counting was successfully established as simple and rapid technique, enabling quantification of dead, viable and persister cell during IVIM experiments. Definition of distinct size thresholds and quantitative discrimination between bacterial subpopulations might be possible leveraging FACS or microfluidic systems as complementary methods to the developed electronic cell counting approach. Furthermore, quantitative real time PCR could provide further insights in expression of the genes involved in SOS response and persister cell formation, such as *hipA, recA* and *lexA* [120,123]. So far, the developed method to quantify filamentation of *E. coli* under LEV exposure indicated relevant contribution of persister cell formation for ST88 and ST167, being most pronounced for ST88. PK/PD analysis based on the novel parameters $cumAUC_{50}$ and $cumAUC_{reg}$, as well as simulations based on the developed NLME model were in agreement with these findings. Further application of the developed approach, investigating various strains in static and dynamic IVIM experiments could support the determination of a PK/PD parameter target value, such as a $cumAUC_{50}$ value, preventing regrowth of persister cells and thereby contribute to optimised antibiotic dosing.

4.3 Pharmacokinetic/pharmacodynamic modelling

4.3.1 Characterisation of the exposure-effect relationship

PK/PD relationships of antibiotics are typically characterised by relating an exposure metric, such as fC_{max}, $fAUC_{24h}$ or $\%fT_{>MIC}$, to an effect metric, the MIC of the pathogen [28,32,33,201]. In preclinical *in vitro* and animal studies, target values for these PK/PD indices, required to reach a desired antibiotic effect, are determined [28,52,201]. Based on the PK of an antibiotic compound, characterised by an appropriate NLME model, and the desired PK/PD target values, clinical susceptibility breakpoints and dosing recommendations are derived [27,28,44,201]. At the same time, severe limitations of the MIC as the guiding principle in antibiotic dosing are well known (chapter 4.1), [126,127,178,179]. Hence, a paradigm shift in antibiotic dosing towards MIC-independent PK/PD targets is highly needed. In this work, alternative PK/PD parameters quantifying the exposure-effect relationship of LEV against *E. coli* were suggested: $cumAUC_{50}$ and $cumAUC_{reg}$. These parameters were derived from novel exposure and effect metrics, which were defined as cumulative exposure and cumulative effect over time and thereby represented (i) the full LEV C(t) profile and, (ii) the bacterial growth, killing and regrowth trajectory, respectively. The suggested effect metric was based on the ABBC, introduced by Firsov et al. [48,49,50], which represents the aggregated effect in a defined period of time and accounts for bacterial growth without antibiotic exposure as baseline. Similar to the AUC_{24h} of a drug, quantifying total exposure in 24 h, ABBC quantifies the overall effect, but does not account for the shape of the bacterial killing and regrowth curve. Hence, in the present analysis, the effect metric was further developed: ABBC(t) was determined cumulatively over time to quantify and discern the different processes constituting the antibiotic effect, i.e. killing and regrowth under antibiotic exposure over time. Normalisation to the cumAUGC(t), representing natural bacterial growth without antibiotic exposure, was performed to account for the increasing maximum possible effect over time. In a similar fashion, LEV exposure was determined as cumAUC(t), accounting for the shape of the full LEV C(t) profile.

Based on the two novel exposure and effect metrics, a semi-mechanistic PK/PD model was developed, combining a sigmoidal E_{max} model with an inhibition term. E_{max} models have been widely used to describe the relationship between the concentration of an antibiotic and the resulting effect [33,47,64,201]. Here, by implementation of cumAUC(t), the concept was extended by leveraging a metric representing the full exposure-time trajectory instead of a single C(t). Thereby, bacterial killing and regrowth under antibiotic exposure were discerned: Initially, the sigmoidal E_{max} model term dominated the exposure-effect relationship, while the impact of the inhibition term increased at higher cumulative exposure values (Figure 3.20).

$CumAUC_{50}$ represented the sigmoidally increasing effect at low exposure, i.e. the strain-specific extent of initial bacterial reduction. Mainly dominating the exposure-effect relationship for initially small cumAUC(t) values, the impact of previous exposure on $cumAUC_{50}$ was small compared to the impact of previous exposure on the regrowth parameter $cumAUC_{reg}$. Hence, for the static and the dynamic exposure pattern, a joint $cumAUC_{50}$ value was estimated, which was probably determined by "inherent" characteristics of an isolate being present prior to antibiotic exposure, i.e. genomic resistance mechanisms. Differently, $cumAUC_{reg}$ reflected the tendency of an isolate to regrow, with lower $cumAUC_{reg}$ estimates for regrowth at lower exposure. According to the increasing impact of the inhibition term at higher exposure (Figure 3.20), $cumAUC_{reg}$ was determined by the full exposure-time trajectory, being different between the static and the dynamic exposure pattern (Figure 3.15). Hence, different $cumAUC_{reg}$ values were estimated for static and dynamic exposure, representing bacterial adaptation under different exposure patterns.

$CumAUC_{50}$ estimates of the three *E. coli* isolates quantitatively described the observed differences in initial reduction of bacterial concentrations in the dIVIM, with the largest extent for ST88, followed by ST167 and being smallest for ST58 (Figure 3.8, Table 3.5). For sIVIM experiments, the exposure-effect relationship was determined by both the bacterial strain and the static C_{LEV} (Figure 3.19, Figure 3.20). Stratification per exposure pattern (dynamic exposure, static exposure to 1-fold MIC and 2-fold MIC) unveiled higher E_{max} values for the same cumAUC(t) under 2-fold MIC compared to 1-fold MIC exposure (Figure 3.19, Table 3.7). Here, the exposure–effect relationship was comparable between dynamic exposure and static exposure to 1-fold MIC for ST58 and ST167. Differently, for ST88, the exposure-effect relationship in the dIVIM was comparable to 2-fold MIC exposure in sIVIM experiments. For ST58, the maximum predicted effect was smaller compared to ST88 and ST167 in all investigated scenarios, and smaller in the dynamic compared to the static setting. For ST88, a higher effect was reached in the static setting under 2-fold MIC exposure at lower cumulative exposure compared to the dynamic setting (Table 3.7). Thus, for ST58, insufficient exposure in the dynamic setting might have contributed to regrowth to a larger extent compared to ST88. The order of the $cumAUC_{reg,static}$ estimates of the three strains was in line with the $cumAUC_{50}$ values (ST88 < ST167 < ST58) and in agreement with observed fractions of increased cells, determined by electronic cell counting in sIVIM experiments (chapter 3.2.2, Figure 3.14). The linear relationship between $cumAUC_{reg,static}$ values and the maximum fraction of prolonged cells was quantitatively demonstrated by an adjusted coefficient of determination of R^2=0.873 (Figure 4.1).

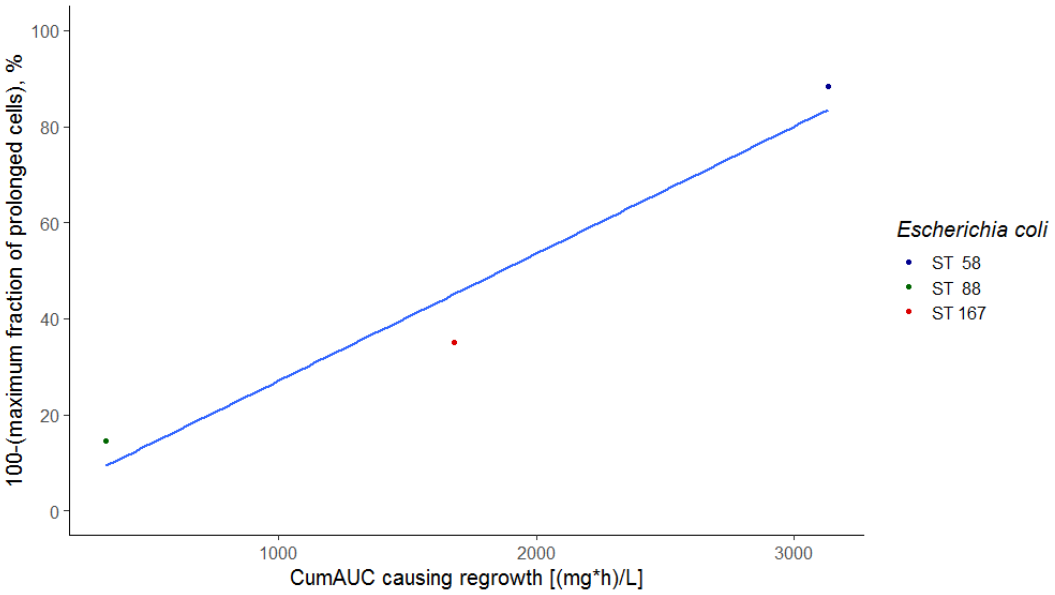

Figure 4.1: Relationship between the maximum fraction of prolonged cells (diameter: >3 µm), assessed by electronic cell counting, and the cumulative area causing regrowth in static *in vitro* infection model experiments, exposing three *Escherichia coli (E. coli)* isolates to constant levofloxacin concentrations, colours: *E. coli* strains, blue line: linear regression line, ST: sequence type.

$CumAUC_{reg,dynamic}$ represented the tendency of a strain to show regrowth in dIVIM experiments and was smallest for ST58, followed by ST88 and ST167 (Table 3.5). The strain-specific differences in the impact of the exposure pattern was quantified by the $cumAUC_{reg,static}/cumAUC_{reg,dynamic}$ ratio. A high $cumAUC_{reg,static}/cumAUC_{reg,dynamic}$ ratio indicated a higher tendency of a strain to show regrowth rather under dynamic LEV exposure than in sIVIM experiments and thereby quantitatively illustrated the relevance of the shape of the C(t) trajectory. Different from ST58 and ST167, the $cumAUC_{reg,static}/cumAUC_{reg,dynamic}$ ratio was < 1 for ST88, indicating a higher tendency to regrow under static exposure. As decreasing antibiotic concentrations were not present under static exposure and could thus not affect bacterial regrowth, adaptation mechanisms, such as persister cell formation, might have contributed more to regrowth under static exposure for ST88 compared to the other isolates. This finding was in agreement with cell size distributions (chapter 3.2.2), indicating the largest extent of filamentation for ST88 (Figure 3.14).

The present investigations demonstrated the limitations of the MIC value as guiding principle for clinical decision making, as differences in the exposure-effect relationship of two strains with the same MIC value (ST58 and ST167) became apparent. Initial bacterial reduction at more than 3-fold higher cumulative exposure ($cumAUC_{50}$: 158 $mg \cdot h \cdot L^{-1}$) quantified the lower susceptibility of ST58 compared to ST167 ($cumAUC_{50}$: 49.4 $mg \cdot h \cdot L^{-1}$, Table 3.5). Currently, antibiotic therapy is guided by MIC-based PK/PD target values. PTA analyses are applied to

predict the therapeutic success of a dosing regimen, given an infection caused by a bacterial strain with a certain MIC value (chapter 4.1, [27]). Here, a MIC-based PD target value is used as surrogate for successful therapy. Stochastic simulations, based on an appropriate NLME model, are leveraged to estimate the PTA for specific patient populations, potentially accounting for relevant covariates, such as renal function. This approach assumes an equal probability of therapeutic success for infections caused by strains displaying equal MIC values. The present analysis demonstrated that a MIC-based approach can miss strain-specific differences in the exposure-effect relationship, which are not captured by the MIC value. Consequently, too low exposure as a result of inappropriate dosing in case of infections caused by strains with reduced susceptibility can result in treatment failure and promote emergence of bacterial adaptation and resistance.

Furthermore, the relevance of the shape of the LEV C(t) profile for the antibiotic effect was shown by comparing static and dynamic IVIM experiments. The newly derived PK/PD parameters $cumAUC_{50}$ and $cumAUC_{reg}$ captured the different processes determining the exposure-effect relationship, i.e. bacterial killing and regrowth. Genomic resistance mechanisms of the isolates did not fully explain the strain-specific exposure-effect relationship, e.g. the small $cumAUC_{50}$ value of ST58 was unexpected with regard to the single *gyrA* mutation of the isolate (Table 3.3). Fitness costs of resistance mutations might have contributed to high $cumAUC_{reg}$ of ST167, i.e. regrowth at higher cumulative exposure in the dynamic setting, which was also indicated by the lower individual relative growth rate constants of ST167 in the dIVIM experiments compared to the other isolates (chapter 3.2.1, Figure 7.13) [108,195]. The exposure pattern had a strain-specific impact, e.g. for ST58, continuously high C_{LEV} in the sIVIM resulted in a higher maximum effect than the dynamic exposure pattern, while for ST88, regrowth was more pronounced in the static setting, indicated by the $cumAUC_{reg,static}/cumAUC_{reg,dynamic}$ ratio. These findings implied that prolonged infusion durations can be beneficial for treatment of infections caused by bacterial strains with low $cumAUC_{reg,static}/cumAUC_{reg,dynamic}$ ratios.

The novel PK/PD parameters $cumAUC_{50}$ and $cumAUC_{reg}$ enabled a MIC-independent characterisation of the exposure-effect relationship and hence, present a promising framework for ranking new antibiotics in drug research and development, to more comprehensively characterise PK/PD relationships and investigate the adequateness of proposed or established dosing regimens. The benefit of the suggested PK/PD metrics and derived PK/PD parameters was shown for LEV as a model compound and a limited number of three clinical *E. coli* isolates. To assess their external validity, these metrics should be applied to a larger number of bacterial species and antibiotics. In particular, applicability of the parameters for antibiotics with a time-dependent PK/PD relationship, such as beta-lactam antibiotics [37], should to be explored.

Further, the developed PK/PD model can be applied to derive MIC-independent PK/PD target values by linking cumulative exposure to *in vitro* eradication or clinical cure.

4.3.2 Characterisation of the bacterial growth and kill behaviour

Building up on the semi-mechanistic model, NLME modelling was leveraged to elucidate the different processes constituting the exposure-effect relationship and to quantify different levels of variability. In a sequential model development strategy, subsets of the full dataset were used to characterise different processes in three submodels: (i) a bacterial growth model, characterising bacterial growth without antibiotic exposure in the static and in the dynamic experimental setting, (ii) a static PK/PD model, describing bacterial killing and persister formation under exposure to constant C_{LEV}, and (iii) a PK model, characterising LEV C(t) profiles in the dIVIM. Finally, the submodels were combined and PK model-predicted C_{LEV} (dIVIM) or nominal C_{LEV} (sIVIM) were linked to viable bacterial concentrations, assessed by the droplet plate assay and to the total counts, assessed by electronic cell counting in a three-bacterial-state PK/PD model. Model development was based on the semi-mechanistic PK/PD model developed by Nielsen et al, who described time-kill curves of *Streptococcus pyogenes* under exposure to five different antibiotics with two bacterial subpopulations [64].

In the **bacterial growth model**, precise parameter estimates and low IIV (Table 3.9) showed adequate reproducibility of the experimental conditions. Different from Nielsen et al., who discerned between bacterial growth and natural death by estimating a growth rate and a death rate constant [64], in the present work, one first-order rate constant quantified net growth, summarising growth and death of the viable bacterial subpopulation in one parameter. Introducing a death rate constant did not improve the model fit of the bacterial growth model, but was ultimately enabled by implementation of electronic cell counting data in the three-bacterial-state PK/PD model (Table 3.13). Here, three bacterial subpopulations were discerned: viable bacteria, persister and dead bacteria. In the bacterial growth model, observed differences in bacterial growth between the static and the dynamic experimental setting were quantified as two distinct growth rates and a fractional change of the maximum bacterial number in the static compared to the dynamic experimental setting. The growth rate constant in the static setting (1.81 h^{-1}) was in agreement with comparable time-kill curve investigations, exposing *E. coli* to various antibiotics and estimating growth rate constants between 1.5 h^{-1} and 2.5 h^{-1} [183,184,189], while the growth rate constant in the dynamic setting was lower (1.15 h^{-1}) and the maximum bacterial number in the stationary growth stage was 11.2% (on a logarithmic scale) higher in the static compared to the dynamic setting (Table 3.9). This finding was unexpected, as entry in the stationary stage is typically attributed to starvation, space and toxic bacterial metabolites [95,96]. Different from the sIVIM, growth medium is

continuously exchanged in the dIVIM, providing steady nutrient supply. In this regard, a higher maximum bacterial number in the dIVIM compared to the sIVIM would have been more plausible. However, biofilm formation might have contributed to lower maximum bacterial numbers in the dIVIM [125]. Biofilm formation might occur preferably in the dIVIM compared to the sIVIM, induced by hydrodynamic agitation due to medium flow [114,125,202]. Shear stress caused by stirring bars, which were not present in the sIVIM, might also have contributed to biofilm formation [134]. The applied sampling technique, i.e. random sampling from the bacterial suspension in the culture vessel using a pipette, only assessed planctonic bacteria and consequently, bacteria in biofilms were not quantified. However, the applied technique is commonly used, while quantification of bacteria in biofilms is not established yet.

Apart from the impact of the experimental setting, fitness costs of mutations might have contributed to strain-dependent differences in growth rate constants. Estimation of a joint growth rate constant for the three strains and its IIV, representing the variability in growth rate constants between the replicates, enabled exploration of individual growth rate constants (post hoc estimates), stratified per strain and experimental setting (Figure 7.13, top). Strain-specific differences between individual growth rate constants became apparent. However, no clear trend was identified for static and dynamic experiments and estimation of distinct growth rate constants for each of the three *E. coli* strains was not supported by the data. Thus, interpretation with regard to fitness costs of the identified mutations remains ambiguous (chapter 4.2.1). Growth competition assays between the strains under controlled experimental conditions without antibiotic exposure could elucidate the contribution of fitness costs. In growth competition assays, bacterial strains harbouring a mutation of interest are co-cultivated with a reference strain, e.g. the wild type, for several growth cycles. After each cycle, the bacterial suspension is plated, bacterial CFU of each strain are quantified by plate counting and the mutant/wild type-ratio is determined. Discrimination between mutant and wild type colonies can be facilitated by utilising a *ΔaraB* wild type strain, resulting in red mutant and white wild type colonies on arabinose containing MacConkey agar plates [195]. Using this approach, the relative fitness of the clinical isolates, compared to a reference strain, can be assessed, to investigate the contribution of fitness costs due to mutations more comprehensively. Drawing conclusions about fitness costs solely based on growth rate constants is not justified, as growth rates and competitive fitness are poorly correlated [196]. However, fitness costs have been previously implemented in a PK/PD model of *E. coli* under ertapenem exposure. Ungphakorn et al. accounted for different growth rate constants of ESBL producing *E. coli* strains by implementing a fractional decrease of growth rate constants of resistant strains compared to the wild type [189]. Differently, Khan et al. described the effect of ciprofloxacin against six mutant *E. coli* strains and the wild type using a PK/PD model,

assuming a less susceptible pre-existing resistant subpopulation, growing with a 5-fold lower growth rate constant compared to the susceptible subpopulation (1.7 h^{-1} vs 0.344 h^{-1}), irrespective of the strain [183]. Here, both “susceptible” and “less susceptible” bacteria were allowed to transform into a non-colony-forming state, comparable to the persister subpopulation in the present three-bacterial-state PK/PD model. In the present work, persister formation and back-transformation rate constants “at baseline”, i.e. without LEV exposure, were fixed to 10^{-6} h^{-1} and 0.1 h^{-1}, respectively, based on Balaban et al. [120], indicating that persister formation was negligible in unexposed bacterial populations compared to exposed populations. This finding was in line with bacterial size distributions, assessed by electronic cell counting (chapter 3.2.2), showing negligible filamentation in the GC replicates compared to exposed bacteria for the three investigated strains (Figure 3.14, Figure 7.8, Figure 7.9, Figure 7.10).

While the developed semi-mechanistic PK/PD model based on cumulative PK and PD metrics quantitatively discerned the exposure-effect relationship of the three *E. coli* isolates and two exposure patterns (chapter 4.3.1), NLME modelling provided deeper insights in the underlying mechanisms, such as the impact of the experimental setting on the growth rate constant and maximum bacterial numbers and the impact of the bacterial strain on LEV effect parameters. As fluoroquinolones target replicating bacteria, reduced growth rates are linked to a decreased fluoroquinolone effect [122,192]. Thus, different growth rate constants in the two experimental settings might have contributed to the exposure pattern-specific LEV effect (Table 3.7).

In the **static PK/PD model**, constant LEV concentrations were related to viable bacterial concentrations, assessed by the droplet plate assay. Nielsen et al. linked the drug effect, described by a sigmoidal E_{max} model, to natural death of bacteria, increasing the first-order death rate constant in a concentration-dependent manner [64]. In the present static PK/PD model, bacterial death was not described as a separate process, and thus, the LEV effect was implemented as a separate first-order killing process of the viable subpopulation, which was linked to the C_{LEV} via a sigmoidal E_{max} model. Here, the strain-dependent killing effect was represented in strain-specific EC_{50} values. Similarly, Khan et al. estimated strain-specific EC_{50} values of ciprofloxacin against *E. coli* and identified a strong correlation between EC_{50} and MIC values [183]. In the present investigation, ST58 and ST167 shared the same MIC value of 8 mg/L, but a 6-fold higher EC_{50} value was estimated in the static PK/PD model for ST58 (14.1 vs. 2.33 mg/L, Table 3.10). This finding can be attributed to the inappropriateness of the MIC value as endpoint metric to represent the full bacterial growth and kill trajectory [127]. Strain-specific EC_{50} values quantitatively demonstrated differences between the isolates in extent and steepness of initial reduction of the viable bacterial population and time of regrowth, which was illustrated by simulated trajectories of bacterial numbers of the growing bacterial

subpopulation (Figure 3.36, green lines). Further, the Nielsen model was extended by implementing a second manifestation of the LEV effect: an additive increase of the perister formation rate constant in the presence of LEV, which was independent of C_{LEV}. Fluoroquinolones cause DNA damage and consequently induce SOS response and persister formation (chapter 1.6, [14,115,123,124]), but a relationship between the antibiotic concentration and the extent of persister formation has not been identified so far [13]. Accordingly, linking C_{LEV} to the persister formation rate constant via a simple or sigmoidal E_{max} model resulted in implausible effect parameter estimates and was therefore not pursued further. Mechanistically, E_{max} models are typically applied to characterise saturable processes, such as drug interaction with receptors or enzymes, where the number of available targets is limited [65]. Here, both manifestations of the LEV effect are quantified as first-order rate constants, representing the number of bacterial cells leaving the viable bacterial subpopulation per hour, depending on the absolute number of viable bacteria. Thus, both the killing effect and the persister formation effect are limited by the number of cells in the viable subpopulation. Different from the killing effect, a very small fraction of the viable bacterial population (1 in 10^6 cells per hour at baseline, i.e., without antibiotic exposure) transforms into persister cells. Hence, saturation of the effect on persister formation could not be identified in the investigated experimental settings.

To characterise experimentally mimicked LEV C(t) profiles, a **PK model** was developed, based on measured C_{LEV} in samples drawn from the dIVIM. Experimental settings, such as pump rates, C_{LEV} in the reservoir and switch time of the pump rates, were determined based on a two-compartmental PK model [55,142], aiming to mimic C(t) profiles in plasma of septic patients, resulting from two LEV dosing regimens: a 750 mg, 90 min i.v. infusion and two 500 mg, 60 min i.v. infusions with a dosing interval of 12 h. Hence, the same structural model as used to derive the experimental settings was identified to describe the experimental data best: a two-compartmental model with zero-order input and linear elimination (Table 3.11, Figure 3.24). Different from the model based on clinical data, PK parameters in the model based on *in vitro* data did not represent mass transfer of LEV molecules, but were determined by experimental settings, such as pump rates. Variability in these experimental settings, caused by e.g. pump rate imprecision, affected the estimated PK parameters in a similar extent, leading to a strong correlation between PK parameters. Thus, a scaling factor between the most strongly correlated parameters V_C and Q was introduced to quantify the relationship between the respective IIV terms, which was estimated to be approx. 1 (0.994 – 1.78).

Overall, PK parameter estimates obtained from experimental data were similar to those obtained from clinical studies [39,42,91], including the PK model, which was used to determine the experimental settings [55,142], highlighting the clinical relevance of the mimicked LEV C(t)

profiles (Table 3.11). The estimate of the total volume of distribution was lower based on experimental data (70.4 L) compared to clinical data (86.1 L), resulting in slightly higher simulated C_{max} values *in vitro* compared to *in vivo* (max. + 14.6%, Table 3.12, Figure 3.23). CL was higher *in vitro* than *in vivo* (8.9 $L \cdot h^{-1}$ vs. 6.24 $L \cdot h^{-1}$), reflected in lower C_{min} values of simulated C(t) profiles based on the *in vitro* model compared to simulations based on clinical data. The elevated C_{max} values might be a consequence of outflow blockage due to bacterial biofilm formation on the membrane filter, enhanced by the high pump rates during the ascending part of the C(t) profile and in the first exponential phase (1.0 and 1.45 mL/min, respectively, Table 2.1, [134]). In the second exponential phase, much lower pump rates were applied, potentially leading to detachment of bacterial cells from the biofilm and thus less hindered outflow. In the replicates mimicking a 500 mg bid dosing regimen, a second dose was administered at t=12 h, and higher pump rates were applied for a second time [131]. The second administration resulted in high variability of observed C_{LEV} between t=12 h and t=14 h, which was apparent in the VPC for the 500 mg bid dosing regimen (Figure 3.31). The PK model was developed based on replicates mimicking both dosing regimens, including 7 replicates mimicking the 500 mg bid regimen and 14 replicates mimicking the 750 mg qd regimen (Table 7.8). Hence, the larger experimental variability related to the 500 mg dosing regimen, quantified as IIV on CL, V_c and V_p, was potentially underestimated due to the lower number of replicates attributed to the dosing regimen. Consequently, a slight trend towards higher individual predicted C_{LEV} compared to observations occurred (Figure 3.29, lower panel). The trend was less pronounced for population predictions (Figure 3.29, upper panel), showing appropriateness of the structural model. The respective observations could be assigned to few very low observed C_{LEV} after the second administration for two replicates (Figure 7.14). Thus, case deletion diagnostics were performed, which did not show a significant impact of these replicates on parameter estimates (Table 7.12). Therefore, all replicates were included in the analysis.

In the **three-bacterial-state PK/PD model**, static C_{LEV} and dynamic C(t) profiles were linked to bacterial concentrations, assessed by the droplet plate assay *and* by electronic cell counting. Implementation of a subpopulation of dead cells was enabled by leveraging the total electronic cell counts as a measure for the aggregated number of bacteria in three bacterial subpopulations. Consequently, a first-order death rate constant was implemented and thus, bacterial growth and natural death were discerned. However, linking the LEV killing effect to the death rate constant was not superior to estimating a separate LEV killing effect. Further, exploiting electronic cell counting data enabled estimation of the number of persister cells being present before antibiotic exposure, after 2 h of pre-incubation, which represented a fraction of 1 in 10^4 of the viable bacterial population ($10^{5.9}$ viable cells vs $10^{2.2}$ persister cells,

Table 3.13, based on SIR). This finding agreed with Keren et al., who report a persister fraction of 10^{-6} to 10^{-4} of the total population [116].

In the three-bacterial-state PK/PD model, the strain-dependent **killing effect**, which was previously described by $cumAUC_{50}$ values (chapter 4.3.1), was quantified by strain-specific EC_{50} values. As the $cumAUC_{50}$ values represented cumulative exposure over time, while EC_{50} values represented a certain C(t), the values of these parameters are not directly comparable. However, the order of the strain-specific estimates was the same, being smallest for ST88 ($cumAUC_{50}$: 28.6 mg·h·L^{-1}; EC_{50}: 3.10 mg·L^{-1}), followed by ST167 ($cumAUC_{50}$: 49.4 mg·h·L^{-1}; EC_{50}: 8.46 mg·L^{-1}) and being largest for ST58 ($cumAUC_{50}$: 158 mg·h·L^{-1}; EC_{50}: 17.2 mg·L^{-1}, Table 3.5, Table 3.13, based on SIR). This finding confirms the previously identified differences between the isolates in LEV susceptibility, which were not captured in their MIC values (ST58 and ST167: 8 mg/L, ST88: 2 mg/L).

The different extent of **persister formation**, which was previously described based on bacterial size distributions (chapter 4.2.2), was quantified by a strain-specific additive increase of the first-order persister formation rate constant $k_{P,LEV}$ under LEV exposure, being most pronounced for ST88 ($1.79 \cdot 10^{-1}$ h^{-1}), followed by ST58 ($1.11 \cdot 10^{-1}$ h^{-1}) and being smallest for ST167 ($4.34 \cdot 10^{-3}$ h^{-1}, Table 3.13, based on SIR). The highest $k_{P,LEV}$ value of ST88 was in agreement with the highest fraction of elongated cells for the isolate under static exposure (Figure 3.14). However, a higher effect on persister formation was expected for ST167, based on the higher fraction of increased cells compared to ST58 (Figure 3.14). Further, estimation of the persister effect was not proven to be robust comparing $k_{P,LEV}$ estimates based on the static PK/PD model (Table 3.10) with estimates based on the full dataset (Table 3.13) and simultaneously re-estimated parameters (Table 3.14). When estimated solely based on static experiments and droplet plate assay data, the effect on the persister formation rate constant was highest for ST167 and lowest for ST88 (Table 3.10). In contrast, when estimated based on the full dataset, the effect was similar for ST58 and ST88 and much higher compared to ST167, when bacterial growth and PK parameters were fixed to values previously obtained in the sequential model development process (Table 3.13). When parameters were simultaneously re-estimated, the effect was highest for ST167, but much lower for ST58 (Table 3.14).

These differences could be explained by the comparably small number of replicates (28.6% of 98 replicates), for which complementary electronic cell counting was carried out (Table 7.8). Further, electronic cell counting was only applied in sIVIM experiments so far. The complementary bacteria quantification method was used to assess filamentation as surrogate for persister cells formation. Similarly, Khan et al. used FACS to characterise filamentation of

E. coli under ciprofloxacin exposure and observed pronounced filamentation under static ciprofloxacin exposure to 0.5- and 1-fold the MIC, concluding that observed regrowth was caused by filaments resuming replication [183]. In the present work, previous analysis of the exposure-effect relationship indicated an impact of the exposure pattern (static or dynamic) on the tendency of a strain to show regrowth (Table 3.5, chapter 4.3.1). Consequently, $k_{P,LEV}$ might be substantially different in the dynamic from the static experimental setting, which was also reported by Thorsted et al. [184]. Their PK/PD model described time-kill behaviour and endotoxin release of *E. coli* under cefuroxime exposure in static and dynamic IVIM experiments and predicted a larger extent of filamentation in the dynamic compared to the static experimental setting [184]. Hence, in the present analysis, robustness of $k_{P,LEV}$ estimates might be improved by including total electronic cell counts, assessed in dIVIM model experiments and, potentially, discerning $k_{P,LEV}$ in the static and in the dynamic experimental setting. Apart from the effect on the persister formation rate constant, most simultaneously re-estimated parameters were comparable to previous estimates, obtained in the sequential model development (Table 3.13, Table 3.14).

Of note, the inoculum number of viable bacteria was estimated lower in simultaneous estimation compared to the previously obtained value ($10^{5.28}$ CFU compared to $10^{5.9}$ CFU), disagreeing with the experimental settings and resulting in systematic deviations between observations and predictions. Therefore, the parameter estimates of the sequential model development were deemed to be more adequate (Table 3.13) and were thus used for stochastic simulations of trajectories in the three bacterial subpopulations based on the full three-bacterial stage PK/PD model (Figure 3.36).

Further, the interplay between the two manifestations of the effect was explored by simulating trajectories of the bacterial subpopulations, omitting each of the two identified effects (killing and persister formation) at a time (Figure 3.37, Figure 7.24). Simulations based on the full model illustrated the lowest killing effect for ST58 under exposure to the 500 mg dosing regimen, showing no initial decline of the median trajectory of growing bacteria (Figure 3.36, green lines). For the 750 mg i.v. dose, initial killing and regrowth was simulated for all of three strains. Bacterial numbers of the persister subpopulation increased continuously under both dynamic and static exposure with a strain-dependent slope, being independent of the simulated dosing regimen or static LEV concentration. When omitting the effect on persister formation (Figure 3.37), trajectories of bacterial subpopulations for the dynamic setting were similar to simulations based on the full model, indicating that regrowth is not necessarily caused by back-transformation of persisters, but can be attributed to decreasing C_{LEV} and thus less killing in the dynamic setting (Figure 3.37, right). Differently, in the static experimental

setting, the viable bacterial population showed unhindered growth for static C_{LEV} below the MIC for ST58 and ST88 and for C_{LEV} < 0.5 MIC for ST167 (Figure 3.37, left). For higher concentrations, killing without regrowth was observed, indicating that the effect on persister formation is necessary to explain observed regrowth under static C_{LEV}.

When omitting the LEV killing effect (Figure 7.24), unhampered growth of viable bacteria was simulated for all strains and scenarios. For ST58 and ST88, continuously increasing numbers of persisters were simulated, while for ST167, the number of persisters was decreasing over time. This can be explained by back-transformation of persisters to growing bacteria without killing effect, indicating that a killing effect is necessary to induce persister formation and prevent back-transformation to the growing state. Simulations for the dynamic setting must be interpreted cautiously, as no electronic cell counting data was obtained in dIVIM experiments yet. However, these findings demonstrate that LEV-induced persister formation was necessary to explain regrowth in the static setting. Contrary, decreasing C_{LEV} were sufficient to explain regrowth due to a declining killing effect in the dynamic setting. ST88 was most prone to transform into the persister state, while for ST58 and ST167, persister formation was less pronounced.

Genomic resistance mechanisms partly explained the strain-specific EC_{50} values, demonstrating a higher LEV potency for ST88 harbouring one *gyrA* mutation and a *qnr* plasmid compared to ST167, harbouring two *gyrA* and one *parC* mutation (chapter 4.2.1, Table 3.3). However, the small killing effect and early regrowth observed for ST58 compared to ST167 under dynamic LEV exposure (Figure 3.36, B) could not be explained by its genomic resistance mechanisms, as the isolate harbours a single *gyrA* mutation, typically leading to a lower resistance level compared to mutations in both target enzymes (chapter 4.2.1, [8,106,109]). Further, persister formation was less pronounced for ST58 compared to the other isolates. Possibly, phenotypic downregulation of porin channels or enhanced expression of chromosomally encoded efflux pumps in combination with the identified *gyrA* mutation can explain the low susceptibility of ST58. Efflux pump upregulation, leading to PK resistance and thus preventing both killing and persister formation by reducing intracellular $C_{LEV,}$ might have played an underestimated role, as suggested by Singh et al. [193]. To quantify the impact of increased efflux pump expression, quantitative real-time PCR can be applied. Further, determination of intracellular antibiotic concentrations, facilitated by fractionation assays, would provide insights in antibiotic uptake and enable investigation of intra-bacterial PK processes [203].

5 Conclusions and perspectives

The present thesis aimed to characterise, as well as mechanistically and quantitatively explain growth and kill behaviour of *E. coli* under LEV exposure, leveraging an integrated *in vitro* and *in silico* PK/PD modelling approach. The case study focussed on the effect of the model compound LEV against three fluoroquinolone resistant clinical *E. coli* isolates, to elucidate the interplay between pre-existing genomic resistance mechanisms and phenotypic adaptation. A novel approach to experimentally assess persister formation based on electronic cell counting was established and successfully employed. New PK/PD metrics were developed and applied to quantitatively characterise the exposure-effect relationship, and a three-bacterial-state PK/PD model provided mechanistic insights into the processes determining the bacterial growth, kill and regrowth curve under LEV exposure.

To characterise the **growth and kill behaviour** of the *E. coli* isolates under static and dynamic LEV exposure, time-kill curve investigations were carried out. Under exposure to constant C_{LEV} in sIVIM experiments, regrowth was observed for all the strains under exposure to $C_{LEV} \leq$ 1-fold the MIC of the isolate, while the extent of initial reduction and regrowth differed between the isolates. In dIVIM experiments, LEV C(t) profiles, resulting from a 750 mg, 90 min LEV i.v. infusion, were successfully mimicked. Dynamic time-kill curve investigations, exposing three *E. coli* isolates to the mimicked LEV C(t) profiles, expectedly demonstrated the incapability of the clinically relevant dosing regimen to eradicate LEV resistant strains. PK/PD target values were not reached and consequently, bacterial regrowth was observed within 24 h. Unexpectedly, the extent of initial bacterial reduction and time and extent of regrowth differed between two strains sharing the same MIC value (8 mg/L). These results highlighted the inappropriateness of the MIC value as an endpoint measurement to comprehensively characterise the bacterial growth and kill trajectory, which is determined by both genomic resistance mechanisms and bacterial adaptation.

To investigate **genomic resistance mechanisms**, leading to PD resistance by hampering the interaction between the drug molecule and its target, bacterial DNA extraction, PCR and electrophoresis were introduced to the Department and successfully applied. Target-site mutations in QRDR and PMQR mechanisms of the investigated isolates were identified by Sanger sequencing and, additionally, WGS was performed in collaboration. ST of the isolates were determined by MLST (ST58, ST88 and ST167). Different widely spread *gyrA* and *parC* mutations were identified in all three strains, and one of the isolates (ST88) harboured *qnr* plasmids. A higher susceptibility of ST88 (MIC: 2 mg/L) compared with ST167 (MIC: 8 mg/L) was partly explained by genomic resistance mechanisms, as ST88 harboured one *gyrA*

mutation and *qnrS* plasmids, and ST167 harboured two *gyrA* mutations and one *parC* mutation. However, the low susceptibility of ST58 (MIC: 8 mg/L) was not fully explained by one *gyrA* mutation, suggesting phenotypic adaptation mechanisms. Fitness costs of resistance mutations might additionally have contributed to the strain-specific growth and kill behaviour, but were out of scope of the present investigations. Perspectively, growth competition assays can be applied to determine the relative fitness of the isolates and elucidate fitness costs. Further, quantification of gene expression by quantitative real-time PCR can provide insights into PK resistance, i.e. decreased intracellular antibiotic concentrations due to increased expression of efflux pumps or downregulation of porin channels in the outer membrane, potentially explaining the reduced susceptibility of ST58.

To investigate **phenotypic adaptation** in terms of persister formation, a simple and rapid electronic cell counting approach, based on the coulter counter technique, was developed and successfully employed to assess bacterial size distributions under LEV exposure over time. A shift of size distributions to larger cell sizes indicated filamentation of bacteria due to persister formation. Pronounced filamentation was observed for ST88 and ST167 under static exposure to 1- and 2-fold the MIC. ST58 displayed increased cell sizes to a smaller extent, indicating less persister formation of the isolate. The total number of electronic cell counts represented the aggregated number of three bacterial subpopulations, comprising viable, dead and persister cells, and was leveraged to inform the developed three-bacterial-state PK/PD model. However, a clear size threshold to discriminate viable and persister cells could not be identified solely based on electronic cell counting. In future, distinct quantification of the bacterial subpopulations could be enabled employing FACS or microfluidic systems.

To quantitatively characterise the **exposure-effect relationship** of LEV against *E. coli* and discriminate the three investigated isolates, novel PK/PD metrics were derived and applied in a semi-mechanistic PK/PD model. LEV exposure over time was determined as the cumulative area under the LEV C(t) profile. The antibiotic effect was computed as the cumulative area between the GC and the bacterial killing and regrowth curve, normalised to the cumulative area under the GC curve. These exposure and effect metrics enabled characterisation of the exposure-effect relationship by a sigmoidal E_{max} model, combined with an inhibition term. Thereby, the full LEV C(t) profile and bacterial growth and kill trajectory were considered. The derived PK/PD parameters $cumAUC_{50}$ and $cumAUC_{reg}$ quantitatively discriminated the investigated isolates and characterised the exposure-effect relationship more comprehensively than the MIC value. Here, $cumAUC_{50}$ represented the initial killing of a strain, while $cumAUC_{reg}$ quantified the cumulative exposure causing regrowth. Furthermore, the semi-mechanistic PK/PD model unveiled a relevant impact of the exposure pattern, i.e. static or dynamic exposure, on the exposure-effect relationship, highlighting the relevance of the shape

of the LEV C(t) profile. As a next step, the PK/PD parameters should be applied to alternative dosing regimens, further antibiotic compounds and bacterial species, to show their broader applicability and appropriateness to guide preclinical research and development, enabling a comprehensive characterisation of novel antibiotic compounds. Finally, the novel PK/PD metrics and derived parameters can be applied to determine MIC-independent PK/PD target values, such as a cumAUC preventing regrowth.

Based on the semi-mechanistic PK/PD model, a **three-bacterial-state PK/PD model** was developed, providing further mechanistic insights into the processes determining the strain-specific exposure-effect relationship and the identified differences between the static and the dynamic experimental setting. Growth and kill behaviour of three clinical *E. coli* isolates under static and dynamic LEV exposure were successfully described by a NLME model, discerning three bacterial subpopulations: viable bacteria, persister and dead bacteria. Two manifestations of the LEV effect were identified: a killing effect, decreasing bacterial numbers of viable bacteria in a concentration-dependent manner, described as a sigmoidal E_{max} model, and an additive increase of persister formation in the presence of LEV. The EC_{50} value quantified the strain-specific LEV potency and agreed with the $cumAUC_{50}$ estimates of the semi-mechanistic PK/PD model, demonstrating the highest LEV potency against ST88 and the lowest LEV potency against ST58. The strain-specific values of the persister formation effect parameter ($k_{P,LEV}$) indicated the highest extent of persister formation for ST88, in agreement with bacterial size distributions. Stochastic simulations based on the PK/PD model showed that in the static experimental setting, LEV-induced persister formation was essential to explain the observed regrowth, while in the dIVIM, decreasing antibiotic concentrations might have been sufficient to explain regrowth. Based on the GC curves, a significant impact of the experimental setting on the bacterial growth rate constants and the maximum bacterial number in the stationary growth stage has been identified, both being higher in the static compared to the dynamic setting. This finding was unexpected and can be further explored by determination of the relative fitness of the strains in both experimental settings. Moreover, a better understanding of the contribution of fitness costs might support the identification of strain-specific growth rate constants. Of note, total electronic cell counts, representing the aggregated bacterial number of the three subpopulations, were solely determined in sIVIM experiments so far. Incorporation of electronic cell counting data, assessed under dynamic exposure, will enable refinement of the PK/PD model. Finally, the developed three-bacterial-state PK/PD model can be applied to simulate time-kill curves of *E. coli* under exposure to alternative LEV dosing regimens, to derive PK/PD targets values and support antibiotic dosing optimisation. External model evaluation utilising time-kill curve data of different compounds

and bacterial species can support the mechanistic understanding of antibiotic resistance and adaptation.

Overall, combining different *in vitro* and *in silico* approaches demonstrated that neither genomic resistance nor phenotypic adaptation mechanisms alone could explain the complex processes underlying bacterial growth and kill behaviour. The present thesis underlined the limitations of the MIC value as the guiding principle in antibiotic dosing and suggested novel PK/PD parameters to quantify exposure-effect relationships more comprehensively. In future, these parameters can be applied to derive PK/PD target values and guide antibiotic dosing. The developed three-bacterial-state PK/PD model provided mechanistic insights and can be employed to simulate the antibiotic effect resulting from various LEV dosing regimens, contributing to antibiotic dosing optimisation and, thus, to overcome the global challenge of antibiotic resistance.

6 Bibliography

[1] https://www.who.int/news-room/fact-sheets/detail/the-top-10-causes-of-death (last access 25 Apr 2021).

[2] World Health Organization (WHO). Global Action Plan on Antimicrobial Resistance. Microbe Mag. 10: 354–355 (2015).

[3] P.R. Shankar. Tackling drug-resistant infections globally. Arch. Pharm. Pract. 7: 110 (2016).

[4] A.H. Holmes, L.S.P. Moore, A. Sundsfjord, M. Steinbakk, S. Regmi, A. Karkey, P.J. Guerin, L.J. V Piddock. Understanding the mechanisms and drivers of antimicrobial resistance. Lancet 387: 176–187 (2016).

[5] D.S. Davies. Sustaining global action on antimicrobial resistance. (2017).

[6] D.I. Andersson, D. Hughes. Microbiological effects of sublethal levels of antibiotics. Nat. Rev. Microbiol. 12: 465–78 (2014).

[7] A. Rodríguez-Rojas, J. Rodríguez-Beltrán, A. Couce, J. Blázquez. Antibiotics and antibiotic resistance: A bitter fight against evolution. Int. J. Med. Microbiol. 303: 293–297 (2013).

[8] K.J. Aldred, R.J. Kerns, N. Osheroff. Mechanism of quinolone action and resistance. Biochemistry 53: 1565–1574 (2014).

[9] D.C. Hooper. Mechanisms of fluoroquinolone resistance. Drug Resist. Updat. 2: 38–55 (1999).

[10] J.M. Rodríguez-Martínez, J. Machuca, M.E. Cano, J. Calvo, Martínez-Martí, L. Nez, A. Pascual. Plasmid-mediated quinolone resistance: Two decades on. Drug Resist. Updat. 29: 13–29 (2016).

[11] R.F. Potter, A.W. D'Souza, G. Dantas. The rapid spread of carbapenem-resistant *Enterobacteriaceae*. Drug Resist. Updat. 29: 30–46 (2016).

[12] K. Lewis. Persister cells, dormancy and infectious disease. Nat. Rev. Microbiol. 5: 48–56 (2007).

[13] N.Q. Balaban, S. Helaine, K. Lewis, M. Ackermann, B. Aldridge, D.I. Andersson, M.P. Brynildsen, D. Bumann, A. Camilli, J.J. Collins, C. Dehio, S. Fortune, J.M. Ghigo, W.D. Hardt, A. Harms, M. Heinemann, D.T. Hung, U. Jenal, B.R. Levin, J. Michiels, G. Storz, M.W. Tan, T. Tenson, L. Van Melderen, A. Zinkernagel. Definitions and guidelines for research on antibiotic persistence. Nat. Rev. Microbiol. 17: 441–448 (2019).

[14] T. Dörr, K. Lewis, M. Vulić. SOS response induces persistence to fluoroquinolones in *Escherichia coli*. PLoS Genet. 5: (2009).

[15] K. Lewis. Persister Cells. Annu. Rev. Microbiol. 64: 357–372 (2010).

[16] U. Theuretzbacher, K. Outterson, A. Engel, A. Karlén. The global preclinical antibacterial pipeline. Nat. Rev. Microbiol. 18: 275–285 (2020).

[17] European Centre for Disease Prevention and Control. Surveillance of antimicrobial resistance in Europe (2019). https://www.ecdc.europa.eu/sites/default/files/documents/surveillance-antimicrobial-resistance-Europe-2019.pdf (last access 25 Apr 2021.)

[18] A. Provenzani, A.R. Hospodar, A.L. Meyer, D. Leonardi Vinci, E.Y. Hwang, C.M. Butrus, P. Polidori. Multidrug-resistant gram-negative organisms: a review of recently approved antibiotics and novel pipeline agents. Int. J. Clin. Pharm. 42: 1016–1025 (2020).

[19] B. McCall. New fund stimulates the ailing antibiotic pipeline. Lancet. Infect. Dis. 20: 1017 (2020).

[20] J.W. Mouton, P.G. Ambrose, R. Canton, G.L. Drusano, S. Harbarth, A. MacGowan, U. Theuretzbacher, J. Turnidge. Conserving antibiotics for the future: New ways to use old and new drugs from a pharmacokinetic and pharmacodynamic perspective. Drug Resist. Updat. 14: 107–117 (2011).

[21] S.G. Wicha. Integrated *in vitro* and *in silico* studies for optimisation of broad-spectrum antibiotic combination therapy. Freie Universitaet Berlin. (2015).

[22] O. Clewe, S.G. Wicha, C.P. de Vogel, J.E.M. de Steenwinkel, U.S.H. Simonsson. A model-informed preclinical approach for prediction of clinical pharmacodynamic interactions of anti-TB drug combinations. J. Antimicrob. Chemother. 73: 437–447 (2017).

[23] S.G. Wicha, M.G. Kees, J. Kuss, C. Kloft. Pharmacodynamic and response surface analysis of linezolid or vancomycin combined with meropenem against *Staphylococcus aureus*. Pharm. Res. 32: 2410–2418 (2015).

[24] A. Olsson, P. Wistrand-Yuen, E.I. Nielsen, L.E. Friberg, L. Sandegren, P. Lagerbäck, T. Tängdén. Evaluation of the efficacy of antibiotic combinations against multidrug-resistant *Pseudomonas aeruginosa* in automated time-lapse microscopy and static time-kill experiments . Antimicrob. Agents Chemother. 46: (2020).

[25] M.S. Baek, E.S. Chung, D.S. Jung, K.S. Ko. Effect of colistin-based antibiotic combinations on the eradication of persister cells in *Pseudomonas aeruginosa*. J. Antimicrob. Chemother. 75: 917–924 (2020).

[26] S. Franck, R. Michelet, F. Casilag, J. Sirard, S.G. Wicha, C. Kloft. A model-based pharmacokinetic/pharmacodynamic analysis of the combination of amoxicillin and monophosphoryl lipid A against *S . pneumoniae* in mice. Pharmaceutics 13: 469 (2021).

[27] European Medicines Agency. Guideline on the use of pharmacokinetics and pharmacodynamics in the development of antibacterial medicinal products. (2015). https://www.ema.europa.eu/en/documents/scientific-guideline/guideline-use-pharmacokinetics-pharmacodynamics-development-antimicrobial-medicinal-products_en.pdf (last access 25 Apr 2021).

[28] F. de Velde, J.W. Mouton, B.C.M. de Winter, T. van Gelder, B.C.P. Koch. Clinical applications of population pharmacokinetic models of antibiotics: Challenges and perspectives. Pharmacol. Res. 134: 280–288 (2018).

[29] W.A. Craig, S.C. Ebert. Protein binding and its significance in antibacterial therapy. Infect. Dis. Clin. North Am. 3: 407–414 (1989).

[30] M.A. Zeitlinger, H. Derendorf, J.W. Mouton, O. Cars, W.A. Craig, D. Andes, U. Theuretzbacher. Protein binding: Do we ever learn? Antimicrob. Agents Chemother. 55: 3067–3074 (2011).

[31] W.A. Craig. Basic pharmacodynamics of antibacterials with clinical applications to the use of beta-lactams, glycopeptides, and linezolid. Infect. Dis. Clin. North Am. 17: 479–501 (2003).

[32] G.L. Drusano. Antimicrobial pharmacodynamics: Critical interactions of “bug and drug.” Nat. Rev. Microbiol. 2: 289–300 (2004).

[33] J.W. Mouton, M.N. Dudley, O. Cars, H. Derendorf, G.L. Drusano. Standardization of pharmacokinetic/pharmacodynamic (PK/PD) terminology for anti-infective drugs: An update. J. Antimicrob. Chemother. 55: 601–607 (2005).

[34] EUCAST-European Committee on Antimicrobial Suscetibility Testing. Breakpoint tables for interpretation of MICs and zone diameters, version 11.0 (2021). http://www.eucast.org (last access 25 April 2021).

[35] G. Kahlmeter. EUCAST proposes to change the definition and usefulness of the susceptibility category 'Intermediate.' Clin. Microbiol. Infect. 23: 894–895 (2017).

[36] M.P. Weinstein. M07. Methods for dilution antimicrobial susceptibility tests for bacteria that grow aerobically. (2018).

[37] G.L. Drusano. Antimicrobial pharmacodynamics: Critical interactions of "bug and drug." Nat. Rev. Microbiol. 2: 289–300 (2004).

[38] G.L. Drusano, S.L. Preston, C. Fowler, M. Corrado, B. Weisinger, J. Kahn. Relationship between fluoroquinolone area under the curve: minimum inhibitory concentration ratio and the probability of eradication of the infecting pathogen, in patients with nosocomial pneumonia. J. Infect. Dis. 189: 1590–1597 (2004).

[39] S.L. Preston, G.L. Drusano, A.L. Berman, C.L. Fowler, A.T. Chow, B. Dornseif, V. Reichl, J. Natarajan, M. Corrado. Pharmacodynamics of levofloxacin: A new paradigm for early clinical trials. JAMA 279: 125–129 (1998).

[40] P.G. Ambrose, D.M. Grasela, T.H. Grasela, J. Passarell, H.B. Mayer, P.F. Pierce. Pharmacodynamics of fluoroquinolones against *Streptococcus pneumoniae* in patients with community-acquired respiratory tract infections. Antimicrob. Agents Chemother. 45: 2793–2797 (2001).

[41] I. Odenholt, O. Cars. Pharmacodynamics of moxifloxacin and levofloxacin against *Streptococcus pneumoniae*, *Staphylococcus aureus*, *Klebsiella pneumoniae* and *Escherichia coli*: Simulation of human plasma concentrations after intravenous dosage in an *in vitro* kinetic model. J. Antimicrob. Chemother. 58: 960–965 (2006).

[42] J.A. Roberts, M.O. Cotta, P. Cojutti, M. Lugano, G. Della Rocca, F. Pea. Does critical illness change levofloxacin pharmacokinetics? Antimicrob. Agents Chemother. 60: 1459–1463 (2016).

[43] V.R. Anderson, C.M. Perry. Levofloxacin: A review of its use as a high-dose, short-course treatment for bacterial infection. Drugs 68: 535–565 (2008).

[44] J.W. Mouton, D.F.J. Brown, P. Apfalter, R. Cantón, C.G. Giske, M. Ivanova, A.P. MacGowan, A. Rodloff, C.J. Soussy, M. Steinbakk, G. Kahlmeter. The role of pharmacokinetics/pharmacodynamics in setting clinical MIC breakpoints: The EUCAST approach. Clin. Microbiol. Infect. 18: E37-45 (2012).

[45] EUCAST-European Committee on Antimicrobial Suscetibility Testing. Levofloxacin : Rationale for EUCAST clinical breakpoints, version 2.0 (2021). http://www.eucast.org/rd (last access 25 Apr 2021).

[46] Clinical and Laboratory Standards Institute-CLSI. Fluoroquinolone breakpoints for *Enterobacteriaceae* and *Pseudomonas aeruginosa*. (2019). https://clsi.org/media/3011/mr02ed1.pdf?utm_source=rm&utm_medium=landingpage&utm_content=MR02&utm_campaign=rationaldocument (last access 25 Apr 2021).

[47] M. Müller, A. Dela Peña, H. Derendorf. Issues in pharmacokinetics and pharmacodynamics of anti-infective agents: Kill curves versus MIC. Antimicrob. Agents Chemother. 48: 369–377 (2004).

[48] A.A. Firsov, V.M. Chernykh, S.M. Navashin. Quantitative analysis of antimicrobial effect kinetics in *in vitro* dynamic model. Microbiology 34: 1312–1317 (1990).

[49] A.A. Firsov, S.N. Vostrov, A.A. Shevchenko, G. Cornaglia. Parameters of bacterial killing and regrowth kinetics and antimicrobial effect examined in terms of area under the concentration-time curve relationships: Action of ciprofloxacin against *Escherichia coli* in an *in vitro* dynamic model. Antimicrob. Agents Chemother. 41: 1281–1287 (1997).

[50] A.A. Firsov, S.N. Vostrov, I.Y. Lubenko, A.P. Arzamastsev, Y.A. Portnoy, S.H. Zinner. ABT492 and levofloxacin: Comparison of their pharmacodynamics and their abilities to prevent the selection of resistant *Staphylococcus aureus* in an *in vitro* dynamic model. J. Antimicrob. Chemother. 54: 178–186 (2004).

[51] J. Gloede, C. Scheerans, H. Derendorf, C. Kloft. *In vitro* pharmakodynamic models to determine the effect of antibacterial drugs. J. Antimicrob. Chemother. 65: 186–201 (2010).

[52] T. Tängdén, C.V. Lundberg, L.E. Friberg, A. Huttner. How preclinical infection models help define antibiotic doses in the clinic. Int. J. Antimicrob. Agents 56: 106008 (2020).

[53] L.F. Amann, E.R. Vicente, M. Rathke, A. Broeker, M. Riedner, S.G. Wicha. Stability studies with tigecycline in bacterial growth medium and impact of stabilizing agents. Eur. J. Clin. Microbiol. Infect. Dis. 40: 215-218 (2021).

[54] E.I. Nielsen. Pharmacometric models for antibacterial agents to improve dosing strategies. Uppsala Universitet. (2011).

[55] D. Busse, A. Schaeftlein, A. Solms, L. Ilia, R. Michelet, M. Zeitlinger, W. Huisinga, C. Kloft. Which analysis aproach is adequate to leverage clinical microdialysis data? A quantitative comparison to investigate exposure and reponse exemplified by levofloxacin. Pharm. Res. 38: 381–395 (2021).

[56] C. Kirbs, C. Kloft. *In vitro* microdialysis recovery and delivery investigation of cytokines as prerequisite for potential biomarker profiling. Eur. J. Pharm. Sci. 57: 48–59 (2014).

[57] I.K. Minichmayr, A. Schaeftlein, J.L. Kuti, M. Zeitlinger, C. Kloft. Clinical determinants of target non-attainment of linezolid in plasma and interstitial space fluid: A pooled population pharmacokinetic analysis with focus on critically ill patients. Clin. Pharmacokinet. 56: 617–633 (2017).

[58] E. Löwdin, I. Odenholt, S. Bengtsson, O. Cars. Pharmacodynamic effects of sub-MICs of benzylpenicillin against *Streptococcus pyogenes* in a newly developed *in vitro* kinetic model. Antimicrob. Agents Chemother. 40: 2478–2482 (1996).

[59] J. Blaser, B.B. Stone, S.H. Zinner. Two compartement kinetic model with multiple artificial capillary units. J. Antimicrob. Chemother. 15: 131–137 (1985).

[60] J.W. Mouton, J.G. Den Hollander. Killing of *Pseudomonas aeruginosa* during continuous and intermittent infusion of ceftazidime in an *in vitro* pharmacokinetic model. Antimicrob. Agents Chemother. 38: 931–936 (1994).

[61] J. Wu, F. Racine, M.K. Wismer, K. Young, D.M. Carr, J.C. Xiao, R. Katwaru, Q. Si, P. Harradine, M. Motyl, P.R. Bhagunde, M.L. Rizk. Exploring the pharmacokinetic/pharmacodynamic relationship of relebactam (MK-7655) in combination with imipenem in a hollow-fiber infection model. Antimicrob. Agents Chemother. 62: 1–13 (2018).

[62] N.S. Ly, J.B. Bulitta, G.G. Rao, C.B. Landersdorfer, P.N. Holden, A. Forrest, P.J. Bergen, R.L. Nation, J. Li, B.T. Tsuji. Colistin and doripenem combinations against *Pseudomonas aeruginosa*: Profiling the time course of synergistic killing and prevention of resistance. J. Antimicrob. Chemother. 70: 1434–1442 (2014).

[63] J.J.S. Cadwell. The hollow fiber infection model : Principles and practice. Adv. Antibiot. Antibodies 1: 1–5 (2015).

[64] E.I. Nielsen, A. Viberg, E. Löwdin, O. Cars, M.O. Karlsson, M. Sandström. Semimechanistic pharmacokinetic/pharmacodynamic model for assessment of activity of antibacterial agents from time-kill curve experiments. Antimicrob. Agents Chemother. 51: 128–136 (2007).

[65] H. Derendorf, T. Gramatté. H.G. Schäfer (eds). Pharmakokinetik. Wissenschaftliche Verlagsgesellschaft Stuttgart, Stuttgart, 2nd ed. (2002).

[66] P.L. Bonate (ed.) Pharmacokinetic-pharmacodynamic modelling and simulation. Springer, New York, 2nd ed. (2011).

[67] A.V. Hill. The possible effects of the aggregation of the molecules of haemoglobin on its dissociation curves. Cambridge Univ. Press 40: 5 (1910).

[68] H. Derendorf, B. Meibohm. Modeling of pharmacokinetic/pharmacodynamic (PK/PD) relationships: Concepts and perspectives. Pharm. Res. 16: 176–185 (1999).

[69] D.R. Mould, R.N. Upton. Basic concepts in population modeling, simulation, and model-based drug development. CPT Pharmacometrics Syst. Pharmacol. 1: 1–14 (2012).

[70] K.M.C. Tjørve, E. Tjørve. The use of Gompertz models in growth analyses, and new Gompertz-model approach: An addition to the Unified-Richards family. PLoS One 12: 1–17 (2017).

[71] M.H. Zwietering, I. Jongenburger, F.M. Rombouts, K. Van't Riet. Modeling of the bacterial growth curve. Appl. Environ. Microbiol. 56: 1875–1881 (1990).

[72] M. Jacobs, N. Grégoire, W. Couet, J.B. Bulitta. Distinguishing antimicrobial models with different resistance mechanisms via population pharmacodynamic modeling. PLoS Comput. Biol. 12: e1004782 (2016).

[73] D.C. Hooper. Topoisomerase inhibitors: Fluoroquinolone mechanisms of action and resistance. Cold Spring Harb. Perspect. Med. 6 (2016).

[74] U.S. Food and Drug Administration. Levaquin prescribing information. (2018). https://www.accessdata.fda.gov/drugsatfda_docs/label/2018/020634s069lbl.pdf (last access 25 Apr 2021).

[75] K. Drlica, M. Malik, R.J. Kerns, X. Zhao. Quinolone-mediated bacterial death. Antimicrob. Agents Chemother. 52: 385–392 (2008).

[76] A. Wohlkonig, P.F. Chan, A.P. Fosberry, P. Homes, J. Huang, M. Kranz, V.R. Leydon, T.J. Miles, N.D. Pearson, R.L. Perera, A.J. Shillings, M.N. Gwynn, B.D. Bax. Structural basis of quinolone inhibition of type IIA topoisomerases and target-mediated resistance. Nat. Struct. Mol. Biol. 17: 1152–1153 (2010).

[77] L. Vinué, M.A. Corcoran, D.C. Hooper, G.A. Jacoby. Mutations that enhance the ciprofloxacin resistance of *Escherichia coli* with *qnrA1*. Antimicrob. Agents Chemother. 60: 1537–1545 (2016).

[78] D.C. Hooper, G.A. Jacoby. Mechanisms of drug resistance: Quinolone resistance. Ann. N. Y. Acad. Sci. 1354: 12–31 (2015).

[79] M.R. Bidell, T.P. Lodise. Fluoroquinolone-associated tendinopathy: Does levofloxacin pose the greatest risk? Pharmacotherapy 36: 679–693 (2016).

[80] European Medicines Agency. Disabling and potentially permanent side effects lead to suspension or restrictions of quinolone and fluoroquinolone antibiotics. (2018). https://www.ema.europa.eu/en/news/disabling-potentially-permanent-side-effects-lead-suspension-restrictions-quinolone-fluoroquinolone (last access 25 Apr 2021).

[81] J. Täubel, K. Prasad, G. Rosano, G. Ferber, H. Wibberley, S.T. Cole, L. Van Langenhoven, S. Fernandes, D. Djumanov, A. Sugiyama. Effects of the fluoroquinolones moxifloxacin and levofloxacin on the QT subintervals: Sex differences in ventricular repolarization. J. Clin. Pharmacol. 60: 400–408 (2020).

[82] Rote Liste® Service GmbH. Summary of product characteristics: Levofloxacin-hameln 5 mg/mL Infusionslösung. (2020).

[83] Rote Liste® Service GmbH. Summary of product characteristics: Levofloxacin Ibisqus 5 mg/mL Infusionslösung. (2013).

[84] D.N. Fish, A.T. Chow. The clinical pharmacokinetics of levofloxacin. Clin. Pharmacokinet. 45: 325–350 (2006).

[85] Rote Liste® Service GmbH. Summary of product charateristics: Tavanic Filmtabletten 250 mg/500 mg Filmtabletten. (2013).

[86] S.C. Chien, M.C. Rogge, L.G. Gisclon, C. Curtin, F. Wong, J. Natarajan, R.R. Williams, C.L. Fowler, W.K. Cheung, A.T. Chow. Pharmacokinetic profile of levofloxacin following once-daily 500-milligram oral or intravenous doses. Antimicrob. Agents Chemother. 41: 2256–2260 (1997).

[87] G.E. Stein, S.L. Schooley, D.P. Nicolau. Urinary bactericidal activity of single doses (250, 500, 750 and 1000 mg) of levofloxacin against fluoroquinolone-resistant strains of *Escherichia coli*. Int. J. Antimicrob. Agents 32: 320–325 (2008).

[88] E. Bergogne-Bérézin. Clinical role of protein binding of quinolones. Clin. Pharmacokinet. 41: 741–750 (2002).

[89] F. Pea, F. Pavan, E. Di Qual, L. Brollo, E. Nascimben, M. Baldassarre, M. Furlanut. Urinary pharmacokinetics and theoretical pharmacodynamics of intravenous levofloxacin in intensive care unit patients treated with 500 mg b.i.d. for ventilator-associated pneumonia. J.Chemother. 15: 563–567 (2003).

[90] F.M.E. Wagenlehner, M. Kinzig-Schippers, U. Tischmeyer, C. Wagenlehner, F. Sörgel, A. Dalhoff, K.G. Naber. Pharmacokinetics of ciprofloxacin XR (1000 mg) versus levofloxacin (500 mg) in plasma and urine of male and female healthy volunteers receiving a single oral dose. Int. J. Antimicrob. Agents 27: 7–14 (2006).

[91] P.G. Cojutti, V. Ramos-Martin, I. Schiavon, P. Rossi, M. Baraldo, W. Hope, F. Pea. Population pharmacokinetics and pharmacodynamics of levofloxacin in acutely hospitalized older patients with various degrees of renal function. Antimicrob. Agents Chemother. 61: 1–11 (2017).

[92] N. Allocati, M. Masulli, M.F. Alexeyev, C. Di Ilio. *Escherichia coli* in Europe: An overview. Int. J. Environ. Res. Public Health 10: 6235–6254 (2013).

[93] J.B. Kaper. Pathogenic *Escherichia coli.* Int. J. Med. Microbiol. 295: 355–356 (2005).

[94] A. Cassini, L.D. Högberg, D. Plachouras, A. Quattrocchi, A. Hoxha, G.S. Simonsen, M. Colomb-Cotinat, M.E. Kretzschmar, B. Devleesschauwer, M. Cecchini, D.A. Ouakrim, T.C. Oliveira, M.J. Struelens, C. Suetens, D.L. Monnet, R. Strauss, K. Mertens, T. Struyf, B. Catry, K. Latour, I.N. Ivanov, E.G. Dobreva, A. Tambic Andraševic, S. Soprek, A. Budimir, N. Paphitou, H. Žemlicková, S. Schytte Olsen, U. Wolff Sönksen, P. Märtin, M. Ivanova, O. Lyytikäinen, J. Jalava, B. Coignard, T. Eckmanns, M. Abu Sin, S. Haller, G.L. Daikos, A. Gikas, S. Tsiodras, F. Kontopidou, Á. Tóth, Á. Hajdu, Ó. Guólaugsson, K.G. Kristinsson, S. Murchan, K. Burns, P. Pezzotti, C. Gagliotti, U. Dumpis, A. Liuimiene, M. Perrin, M.A. Borg, S.C. de Greeff, J.C. Monen, M.B. Koek, P. Elstrøm, D. Zabicka, A. Deptula, W. Hryniewicz, M. Caniça, P.J. Nogueira, P.A. Fernandes, V. Manageiro, G.A. Popescu, R.I. Serban, E. Schréterová, S. Litvová, M. Štefkovicová, J. Kolman, I. Klavs, A. Korošec, B. Aracil, A. Asensio, M. Pérez-Vázquez, H. Billström, S. Larsson, J.S. Reilly, A. Johnson, S. Hopkins. Attributable deaths and disability-adjusted life-years caused by infections with antibiotic-resistant bacteria in the EU and the European Economic Area in 2015: A population-level modelling analysis. Lancet Infect. Dis. 19: 56–66 (2019).

[95] A. Jõers, E. Liske, T. Tenson. Dividing subpopulation of *Escherichia coli* in stationary phase. Res. Microbiol. 171: 153–157 (2020).

[96] R. Kolter, D.A. Siegele, A. Tormo. The stationary phase of the bacterial life cycle. Annu. Rev. Microbiol. 47: 855–874 (1993).

[97] N. Nanninga. Morphogenesis of *Escherichia coli*, Microbiol Mol Biol Rev. Microbiol. Mol. Biol. Rev. 62: 110–125 (1998).

[98] Z.W. El-Hajj, E.B. Newman. How much territory can a single *E. coli* cell control? Front. Microbiol. 6: 1–12 (2015).

[99] B. Volkmer, M. Heinemann. Condition-dependent cell volume and concentration of *Escherichia coli* to facilitate data conversion for systems biology modeling. PLoS One 6: 1–6 (2011).

[100] J. Cho, A.N. Carr, L. Whitworth, B. Johnson, K.S. Wilson. MazEF toxin-antitoxin proteins alter *Escherichia coli* cell morphology and infrastructure during persister formation and regrowth. Microbiol. (United Kingdom) 163: 308–321 (2017).

[101] M. Hoppert, F. Mayer. Principles of macromolecular organization and cell function in bacteria and archaea. Cell Biochem. Biophys. 31: 247–284 (1999).

[102] J.L. Martinez, F. Baquero. Minireview Mutation frequencies and antibiotic resistance. Antimicrob. Agents Chemother. 44: 1771–1777 (2000).

[103] S. Correia, P. Poeta, M. Hébraud, J.L. Capelo, G. Igrejas. Mechanisms of quinolone action and resistance: Where do we stand? J. Med. Microbiol. 66: 551–559 (2017).

[104] A. Carattoli. Plasmids and the spread of resistance. Int. J. Med. Microbiol. 303: 298–304 (2013).

[105] L. Martínez-Martínez, A. Pascual, G.A. Jacoby. Quinolone resistance from a transferable plasmid. Lancet 351: 797–799 (1998).

[106] L.S. Redgrave, S.B. Sutton, M.A. Webber, L.J.V. Piddock. Fluoroquinolone resistance: Mechanisms, impact on bacteria, and role in evolutionary success. Trends Microbiol. 22: 438–445 (2014).

[107] E.S. Kim, C. Chen, M. Braun, H.Y. Kim, R. Okumura, Y. Wang, G.A. Jacoby, D.C. Hooper. Interactions between QnrB, QnrB mutants, and DNA gyrase. Antimicrob. Agents Chemother. 59: 5413–5419 (2015).

[108] J. Machuca, A. Briales, P. Díaz-de-Alba, L. Martínez-Martínez, Á. Pascual, J.M. Rodríguez-Martínez. Effect of the efflux pump QepA2 combined with chromosomally mediated mechanisms on quinolone resistance and bacterial fitness in *Escherichia coli*. J. Antimicrob. Chemother. 70: 2524–2527 (2015).

[109] J.H. Han, I. Nachamkin, P. Tolomeo, X. Mao, W.B. Bilker, E. Lautenbach. Temporal changes in resistance mechanisms in colonizing *Escherichia coli* isolates with reduced susceptibility to fluoroquinolones. Diagn. Microbiol. Infect. Dis. 76: 491–496 (2013).

[110] X. Xie, R. Lv, C. Yang, Y. Song, Y. Yan, Y. Cui, R. Yang. Soft sweep development of resistance in *Escherichia coli* under fluoroquinolone stress. J. Microbiol. 57: 1056–1064 (2019).

[111] D.C. Moon, S.Y. Seol, M. Gurung, J.S. Jin, C.H. Choi, J. Kim, Y.C. Lee, D.T. Cho, J.C. Lee. Emergence of a new mutation and its accumulation in the topoisomerase IV gene confers high levels of resistance to fluoroquinolones in *Escherichia coli* isolates. Int. J. Antimicrob. Agents 35: 76–79 (2010).

[112] M.J. Ellington, O. Ekelund, F.M. Aarestrup, R. Canton, M. Doumith, C. Giske, H. Grundman, H. Hasman, M.T.G. Holden, K.L. Hopkins, J. Iredell, G. Kahlmeter, C.U. Köser, A. MacGowan, D. Mevius, M. Mulvey, T. Naas, T. Peto, J.M. Rolain, Samuelsen, N. Woodford. The role of whole genome sequencing in antimicrobial susceptibility testing of bacteria: Report from the EUCAST Subcommittee. Clin. Microbiol. Infect. 23: 2–22 (2017).

[113] Y. Pu, Z. Zhao, Y. Li, J. Zou, Q. Ma, Y. Zhao, Y. Ke, Y. Zhu, H. Chen, M.A.B. Baker, H. Ge, Y. Sun, X.S. Xie, F. Bai. Enhanced efflux acativity facilitates drug tolerance in dormant bacterial cells. Mol. Cell 62: 284–294 (2016).

[114] J.E. Michiels, B. Van den Bergh, N. Verstraeten, J. Michiels. Molecular mechanisms and clinical implications of bacterial persistence. Drug Resist. Updat. 29: 76–89 (2016).

[115] T.C. Barrett, W.W.K. Mok, A.M. Murawski, M.P. Brynildsen. Enhanced antibiotic resistance development from fluoroquinolone persisters after a single exposure to antibiotic. Nat. Commun. 10: 1–11 (2019).

[116] I. Keren, N. Kaldalu, A. Spoering, Y. Wang, K. Lewis. Persister cells and tolerance to antimicrobials. FEMS Microbiol. Lett. 230: 13–18 (2004).

[117] B.R. Levin, D.E. Rozen. Non-inherited antibiotic resistance. Nat. Rev. Microbiol. 4: 556–562 (2006).

[118] T.K. Wood, S.J. Knabel, B.W. Kwan. Bacterial persister cell formation and dormancy. Appl. Environ. Microbiol. 79: 7116–7121 (2013).

[119] M.A. Orman, M.P. Brynildsen. Dormancy is not necessary or sufficient for bacterial persistence. Antimicrob. Agents Chemother. 57: 3230–3239 (2013).

[120] N.Q. Balaban, J. Merrin, R. Chait, L. Kowalik, S. Leibler. Bacterial persistence as a phenotypic switch. Science. 305: 1622–1625 (2004).

[121] I. Keren, D. Shah, A. Spoering, N. Kaldalu, K. Lewis. Specialized persister cells and the mechanism of multidrug tolerance in *Escherichia coli*. J. Bacteriol. 186: 8172–8180 (2004).

[122] K.J. Kristina Heinrich, David J. Leslie. Chapter four - Modulation of bacterial proliferation as a survival strategy. In: Advances in Applied Microbiology. Pages 127-171 (2015).

[123] R. Pourahmad Jaktaji, S. Pasand. Overexpression of SOS genes in ciprofloxacin resistant *Escherichia coli* mutants. Gene 576: 115–118 (2016).

[124] F. Goormaghtigh, L. Van Melderen. Single-cell imaging and characterization of *Escherichia coli* persister cells to ofloxacin in exponential cultures. Sci. Adv. 5: 1–14 (2019).

[125] G. Sharma, S. Sharma, P. Sharma, D. Chandola, S. Dang, S. Gupta, R. Gabrani. *Escherichia coli* biofilm: Development and therapeutic strategies. J. Appl. Microbiol. 121: 309–319 (2016).

[126] J.W. Mouton, J. Meletiadis, A. Voss, J. Turnidge. Variation of MIC measurements: The contribution of strain and laboratory variability to measurement precision. J. Antimicrob. Chemother. 73: 2374–2379 (2018).

[127] J.W. Mouton, A.E. Muller, R. Canton, C.G. Giske, G. Kahlmeter, J. Turnidge. MIC-based dose adjustment: Facts and fables. J. Antimicrob. Chemother. 73: 564–568 (2018).

[128] L.R. Peterson, C.J. Shanholtzer. Tests for bactericidal effects of antimicrobial agents: Technical performance and clinical relevance. Clin. Microbiol. Rev. 5: 420–432 (1992).

[129] Thermo Fisher Scientific. http://www.oxoid.com/UK/blue/prod_detail/prod_detail.asp?pr=CM0405&c=UK&lang=EN (last access 25 Apr 2021).

[130] EUCAST-European Committee on Antimicrobial Suscetibility Testing. Media preparation for EUCAST disk diffusion testing and for determination of MIC values by the broth microdilution method, version 6 (2020). https://www.eucast.org/fileadmin/src/media/PDFs/EUCAST_files/Disk_test_documents/2020_manuals/Media_preparation_v_6.0_EUCAST_AST.pdf (last access 25 Apr 2021).

[131] J. Seeger. Vergleich des pharmakodynamischen Effekts von Levofloxacin 750 mg qd und 500 mg bid auf resistente *Escherichia coli* im dynamischen *In-vitro*-Infektionsmodell. Freie Universitaet Berlin. (2017).

[132] B. Herigstad, M. Hamilton, J. Heersink. How to optimize the drop plate method for enumerating bacteria. J. Microbiol. Methods 44: 121–129 (2001).

[133] E.B. Goebgen. Entwicklung und Evaluierung eines elektronischen Bakterienzählverfahrens und Untersuchungen unter Linezolidexposition. Freie Universitaet Berlin. (2014).

[134] E.B. Goebgen. Impact of human levofloxacin concentrations on *Escherichia coli* growth/kill/adaption dynamics in an integrated experimental and semi-mechanistic pharmacocinetic/pharmacodynamic modelling approach. Freie Universitaet Berlin. (2018).

[135] I.K. Bartels. Validierung des dynamischen *In-vitro*-Infektionsmodells zur Bestimmung des pharmakodynamischen Effekts von Levofloxacin auf *Escherichia coli*. Freie Universitaet Berlin. (2015).

[136] EMA-European Medicines Agency. Guideline on bioanalytical method validation. (2012). https://www.ema.europa.eu/en/documents/scientific-guideline/guideline-bioanalytical-method-validation_en.pdf (last access 25 Apr 2021).

[137] J. Beer, C.C. Wagner, M. Zeitlinger. Protein binding of antimicrobials: Methods for quantification and for investigation of its impact on bacterial killing. AAPS J. 11: 1–12 (2009).

[138] D.G. Levitt, M.D. Levitt. Human serum albumin homeostasis: A new look at the roles of synthesis, catabolism, renal and gastrointestinal excretion, and the clinical value of serum albumin measurements. Int. J. Gen. Med. 9: 229–255 (2016).

[139] M. Zeitlinger, R. Sauermann, M. Fille, J. Hausdorfer, I. Leitner, M. Müller. Plasma protein binding of fluoroquinolones affects antimicrobial activity. J. Antimicrob. Chemother. 61: 561–567 (2008).

[140] J. Michael. Pharmacodynamic *in vitro* studies contributing to the rational use of linezolid in infections by vancomycin resistant *Enterococcus faecium*. Martin-Luther-Universitaet Halle-Wittenberg. (2011).

[141] J. Michael. Disputation. (2011).

[142] A. Schaeftlein. Neue Wege in der Modellierung von Mikrodialysatdaten im Menschen: Charakterisierung der klinischen ADMER-Prozesse von Moxifloxacin, Levofloxacin und Linezolid in Gesunden und Hochrisikopopulationen. Freie Universitaet Berlin. (2013).

[143] E. Zankari, H. Hasman, S. Cosentino, M. Vestergaard, S. Rasmussen, O. Lund, F.M. Aarestrup, M.V. Larsen. Identification of acquired antimicrobial resistance genes. J. Antimicrob. Chemother. 67: 2640–2644 (2012).

[144] https://www.geneon.net/products/dna-rna-extraction-1/tissue-dna-purification-de/ (last access 25 Apr 2021).

[145] https://www.illumina.com/documents/products/technotes/technote_Q-Scores.pdf (last access 25 Apr 2021).

[146] National Center for Biotechnology Information. https://www.ncbi.nlm.nih.gov (last access 25 Apr 2021).

[147] Illumina® Sequencing Technology. https://www.illumina.com/documents/products/techspotlights/techspotlight_sequencing.pdf (last access 25 Apr 2021).

[148] Center for Genomic Epidemilogy. https://cge.cbs.dtu.dk/services/MLST/ (last access 25 Apr 2021).

[149] M. V. Larsen, S. Cosentino, S. Rasmussen, C. Friis, H. Hasman, R.L. Marvig, L. Jelsbak, T. Sicheritz-Pontén, D.W. Ussery, F.M. Aarestrup, O. Lund. Multilocus sequence typing of total-genome-sequenced bacteria. J. Clin. Microbiol. 50: 1355–1361 (2012).

[150] L. Uelze, J. Grützke, M. Borowiak, J.A. Hammerl, K. Juraschek, C. Deneke, S.H. Tausch, B. Malorny. Typing methods based on whole genome sequencing data. One Heal. Outlook 2: 3 (2020).

[151] O. Clermont, D. Gordon, E. Denamur. Guide to the various phylogenetic classification schemes for *Escherichia coli* and the correspondence among schemes. Microbiol. (United Kingdom) 161: 980–988 (2015).

[152] Basic Local Alignment Search Tool. https://blast.ncbi.nlm.nih.gov/Blast.cgi (last access 25 Apr 2021).

[153] OMNI Life Science. CASY® Cell counter & analyzer - Manual. (2019).

[154] D.R. Mould, R.N. Upton. Basic concepts in population modeling, simulation, and model-based drug development—Part 2: Introduction to pharmacokinetic modeling methods. CPT Pharmacometrics Syst. Pharmacol. 2: e38 (2013).

[155] I.J. Myung. Tutorial on maximum likelihood estimation. J. Math. Psychol. 47: 90–100 (2003).

[156] C.C. Peck, S.L. Beal, L.B. Sheiner, A.I. Nichols. Extended least squares nonlinear regression: A possible solution to the “choice of weights” problem in analysis of individual pharmacokinetic data. J. Pharmacokinet. Biopharm. 12: 545–558 (1984).

[157] J.A. Nelder, R. Mead. A simplex method for function minimization. Comput. J. 7: 308–313 (1965).

[158] J.R. Shewchuk. An introduction to the conjugate gradient method without the agonizing pain. Evolution (N. Y). 61: 708–712 (2007).

[159] H. Akaike. A new look at the statistical model identification. IEEE Trans. Automat. Contr. 19: 716–723 (1974).

[160] R.J. Bauer. NONMEM tutorial part I: Description of commands and options, with simple examples of population analysis. CPT Pharmacometrics Syst. Pharmacol. 8: 525–537 (2019).

[161] J.E. Ahn, M.O. Karlsson, A. Dunne, T.M. Ludden. Likelihood based approaches to handling data below the quantification limit using NONMEM VI. J. Pharmacokinet. Pharmacodyn. 35: 401–421 (2008).

[162] E.B. Goebgen, J. Seeger, A. Schaeftlein, C. Kloft. Levofloxacin in resistant *Escherichia coli* : Is there a difference between 750 mg once a day and 500 mg twice a day? 27th European Congress of Clinical Microbiology and Infectious Diseases, Vienna, Austria, 22-25 April (2017). [https://www.escmid.org/escmid_publications/escmid_elibrary/material/?mid=40622], P1206 (2017).

[163] U. Wahlby, E.N. Jonsson, M.O. Karlsson. Comparison of stepwise covariate model building strategies in population pharmacokinetic-pharmacodynamic analysis. AAPS PharmSci 4: 1–12 (2002).

[164] R.N. Upton, D.R. Mould. Basic concepts in population modeling, simulation, and model-based drug development: Part 3-Introduction to pharmacodynamic modeling methods. CPT Pharmacometrics Syst. Pharmacol. 3: e88 (2014).

[165] L.F. Lacey, O.N. Keene, J.F. Pritchard, A. Bye. Common noncompartmental pharmacokinetic variables: Are they normally or log-normally distributed? J. Biopharm. Stat. 7: 171–178 (1997).

[166] R.J. Bauer, S. Guzy, C. Ng. A survey of population analysis methods and software for complex pharmacokinetic and pharmacodynamic models with examples. AAPS J. 9: (2007).

[167] T.H.T. Nguyen, M.S. Mouksassi, N. Holford, N. Al-Huniti, I. Freedman, A.C. Hooker, J. John, M.O. Karlsson, D.R. Mould, J.J. Perez Ruixo, E.L. Plan, R. Savic, J.G.C. Van Hasselt, B. Weber, C. Zhou, E. Comets, F. Mentre. Model evaluation of continuous data pharmacometric models: Metrics and graphics. CPT Pharmacometrics Syst. Pharmacol. 6: 87–109 (2017).

[168] A.C. Hooker, C.E. Staatz, M.O. Karlsson. Conditional weighted residuals (CWRES): A model diagnostic for the FOCE method. Pharm. Res. 24: 2187–2197 (2007).

[169] A.G. Dosne, M. Bergstrand, K. Harling, M.O. Karlsson. Improving the estimation of parameter uncertainty distributions in nonlinear mixed effects models using sampling importance resampling. J. Pharmacokinet. Pharmacodyn. 43: 583–596 (2016).

[170] A.G. Dosne, M. Bergstrand, M.O. Karlsson. An automated sampling importance resampling procedure for estimating parameter uncertainty. J. Pharmacokinet. Pharmacodyn. 44: 509–520 (2017).

[171] https://www.r-project.org/ (last access 25 Apr 2021).

[172] https://www.rstudio.com/ (last access 25 Apr 2021).

[173] H. Wätzig, W. Mehnert, W. Bühler (eds.). Mathematik und Statistik kompakt. Wissenschaftliche Verlagsgesellschaft Stuttgart, Stuttgart, 1st ed. (2009).

[174] The European Molecular Biology Open Software Suite. http://emboss.open-bio.org/ (last access 25 Apr 2021).

[175] A.C. Matos, R. V. Pinto, A.F. Bettencourt. Easy assessment of levofloxacin and minocycline in relevant biomimetic media by HPLC-UV Analysis. J. Chromatogr. Sci. 55: 757–765 (2017).

[176] A. Nussbaumer-Pröll, M. Zeitlinger. Use of supplemented or human material to simulate PD behavior of antibiotics at the target site *in vitro*. Pharmaceutics 12: 1–18 (2020).

[177] A.K. Nussbaumer-Pröll, S. Eberl, B. Reiter, T. Stimpfl, W. Jäger, S. Poschner, M. Zeitlinger. Impact of thrombocytes, on bacterial growth and antimicrobial activity of selected antibiotics. Eur. J. Clin. Microbiol. Infect. Dis. 39: 593–597 (2020).

[178] M. Hombach, C. Ochoa, F.P. Maurer, T. Pfiffner, E.C. Böttger, R. Furrer. Relative contribution of biological variation and technical variables to zone diameter variations of disc diffusion susceptibility testing. J. Antimicrob. Chemother. 71: 141–151 (2016).

[179] M. Ballestero-Téllez, E. Jiménez-Morgades, Camachom Pilar Arjona. Inter-technique variability between antimicrobial susceptibility testing methods affects clinical classification of cefuroxime in strains close to breakpoints. Clin. Microbiol. Infect. 26: (2020).

[180] A. Soares, M. Pestel-Caron, F. Leysour de Rohello, G. Bourgoin, S. Boyer, F. Caron. Area of technical uncertainty for susceptibility testing of amoxicillin/clavulanate against *Escherichia coli*: Analysis of automated system, Etest and disk diffusion methods compared to the broth microdilution reference. Clin. Microbiol. Infect. 26: (2020).

[181] EUCAST-European Committee on Antimicrobial Suscetibility Testing. Standard Operating Procedure 10.1. MIC distributions and the setting of epidemiological cut-off (ECOFF) values. (2017). https://www.eucast.org/fileadmin/src/media/PDFs/EUCAST_files/EUCAST_SOPs/EUCAST_SOP_10.1_MIC_distributions_and_epidemiological_cut-off_value__ECOFF__setting_20191130.pdf (last access 25 Apr 2021).

[182] EUCAST-European Committee on Antimicrobial Susceptibility Testing. Definitions of clinical breakpoints and epidemiological cut-off values. (2017). https://www.eucast.org/fileadmin/src/media/PDFs/EUCAST_files/EUCAST_SOPs/EUCAST_definitions_of_clinical_breakpoints_and_ECOFFs.pdf (last access 25 Apr 2021).

[183] D.D. Khan, Lagerbaeck, Pernilla, S. Cao, U. Lustig, E.I. Nielsen, O. Cars, D. Hughes, D.I. Andersson, L.E. Friberg. A mechanism-based pharmacokinetic/pharmacodynamic model allows prediction of antibiotic killing from MIC values for WT and mutants. J. Antimicrob. Chemother. 70: 3051–3060 (2015).

[184] A. Thorsted, E. Tano, K. Kaivonen, J. Sjölin, L.E. Friberg, E.I. Nielsen. Extension of pharmacokinetic/pharmacodynamic (PK/PD) time-kill studies to include LPS/endotoxin release from *E. coli* exposed to cefuroxime . Antimicrob. Agents Chemother. 64: 1–12 (2020).

[185] L. Drago. Activity of levofloxacin and ciprofloxacin against urinary pathogens. J. Antimicrob. Chemother. 48: 37–45 (2001).

[186] H.K. Lee, V. DeVito, C. Vercelli, C. Tramuta, P. Nebbia, G. Re, K. Kovalenko, M. Giorgi. *Ex vivo* antibacterial activity of levofloxacin against *Escherichia coli* and its pharmacokinetic profile following intravenous and oral administrations in broilers. Res. Vet. Sci. 112: 26–33 (2017).

[187] L. Tasso, C. De Andrade, T. Dalla Costa. Pharmacokinetic/pharmacodynamic modelling of the bactericidal activity of free lung concentrations of levofloxacin and gatifloxacin against *Streptococcus pneumoniae*. Int. J. Antimicrob. Agents 38: 307–313 (2011).

[188] J.B. Bulitta, N.S. Ly, J.C. Yang, A. Forrest, W.J. Jusko, B.T. Tsuji. Development and qualification of a pharmacodynamic model for the pronounced inoculum effect of ceftazidime against *Pseudomonas aeruginosa*. Antimicrob. Agents Chemother. 53: 46–56 (2009).

[189] W. Ungphakorn, T. Tängdén, L. Sandegren, E.I. Nielsen. A pharmacokinetic-pharmacodynamic model characterizing the emergence of resistant *Escherichia coli* subpopulations during ertapenem exposure. J. Antimicrob. Chemother. 71: 2521–2533 (2016).

[190] E.B. Goebgen, N. Hartung, J Seeger, A. Schaeftlein, C. Kloft. Treatment of catheterized ICU patients with levofloxacin - How *in silico* models help to streamline *in vitro* investigations of treatment efficacy at the target site. Annual Meeting of the Deutsche Pharmazeutische Gesellschaft (DPhG), Munich, Germany, 04-07 October 2016. Abstract book, POS.89 (2016).

[191] N. Hartung, C. Hethey, E.B. Goebgen, C. Kloft, W. Huisinga. Quantifying adaptive resistance in bacteria using well-designed dynamic time-kill curve experiments. 26th Population Approach Group Europe (PAGE), Budapest, Hungary, 06-09 June 2017, PAGE 26: 7210 [www.page-meeting.org/default.asp?abstract=7210], (2017).

[192] P.G. Ambrose, B. VanScoy, H. Conde, J. McCauley, C.M. Rubino, S.M. Bhavnani. Bacterial replication rate modulation in combination with antimicrobial therapy: Turning the microbe against itself. Antimicrob. Agents Chemother. 61: 1–6 (2017).

[193] R. Singh, M.C. Swick, K.R. Ledesma, Z. Yang, M. Hu, L. Zechiedrich, V.H. Tama. Temporal interplay between efflux pumps and target mutations in development of antibiotic resistance in *Escherichia coli*. Antimicrob. Agents Chemother. 56: 1680–1685 (2012).

[194] Biomatters Ltd. Geneious 11.1. (2018).

[195] L.L. Marcusson, N. Frimodt-Møller, D. Hughes. Interplay in the selection of fluoroquinolone resistance and bacterial fitness. PLoS Pathog. 5: (2009).

[196] A.H. Melnyk, A. Wong, R. Kassen. The fitness costs of antibiotic resistance mutations. Evol. Appl. 8: 273–283 (2015).

[197] H.E. Kubitschek, J.A. Friske. Determination of bacterial cell volume with the coulter counter. J. Bacteriol. 168: 1466–1467 (1986).

[198] E.M. Swanton, W.A. Curby, H.E. Lind. Experiences with the coulter counter in bacteriology. Appl. Microbiol. 10: 480–485 (1962).

[199] M.K. Alexander, M.S. Khan, C.S. Dow. Rapid screening for bacteriuria using a particle counter, pulse-height analyser, and computer. J. Clin. Pathol. 34: 194–198 (1981).

[200] G. Toennies, L. Iszard, N.B. Rogers, G.D. Shockman. Cell multiplication studied with an electronic particle counter. J. Bacteriol. 82: 857–866 (1961).

[201] A. McAleenan, P.G. Ambrose, S.M. Bhavnani, G.L. Drusano, W.W. Hope, J.W. Mouton, J.P.T. Higgins, A.P. MacGowan. Methodological features of clinical pharmacokinetic–pharmacodynamic studies of antibacterials and antifungals: A systematic review. J. Antimicrob. Chemother. 75: (2020).

[202] J.S. Teodósio, M. Simões, L.F. Melo, F.J. Mergulhão. Flow cell hydrodynamics and their effects on *E. coli* biofilm formation under different nutrient conditions and turbulent flow. Biofouling 27: 1–11 (2011).

[203] H. Prochnow, V. Fetz, S.K. Hotop, M.A. García-Rivera, A. Heumann, M. Brönstrup. Subcellular quantification of uptake in Gram-negative bacteria. Anal. Chem. 91: 1863–1872 (2019).

[204] EUCAST-European Committee on Antimicrobial Suscetibility Testing. Antimicrobial wild type distributions of microorganisms. https://mic.eucast.org (last access 11 Apr 2021).

7 Appendix

7.1 Figures

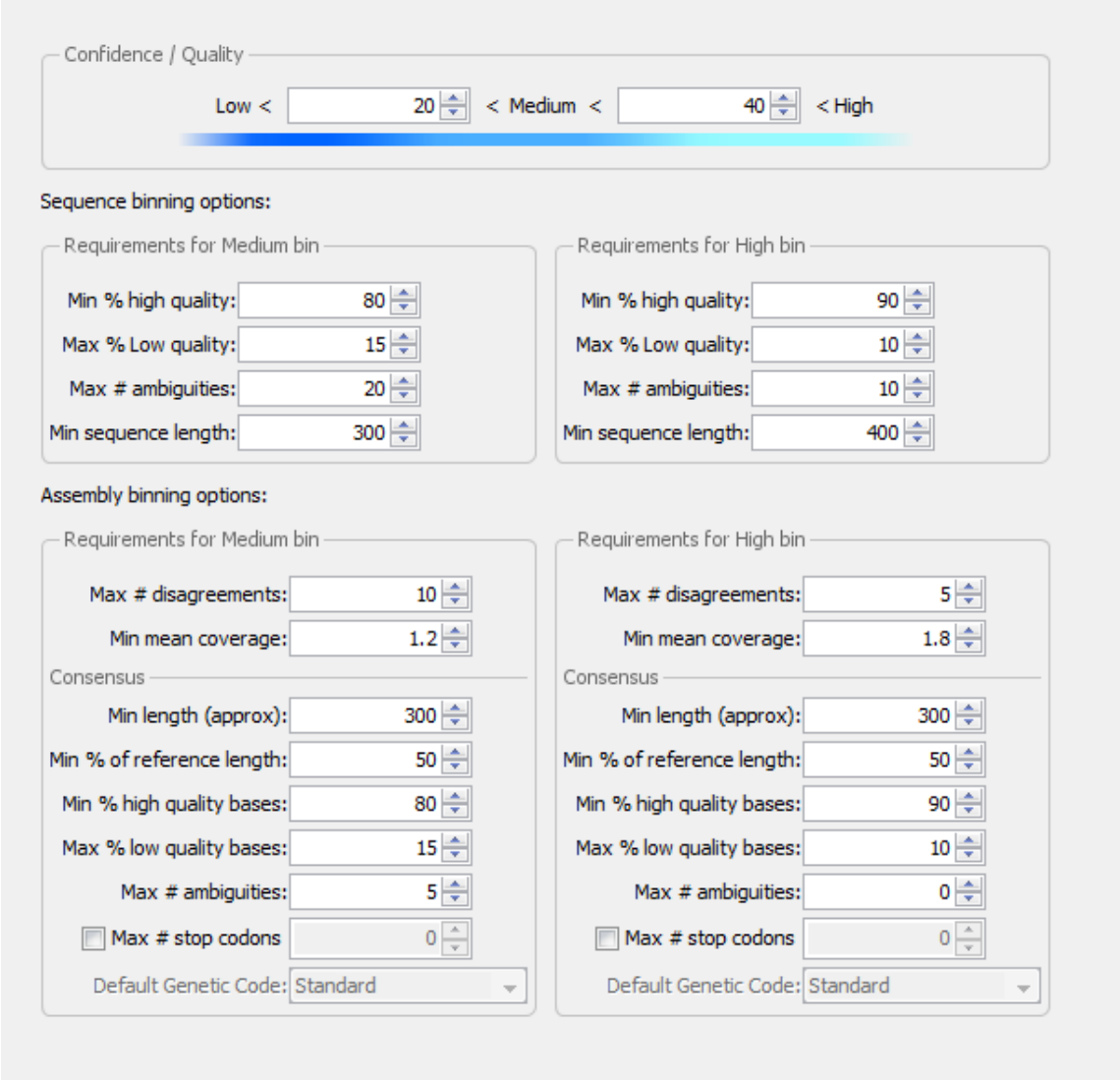

Figure 7.1: Settings for the assignment of quality categories in geneious® and representation of sequence quality on a colour scale.

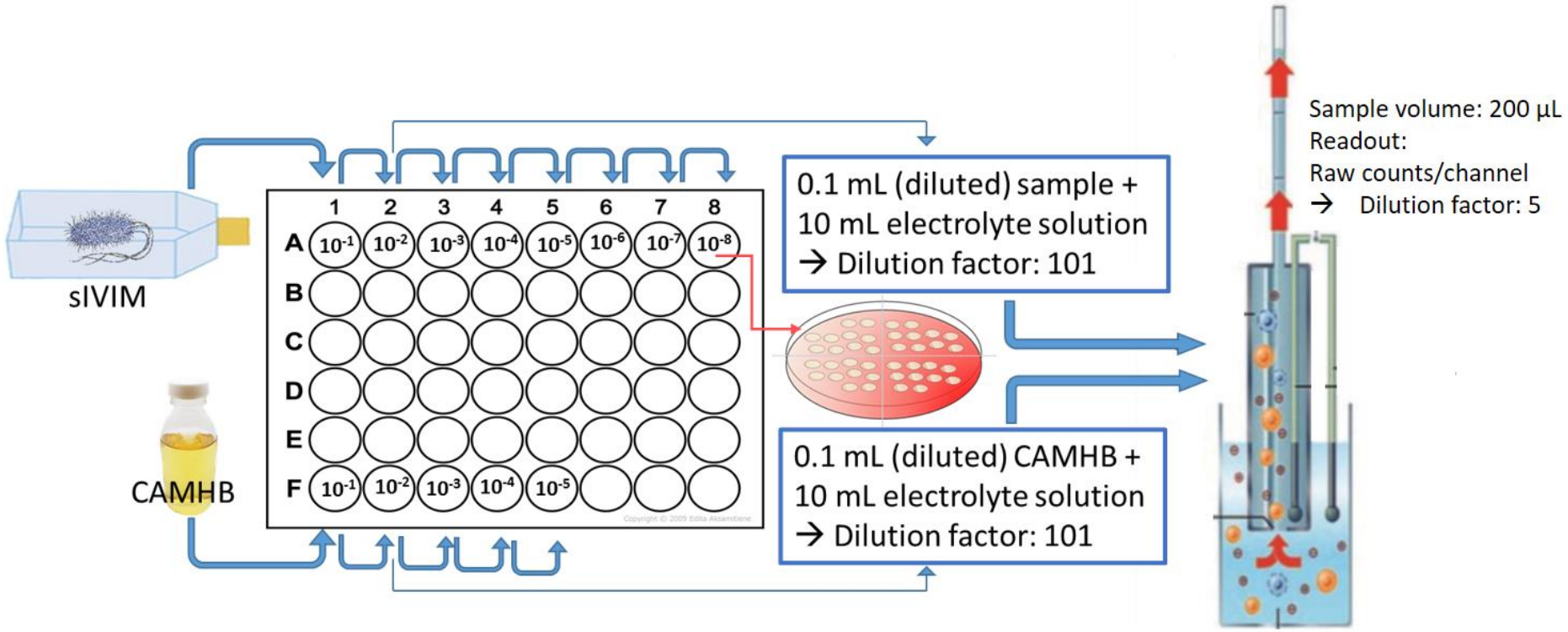

Figure 7.2: Experimental workflow and dilution steps for bacterial quantification by droplet plate assay (chapter 2.2.1.3) and cell counter and analyser system (CASY®) in static *in vitro* infection model (sIVIM) experiments. CAMHB: cation adjusted Mueller Hinton broth.

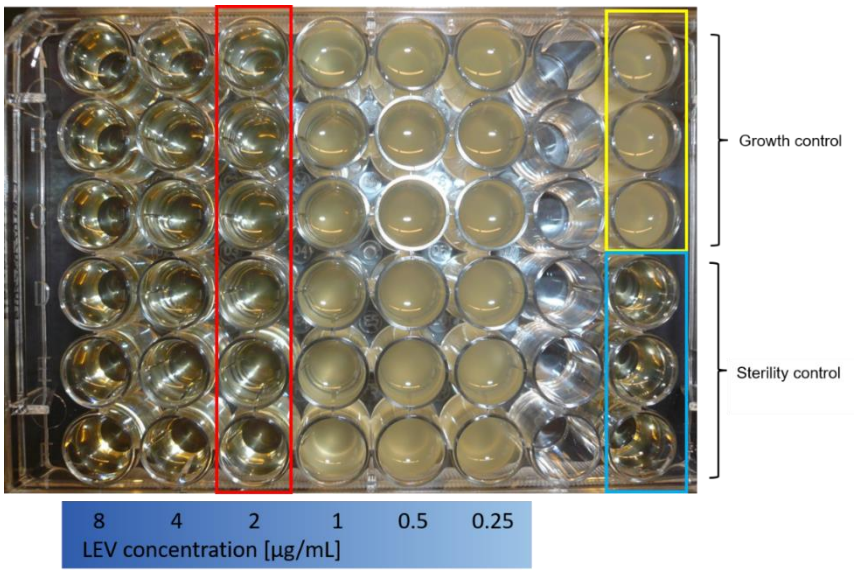

Figure 7.3: Minimal inhibitory concentration (MIC) of *Escherichia coli* sequence type 88**,** determined by the microdilution method. Levofloxacin (LEV) concentrations in each well in a vertical row are displayed below the corresponding row; growth control (yellow frame): bacterial suspension without LEV addition; sterility control (blue frame): growth medium without bacteria or drug; red frame indicates LEV MIC of the isolate (2 µg/mL).

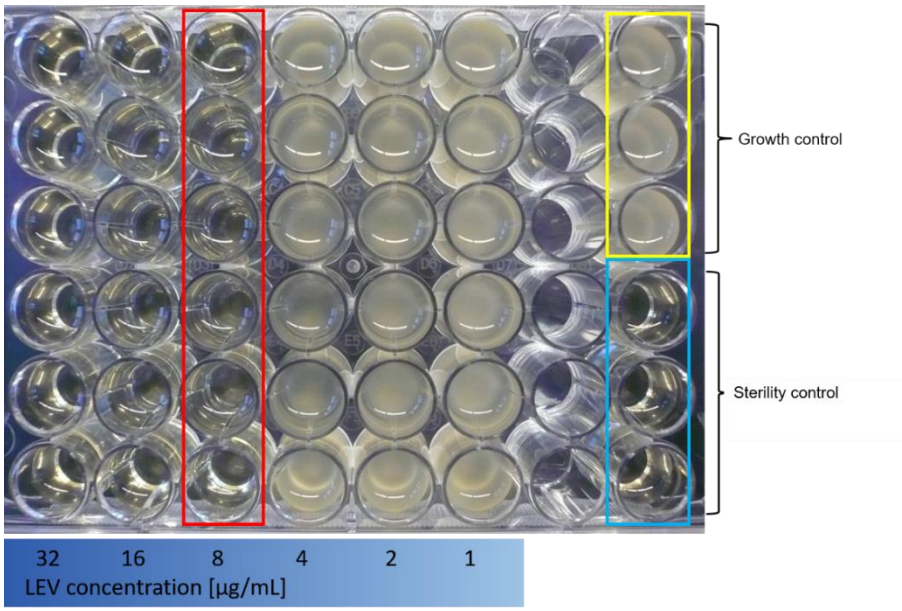

Figure 7.4: Minimal inhibitory concentration (MIC) of *Escherichia coli* sequence type 167**,** determined by the microdilution method. Levofloxacin (LEV) concentrations in each well in a vertical row are displayed below corresponding row; growth control (yellow frame): bacterial suspension without LEV addition; sterility control (blue frame): growth medium without bacteria or drug; red frame indicates LEV MIC of the isolate (8 µg/mL).

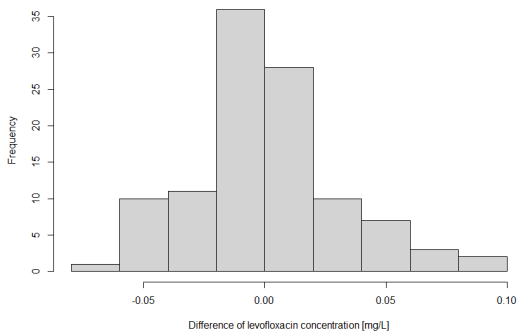

Figure 7.5: Frequency distribution of differences in levofloxacin concentration between calibrator solutions before ultrafiltration and in ultrafiltrate, n=108.

MLST-2.0 Server - Results

mlst Profile: *ecoli*

Organism: *Escherichia coli#1*

Sequence Type: *58*

Locus	Identity	Coverage	Alignment Length	Allele Length	Gaps	Allele
adk	100	100	536	536	0	adk_6
fumC	100	100	469	469	0	fumC_4
gyrB	100	100	460	460	0	gyrB_4
icd	100	100	518	518	0	icd_16
mdh	100	100	452	452	0	mdh_24
purA	100	100	478	478	0	purA_8
recA	100	100	510	510	0	recA_14

extended output

Input Files: *FU1.fasta*

MLST-2.0 Server - Results

mlst Profile: *ecoli_2*

Organism: *Escherichia coli#2*

Sequence Type: *24*

Locus	Identity	Coverage	Alignment Length	Allele Length	Gaps	Allele
dinB	100	100	450	450	0	dinB_7
icdA	100	100	516	516	0	icdA_32
pabB	100	100	468	468	0	pabB_18
polB	100	100	450	450	0	polB_2
putP	100	100	456	456	0	putP_5
trpA	100	100	561	561	0	trpA_8
trpB	100	100	594	594	0	trpB_2
uidA	100	100	600	600	0	uidA_2

extended output

Input Files: *FU1.fasta*

mlst Profile: *ecoli*

Organism: *Escherichia coli#1*

Sequence Type: *88*

Locus	Identity	Coverage	Alignment Length	Allele Length	Gaps	Allele
adk	100	100	536	536	0	adk_6
fumC	100	100	469	469	0	fumC_4
gyrB	100	100	460	460	0	gyrB_12
icd	100	100	518	518	0	icd_1
mdh	100	100	452	452	0	mdh_20
purA	100	100	478	478	0	purA_12
recA	100	100	510	510	0	recA_7

extended output

Input Files: *FU2.fasta*

mlst Profile: *ecoli_2*

Organism: *Escherichia coli#2*

Sequence Type: *66*

Locus	Identity	Coverage	Alignment Length	Allele Length	Gaps	Allele
dinB	100	100	450	450	0	dinB_6
icdA	100	100	516	516	0	icdA_5
pabB	100	100	468	468	0	pabB_3
polB	100	100	450	450	0	polB_2
putP	100	100	456	456	0	putP_6
trpA	100	100	561	561	0	trpA_7
trpB	100	100	594	594	0	trpB_2
uidA	100	100	600	600	0	uidA_4

extended output

Input Files: *FU2.fasta*

mlst Profile: *ecoli*

Organism: *Escherichia coli#1*

Sequence Type: *167*

Locus	Identity	Coverage	Alignment Length	Allele Length	Gaps	Allele
adk	100	100	536	536	0	adk_10
fumC	100	100	469	469	0	fumC_11
gyrB	100	100	460	460	0	gyrB_4
icd	100	100	518	518	0	icd_8
mdh	100	100	452	452	0	mdh_8
purA	100	100	478	478	0	purA_13
recA	100	100	510	510	0	recA_2

extended output

Input Files: *FU3.fasta*

mlst Profile: *ecoli_2*

Organism: *Escherichia coli#2*

Sequence Type: *877*

Locus	Identity	Coverage	Alignment Length	Allele Length	Gaps	Allele
dinB	100	100	450	450	0	dinB_8
icdA	100	100	516	516	0	icdA_2
pabB	100	100	468	468	0	pabB_7
polB	100	100	450	450	0	polB_190
putP	100	100	456	456	0	putP_7
trpA	100	100	561	561	0	trpA_1
trpB	100	100	594	594	0	trpB_4
uidA	100	100	600	600	0	uidA_2

extended output

Input Files: *FU3.fasta*

Figure 7.6: Screenshots of multilocus sequence typing (MLST) output of the MLST-2.0 tool by the Center for Genomic Epidemiology [143] for 3 *Escherichia coli* isolates according to the Warwick medical school scheme (scheme 1, left panel) and Pasteur institute scheme (scheme 2, right panel).

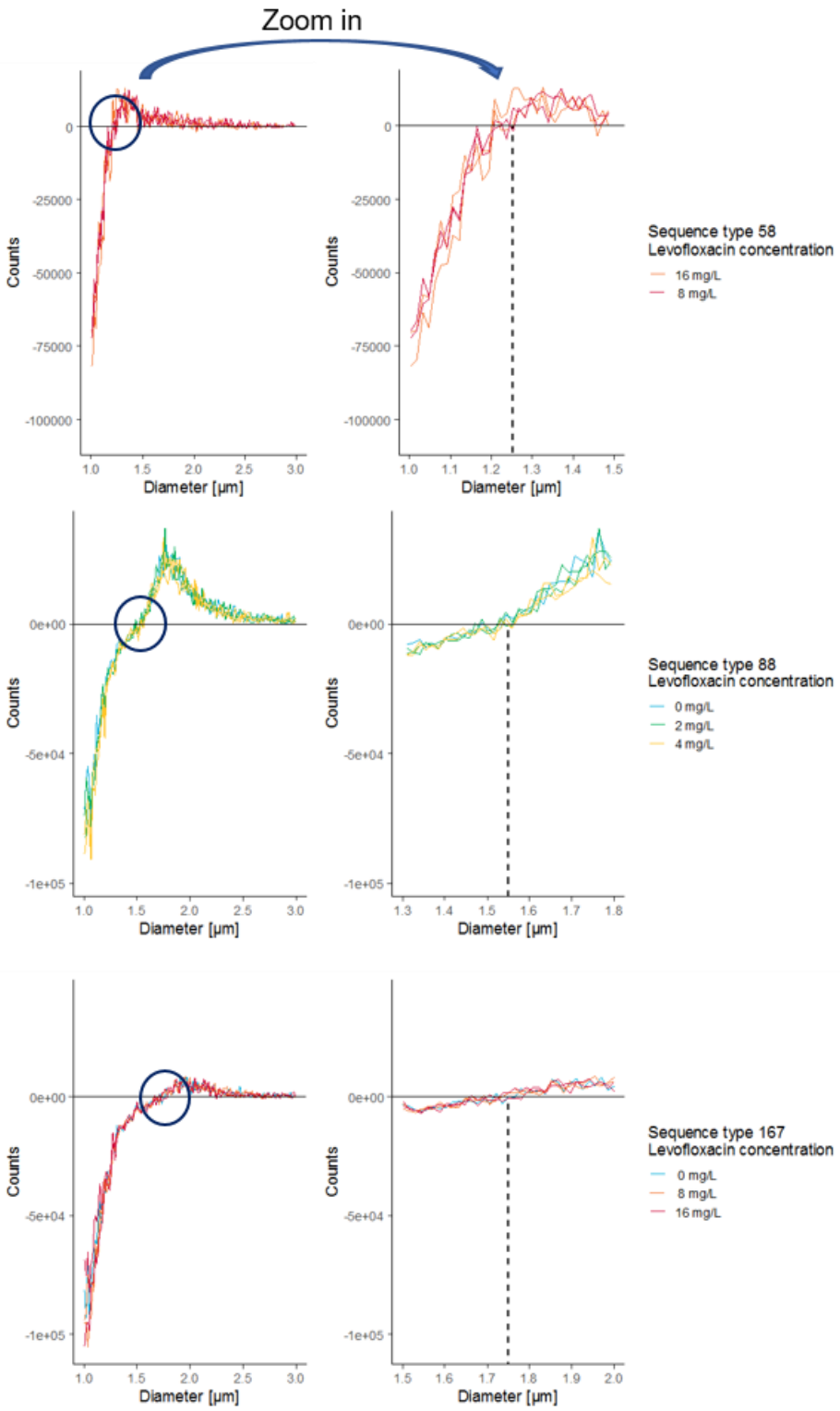

Figure 7.7: Background-corrected size distributions of three *Escherichia coli* isolates (sequence type 58, 88 and 167), before levofloxacin exposure in the static *in vitro* infection model, diameter range between 1.0 and 3.0 µm (left) and zoomed in to strain-specific diameter thresholds between debris and bacteria (right), colours represent mean of ≥ 2 replicates per levofloxacin concentration.

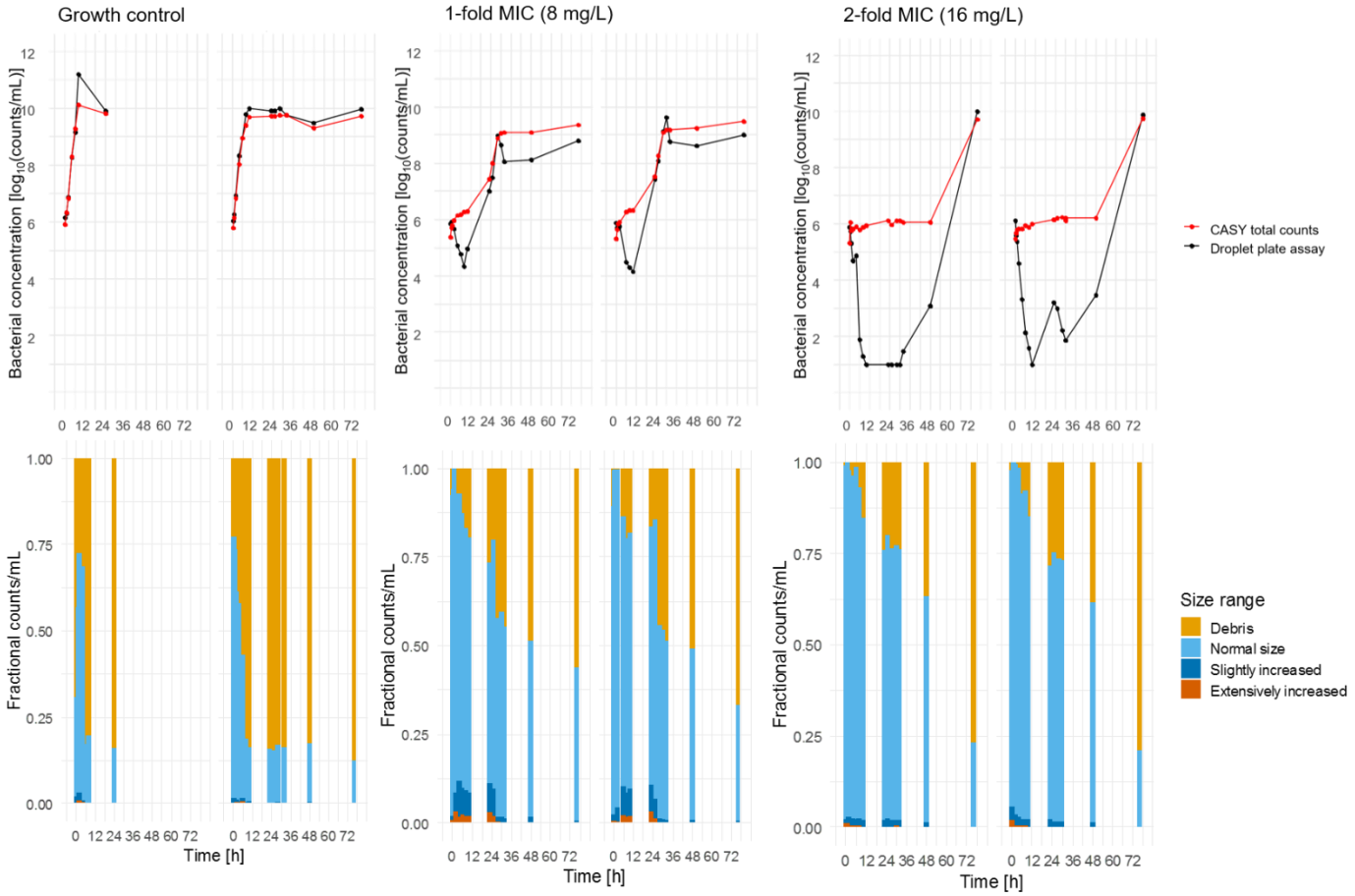

Figure 7.8: Bacterial growth, kill and regrowth behaviour of *Escherichia coli* sequence type 58 in static *in vitro* infection model experiments without antibiotic exposure (left), under exposure to 8 mg/L levofloxacin (LEV), corresponding to the minimal inhibitory concentration (MIC) of the isolate (middle) and under exposure to 2-fold the MIC of the isolate (right). Upper panel: Viable bacteria, quantified as colony forming units/mL (black points and lines) and total counts, quantified by electronic cell counting (red points and lines), over time. Lower panel: fractional counts per size range over time; full height of bars corresponds to total counts of the respective sample, colours correspond to fractional counts of different size ranges; n=2 replicates per levofloxacin concentration.

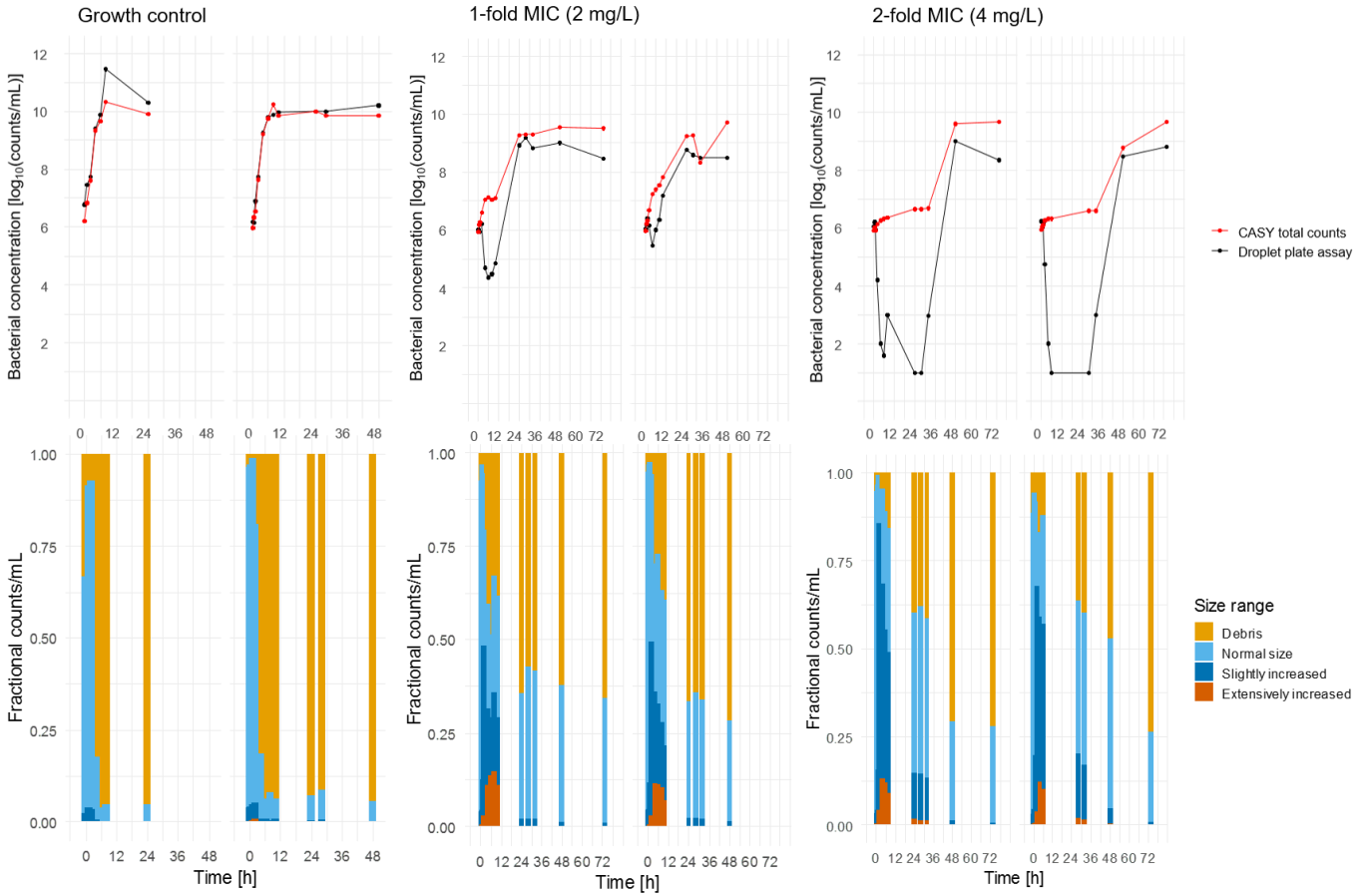

Figure 7.9: Bacterial growth, kill and regrowth behaviour of *Escherichia coli* sequence type 88 in static *in vitro* infection model experiments without antibiotic exposure (left), under exposure to 2 mg/L levofloxacin, corresponding to the minimal inhibitory concentration (MIC) of the isolate (middle) and under exposure to 2-fold the MIC of the isolate (right). Upper panel: Viable bacteria, quantified as colony forming units/mL (black points and lines) and total counts, quantified by electronic cell counting (red points and lines), over time. Lower panel: fractional counts per size range over time; full height of bars corresponds to total counts of the respective sample, colours correspond to fractional counts of different size ranges; n=2 replicates per levofloxacin concentration.

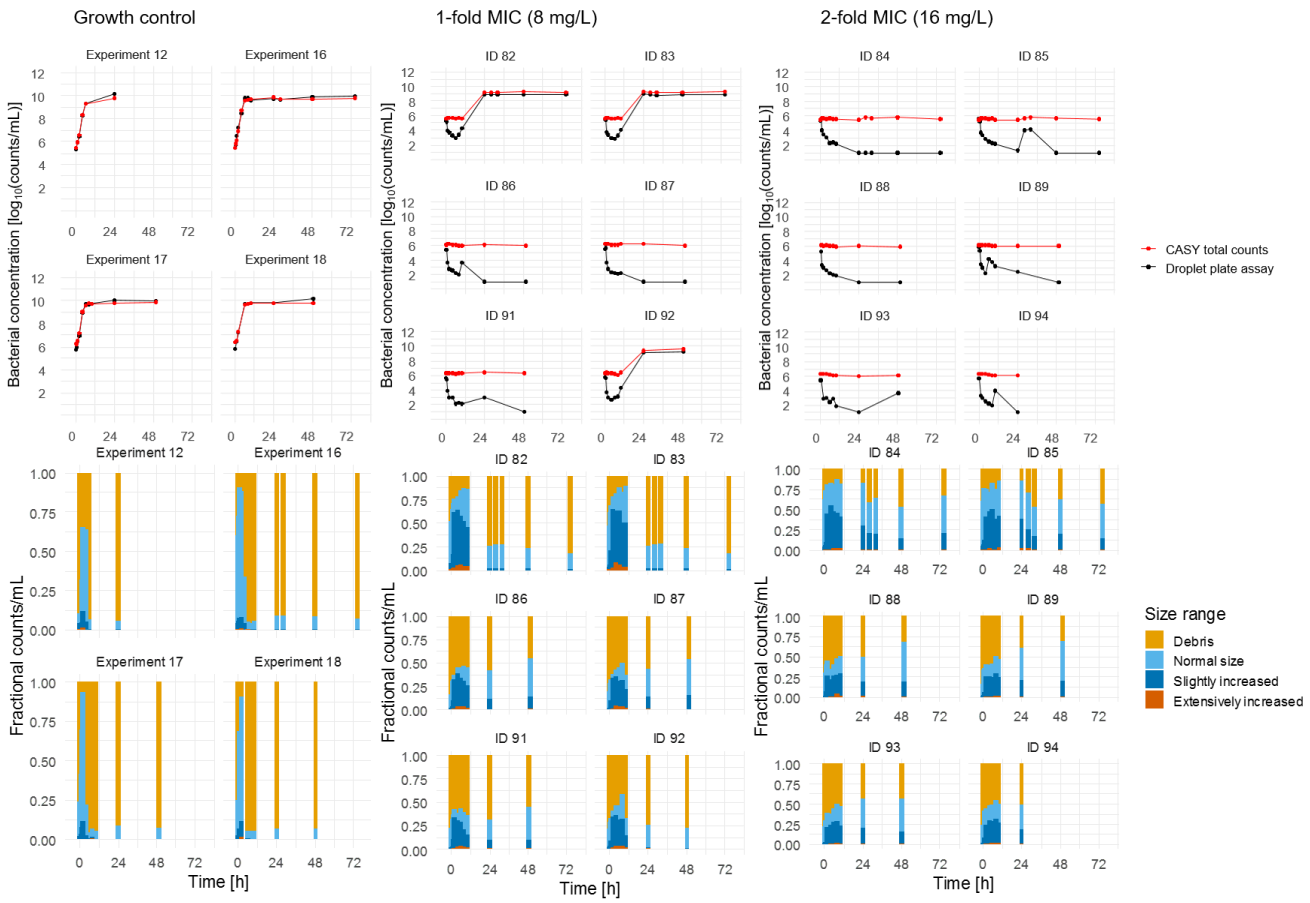

Figure 7.10: Bacterial growth, kill and regrowth behaviour of *Escherichia coli* sequence type 167 in static *in vitro* infection model experiments without antibiotic exposure (left, n=4), under exposure to 8 mg/L levofloxacin, corresponding to the minimal inhibitory concentration (MIC) of the isolate (middle, n=6) and under exposure to 2-fold the MIC of the isolate (right, n=6). Upper panel: Viable bacteria, quantified as colony forming units/mL (black points and lines) and total counts, quantified by electronic cell counting (red points and lines), over time. Lower panel: fractional counts per size range over time; full height of bars corresponds to total counts of the respective sample, colours correspond to fractional counts of different size ranges.

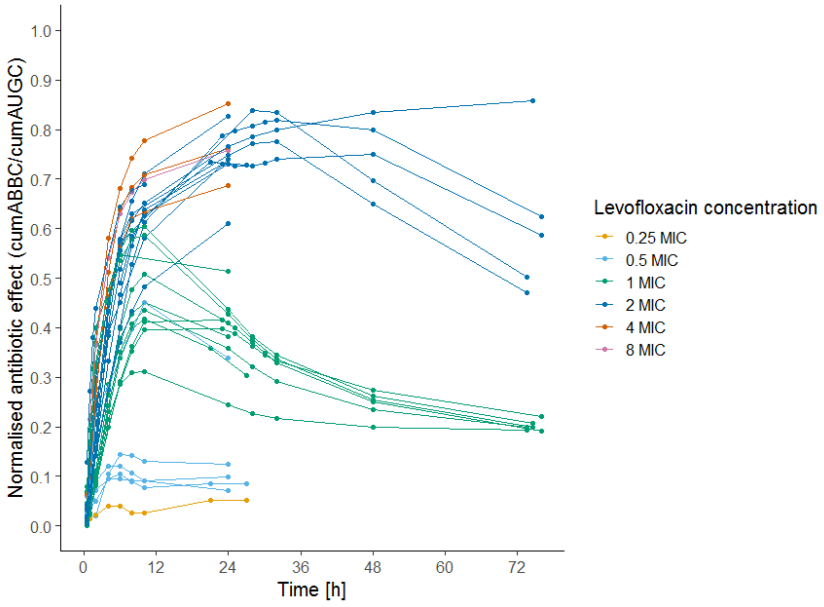

Figure 7.11: Antibiotic effect of levofloxacin against 3 *Escherichia coli* isolates, determined as the cumulative area between the growth control and the bacterial killing and regrowth curve (cumABBC(t)), normalised to the area under the growth control curve (AUGC(t)) of unexposed bacteria over time in static *in vitro* infection model experiments (n=43 replicates), colours: static levofloxacin concentrations, normalised to the minimal inhibitory concentration (MIC) of the isolate, points: sampling times.

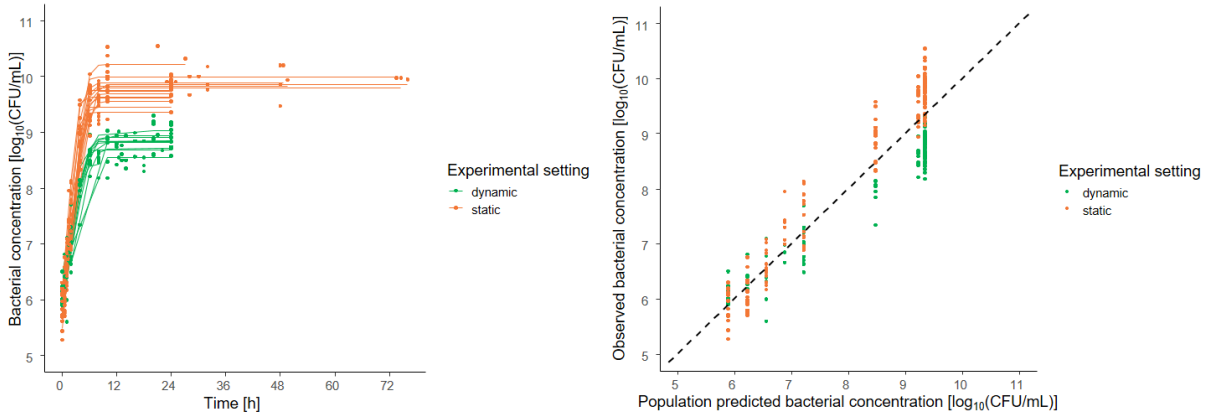

Figure 7.12: Observed bacterial concentrations (symbols) and individual predictions (solid lines) versus time (left) and population predictions (right) in growth control replicates (n=28) in static (orange) and dynamic (green) *in vitro* infection model experiments; predictions based on bacterial growth model without accounting for covariate effect of the experimental setting; dashed line: line of identity.

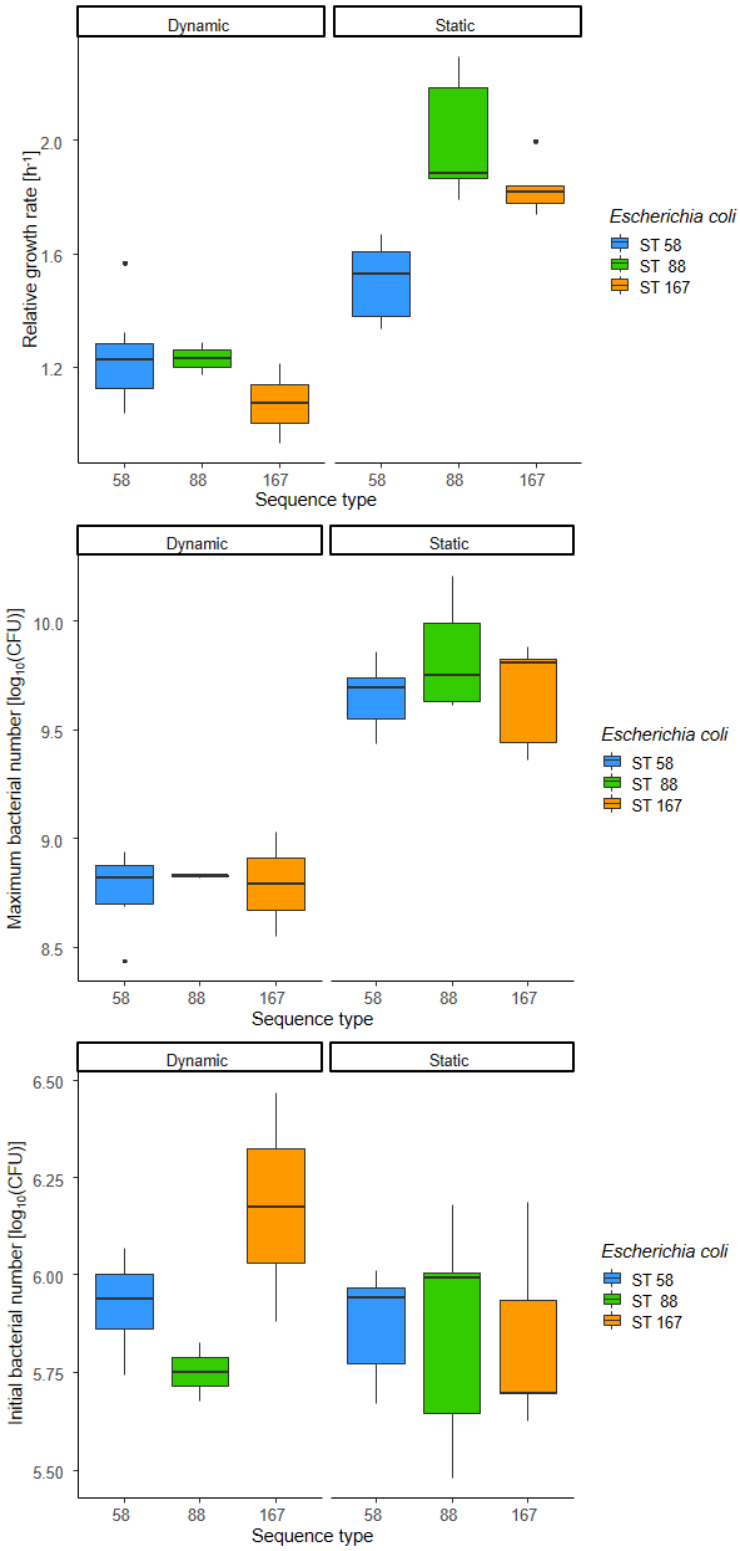

Figure 7.13: Parameter estimates (relative growth rate constant, maximum bacterial number and initial bacterial number) of the bacterial growth model without accounting for covariate effect of the experimental setting, solid lines: median, lower and upper hinge: 25th and 75th percentile, lower and upper whiskers: 1.5·interquartile range, stratified per experimental setting (dynamic and static *in vitro* infection model), colours: bacterial isolate (*Escherichia coli* sequence type 58, 88 and 167), ST: sequence type, CFU: colony forming units.

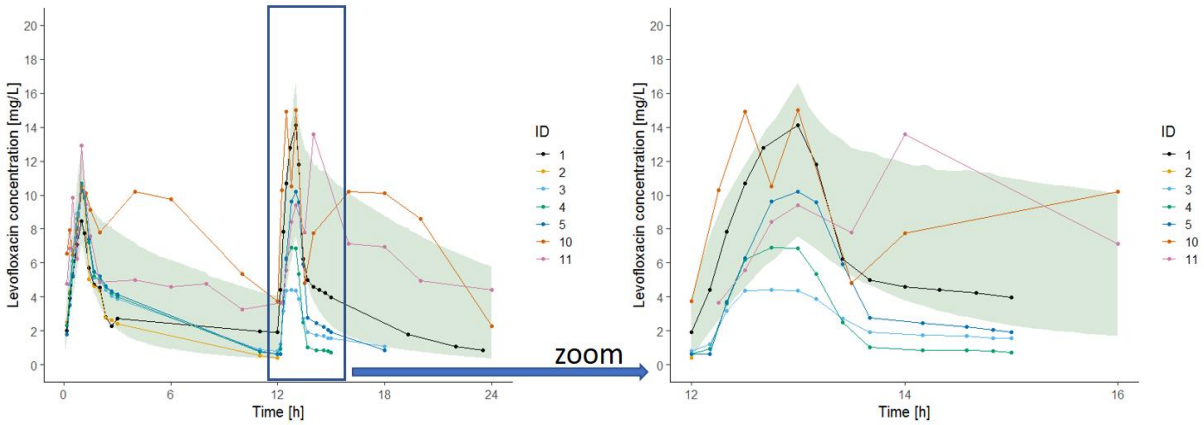

Figure 7.14: Observed levofloxacin (LEV) concentrations in dynamic *in vitro* infection model experiments (n=7 replicates), mimicking 500 mg, 60 min LEV infusions twice daily (lines and symbols) and 90% confidence interval of 1000 simulations (shaded area) based on an interim pharmacokinetic model of LEV concentration-time profiles in dynamic *in vitro* infection model experiments over 24 h (left) and zoomed in for t=12-16 h (right), colours: experimental replicates (IDs).

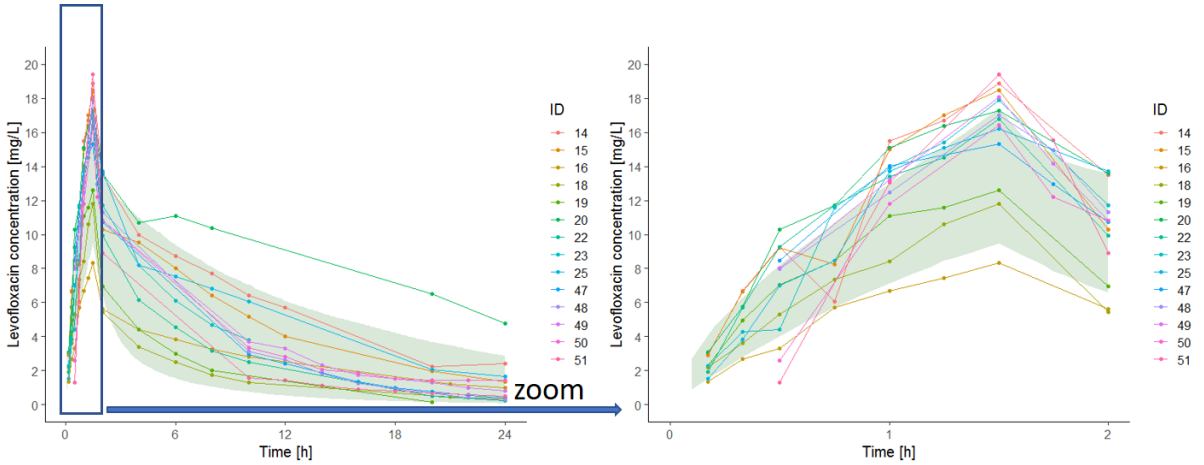

Figure 7.15: Observed levofloxacin (LEV) concentrations in dynamic *in vitro* infection model experiments (n=14 replicates), mimicking a 750 mg, 90 min LEV infusions (lines and symbols) and 90% confidence interval of 1000 simulations (shaded area) based on an interim pharmacokinetic model of LEV concentration-time profiles in dynamic *in vitro* infection model experiments over 24 h (left) and zoomed in for t=0-2 h (right), colours: experimental replicates (IDs).

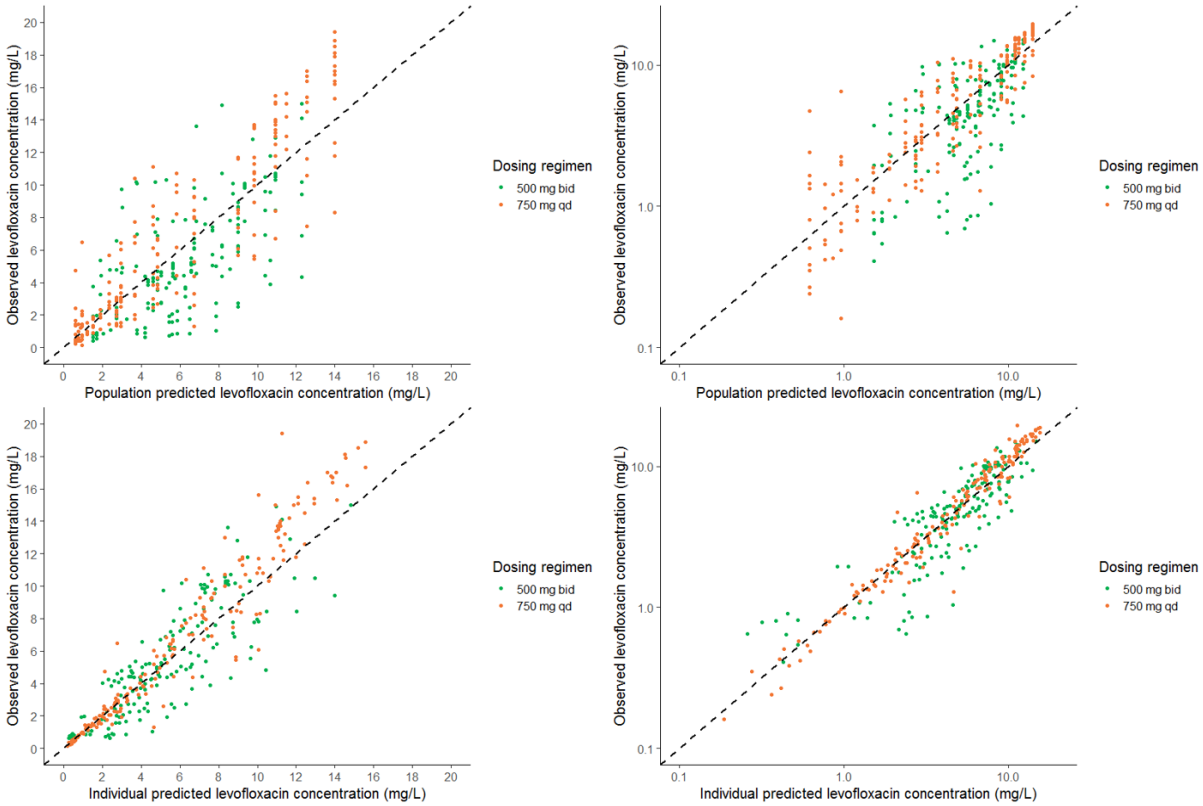

Figure 7.16: Observed levofloxacin (LEV) concentrations in dynamic *in vitro* infection model experiments, mimicking LEV concentration-time profiles resulting from mimicking administration of 500 mg, 60 min LEV i.v. infusions twice daily (bid, green symbols, n=7 replicates) or a 750 mg, 90 min i.v. LEV infusion once daily (qd, orange symbols, n=14 replicates) versus population predictions (upper panel) and individual predictions (lower panel) based on the final three-bacterial-state pharmacokinetic/pharmacodynamic model, left: linear scaling: right: logarithmic scaling; dashed lines: lines of identity, symbols: LEV concentrations.

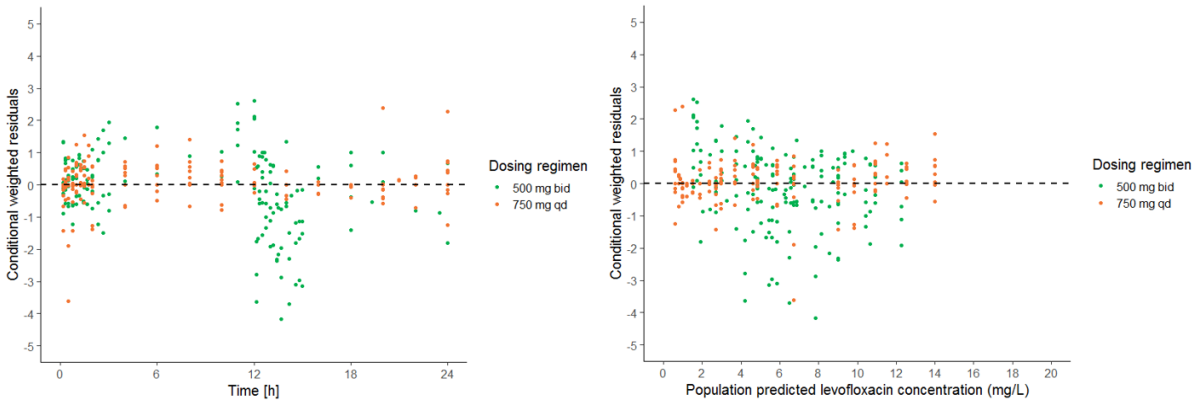

Figure 7.17: Conditional weighted residuals (CWRES) versus time (left) and population predictions (right) of levofloxacin (LEV) concentrations in dynamic *in vitro* infection model experiments, mimicking LEV concentration-time profiles resulting from mimicking administration of 500 mg, 60 min LEV i.v. infusions twice daily (bid, green symbols, n=7 replicates) or a 750 mg, 90 min i.v. LEV infusion once daily (qd, orange symbols, n=14 replicates) based on the final three-bacterial-state pharmacokinetic/pharmacodynamic model, dashed lines: CWRES=0; symbols: CWRES.

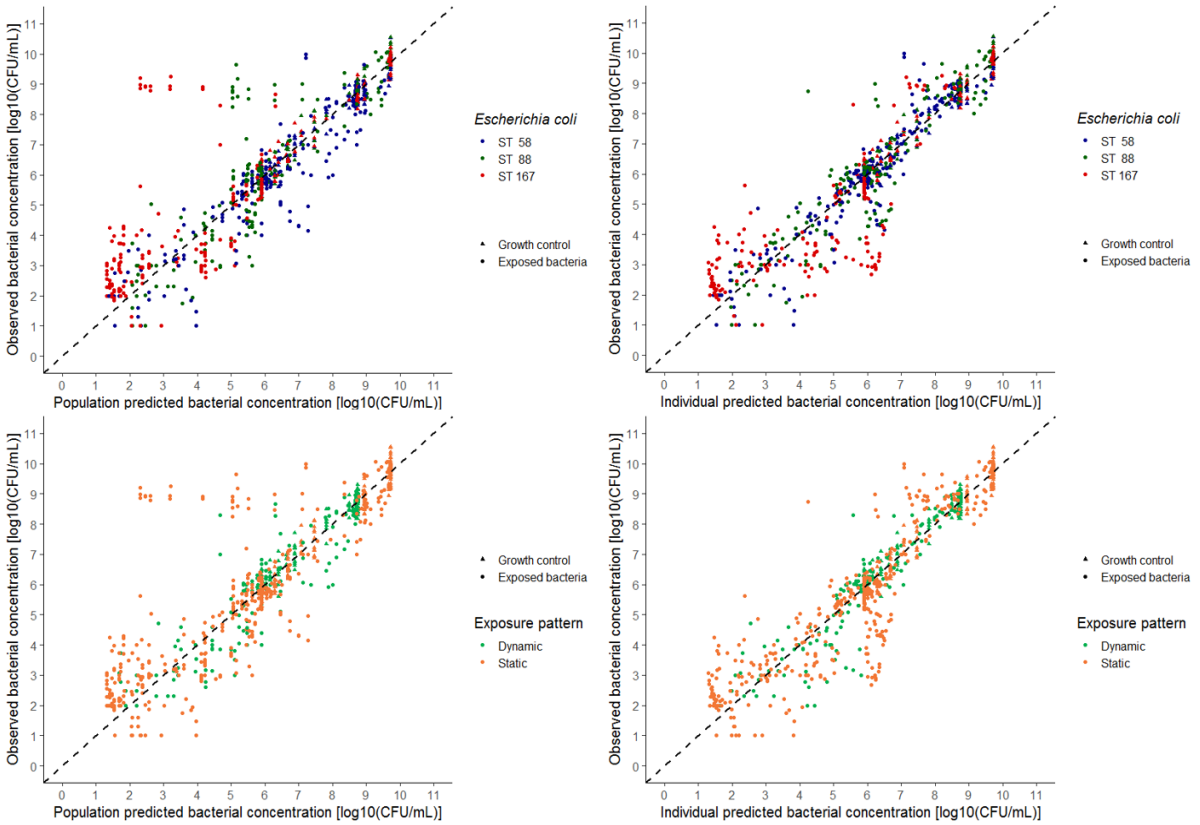

Figure 7.18: Observed bacterial concentrations in static and dynamic *in vitro* infection model experiments, assessed via droplet plate assay, versus population predictions (left) and individual predictions (right), based on the final three-bacterial-state pharmacokinetic/pharmacodynamic model; upper panel: stratified per *Escherichia coli* strain (ST58: blue, ST88: green, ST167: red symbols) and between growth controls (filled triangles) and exposed bacteria (filled circles); lower panel: stratified per exposure pattern (green: dynamic, orange: static) and between growth controls (filled triangles) and exposed bacteria (filled circles); dashed lines: lines of identity, CFU: colony forming units, ST: sequence type.

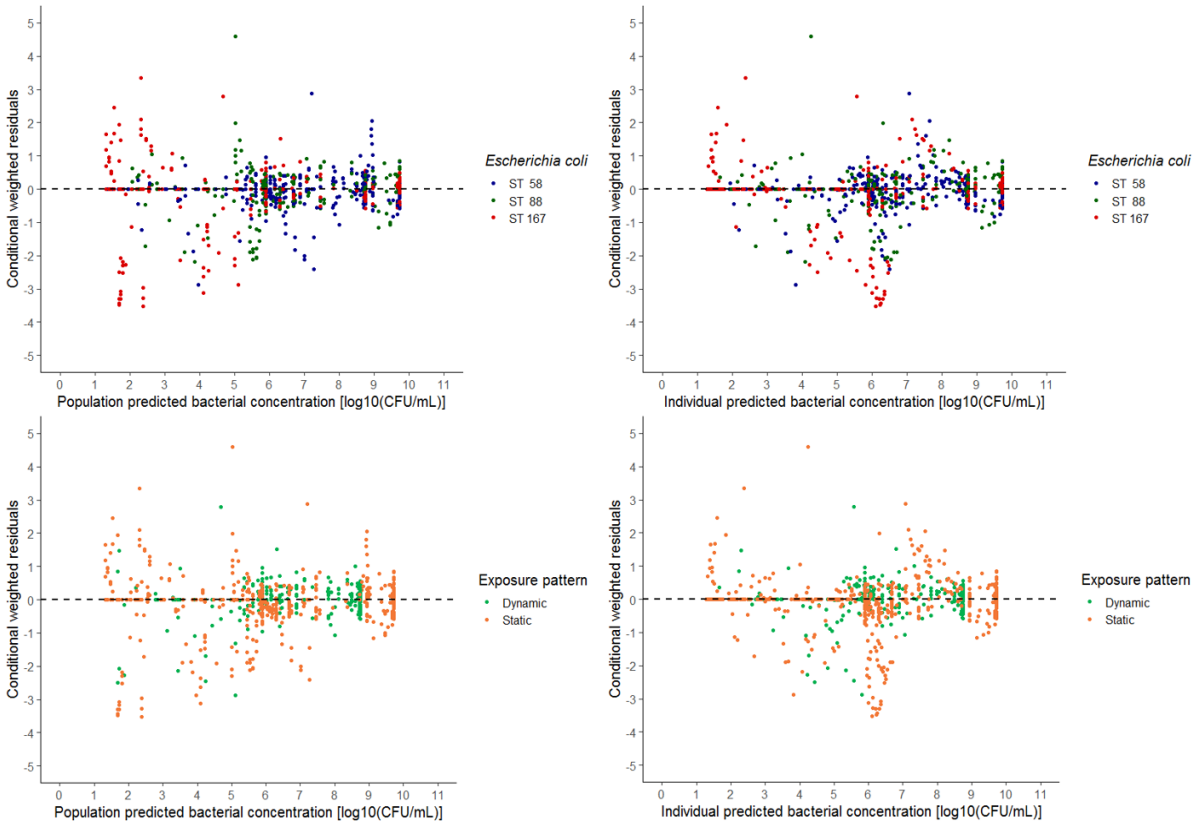

Figure 7.19: Conditional weighted residuals (CWRES) versus population predictions (left) and individual predictions (right) of bacterial concentrations, assessed via droplet plate assay, in static and dynamic *in vitro* infection model experiments, based on the final three-bacterial-state pharmacokinetic/pharmacodynamic model, colours (upper panel): *Escherichia coli* strain (ST58: blue, ST88: green, ST167: red symbols), lower panel: exposure pattern (green: dynamic, orange: static); dashed lines: CWRES=0; ST: sequence type.

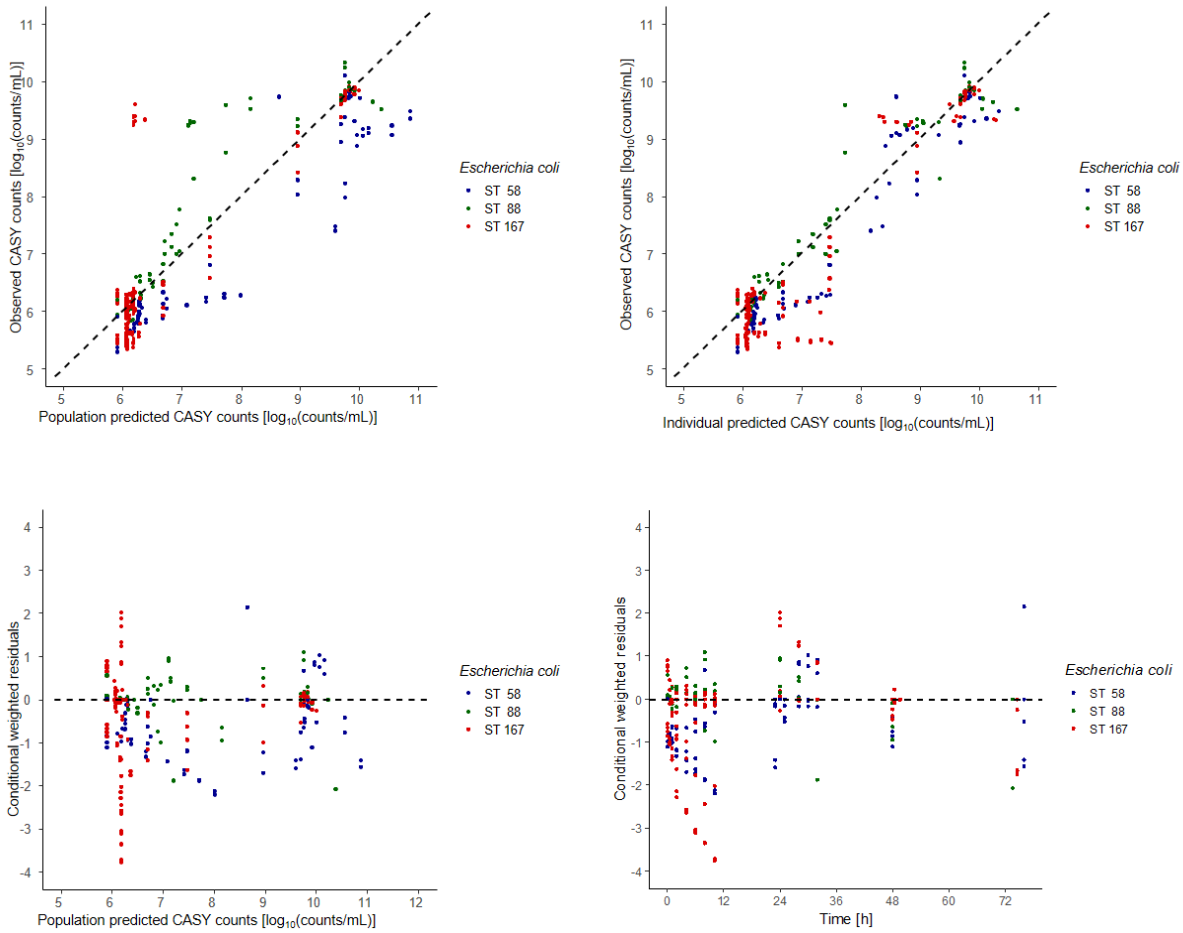

Figure 7.20: Upper panel: observed bacterial concentrations, assessed via electronic cell counting in static *in vitro* infection model experiments versus population predictions (left) and individual predictions (right) based on the final three-bacterial-state pharmacokinetic/pharmacodynamic model; lower panel: conditional weighted residuals (CWRES) versus population predicted electronic cell counts (left) and time (right); colours: *Escherichia coli* strains (ST58: blue, ST88: green, ST167: red symbols); dashed lines: lines of identity (upper panel) or CWRES=0 (lower panel), ST: sequence type.

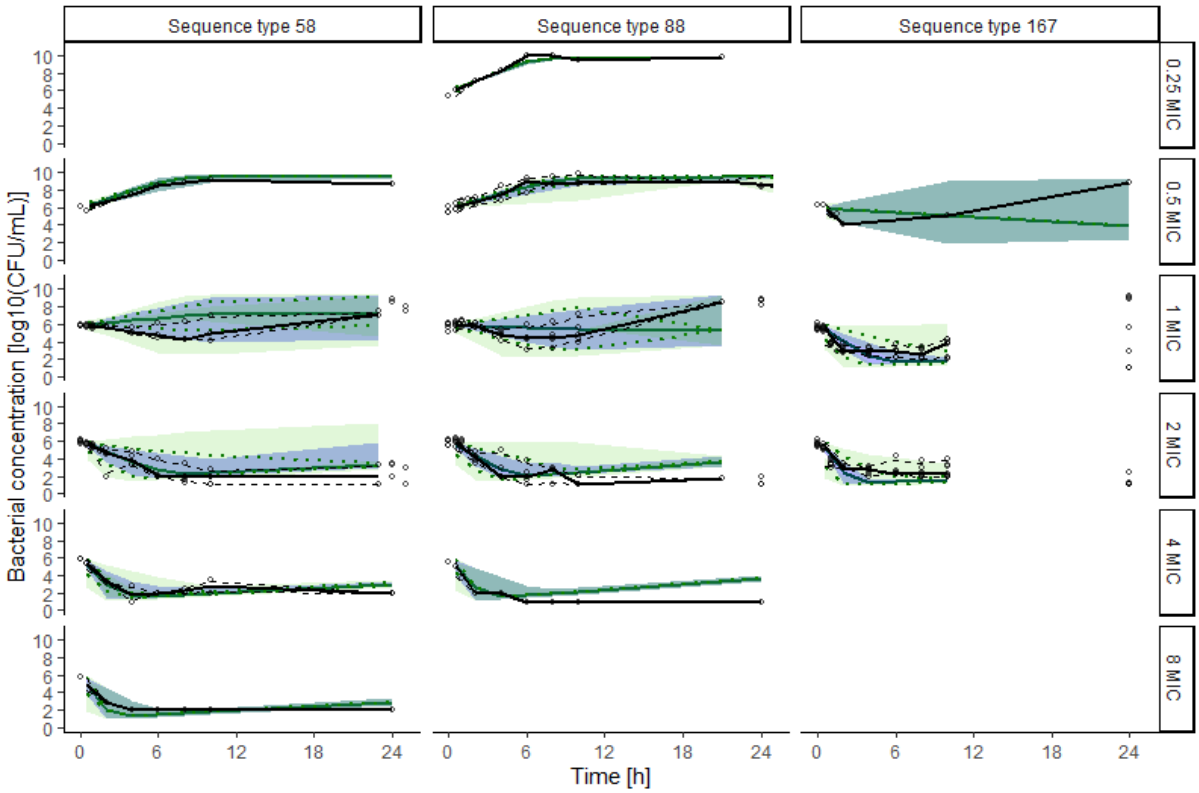

Figure 7.21: Visual predictive check (n=1000 simulations) of the final three-bacterial-state pharmacokinetic/pharmacodynamic model for growth and kill behaviour of three *Escherichia coli* isolates (Sequence type 58, 88 and 167) under levofloxacin (LEV) exposure in static *in vitro* infection model experiments, stratified by bacterial strain and applied LEV concentration, normalised to the minimal inhibitory concentration (MIC), static LEV concentration between 0.25- and 8-fold the MIC, black solid line: median of observed bacterial concentrations, black dashed lines: 5th and 95th percentile of observations, green solid line and blue shaded area: median and 90% confidence interval of simulations, green dashed lines and green areas: 5th and 95th percentile and 90% confidence interval of simulations, CFU: colony forming units.

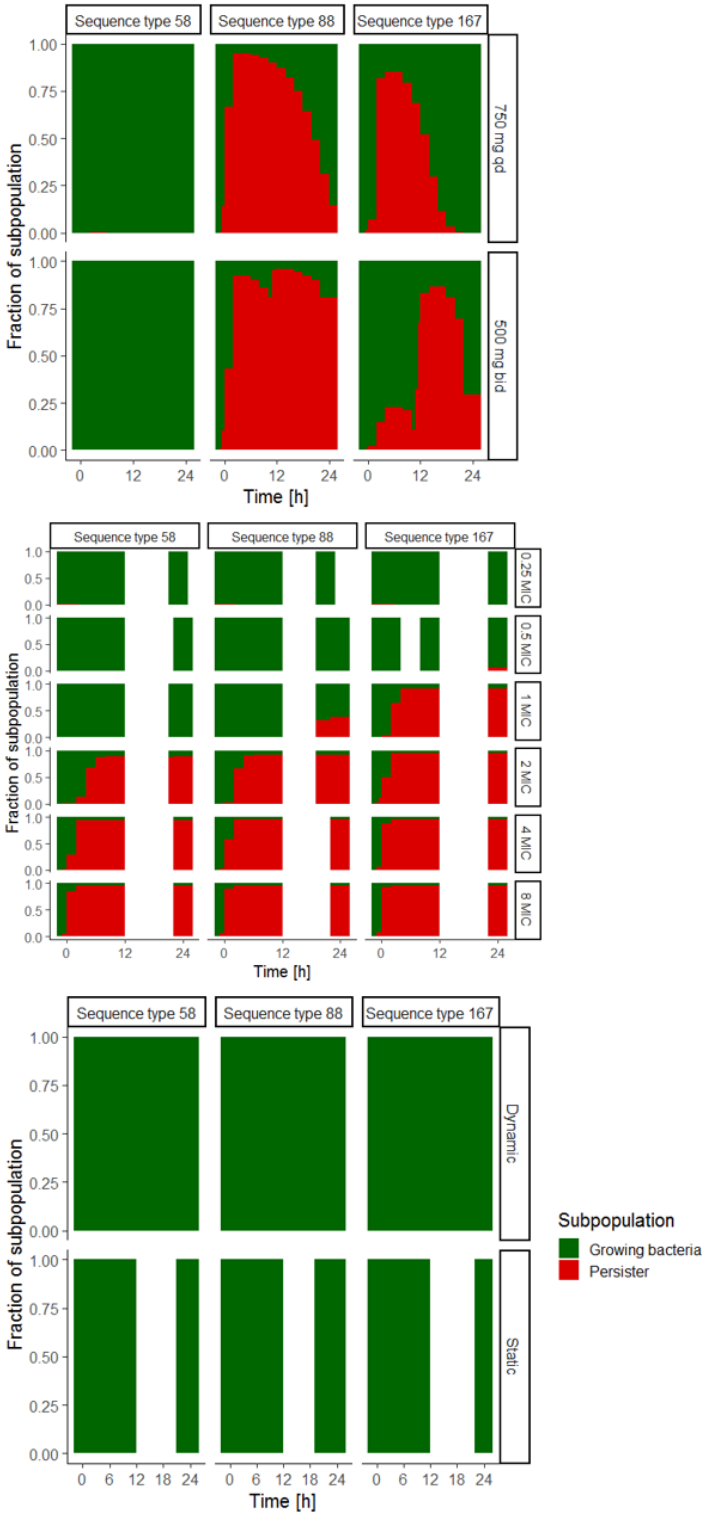

Figure 7.22: Fractions of growing bacteria and persister cells in not-dead bacterial subpopulations (viable+persister) over time based on 1000 stochastic simulations for three *Escherichia coli* isolates (sequence type 58, 88 and 167) under dynamic levofloxacin (LEV) exposure (top), static LEV exposure (middle) and without LEV exposure in static and dynamic *in vitro* infection model experiments (bottom), qd: quaque die (once daily), bid: bis in die (twice daily), MIC: minimal inhibitory concentration.

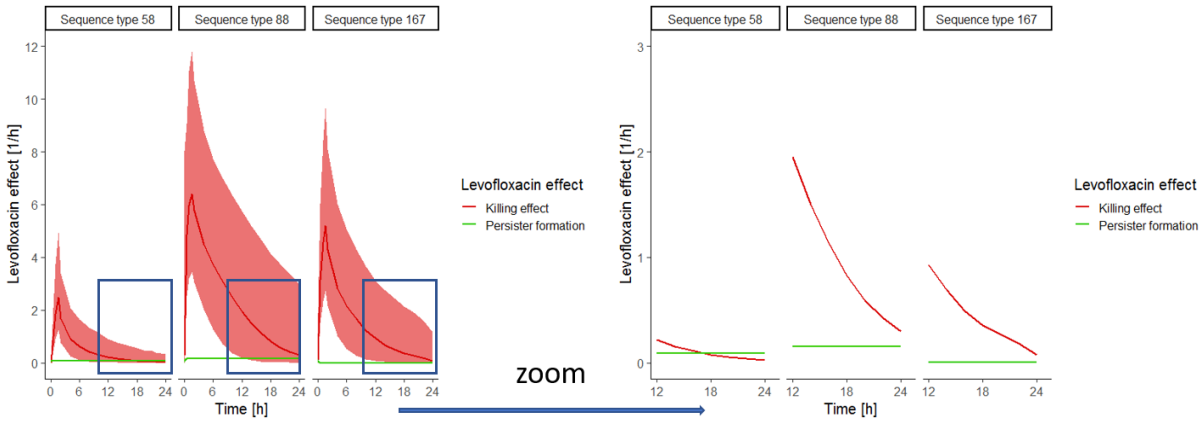

Figure 7.23: Levofloxacin (LEV) killing effect (red), simulated omitting the effect on persister formation by fixing $k_{P,LEV}$ to 0, and LEV effect on persister formation (green), simulated omitting the killing effect by fixing E_{max} to 0, in stochastic simulations based on the final three-bacterial-state pharmacokinetic/pharmacodynamic model for three *Escherichia coli* isolates under LEV exposure in dynamic *in vitro* infection model experiments, mimicking a 750 mg, 90 min LEV i.v. infusion for 24 h (left) and zoomed in for t=12 h to t=24 h (right), median (solid lines) and 90% confidence interval (shaded area) of simulations (n=1000).

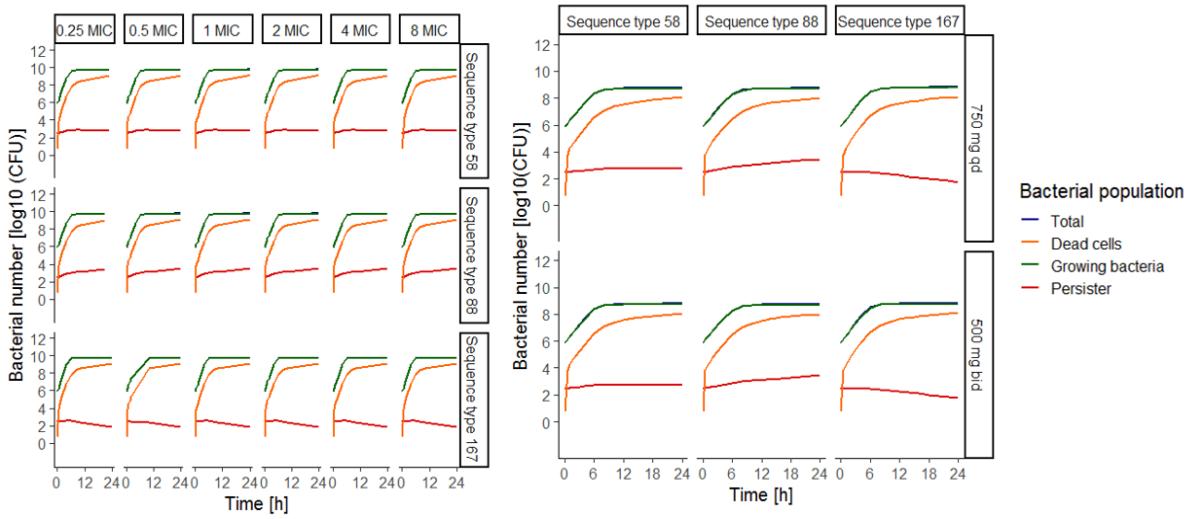

Figure 7.24: Bacterial numbers in different bacterial populations over time under levofloxacin (LEV) exposure in static (left) and dynamic (right) *in vitro* infection model experiments, simulated omitting the LEV killing effect by fixing E_{max} to 0; exposing three *Escherichia coli* isolates (sequence type 58, 88 and 167) to constant LEV concentrations between 0.25- and 8-fold the minimal inhibitory concentration (MIC) of the isolate (left), and to concentration-time profiles resulting from a 750 mg, 90 min i.v. infusion once daily (qd, right, upper panel) and from a 500 mg, 60 min LEV i.v. infusion twice daily (bid, right, lower panel); n=1000 simulations; CFU: colony forming units.

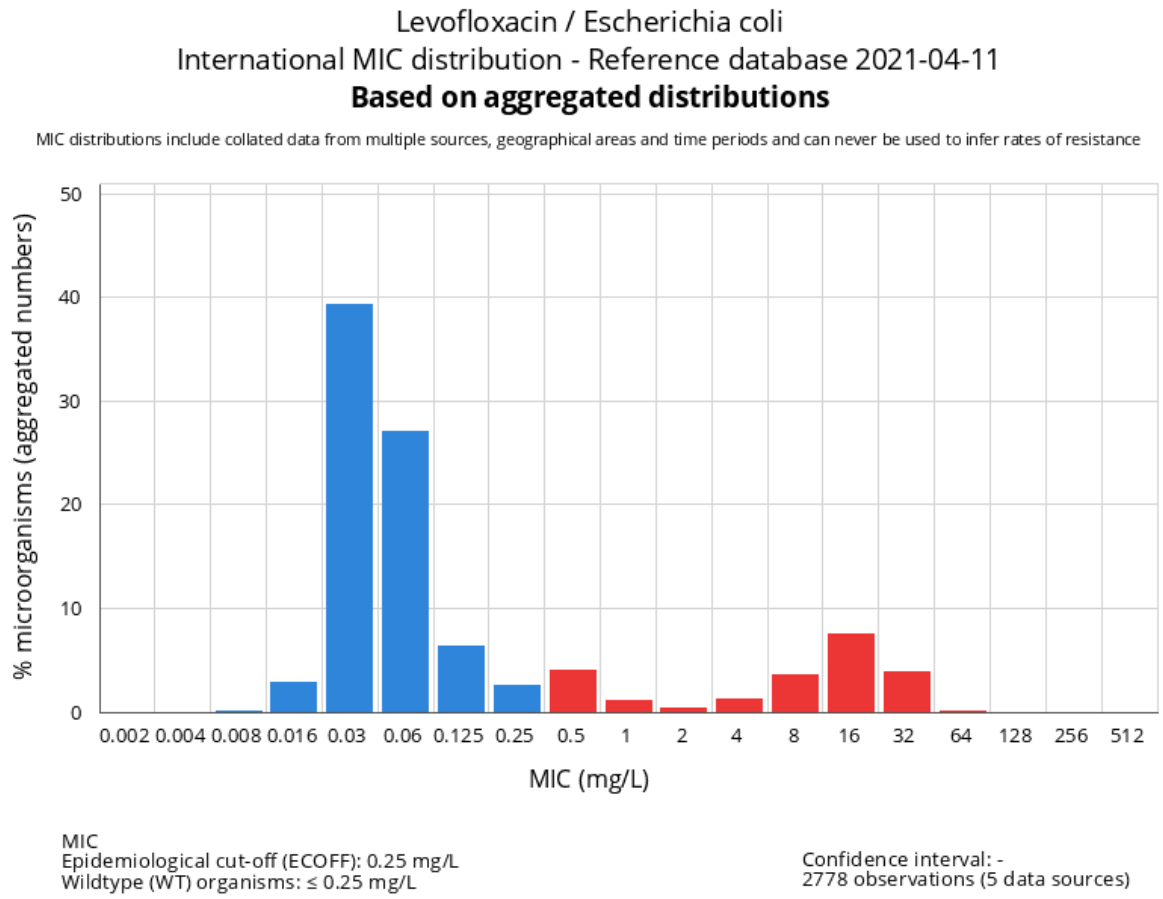

Figure 7.25: Distribution of minimal inhibitory concentration values of levofloxacin against *Escherichia coli,* obtained from EUCAST [204].

7.2 Tables

Table 7.1: Experimental settings of each of the 13 experiments in a static *in vitro* infection model, exposing three *Escherichia coli* isolates and the reference strain *Escherichia coli* ATCC 25922 to constant levofloxacin concentrations: bacterial strain, investigated levofloxacin concentrations, normalised to the minimal inhibitory concentration (MIC) of the strain and in mg/L and duration of the experiment, in grey: experiments with additional assessment of bacterial size distributions using the cell counter and analyser system (chapter 2.3.2), in bold: additional experiments (chapter 2.4.1.2). ATCC: American Type Culture Collection, ST: Sequence type.

Bacterial strain	Levofloxacin concentrations [x-fold MIC]	Levofloxacin concentrations [mg/L]	Time of levofloxacin exposure [days]
ATCC 25922	0.5; 1; 2	0.016; 0.032; 0.064 (n=1, each)	1
ST 58	0.5; 1; 2	4; 8; 16 (n=1, each)	1
ST 58	1; 2; 4	8; 16; 32 (n=1, each)	1
ST 58	2; 4; 8	16, 32, 64 (n=1, each)	1
ST 58	1; 2	8; 16 (n=2, each)	3
ST 88	0.5; 1; 2; 4	1; 2; 4; 8 (n=1, each)	1
ST 88	0.5; 1; 2	1; 2, 4 (n=1, each)	1
ST 88	0.25; 0.5; 1; 2	0.5; 1; 2; 4 (n=1, each)	1
ST 88	1; 2	2; 4 (n=2, each)	3
ST 167	0.5; 1; 2	4, 8, 16 (n=1, each)	1
ST 167	1; 2	8; 16 (n=2, each)	3
ST 167	**1; 2**	**8; 16 (n=2, each)**	**2**
ST 167	**1; 2**	**8; 16 (n=2, each)**	**2**

Table 7.2: Parameter estimates and precision of a pharmacokinetic nonlinear mixed-effect model [55,142], applied for simulation of 1000 levofloxacin concentration-time profiles resulting from a 750 mg, 90 min i.v. infusion in plasma of septic patient and computing experimental parameters for the dynamic *in vitro* infection model.

Parameter [unit]	**Estimate [RSE, %]**
CL [L/h]	6.91 (7.1)
V_c [L]	21.7 (9.5)
V_p [L]	64.4 (7.3)
Q [L/h]	60.3 (9.6)
$CLCR_{CL}$ [% per mL/min]	1.09 (20)
Interindividual variability parameters [CV, %]	
in CL	40.2 [34]
in V_c	51.8 [23]
in V_p	42.4 [36]
in Q	46.6 [62]

Table 7.3: *In vitro* experiments exposing 3 clinical *Escherichia coli* isolates to levofloxacin concentration-time profiles resulting from a 750 mg, 90 min i.v. infusion in plasma of a septic patient, mimicked in the dynamic *in vitro* infection model, GC: Growth control.

Bacterial strain (Sequence type)	**Sampling times after start of experimet [h]**	**Number of replicates**
58	0; 0.5; 1; 1.5; 2; 4; 6; 8; 10; 20; 24	2 + GC
58	0; 0.5; 1; 1.5; 2; 4; 6; 8; 10; 20; 24	1 + GC
58	0; 0.5; 1; 1.5; 2; 10;12;14;16;18;20;22;24	2 (no GC)
88	0; 0.5; 1; 1.5; 2; 4; 6; 8; 10; 20; 24	2 + GC
88	0; 0.5; 1; 1.5; 2; 10;12;14;16;18;20;22;24	2+GC
167	0; 0.5; 1; 1.5; 2; 10;12;14;16;18;20;22;24	1 + GC
167	0; 0.5; 1; 1.5; 2; 4; 6; 8; 10; 20; 24	2 + GC

Table 7.4: Components of master mixes used for polymerase chain reaction for amplification of *gyrA, parC* and *qnrA/B/*S and their respective volumes, for one DNA sample. dNTP: deoxynucleotides, primer F and R: forward and reverse primer, *Taq: Thermus aquaticus.*

Components of master mix	Volume [µL]		
	gyrA	*parC*	*qnrA/B/S*
dNTP mix in 10x Green Buffer (10mM)	29.0	29.0	15.67
Primer mix (F and R, 10 µM)	1.00	0.50	0.25
Dream *Taq* polymerase	0.05	0.05	0.08

Table 7.5: Sizes of polymerase chain reaction (PCR) products of fluoroquinolone resistance determining regions (*gyrA, parC*) and *qnr* plasmids**,** bp: base pairs.

Target gene	PCR product size [bp]
gyrA	647
parC	509
qnrA	516
qnrB	469
qnrS	417

Table 7.6: Investigated models to describe the exposure-effect relationship of levofloxacin against *Escherichia coli* in the static and in the dynamic *in vitro* infection model.

Model	Description	Equation
1	Sigmoidal E_{max} model	$Effect = \frac{cumABBC(t)}{cumAUGC(t)} = \frac{cumABBC_{max} \cdot cumAUC(t)^n}{cumAUC_{50}^n + cumAUC(t)^n}$
2	E_{max} model + inhibition term	$Effect = \frac{cumABBC(t)}{cumAUGC(t)} = \frac{cumABBC_{max}}{1 + \frac{cumAUC_{50}}{cumAUC(t)} + \frac{cumAUC(t)}{cumAUC_{reg}}}$
3	E_{max} model + inhibition term; E_{max} fixed to 1	$Effect = \frac{cumABBC(t)}{cumAUGC(t)} = \frac{1}{1 + \frac{cumAUC_{50}}{cumAUC(t)} + \frac{cumAUC(t)}{cumAUC_{reg}}}$
4	Sigmoidal inhibition model	$Effect = \frac{cumABBC(t)}{cumAUGC(t)} = \left(\frac{cumABBC_{max} \cdot cumAUC(t)^n}{cumAUC_{50}^n + cumAUC(t)^n}\right) \cdot \frac{1}{1 + \frac{cumAUC(t)}{cumAUC_{reg}}}$
5	Sigmoidal inhibition model, E_{max} fixed to 1	$Effect = \frac{cumABBC(t)}{cumAUGC(t)} = \left(\frac{cumAUC(t)^n}{cumAUC_{50}^n + cumAUC(t)^n}\right) \cdot \frac{1}{1 + \frac{cumAUC(t)}{cumAUCreg}}$

E_{max}: maximum effect = $cumABBC_{max}$ = maximum effect, determined as cumAUGC(t)-normalised cumABBC(t), cumABBC(t): cumulative area between the growth control and the bacterial killing and regrowth curve as function of time, cumAUGC(t): cumulative area under the growth control curve as function of time, cumAUC(t): cumulative area under the levofloxacin concentration-time curve as function of time, $cumAUC_{50}$: exposure, determined as cumAUC(t), causing 50% of the maximum effect, $cumAUC_{reg}$: exposure causing regrowth in *in vitro* infection model experiments, n: Hill factor (steepness of exposure-effect relationship).

Table 7.7: Subset of NONMEM® dataset, exemplified for *Escherichia coli* sequence type 58, exposed to a levofloxacin concentration-time profile resulting from a 500 mg, 60 min levofloxacin i.v. infusion, mimicked in the dynamic *in vitro* infection model.

ID	TIME	CON	STRN	EXPNR	DV_LIN	FLAG	DV	LDV	AMT	MDV	RATE	EVID	STDY	STAT	BQL	LLOQ	REGIM	…
10	0	0	1	5	.	1	.	.	0	1	0	3	1	0	0	0.25	2	…
10	0	0	1	5	.	3	.	.	0	1	0	3	1	0	0	100	2	…
10	0	0	1	5	7.20E+05	3	13.4	5.86	0	0	0	0	1	0	0	100	2	…
10	0	0	1	5	0.00E+00	1	.	0	500	1	500	1	1	0	0	0	2	…
10	0.17	0	1	5	6.55E+00	1	1.88	6.55	0	0	0	0	1	0	0	0.25	2	…
10	0.33	0	1	5	7.92E+00	1	2.07	7.92	0	0	0	0	1	0	0	0.25	2	…
10	0.5	0	1	5	6.45E+00	1	1.86	6.45	0	0	0	0	1	0	0	0.25	2	…
10	0.5	0	1	5	8.80E+05	3	13.7	5.94	0	0	0	0	1	0	0	0.25	2	…
10	0.75	0	1	5	7.96E+00	1	2.07	7.96	0	0	0	0	1	0	0	100	2	…
10	1	0	1	5	1.05E+01	1	2.35	10.5	0	0	0	0	1	0	0	0.25	2	…
10	1	0	1	5	1.94E+06	3	14.5	6.29	0	0	0	0	1	0	0	0.25	2	…
10	1.25	0	1	5	1.01E+01	1	2.31	10.1	0	0	0	0	1	0	0	100	2	…
10	1.5	0	1	5	9.15E+00	1	2.21	9.15	0	0	0	0	1	0	0	0.25	2	…
10	1.5	0	1	5	7.15E+05	3	13.5	5.85	0	0	0	0	1	0	0	100	2	…
10	2	0	1	5	7.79E+00	1	2.05	7.79	0	0	0	0	1	0	0	0.25	2	…
10	2	0	1	5	9.15E+05	3	13.7	5.96	0	0	0	0	1	0	0	100	2	…
10	4	0	1	5	1.02E+01	1	2.32	10.2	0	0	0	0	1	0	0	0.25	2	…
10	4	0	1	5	1.00E+06	3	13.8	6.00	0	0	0	0	1	0	0	100	2	…
10	6	0	1	5	9.74E+00	1	2.28	9.74	0	0	0	0	1	0	0	0.25	2	…
10	6	0	1	5	2.90E+06	3	14.9	6.46	0	0	0	0	1	0	0	100	2	…
10	8	0	1	5	1.00E+06	3	13.8	6.00	0	0	0	0	1	0	0	100	2	…
10	10	0	1	5	5.34E+00	1	1.68	5.34	0	0	0	0	1	0	0	0.25	2	…
10	10	0	1	5	1.00E+06	3	13.8	6.00	0	0	0	0	1	0	0	100	2	…
10	12	0	1	5	3.75E+00	1	1.32	3.75	0	0	0	0	1	0	0	0.25	2	…

[continued on next page]

ID	TIME	CON	STRN	EXPNR	DV_LIN	FLAG	DV	LDV	AMT	MDV	RATE	EVID	STDY	STAT	BQL	LLOQ	REGIM	…
10	12	0	1	5	2.80E+07	3	17.1	7.45	0	0	0	0	1	0	0	100	2	…
10	12	0	1	5	0.00E+00	1	.	0	500	1	500	1	1	0	0	0	2	…
10	12.25	0	1	5	1.03E+01	1	2.33	10.3	0	0	0	0	1	0	0	0.25	2	…
10	12.5	0	1	5	1.49E+01	1	2.70	14.9	0	0	0	0	1	0	0	0.25	2	…
10	12.75	0	1	5	1.05E+01	1	2.35	10.5	0	0	0	0	1	0	0	0.25	2	…
10	13	0	1	5	1.50E+01	1	2.71	15.0	0	0	0	0	1	0	0	0.25	2	…
10	13	0	1	5	2.20E+07	3	16.9	7.34	0	0	0	0	1	0	0	100	2	…
10	13.5	0	1	5	4.83E+00	1	1.57	4.83	0	0	0	0	1	0	0	0.25	2	…
10	13.5	0	1	5	5.00E+06	3	15.4	6.70	0	0	0	0	1	0	0	100	2	…
10	14	0	1	5	7.76E+00	1	2.05	7.76	0	0	0	0	1	0	0	0.25	2	…
10	14	0	1	5	2.80E+06	3	14.8	6.45	0	0	0	0	1	0	0	100	2	…
10	16	0	1	5	1.02E+01	1	2.32	10.2	0	0	0	0	1	0	0	0.25	2	…
10	16	0	1	5	8.50E+05	3	13.7	5.93	0	0	0	0	1	0	0	100	2	…
10	18	0	1	5	1.01E+01	1	2.31	10.1	0	0	0	0	1	0	0	0.25	2	…
10	18	0	1	5	8.00E+06	3	15.9	6.90	0	0	0	0	1	0	0	100	2	…
10	20	0	1	5	8.60E+00	1	2.15	8.6	0	0	0	0	1	0	0	0.25	2	…
10	20	0	1	5	1.50E+07	3	16.5	7.18	0	0	0	0	1	0	0	100	2	…
10	24	0	1	5	2.28E+00	1	0.824	2.28	0	0	0	0	1	0	0	0.25	2	…
10	24	0	1	5	2.00E+08	3	19.1	8.30	0	0	0	0	1	0	0	100	2	…

Abbreviations: ID: individual (replicate) identifier, TIME: time [h], CON: levofloxacin concentration in static *in vitro* infection model experiments [mg/L], STRN: exposed bacterial strain, EXPNR: experiment number, DV_LIN: dependent variable (i.e. see “FLAG”), linear scale, FLAG: identifier for different records, here: 1=levofloxacin concentration in dynamic *in vitro* infection model; 2=bacterial concentration, determined by droplet plate assay (growth control), 3=bacterial concentration, determined by droplet plate assay (exposed bacteria), 4=bacterial concentration, determined by electronic cell counting, DV: dependent variable on ln scale, LDV= dependent variable on $\log_{10}$ scale (only bacterial concentrations; levofloxacin concentrations: linear scale), AMT: amount (here: levofloxacin dose in dynamic *in vitro* infection model), MDV: missing dependent variable (0=no, 1=yes), rate: mimicked infusion rate [mg/h], EVID: event identification (here: 0=observation, 1=dosing event, 3=reset event), STDY: study identification number, STAT: indicates experimental setting (0=dynamic *in vitro* infection model, 1=static *in vitro* infection model), BLQ: observation below quantification limit (0=no, 1=yes), LLOQ: lower limit of quantification [CFU/mL for bacterial concentration; mg/L for levofloxacin concentration], REGIM: mimicked dosing regimen in dynamic *in vitro* infection model (1=750 mg once daily; 2=500 mg twice daily).

Table 7.8: Experiments included in the development of a pharmacokinetic/pharmacodynamic (PK/PD) model characterising the growth and kill behaviour of *Escherichia coli* under levofloxacin (LEV) exposure; experiment number, individual identifiers (ID) of the replicates, exposed *Escherichia coli* strain (0: only PK; 1: Sequence type (ST) 58; 2: ST88, 3: ST167; 4: ATCC 25922); *in vitro* infection model (IVIM) type; LEV concentrations in the static or mimicked dosing regimen in the dynamic IVIM; sampling times. Bid: bis in die, qd: quaque die, GC: growth control.

Experiment Number	ID	Strain	IVIM type	Dosing regimen/ LEV concentrations [mg/L]	Sampling times [h]	Comment
1	1,2	0	dynamic	500 mg bid	0; 0.17; 0.33; 0.5; 0.75; 1.0; 1.17; 1.52; 1.67; 2.0; 2.3, 2.6; 3.0; 11; 12.0; 12.2; 12.3; 12.5; 13.0; 13.2; 13.4; 13.7; 14.0; 14.3; 14.6; 15.0; 19.3; 22.0; 23.5	Feasibility experiment (PK only)
2	3,4,5	0	dynamic	500 mg bid	0; 0.17; 0.33; 0.5; 0.75; 1.0; 1.17; 1.52; 1.67; 2.0; 2.3, 2.6; 3.0; 11; 12.0; 12.2; 12.3; 12.5; 13.0; 13.2; 13.4; 13.7; 14.0; 14.3; 14.6; 15.0; 18.0; 24.0	Feasibility experiment (PK only)
3	6,7	1	dynamic	GC only	0; 0.5; 1; 1.5; 2; 4; 6; 8; 10; 24	Pump rates according to 750 mg qd
4	8,9	1	dynamic	GC only	0; 0.5; 1; 1.5; 2; 4; 6; 8; 10; 24	Pump rates according to 500 mg bid
5	10,11,12	1	dynamic	500 mg bid	0; (0.17; 0.33)*; 0.5; (0.75)*; 1.0; (1.25)*; 2.0; 4.0; 6.0; 8.0; 10.0; 12.0; (12.2; 12.3)*; 12.5; (12.8)* 13.0; 13.5; 14.0; 16.0; 18.0; 20.0; 24.0	PK and PD
6	13,14,15	1	dynamic	750 mg qd	0; (0.17; 0.33)*; 0.5; (0.75)*; 1.0; (1.25)*; 1.5; 2.0; 4.0; 6.0; 8.0; 10.0; 12.0; 20.0; 24.0	PK and PD
7	16	0	dynamic	750 mg qd	0; 0.17; 0.33; 0.5; 0.75; 1.0; 1.25; 1.5; 2.0; 4.0; 6.0; 8.0; 10.0; 21.0; 24.0	PK only
8	17,18	1	dynamic	750 mg qd	0; (0.17; 0.33)*; 0.5; (0.75)*; 1.0; (1.25)*; 1.5; 2.0; 4.0; 6.0; 8.0; 10.0; 20.0; 24.0	PK and PD
9	19,20,21	3	dynamic	750 mg qd	0; (0.17; 0.33)*; 0.5; (0.75)*; 1.0; (1.25)*; 1.5; 2.0; 4.0; 6.0; 8.0; 20.0; 24.0	PK and PD
10	22,23,24	2	dynamic	750 mg qd	0; (0.17; 0.33)*; 0.5; (0.75)*; 1.0; (1.25)*; 1.5; 2.0; 4.0; 6.0; 8.0; 10.0; 20.0; 24.0	PK and PD

Experiment Number	ID	Strain	IVIM type	Dosing regimen/ LEV concentrations [mg/L]	Sampling times [h]	Comment
11	25	0	dynamic	750 mg qd	0; (0.17; 0.33)*; 0.5; (0.75)*; 1.0; (1.25)*; 1.5; 2.0; 4.0; 6.0; 8.0; 10.0; 20.0; 24.0	Feasibility experiment (PK only)
12	26,27,28,29,30	2	static	1; 2; 4; 8	0; 0.5; 1; 2; 4; 6; 8; 10; 24	PD only
13	31,32,33,34	1;2;3;4	static	GC only	0; 0.5; 1; 1.5; 2; 4; 6; 8; 10; 24	PD only
14	35,36,37,38	1	static	4; 8; 16	0; 0.5; 1; 1.5; 2; 4; 6; 8; 10; 24	PD only
15	39,40,41,42	2	static	1; 2; 4	0; 0.5; 1; 1.5; 2; 4; 6; 8; 10; 24	PD only
16	43,44,45,46	3	static	4; 8; 16	0; 0.5; 1; 1.5; 2; 4; 6; 8; 10; 24	PD only
17	47,48, 52	2	dynamic	750 mg qd	0; 0.5; 1.0; 1.5; (1.75)*; 2.0; 10.0; 12.0; 14.0; 16.0; 18.0; 20.0; 22.0; 24.0	PK and PD
18	49, 53	3	dynamic	750 mg qd	0; 0.5; 1.0; 1.5; (1.75)*; 2.0; 10.0; 12.0; 14.0; 16.0; 18.0; 20.0; 22.0; 24.0	PK and PD
19	50,51	1	dynamic	750 mg qd	0; 0.5; 1.0; 1.5; (1.75)*; 2.0; 10.0; 12.0; 14.0; 16.0; 18.0; 20.0; 22.0; 24.0	PK and PD
20	54,55,56,57	4	static	0, 0.016,0.032, 0.064	0; 0.5; 1; 1.5; 2.15; 4; 6; 8; 10; 25	PD only
21	58,59,60,61	1	static	0; 8; 16; 32	0; 0.5; 1; 2; 4; 6; 8; 10; 24	PD only
22	62, 63, 64, 65	1	static	16, 32, 64	0; 0.5; 1; 2; 4; 6; 8; 10; 24	PD only
23	66, 67, 68, 69, 70	2	static	0.5; 1; 2; 4	0; 0.5; 1; 2; 4; 6; 8; 10; 21; 27	PD only
24	71, 72, 73, 74, 75	1	static	2x8 and 2x16	0; 0.5; 1.0; 2.0; 4.0; 6.0; 8.0; 10.0; 23.0; 25.0; 28.0; 30.0; 32.0; 48.0; 76.0	Additional electronic cell counting
25	76, 77, 78, 79, 80	2	static	2x2 and 2x4	0; 0.5; 1.0; 2.0; 4.0; 6.0; 8.0; 10.0; 24.0; 25.0; 28.0; 30.0; 32.0; 48.0; 73.5	Additional electronic cell counting
26	81, 82, 83, 84, 85	3	static	2x8 and 2x16	0; 0.5; 1.0; 2.0; 4.0; 6.0; 8.0; 10.0; 24.0; 25.0; 28.0; 32.0; 48.0; 74.5	Additional electronic cell counting
27	86, 87, 88, 89, 90	3	static	2x8 and 2x16	0; 0.5; 1.0; 2.0; 4.0; 6.0; 8.0; 10.0; 24.0; 49.5	Additional electronic cell counting
28	91, 92, 93, 94, 95	3	static	2x8 and 2x16	0; 0.5; 1.0; 2.0; 4.0; 6.0; 8.0; 10.0; 24.0; 48.5	Additional electronic cell counting
29	96, 97, 98	1,2,3	static	GC only	0; 0.5; 1.0; 2.0; 4.0; 6.0; 8.0; 24.0	Additional electronic cell counting

*****Sampling times for assessment of LEV concentrations only (no assessment of bacterial concentrations).

Table 7.9: Sequence quality of 8 polymerase chain reaction (PCR) products of quinolone resistance determining regions (*gyrA* and *parC)* of 3 clinical *Escherichia coli* isolates: percentage of high quality base calls, based on Phred quality score, corresponding assignment to quality bin (in green: high quality, yellow: medium quality, red: low quality) and percentage of identical bases for PCR product, sequenced with forward (F) or reverse (R) primer, respectively; percentage of identical bases with reference strain, obtained from the National Center for Biotechnology [146]; in grey: sequences used for further analysis, ST: sequence type, "post" indicates that PCR was performed with DNA extracted from isolate after levofloxacin exposure in the static *in vitro* infection model.

	High quality score, %		Quality bin		Identity Primer F and Primer R, %	Identity with reference, %	
Isolate, gene	**Primer F**	**Primer R**	**Primer F**	**Primer R**		**Primer F**	**Primer R**
ST 58 *gyrA*	92.7	93.3	high	high	97.5	98.3	94.4
ST 58 *parC*	0.0	90.6	low	high	94.4	98.3	98.3
ST 88 *gyrA*	92.0	93.6	high	high	97.3	99.4	99.4
ST 88 *parC*	84.0	93.3	medium	high	99.1	98.9	99.1
ST 88 post *gyrA*	94.3	19.8	high	low	91.4	99.4	83.9
ST 88 post *parC*	69.4	92.8	low	high	97.9	97.0	98.7
ST 167 *gyrA*	91.6	90.4	high	high	97.5	96.7	92.9
ST 167 *parC*	34.3	90.5	low	high	98.4	80.9	98.5

Table 7.10: Acquired antimicrobial resistance mechanisms of three investigated *Escherichia coli* isolates according to ResFinder 3.2 [143].

Sequence type 58	Sequence type 88	Sequence type 167
• Aminoglycosides • Beta-lactamases • Sulphonamides • Macrolides	• Aminoglycosides • Beta-lactamases • Sulphonamides • Macrolides • Tetracyclines	• Aminoglycosides • Beta-lactamases • Macrolides

Table 7.11: Parameter estimates of different models (Table 7.6) describing the exposure-effect relationship of levofloxacin against 3 clinical *Escherichia coli* isolates in static and in dynamic *in vitro* infection model (IVIM) experiments.

	Static IVIM Estimate [RSE,%]					Dynamic IVIM Estimate [RSE,%]				
Parameter [unit]	**Model 1**	**Model 2**	**Model 3**	**Model 4**	**Model 5**	**Model 1**	**Model 2**	**Model 3**	**Model 4**	**Model 5**
Strain 1 (ST 58)										
$cumAUC_{50}$ [mg·h·L^{-1}]	154 [29.6]	325 [28.1]	160 [6.95]	144 [17.7]	167 [10.7]	34.1 [38.7]	171 [15.7]	154 [15.8]	102 [69.8]	83.0 [30.5]
E_{max}	0.933 [12.5]	1.10 [15.5]	FIX 1	1.10 [9.86]	FIX1	0.332 [19.3]	1.10 [0.0]	FIX 1	1.10 [43.4]	FIX1
Hill	0.949 [8.42]	-	-	1.07 [5.81]	0.951 [6.25]	1.30 [12.8]	-	-	1.27 [18.9]	1.28 [12.3]
$cumAUC_{reg}$ [mg·h·L^{-1}]	-	317 [19.1]	4751 [60.7]	1020 [17.02]	7843 [92.2]	-	66.2 [34.7]	76.5 [36.2]	62.6 [38.5]	87.5 [44.0]
Proportional residual variability, % CV	2.76	23.2	2.80	3.53	2.72	5.05	4.64	4.64	10.7	4.85
Strain 2 (ST 88)										
$cumAUC_{50}$ [mg·h·L^{-1}]	22.9 [25.2]	34.4[16.0]	32.6 [7.15]	25.9 [21.0]	27.2 [11.2]	26.9 [19.6]	40.9 [16.5]	38.0 [8.05]	32.5 [16.8]	32.2 [10.1]
E_{max}	0.885 [13.1]	1.10 [9.65]	FIX 1	1.10 [14.4]	FIX1	0.842 [8.13]	1.10 [6.70]	FIX 1	1.10 [10.8]	FIX1
Hill	1.21 [9.28]	-	-	1.26 [7.04]	1.17 [7.39]	1.20 [10.1]	-	-	1.27 [7.24]	1.20 [8.04]
$cumAUC_{reg}$ [mg·h·L^{-1}]	-	139.3 [17.6]	$2.55 \cdot 10^6$ [9.3]	249 [31.4]	1441 [140]	-	279 [16.7]	1809 [107]	300 [30.03]	615.5 [44.7]
Proportional residual variability, % CV	3.14	4.04	3.11		3.14	0.734	1.14	0.762	0.711	0.694
Strain 3 (ST 167)										
$cumAUC_{50}$ [mg·h·L^{-1}]	13.9 [18.6]	42.0 [6.20]	36.1 [9.45]	13.8 [18.6]	31.8 [17.4]	12.7 [11.4]	40.2 [28.2]	35.1 [7.63]	16.6 [19.3]	27.2 [8.45]
E_{max}	0.598 [8.05]	1.10 [8.92]	FIX 1	0.597 [8.04]	FIX1	0.564 [4.09]	1.10 [18.8]	FIX 1	0.692 [12.6]	FIX1
Hill	1.47 [16.9]	-	-	1.47 [16.9]	1.085 [13.5]	1.66 [9.99]	-	-	1.48 [10.43]	1.28 [7.62]
$cumAUC_{reg}$ [mg·h·L^{-1}]	-	325 [40.2]	327 [28.2]	$1.96*10^6$ [20.9]	338 [34.0]	-	177 [45.4]	223 [14.1]	540 [58.7]	195 [14.2]
Proportional residual variability, % CV	1.19	1.53	1.35	1.19	1.30	0.830	0.800	0.829	0.697	0.702

ST: Sequence type, RSE: Relative standard error (imprecision of parameter estimates); E_{max}: maximum effect, $cumAUC_{50}$: exposure, determined as cumulative area under the levofloxacin concentration-time curve, causing 50% of the maximum effect, $cumAUC_{reg}$: exposure causing regrowth in *in vitro* infection model experiments, Hill: Hill factor (steepness of exposure-effect relationship), CV: coefficient of variation.

Table 7.12: Parameter estimates and imprecision (based on SIR) of pharmacokinetic model, based on levofloxacin concentrations in dynamic *in vitro* infection model experiments (full dataset: n=21 experimental replicates and excluding ID 3, ID 4, ID 10 or ID 20), resulting from a 750 mg, 90 min i.v. infusion qd (n=14 replicates) or a 500 mg, 60 min i.v. infusions bid (n=7 replicates).

	Full dataset		**Case deletion: ID 3**		**Case deletion: ID 4**		**Case deletion: ID 10**		**Case deletion: ID 20**	
Parameter [unit]	Estimate (RSE, %)	95% CI	Estimate (RSE, %)	95% CI	Estimate (RSE, %)	95% CI	Estimate (RSE, %)	95% CI	Estimate (RSE, %)	95% CI
θ CL [L/h]	8.90 (10.7)	7.21 – 10.9	8.52 (10.3)	6.81 – 10.5	8.50 (10.2)	6.91 – 10.3	9.24 (10.9)	7.36 - 11.3	9.49 (10.1)	7.82 – 11.4
θ V_c [L]	28.3 (8.80)	23.8 – 33.3	27.7 (9.29)	23.1 - 33.5	27.5 (9.23)	23.0 – 33.0	30.2 (7.14)	26.5 - 34.6	28.7 (10.4)	23.5 – 35.1
θ V_p [L]	42.1 (7.71)	35.6 - 48.9	41.0 (8.80)	34.8 – 48.5	41.7 (7.27)	34.2 – 49.2	41.9 (8.94)	36.0 – 50.7	42.5 (9.21)	36.4 – 51.2
θ Q [L/h]	26.6 (14.7)	19.6 - 34.6	25.7 (15.1)	18.7 – 33.6	26.4 (14.4)	18.9 – 33.6	24.1 (14.0)	17.7 – 31.2	26.3 (17.5)	18.8 – 36.8
θ SF [unitless]	1.39 (14.6)	0.994 - 1.78	1.48 (12.6)	1.11 – 1.83	1.43 (14.8)	1.04 – 1.85	1.47 (19.4)	0.849– 1.95	1.38 (16.7)	0.916 – 1.82
Interindividual variability parameters, %CV										
ω CL	57.3 (27.1)	44.7 – 77.3	56.6 (30.8)	42.1-80.9	56.6 (26.7)	43.4 – 75.8	55.0 (29.2)	41.5 – 75.5	49.2 (31.6)	38.6 – 70.7
ω V_c	42.0 (36.5)	29.9 – 60.1	43.0 (36.8)	30.2 – 62.2	43.0 (33.7)	32.1 – 61.8	35.0 (39.3)	23.8 – 51.7	42.7 (48.4)	30.5 – 69.1
ω V_p	28.3 (66.1)	15.8 - 49.5	29.5 (54.9)	19.7 – 49.1	30.3 (46.4)	18.5 – 46.4	31.6 (56.8)	18.3 – 52.5	29.0 (63.7)	17.5 - 52.0
Residual unexplained variability, %										
σ	26.9 (4.33)	24.9 - 29.2	24.9 (4.47)	23.0–27.3	24.5 (4.29)	22.5 – 26.6	26.5 (4.65)	24.4- 29.3	27.3 (4.62)	24.9 – 30.0

Abbreviations: RSE: Relative standard error, SIR: sampling importance resampling, %CV: coefficient of variation, calculated according to Equation 2.27; CI: confidence interval, determined by SIR, SF: scaling factor; bid: bis in die (twice daily), qd: quaque die (once daily).

7.3 NONMEM® script

```
; 1. Based on: RUV_CASY_fixrates
; 2. Description: Final PK/PD model

$SIZES MAXFCN=100000000
$PROBLEM PKPD
$INPUT
ID          ; replicate identifier
TIME        ; time [h]
CON         ; levofloxacin concentration in static in vitro infection model
STRN        ; bacterial strain (0=PK feasibility experiment; 1:ST58; 2:ST88; 3:ST167;
              4: ATCC25922 (not included))
EXPNR       ; experiment number
DV_LIN      ; dependent variable, linear scale
FLAG        ; 0: dosing record; 1: PK observation [mg/L]; 2: PD observation, growth control
              [droplet plate, CFU/mL]; 3: PD observation, exposed bacteria [droplet plate,
              CFU/mL] 4: PD observation [total CASY counts/mL])
DV          ; dependent variable on ln scale
LDV         ; dependent variable on log10 scale (only bacterial concentrations;
              levofloxacin concentrations: linear scale)
AMT         ; administered levofloxacin amount in dynamic in vitro infection model
MDV         ; missing dependent variable (0: no; 1: yes)
RATE        ; mimicked infusion rate in dynamic in vitro infection model [mg/h]
CMT         ; compartment (1: central)
EVID        ; event identification (0: observation, 1: dosing, 2: other event, 3: reset event)
STDY        ; study number
STAT        ; indicates in vitro infection model type  (0: dynamic, 1: static)
BQL         ; below quantification limit (0: no, 1: yes)
LLOQ        ; lower limit of quantification (levofloxacin concentration [mg/L]; bacterial
            concentration [CFU/mL])
REGIM       ; mimicked dosing regimen in dynamic in vitro infection model  (1: 750 mg qd;
              2: 500 mg bid)
DOSE        ; levofloxacin dose
NAME=DROP

$DATA 20200824_PKPD_CASY.csv IGNORE=@ IGNORE=(STRN.EQ.4)
        ; STRN4 (ATCC25922) not included

$SUBROUTINES ADVAN13 TOL=9

$MODEL

COMP(CENT)      ; central (PK)
COMP(PERIPH)    ; peripheral (PK)

COMP(ALIVE_N)   ; viable bacteria
COMP(ALIVE_P)   ; persister
COMP(DEAD)      ; dead cells
```

$PK

```
MXSTEP = 1000000

; Exposure parameters

TVCL  =    THETA(1)
CL    =    TVCL*EXP(ETA(1))
TVV1  =    THETA(2)
V1    =    TVV1 * EXP(ETA(2))
TVQ   =    THETA(3)
SCALE=     THETA(4)
Q     =    TVQ*EXP(-ETA(2)*SCALE)
TVV2  =    THETA(5)
V2    =    TVV2*EXP(ETA(3))
K12   =    Q/V1
K21   =    Q/V2
K10   =    CL/V1
;-------------------------------------------------------------------------------
; Bacterial growth parameters

IF(STAT.EQ.0)TVKGN = THETA(6)        ; relative growth rate, dynamic ; h-1
IF(STAT.EQ.1)TVKGN = THETA(7)        ; relative growth rate, static ; h-1
KG_N = TVKGN * EXP(ETA(4))
KG_P = KG_N/10                       ; persister growth rate (1/10 of "viable growth
                                       rate")

TVN0 = THETA(8)                      ; log10 initial viable bacterial number, (N)
                                       [log10(CFU)]
N0 = TVN0 * EXP(ETA(5))

IF(STAT.EQ.0)TVLOGMAX = THETA(9) ; maximum bacterial number dynamic [log10(CFU)]
IF(STAT.EQ.1)TVLOGMAX = THETA(9)*(1+THETA(10)) ; fractional change of maximum
                                  bacterial number static from dynamic [log10(CFU)]

LOGMAX = TVLOGMAX * EXP(ETA(6))

TVKD = THETA(11)                     ; death rate [h-1]
KD = TVKD * EXP(ETA(7))

TVKPER = THETA(12)                   ; transfer to persister state [h-1]
KPER = TVKPER*EXP(ETA(8))

TVKNOR = THETA(13)                   ; back-transfer to viable state [h-1]
KNOR = TVKNOR*EXP(ETA(9))
```

```
; Levofloxacin effect parameters

; Levofloxacin killing effect (Emax model parameters)

TVEMAX = THETA(14)                          ; Emax
EMAX = TVEMAX* EXP(ETA(10))
IF(STRN.EQ.1)   TVEC50  = THETA(15)         ; EC50 ST58
IF(STRN.EQ.2)   TVEC50  = THETA(16)         ; EC50 ST88
IF(STRN.EQ.3)   TVEC50  = THETA(17)         ; EC50 ST167
EC50 = TVEC50*EXP(ETA(11))

HILL     = TVHILL*EXP(ETA(12))              ; Hill
TVHILL = THETA(18)

; Levofloxacin effect on persister formation

IF(STRN.EQ.1)   TVPMAX  = THETA(19)         ; additive increase KPER ST58
IF(STRN.EQ.2)   TVPMAX  = THETA(20)         ; additive increase KPER ST88
IF(STRN.EQ.3)   TVPMAX  = THETA(21)         ; additive increase KPER ST167

PMAX = TVPMAX*EXP(ETA(13))
;-------------------------------------------------------------------------------
; Initial bacterial numbers in persister and dead cell compartment

TVNP = THETA(22)                            ; log10 initial persister (P) [log10(CFU)]
NP = TVNP * EXP(ETA(14))
TVND = THETA(23)                            ; log10 initial dead bacteria (D) [log10(CFU)]
ND = TVND * EXP(ETA(15))
;-------------------------------------------------------------------------------
; Initialise compartments

A_0(1) = 0          ; Central compartment PK
A_0(2) = 0          ; Peripheral compartment PK
A_0(3) = 10**N0     ; Number of normal growers at t=0
A_0(4) = 10**NP     ; Number of persisters  at t=0
A_0(5) = 10**ND     ; Number of dead cells at t=0
;-------------------------------------------------------------------------------
$DES

; Levofloxacin concentrations
  CLEV=CON                          ; Static levofloxacin concentration
  IF(STAT.EQ.0)CLEV = (A(1)/V1)     ; Dynamic levofloxacin concentration

; Levofloxacin effect
  ELEV=0                            ; No killing effect for growth controls (CLEV=0)
  PLEV=0                            ; No effect on persister formation for growth controls

  IF(CLEV.GT.0)THEN
  ELEV = (EMAX*(CLEV)**HILL)/((CLEV)**HILL+EC50**HILL)          ; Killing effect
  PLEV =  PMAX                                                  ; Effect on persister formation
  ENDIF

  KILL = ELEV
  IF(KILL.LT.0)KILL=0
  KNPo = KPER * (A(3))/(10**LOGMAX)
  KNP = KNPo + PLEV
```

```
  IF(KNP.LT.0)KNP=0
  KGPER = (KG_P * (1- (A(3)+A(4)/10)/10**LOGMAX))
  IF(KGPER.LT.0)KGPER=0
  IF(KD.LT.0)KD=0

; PK
  DADT(1)=0
  IF(STAT.EQ.0)DADT(1) = -K12*A(1) + K21*A(2) - K10*A(1)       ; central compartment
  DADT(2)=0
  IF(STAT.EQ.0)DADT(2) =  K12*A(1) - K21*A(2)                  ; peripheral compartment

; PD

; Viable bacteria
DADT(3) =  (KG_N * (1- (A(3)+A(4)/10)/10**LOGMAX)) * A(3) - KNP*A(3) + 2*KNOR*A(4) -
KD * A(3) - KILL*A(3)

; Persister
DADT(4) =  (KG_P * (1- (A(3)+A(4)/10)/10**LOGMAX)) * A(4) + KNP*A(4) - KNOR*A(4)

; Dead bacteria
  DADT(5)=  (KD * A(3)) + (KILL * A(3))
;-------------------------------------------------------------------------------

$ERROR
CALLFL=0
CONC= A(1)/V1
NOR = LOG10(A(3)+0.0001)
PER = LOG10(A(4)+0.0001)
DEAD = LOG10(A(5)+0.0001)
SUM_ALL = LOG10(10**NOR + 10**PER+ 10**DEAD)
CASY_TOTAL = LOG(10**SUM_ALL)

IPRED=-3
IF(FLAG.EQ.1)THEN                       ; Levofloxacin concentrations
IPRED = LOG(A(1)/V1+0.0001)
W = SQRT(THETA(24)**2)                  ; RUV PK
ENDIF
IF(FLAG.EQ.2)THEN                       ; Growth controls
IPRED = LOG(A(3)+0.0001)
W = SQRT(THETA(25)**2)                  ; RUV PD (droplet plate)
ENDIF
IF(FLAG.EQ.3)THEN                       ; Exposed bacteria
IPRED = LOG(A(3)+0.0001)
W = SQRT(THETA(25)**2)                  ; RUV PD  (droplet plate)
ENDIF
IF (FLAG.EQ.4) THEN                     ; Total CASY counts
  IPRED = CASY_TOTAL
        IRES = DV-IPRED
  W = SQRT(THETA(26)**2)                ; RUV PD (CASY)
        IWRES = IRES/W
        F_FLAG=0
        Y = IPRED + W*EPS(2)
ENDIF
; Observations below the LLOQ: M3 method
LOQ    = LLOQ+0.0001
```

```
LOQ10 = LOG10(LLOQ+0.0001)
LOQN  = LOG(LLOQ+0.0001)

DUM   = (LOQN-IPRED)/W
CUMD = PHI(DUM)

IF (FLAG.EQ.1) THEN                     ; Levofloxacin concentrations
        IRES = DV-IPRED
        IWRES = IRES/W
        F_FLAG=0
        Y = IPRED + W*EPS(1)
ENDIF

IF (FLAG.EQ.2) THEN                     ; Growth control (droplet plate)
        IRES = DV-IPRED
        IWRES = IRES/W
        F_FLAG=0
        Y = IPRED + W*EPS(2)
ENDIF

IF (FLAG.EQ.3.AND.BQL.EQ.0) THEN        ; Exposed Bacteria (droplet plate) > LLOQ
        IRES = DV-IPRED
        IWRES = IRES/W
        F_FLAG=0
        Y = IPRED + W*EPS(2)
ENDIF

IF (FLAG.EQ.3.AND.BQL.EQ.1) THEN        ; Exposed Bacteria (droplet plate) < LLOQ
      IRES=0
      IWRES=0
      F_FLAG=1
  Y=CUMD
ENDIF
;-------------------------------------------------------------------------------
$THETA
; PK
(8.9)          FIX              ; CL, L/h
(28.3)         FIX              ; Vc, L
(26.6)         FIX              ; Q, L/h
(1.39)         FIX              ; Scale, -
(42.1)         FIX              ; Vp, L

; Bacterial growth
 1.15          FIX              ; Kg_n, dynamic,h-1
 1.81          FIX              ; kg_n, static, h-1
 5.9           FIX              ; Log10(N0)
 8.75          FIX              ; Log10(PopMAX_DYN)
 0.112         FIX              ; Fractional change popmax [log10(CFU)]
 0.0123        FIX              ; KD, h-1
(0.000001)     FIX              ; KPER, h-1
(0.1)          FIX              ; KNOR, h-1
```

```
; LEV effect
(0, 10.1,40)                    ; Emax, h-1
(0, 42.7)                       ; EC501,mg/L
(0, 8.97)                       ; EC502,mg/L
(0, 10.5)                       ; EC503,mg/L
(0, 1.04,20)                    ; HILL
(0, 0.00019)                    ; Pmax1, h-1
(0, 0.0343)                     ; Pmax2, h-1
(0, 0.121)                      ; Pmax3, h-1
(0, 3.07,6)                     ; Log10(NP)
(0, 0.45,1)                     ; log10(ND)

; RUV
(0, 0.346)                      ; Add REPK in LOG
(0, 1.78)                       ; Add REDP in LOG
(0, 1.06)                       ; Add RECASY in LOG

$OMEGA
;PD
 0.331                          ;  IIV CL
 0.142 FIX                      ;  IIV V1/Q
 0 FIX                          ;  IIV_V2
 0 FIX                          ;  IIV Kgn
 0 FIX                          ;  IIV N0
 0 FIX                          ;  IIV popMax
 0 FIX                          ;  IIV KD
 0 FIX                          ;  IIV KPER
 0 FIX                          ;  IIV KNOR
 0.0462                         ;  IIV Emax
 0 FIX                          ;  IIV EC50
 0 FIX                          ;  IIV HILL
 0 FIX                          ;  IIV PMax
 0 FIX                          ;  IIV NP
 0 FIX                          ;  IIV ND

$SIGMA
 1 FIX                          ; Proportional error PK
 1 FIX                          ; Error PD

$EST METHOD=1 LAPLACIAN NUMERICAL SIGDIG=3 SIGL=9 SIGLO=9
MAXEVAL=100000 NOABORT PRINT=1 POSTHOC NOABORT

$COV UNCONDITIONAL PRINT=E

$TABLE ID TIME AMT BQL LOQ LOQN LOQ10 LDV STRN ELEV PLEV CON
CASY_TOTAL DEAD NOR PER FLAG DV MDV EVID IPRED IWRES CWRES EXPNR
ONEHEADER NOPRINT FILE=sdtab_STAT_on_KG_popmax1

$TABLE ID AMT IPRED IWRES CWRES FLAG NP KG_N KD LOGMAX KNOR Kper EMAX
EC50 HILL PMAX EXPNR STRN ONEHEADER NOPRINT FIRSTONLY
FILE=patab_STAT_on_KG_popmax1
```

8 Publications

Original articles

J. Seeger[#], R. Michelet[#], C. Kloft.
Quantification of persister formation of *Escherichia coli* leveraging electronic cell counting and semi-mechanistic pharmacokinetic/pharmacodynamic modelling.
J. Antimicrob. Chemother 76: 2088-2096.
doi: 10.1093/jac/dkab146.
[#]equal contribution

J. Seeger, S. Guenther, K. Schaufler, S.E. Heiden, R. Michelet[#], C. Kloft[#].
Novel pharmacokinetic/pharmacodynamic parameters quantify the exposure-effect relationship of levofloxacin against fluoroquinolone resistant *Escherichia coli*.
Antibiotics 10: 615 (2021).
doi: 10.3390/antibiotics10060615.
[#]shared senior authorship

Review article

C.V. Montefusco-Pereira, C. de Souza Carvalho-Wodaz, **J. Seeger**, C. Kloft, R. Michelet, C. Lehr.
Translating (patho-)physiology by advanced cell culture models to develop new pulmonary anti-infectives.
Drug Discov. Today. 26: 148-163 (2021).
doi: 10.1016/j.drudis.2020.10.016

Oral presentations

J. Seeger, R. Michelet, C. Kloft.
Exploring the exposure-effect relationship of levofloxacin against fluoroquinolone resistant *Escherichia coli* isolates in a dynamic *in vitro* infection model.
Annual meeting of the International Society of Anti-Infective Pharmacology (ISAP) 2019, Rotterdam, The Netherlands, 12 April 2019.
https://isap.org/index.php/annual-meeting/annual-meeting-2019, (2019).

J. Seeger, R. Michelet, S. Günther, C. Kloft.
Determinants of growth-kill behaviour of fluoroquinolone resistant *Escherichia coli* under levofloxacin exposure in a dynamic *in vitro* infection model.
Annual Meeting of the Deutsche Pharmazeutische Gesellschaft (DPhG), Heidelberg, Germany, 01-04 September 2019.
https://www.dphg.de/fileadmin/downloads/DPhG-ConferenceBook_2019.pdf, 162, (2019).

Conference abstracts

J. Seeger, R. Michelet, C. Kloft. Electronic cell counting facilitates quantification of persister formation of *Escherichia coli* under levofloxacin exposure in static and dynamic *in vitro* infection model experiments.
31st European Congress of Clinical Microbiology and Infectious Diseases (ECCMID). Accepted (2021).

J. Seeger, R. Michelet, S. Guenther, C. Kloft. Beyond the minimal inhibitory concentration: Novel pharmacokinetic/pharmacodynamic metrics quantify the exposure-effect relationship of levofloxacin against fluoroquinolone resistant *Escherichia coli* based on *in vitro* infection models.
30th European Congress of Clinical Microbiology and Infectious Diseases (ECCMID), Paris, France, 18-21 April 2020. Abstract book, 3065, (2020).

R. Michelet, **J. Seeger**, C. Kloft. A mechanism-based pharmacokinetic/pharmacodynamic model based on pharmacokinetic and static time-kill data alone can predict the *in vitro* bacterial regrowth of 3 fluoroquinolone-resistant *Escherichia coli* strains after dynamic exposure.
30th European Congress of Clinical Microbiology and Infectious Diseases (ECCMID), Paris, France, 18-21 April 2020. Abstract book, 1243, (2020).

J. Seeger, R. Michelet, C. Kloft.
What drives regrowth of fluoroquinolone resistant *Escherichia coli* under levofloxacin exposure in a dynamic *in vitro* infection model?
American Society for Microbiology (ASM) Microbe, San Francisco, USA, 20-24 June 2019.
https://www.abstractsonline.com/pp8/#!/7859/presentation/16865, (2019).

J. Seeger, C. Kloft.
Exploring pharmacokinetic/pharmacodynamic relationships of levofloxacin against resistant *Escherichia coli* in a dynamic *in vitro* infection model.
Annual Meeting of the Deutsche Pharmazeutische Gesellschaft (DPhG), Hamburg, Germany, 02-05 October 2018.
https://www.dphg.de/fileadmin/downloads/DPhG2018_ConferenceBook_Final_27-09-2018.pdf, 139, (2018).

E.B. Goebgen, **J. Seeger**, A. Schaeftlein, C. Kloft.
Levofloxacin in resistant *Escherichia coli*: Is there a difference between 750 mg once a day and 500 mg twice a day?
27th European Congress of Clinical Microbiology and Infectious Diseases (ECCMID), Vienna, Austria, 22-25 April 2017.
https://www.escmid.org/escmid_publications/escmid_elibrary/material/?mid=40622, (2017).

J. Seeger, E.B. Goebgen, C. Kloft.
The effect of levofloxacin 500 mg bid and 750 mg qd against resistant *Escherichia coli* in the *in vitro* dynamic infection model.
Annual Meeting of the Deutsche Pharmazeutische Gesellschaft (DPhG), Munich, Germany, 04-07 October 2016.
www.dphg.de/fileadmin/downloads/DPhG2016_ConferenceBook_final.pdf, 172, (2016).

E.B. Goebgen, N. Hartung, **J. Seeger**, A. Schäftlein, C. Kloft.
Treatment of catheterised ICU patients with levofloxacin - How *in silico* models help to streamline *in vitro* investigations of treatment efficacy at the target site.
Annual Meeting of the Deutsche Pharmazeutische Gesellschaft (DPhG), Munich, Germany, 04-07 October 2016.
www.dphg.de/fileadmin/downloads/DPhG2016_ConferenceBook_final.pdf, 121, (2016).

Diploma thesis

J. Seeger. Vergleich des pharmakodynamischen Effekts von Levofloxacin 750 mg qd und 500 mg bid auf resistente *Escherichia coli* im dynamischen *In-vitro*-Infektionmodell. Freie Universitaet Berlin. (2017).

Further publication

J. Seeger, J. Schulz.
Patienten im Fokus. Klinische Pharmazie weitergedacht.
Deutsche Apotheker Zeitung 160: 4230-4232 (2020).